Lawrence Berkeley National Laboratory
Recent Work

Title
Atomic processes for heavy ion inertial fusion

Permalink
https://escholarship.org/uc/item/52h8h3sw

Author
Armel, Michael Scott

Publication Date
2000-11-01

eScholarship.org Powered by the California Digital Library
University of California

Atomic Processes for Heavy Ion Inertial Fusion

by

Michael Scott Armel

B.S. (University of Virginia) 1992
M.S. (Yale University) 1994

A dissertation submitted in partial satisfaction of the
requirements for the degree of
Doctor of Philosophy

in

Engineering - Nuclear Engineering

in the

GRADUATE DIVISION

of the

UNIVERSITY OF CALIFORNIA, BERKELEY

Committee in charge:

Professor Per Peterson, Chair
Professor Stan Prussin
Professor Richard Marrus

Fall, 2000

The dissertation of Michael Scott Armel is approved:

Chair Date

Date

Date

University of California, Berkeley

Fall, 2000

Atomic Processes for Heavy Ion Inertial Fusion

Copyright 2000

by

Michael Scott Armel

Abstract

Atomic Processes for Heavy Ion Inertial Fusion

by

Michael Scott Armel

Doctor of Philosophy in Engineering - Nuclear Engineering

University of California, Berkeley

Professor Per Peterson, Chair

Heavy ion beams which may be used as drivers for inertial fusion energy power generation exhibit a wide array of atomic phenomena in connection to their penetration through the chamber environments and into the target materials associated with current heavy ion fusion (HIF) scenarios. The modeling of many of these atomic processes has been complicated due to uncertainties, including many difficult-to-quantify atomic processes of ion-plasma interactions. This work has been directed to address some of the issues of greatest import to HIF and atomic physics in general.

A comprehensive model is presented in this dissertation which enables calculation of important atomic reactions and an improved understanding of the processes responsible for errors in previous calculations. This work demonstrates that the standard binary encounter models (BEM) for direct ionization can be used reliably in HIF-related calculations of beam ionization in gaseous chambers and the charge evolution of ions penetrating solids.

Much of the miscalculation of enhanced ionization previously encountered is shown not to be due to shortcomings in the BEM, but rather to incomplete application of the Lotz free electron formula to highly-charged ions. Included are recommendations for obtaining better HIF-related ionization cross sections experimentally. This can be done by reversing the target and beam frames, using nuclear or electron beams to ionize heavy ions, which can have an initial charge state as high as 10+ [50].

Herein is demonstrated for the first time the successful use of first-principle charge-changing reaction models to replicate the Bohr semi-empirical formula for equilibrium charge states of ions penetrating cold solids. This success, along with an improved understanding of the ionization and capture processes in beams penetrating plasmas are combined to establish trends in the charge state evolution of heavy ions in plasma targets. This enables the development of a new equilibrium charge state formula giving the equilibrium charge evolution of a beam penetrating a dense, partially ionized plasma target.

Professor Per Peterson
Dissertation Committee Chair

To the cathedral builders, who toil in love for that whose culmination they may never know,

Contents

List of Figures

List of Tables

Acknowledgements

My first scientific acknowledgements are due to my dissertation advisor, professor Per Peterson. It has been an honor to be his student in the classroom learning thermal-hydraulics and his student research advisee. When I first visited Berkeley I met with Per among the other faculty members, and frankly I had no idea what heavy ion inertial fusion meant. Since then I have learned not only what HIF is, but who the next world expert will be. I especially thank Per for his amazingly attentive and rapid feedback on my dissertation. It has just been announced publicly that Per will be the next chairperson of the nuclear engineering department at Berkeley. I leave knowing that it is in very capable hands.

I offer thanks also to the other two members of my dissertation committee, Professor Stan Prussin of nuclear engineering and Professor Richard Marrus of the physics department. Professor Prussin's lectures on energy deposition in his nuclear physics course formed the basis for much of my knowledge of atomic interactions. Stan has enthusiastically advised me on post-graduate research and I hope that his talents and physical knowledge will continue to be applied to research projects in nuclear physics. My dissertation benefited immensely from his thorough reading and painfully honest suggestions. It is an honor to be associated with such academic integrity. Professor Marrus may have finished with my dissertation, but I hope to continue the informal weekly meetings with him at La Strada and to discuss relativistic atomic physics over coffee. Examination of the ancillary problems he posed to me actually spurred me to learn some important physics which helped to solidify my understanding of a universal ionization formula. More importantly, I've found a friend in another atomic physicist.

The members of my oral exam committee, Professor Jasmina Vujic, Professor Ken Fowler, Professor Jonathan Wurtele and Per all were appreciated greatly in December of 1999. They did not disappoint my expectations of an exhausting but fair oral qualifying exam.

I also am honored and immensely appreciative of the participation of several other co-advisors who represent the most prominent fusion scientists in the world today. Roger Bangerter at Lawrence Berkeley National Lab originated the idea for the topic which became my dissertation body. From him I learned a great amount of physics and fusion science, as well as an enthusiasm and optimism for pursuing national-scale science projects. Roger is the kind of project leader and scientist who engenders the confidence which proponents of fusion require. Unfortunately, as I finish my work I learn of Roger's retirement. I hope that a leader with his integrity will emerge to continue his efforts in bringing HIF to the attention of the world. Max Tabak and Debbie Callahan-Miller gave me an education in capsule and hohlraum physics and generously made arrangements for me to work at LLNL. Though my atomic physics work eventually overshadowed the other projects which Roger, Max and Debbie considered for me, I hope to be able to work in the future with them on the many other exciting issues.

A number of individuals at Berkeley and Livermore also contributed to my education. Ed Lee entertained many of my breathless knocks at his door and subsequent whiteboard demonstrations and offered his time and wisdom generously. Bill Sharp provided many very useful discussions and suggestions and is largely responsible for allowing my work to be extended from the originally envisioned target regime to chamber applica-

tions as well. Harvey Gould of LBNL provided some sorely needed experimentalist expertise and introduced me to a large body of measurements which helped me to validate my calculations.

Outside of Livermore I have benefited from many e-mail and phone conversations with some very prominent atomic scientists. I was able to secure a copy of the classic text *The Theory of Atomic Structure and Spectra* by Bob Cowan from none other than Dr. Cowan himself. Bob kindly answered e-mails and discussed by phone the questions I posed to him. I'll cherish the autographed copy of his text which he sent me. Charlotte Fischer of Vanderbilt University provided suggestions on using screening functions for ionization potential scaling which enabled my research to sustain a quantum leap in quality. Yong-Ki Kim at NIST kindly offered much advise on problems in ionization calculations and introduced me to some of his most excellent previous work in HIF atomic physics. Professor Sumner Davis also entertained several meetings and e-mail discussions and put me in touch with some very valuable people, including Dr. Kim.

I would also like to thank my colleagues at Princeton Plasma Physics Lab. PPPL as well as Livermore lab have both been part of the dream which began in middle school and which lead eventually to my pursuit of a fusion-related dissertation. Just when I was about to forget about fusion, I was reminded of the magnetic fusion effort at Princeton in a film I saw at Disney World. The dream is still alive. Igor Kaganovich at Princeton kindly arranged for me to visit. It was an honor to give a presentation of my research there and to work with him and the others. Igor also has rigorously reviewed much of my dissertation and research and has contributed to my physical understanding for which I

am greatly appreciative. It has also been an honor to enjoy many sincere discussions with Larry Grisham concerning fusion, science and especially cathedrals. It is great to have a soul mate working for the 'other side' and I wish the best and much success for him and the rest of the group at Princeton.

I give special thanks to the staffs of my department and the national labs where I have worked. From finances to course registration to conferences, people like Sara Hill, Lisa Zemelman, Pat Sizer, Carol Schun, Lynn Heimbucher and Sharon Buckley have facilitated every step of the way.

Personal acknowledgements are due to my mother and grandparents and brother and sister and other family members for providing me with the love and encouragement which sustained me throughout my academic years through everything else through which we have lived. To be blessed with people who believe that you are special is greater than any inheritance. Your participation in my life has made all of the difference.

I thank the spice boys of Za'atar for giving me a most wonderful set of cultural, social and musical experiences outside of the computer lab. The times I've enjoyed playing in Za'atar alone would justify having moved across the country to California. I am sad to have to say farewell to my friends in the department and in the Accelerator and Fusion Research Division at Berkeley Lab who have shared these years with me. I will miss the daily seminars in building 54 with the AFRD student fusion group. Discussing progress in that way greatly enhances fusion research, even if only by sustaining friendships.

I consider it a privilege to have been able to study fusion in California as the year 2000 was greeted. The aquarian notions which I have perennially entertained have

continued to bloom in Berkeley. Like the NorCal sun, they never fail to re-invigorate me just as I can no longer tolerate the fog. From Dr. Kastenberg's feminization of science education to finding gold in a forgotten room in Etcheverry with the Nukees after lunch, this department has offered a fulfilling set of experiences which have made the last years of my 'youth' immensely enriched.

I now move on to astrophysics. Berkeley has changed my life. In many ways I am disillusioned, yet I have been lead now to the greater illusions. It has been a sublime pleasure and awakening to walk the streets of Berkeley, shopping for vintage shirts and climbing stairways which lead only from jasmine to eucalyptus and maybe to the next dream.

Chapter 1

Introduction and Heavy Ion Fusion

The Earth in all of its nearly five billion years has been powered by fusion energy. Ninety-three million miles away seethes a ball of fusion generating almost 4×10^{26} joules of energy every second with philanthropically anthropic precision and beneficence. The mass of the sun, a third of a million times greater than that of our planet, creates the gravitational conditions necessary to sustain astrophysical thermonuclear reactions and contains enough nuclear fusion fuel for billions more years. With epic determination to replicate jealously that orb which was once worshiped, many members of the world's scientific community have endeavored to fashion a golden calf of brilliant fusion energy here amongst ourselves.

1.1 The Challenge of Fusion

In order to achieve fusion energy, a great hill must be ascended. This hill is the barrier of electrostatic repulsion which acts to repel the nuclei which fusion scientists aim to bring together. That 'hill' is in fact much too great to be conquered by ordinary kinetic

collisions. Even the sun, if it were to rely on brute-force mechanical collision to bring two light elements together, would collapse cold. Only by a trick of quantum mechanical tunneling can the barrier of Coulomb repulsion be breached effectively enough to allow energy to be produced in any significant manner.

This struggle to unite light elements is in contrast to the relative ease with which nuclear fission occurs. The fissioning of a heavy nucleus occurs not by a mad melee among particles, but by the subtle assumption of a slowly moving neutron. The subatomic instability which results enables a chain reaction of more fissions which can continue in a sustained manner if the conditions should be appropriate. Nuclear fission is in principle so easy to achieve that it once occurred naturally on earth in places such as the Gabon province of Africa. The now-famous Oklo natural reactor simmered there billions of years ago before the Earth's supply of precious ^{235}U decayed, leaving mostly the less fissionable ^{238}U [12].

Yet fusion, as currently understood, requires a struggle. In hydrogen powered 'H-bombs', thermonuclear fusion produces significant amounts of energy, usually having been initiated by a primary explosion generated with facility by nuclear fission. This only truly successful terrestrial fusion represents well some components of the conditions required to create significant quantities of thermonuclear energy.

The challenge of confining and heating isotopes of hydrogen or other light elements in appropriate quantities for appropriate lengths of time is the pivotal challenge in thermonuclear fusion energy research. The prefix '*thermo*' implies that heat is involved in the approach to generate fusion. The role of this heat is to provide the fuel atoms, usually hydrogen isotopes, with enough average kinetic energy (temperature) to enable them

to tunnel through their associated Coulomb barriers. Another requirement intuitively expected is that collisions among nuclei should be frequent enough, relative to the time of the containment of the ensemble, to allow enough reactions to occur.

Traditionally $n\tau$, the product of the number density of a fusion fuel and its confinement time, is the primary measure of how well an ensemble of particles has been prepared to undergo thermonuclear fusion. Broadly interpreted, its merit emphasizes that a combination of containment and density must be achieved in order for a substantial fraction of collected nuclei to interact and fuse. According to the Lawson criterion, the product $n\tau$ must be of the order of 10^{14}s/cm^3 for successful fusion energy production.

1.1.1 Magnetic Confinement

If the heated collection of fusing particles should be in the form of a relatively low density plasma, whose ionic density n is much less than about $10^{18}/\text{cm}^3$ it could produce significant thermonuclear energy if it were contained appropriately. The reduction of the product $n\tau$ due to the low density would be compensated by a larger confinement time τ. This is the general approach of magnetic confinement fusion. In magnetic confinement schemes, containment of a rarefied fusion plasma is achieved by arranging magnetic fields within a large volume to contain the electrons and nuclei of the fusion plasma as they swirl along magnetic field lines. This magnetic fusion energy (MFE) approach has been pursued with increasing success over the last half-century.

The density characteristic to such MFE plasmas is low, of the order of $10^{14}/\text{cm}^3$. However, ambitious confinement times are sought in such plasmas, from milli-seconds to seconds. The complexities of magneto-hydrodynamics including a number of plasma insta-

bilities have made the research associated with MFE a very rich endeavor.

1.1.2 Inertial Confinement

Instead of creating the necessary combination of fusion fuel density and containment time by striving for an extensively contained but rarefied ensemble, suppose that the obverse conditions could be achieved. Alternatively, a small but dense ensemble of thermonuclear fuel would be required to be confined only momentarily to achieve the confinement criterion.

Recalling the explosion of an H-bomb, suppose that a small, dense capsule of fusion isotopes were to be gathered and compressed, generating a miniature bang from which energy could be extracted. The confinement would be achieved by the slight but effective inertial reluctance of the inwardly imploding shell to change its direction once thermonuclear burn should begin. In the brief moment of thermonuclear propagation through the fuel, it would adequately resist disassembly due to the momentum which it had received from implosion. In more explicit terms, fusion can be achieved effectively since the characteristic burn propagation time is less than the disassembly time of the compressed hydrogen isotopes. This approach to creating fusion energy, relying on the inertia of the fuel to provide the confinement of the elements to be fused, is known as inertial confinement fusion, or ICF. The extraction of energy from such ICF processes is known as inertial fusion energy, or IFE.

1.2 IFE Power Generation

There are at least four macro-components to a scheme to extract energy from thermonuclear reactions in ignited IFE fuel capsules [3]. (1)A driver energy source is required to provide the energy which compresses and heats the capsules; (2)Fuel capsules must be developed and fabricated for use in power plant systems; (3)A chamber for containing the miniature fusion explosions must be designed to handle the energy of the thermonuclear yield and the radiation generated; (4)Some suitable turbine system is required to convert the heat energy from the chamber into electrical energy.

1.2.1 IFE Drivers and HIF

In order for a thermonuclear implosion and ignition to be generated in a small hydrogen fuel capsule by compression, a large amount of energy must be directed onto the capsule. This energy which drives the compression of the capsule would blast away the outer layers of the capsule's shell resulting in a recoil of the capsule's main body of fusion fuel inward. At the appropriate point, thermonuclear reactions would be initiated and spread through the compressed and heated fuel.

The energy source required to perform this compression is immense, but the benefits in terms of the thermonuclear energy yield can be great. The first challenge in developing power from IFE is to identify an appropriate source of energy necessary to compress and ignite the fuel pellets. Currently two general types of these driver sources are being considered: lasers and heavy ion beams. In either case, the driver beam would deposit its energy on or around the fusion fuel capsule providing the necessary energy for implosion

and thermonuclear 'bang'.

Indirect and Direct Drive

The energy necessary for the compression and ignition of a thermonuclear fuel pellet can be delivered to the capsule in two general ways. A driver laser pulse or ion beam pulse can be deposited into a material on the capsule surface itself or into a secondary material encasing the capsule. The former approach is known as *direct drive*. The sudden deposition of driver energy just beneath the surface of a coating on the capsule is intended to cause an explosion below the surface, the recoil of which would drive the main body inward. The driver energy must be deposited symmetrically over the surface of the spherical capsule in order to achieve an efficient implosion. In *indirect drive* schemes, the driver energy is not applied directly onto the fusion fuel capsule but into a surrounding container in whose cavity the capsule is located. This method relies on the radiation emitted by the secondary materials surrounding the capsule to heat and ablate away its surface, generating a recoil which sends the body of thermonuclear fuel inward.

Currently among most HIF power plant design groups at the Virtual National Laboratory for Heavy Ion Fusion (VNL), indirect drive is regarded as a more favorable approach. The advantages of indirect drive include improved ablation symmetry. Rather than laser or ion beam intrinsic non-uniformities being sensed directly by the surface of the capsule as in direct drive methods, indirect drive offers a significant degree of smoothing. The non-uniformities of the driver beam are generally lost as it is deposited into the radiating materials of the hohlraum. Those materials re-radiate the energy in a manner whose symmetry depends on their spatial distribution and hydrodynamic motions, not on

Figure 1.1: An idealized ICF hohlraum; Arrows indicate application of driver energy

the imperfections of the beam. However, direct drive schemes are still being considered and may eventually represent a competitive alternative to indirect drive.

ICF Hohlraums

In indirect drive implosions systems, the fusion fuel capsule is contained within a structure designed to receive the driver's energy and to re-radiate that energy onto the capsule within. The structure containing the capsule is known as a *hohlraum*, which means 'cavity' in German. The principle motivating this name is that the cavity between the absorbing and radiating materials and the capsule itself houses the radiation field which ablates away the surface of the capsule. This is represented graphically in figure 1.1.

The materials within the hohlraum which receive the driver energy, either laser or ion beam, are known by several names, the most common being 'radiators' or 'convertors'. These materials re-radiate the driver energy, converting it into an X-ray black-body field in the cavity in the hohlraum.

Heavy Ion Indirect Drive

Among the many possible manners of driving an IFE fuel capsule implosion, this dissertation will be directed to the study of one in particular. The use of beams of heavy ions to supply the driver energy for an IFE power plant is regarded as a potentially economically successful mode of fusion power generation. This dissertation addresses some atomic physics issues associated with the use of such driver beams, which may consist of lead ions with a beam energy of 20MeV/u.

1.2.2 IFE Fuel Capsules

After the driver, the second general component of an IFE power scheme is the the thermonuclear fuel capsule itself. Whether driven by direct beam deposition onto their surfaces or by indirect radiation, the science of small, dense arrangements of hydrogen isotopes is a refined concert of hydrodynamics, radiation transport and thermonuclear reactions. The concept of ignition of a compressed fuel capsule in general terms is a realistic and well-understood approach to generating fusion power. This section covers the nature of these remarkable fusion fuel capsules and their performance in thermonuclear power generation.

Pellet Function and Form

The general principle on which IFE fuel capsules are designed is that it is energetically easier to accelerate inwardly and implode a spherical shell than a sphere. This is the same principle behind the designs of early fission weapons in which a critically dense and confined fissioning fuel mass was assembled by imploding hollow spheres [56]. For IFE fuel capsules, the analogous solid shell is intended to consist of cryogenic hydrogen which

would be imploded inward to create the final conditions appropriate for a rapid spread of thermonuclear burn through the compressed lump. Another nuclear component is needed for this to be achieved. Current designs require a rarefied gas of fusion fuel to be present in the hollow center of the cryogenic shell. It is this gas which, when compressed by the imploding main fuel shell, first initiates thermonuclear burn. This burn then propagates into the main fuel, ideally at the appropriate point of compression. Just as a rocket can be propelled by releasing fuel exhaust, a spherical shell can be compressed by sending exhaust off of its surface, propelling the shell inward at all points to its center. In this manner, by applying an external energy source, an outer layer covering a shell of hydrogen isotopes could be ablated away while driving the fuel shell inward by conservation of momentum. The imploding shell of fuel within the capsule could be initiated to fuse at the proper point of compression. In that situation, as a function of the density of the fuel, the thermonuclear reactions once initiated would propagate or "boot-strap" through the compressed, dense fuel at the right instant. The fuel would burn up creating a thermonuclear explosion. This explosion could be designed to be a small, manageable event from which useful energy could be extracted.

Pellet $n\tau$

In inertial confinement fusion systems, the time scale of the confinement is the duration of the 'bang', the propagation of the thermonuclear burn wave through the main fuel. For IFE capsules this time is of the order of tens of picoseconds, 10^{-11} seconds. This, as often remarked, is hardly confinement at all. The figure of merit $n\tau$ is rescued by the high densities of the thermonuclear fuel involved. The main fuel shells of fuel capsules are

to be constructed of cryogenic hydrogen. This solid-density fuel is then compressed by a series of pulse-induced shocks which increase the density even more. Final densities are achieved which are 1000 times greater than the initial cryogenic density, creating a dense DT (deuterium + tritium) mass compressed to the astronomically tight ionic density of $10^{25}/\mathrm{cm}^3$. [58]

The Fermi Adiabat

In order to achieve such high final densities, the fuel shell must be compressed in a careful manner. The foremost principle in ICF fuel compression is that solid fuel compressibility is hindered by entropy increase. In order to compress the main fuel shell to high final densities by shock penetration, the entropy added to the fuel by each shock must be minimized. A measure of how well this is done is the ratio of the pressure of the solid fuel to its Fermi pressure during the compression. Ideally, the compression is performed keeping the pressure of the fuel as close to the Fermi pressure as possible, ensuring adiabatic compression and maximizing the possible final densities. The Fermi pressure of an electron-degenerate medium is calculated as follows.

The condition of Fermi degeneracy entails that the constituent electrons in a material have been arranged such that their six-dimensional volume in momentum-position space V_6 is quantum-limited. This means that each electron's individual 6-volume is reduced to the Planckian value of h^3, having units of $(length \times momentum)^3$. This condition for a material having N electrons is expressed as

$$V_6 = \sum_s \int \int d^3x d^3p = (2s+1)V_x V_p = Nh^3 \tag{1.1}$$

with $(2s+1)$ representing the multiplicity of combinations of spin angular momenta of spin-s particles, and V_x and V_p representing volumes in position and momentum space, respectively. For electrons $s = 1/2$. The Fermi momentum is derived from this by

$$V_p = \frac{4}{3}\pi p_f^3 = \frac{Nh^3}{(2s+1)V_x} \tag{1.2}$$

$$p_f^3 = \frac{3nh^3}{8\pi} = \frac{(2\pi)^3 3n\hbar^3}{8\pi} \tag{1.3}$$

$$p_f = (3\pi^2 n)^{1/3}\hbar \tag{1.4}$$

The electronic number density $n = N/V_x$ for hydrogen isotopes is identical to the ionic density. The ionic density of a medium is

$$n = \frac{\rho}{\bar{A}m_u} \tag{1.5}$$

where ρ is its mass density, $\bar{A}$ is the average atomic mass number and m_u is the atomic mass unit. The Fermi energy for a degenerate electron gas is

$$\epsilon_f = \frac{p_f^2}{2m_e} = \frac{\hbar^2}{2m_e}\left(\frac{3\pi^2}{2.5m_u}\rho\right)^{2/3} \tag{1.6}$$

Converting to familiar energy units this becomes

$$\epsilon_f = 14.03\text{eV}\frac{\text{cm}^2}{\text{g}^{2/3}}\rho^{2/3} = 2.247\times 10^{-11}\text{erg}\frac{\text{cm}^2}{\text{g}^{2/3}}\rho^{2/3} \tag{1.7}$$

The Fermi pressure P_f which will be compared to the actual material pressure is determined by [70]

$$P_f = -\frac{dE}{dV} = \frac{2}{3}\frac{\epsilon_f}{V} \tag{1.8}$$

Since the average kinetic energy of an electron is $\frac{3}{5}\epsilon_f$ this Fermi pressure can be related to the Fermi energy as

$$P_f = \frac{2}{5}n\epsilon_f = \frac{2}{5}5.416\times 10^{12}\frac{\text{erg cm}^2}{\text{g}^{5/3}}\rho^{5/3} \tag{1.9}$$

This expression can be used to state a ratio of the material's kinetic pressure to its Fermi pressure. This ratio is usually expressed by the term α. Converting to appropriate pressure units using 1dyne = 1erg/cm^3 and 1Bar = 10^6dyne, the standard relationship is obtained

$$\alpha = \frac{P[\mathrm{MBar}]}{2.166\mathrm{MBar}\frac{\mathrm{cm}^5}{\mathrm{g}^{5/3}}\rho^{5/3}} \tag{1.10}$$

For situations such as IFE fuel capsule compression the pressure of the hydrogen mass is sought to be kept close to that of the Fermi pressure throughout the compression. Thus, ideally α should be close to 1 for the dense main fuel in the capsule. Compressibility decreases with increasing α.

Burn-up and ρR

The need for this terrific compression can be understood through an examination of the propagation of thermonuclear burn in a solid fuel. The fuel's burn fraction is expressed as the ratio

$$f_b = \frac{n_b}{n} \tag{1.11}$$

where n_b is the density of hydrogen isotopes which have fused and n is just the total ionic density. The number of isotopes remaining to be burned is just $n_r = n - n_b$. In standard DT fuel capsules the rate at which this burn-up occurs is twice the reaction rate density of the DT fusion reactions since each fusion reaction causes two ions, one deuterium and one tritium, to burn:

$$\dot{n}_b = n\dot{f}_b = 2n_{Dr}n_{Tr} < \sigma v_{th} > . \tag{1.12}$$

The brackets <> indicate that the DT fusion cross section σ is to be averaged over the the distribution of thermal ionic velocities v_{th}. Since the fuel ideally consists of an equal mixture of D and T this reduces to

$$\dot{nf_b} = 2\frac{n_r}{2}\frac{n_r}{2} < \sigma v_{th} > \tag{1.13}$$

$$\dot{nf_b} = \frac{n_r^2}{2} < \sigma v_{th} > . \tag{1.14}$$

With the substitution of $n(1 - f_b)$ for n_r a convenient expression is written

$$\dot{f_b} = \frac{(1 - f_b)^2}{2} n < \sigma v_{th} > . \tag{1.15}$$

The product $n < \sigma v_{th} >$ is a reaction rate for fusion reactions and its inverse is a characteristic reaction time τ.

When this expression is written as a differential equation and integrated from $t = 0$ to the confinement time of the ensemble t_c the following relationships develop

$$\int_{f(0)}^{f(t_c)} \frac{df}{(1 - f)^2} = \int_0^{t_c} \frac{dt}{2\tau} \tag{1.16}$$

$$= \frac{f_b}{1 - f_b} = \frac{t_c}{2\tau} \tag{1.17}$$

$$f_b = \frac{t_c/2\tau}{1 + t_c/2\tau}. \tag{1.18}$$

From this we see that as the confinement time increases so does the burn fraction with a logical limit of 1.[58]

After the fuel pellet has been compressed and thermonuclear burn has been initiated, a rarefaction wave propagates into the fuel shell from without. This is equivalent to saying that the DT main fuel shell hydrodynamically diffuses into the hohlraum's cavity.

The speed with which this rarefaction penetrates into the fuel is the sound speed of the fuel

$$c_s = \left(\frac{\gamma P}{\rho}\right)^{1/2}. \tag{1.19}$$

During compression, the pressure of the fuel had ideally been kept near the electron Fermi degeneracy pressure. However, after burn begins, the heat of the fusing ions rapidly dominates the pressure term. Therefore,

$$c_s = \left(\frac{\gamma n_i k_B T_i}{\bar{A} n_i m_u}\right)^{1/2} \tag{1.20}$$

where n_i is the density of hydrogen isotopes, T_i is the ion temperature, $\gamma = 5/3$ is the heat capacity ratio of the fuel, $\bar{A}$ is the average atomic mass number ($= 2.5$ for DT) and m_u is the atomic mass unit. These values give

$$c_s = \left(\frac{\gamma k_B T_i}{\bar{A} m_u}\right)^{1/2} \tag{1.21}$$

$$c_s = \left(\frac{(5/3) k_B T_i[\mathrm{eV}] 1.602 \times 10^{-12} \mathrm{erg/eV}}{(2.5) 1.66 \times 10^{-24}}\right)^{1/2} \tag{1.22}$$

$$c_s = 8.02 \times 10^5 \frac{\mathrm{cm/s}}{\mathrm{eV}^{1/2}} \sqrt{T_i}. \tag{1.23}$$

The confinement time of the fuel is the time in which this thermonuclear burn wave propagates throughout most of the shell. A competition thus exists between the time scale of the propagation of thermonuclear burn and the time scale for the dissociation of the fusion fuel mass by rarefaction. A general estimate for the effective confinement time is given as the time for the rarefaction to penetrate into a fraction of the compressed fuel mass. A figure usually cited is [58]

$$t_c = \frac{R}{4 c_s} \tag{1.24}$$

where R is the capsule outer radius at stagnation.

Continuing to solve now for the term $t_c/2\tau$ in the burn fraction equation 1.18,

$$\frac{t_c}{2\tau} = \frac{R < n\sigma v >}{8c_s} \tag{1.25}$$

$$\frac{t_c}{2\tau} = \frac{\bar{A}m_u nR < \sigma v >}{8\bar{A}m_u c_s} \tag{1.26}$$

$$\frac{t_c}{2\tau} = \frac{\rho R < \sigma v >}{8\bar{A}m_u c_s} \tag{1.27}$$

in which the familiar areal density ρR is introduced. In order to complete the expression for burn fraction, the terms relating to the cross section and speed of sound must be evaluated. The typical temperature of burning solid DT fuel should be about 30keV in these applications. At this point the value of the sound speed, from equation 1.23, is about 1.4×10^8cm/s. The value of the velocity-averaged reaction cross section at this temperature is near $6.5 \times 10^{-16}\text{cm}^3\text{s}^{-1}$. Using these values and the usual $\bar{A} = 2.5$ for an even mix of deuterium and tritium,

$$\frac{8\bar{A}m_u c_s}{< \sigma v >} \simeq 7\text{g/cm}^2. \tag{1.28}$$

Hence, a generalized relationship between the burn fraction and the areal density can be obtained by substituting this re-expressed form of $t_c/2\tau$ into equation 1.18:

$$f_b = \frac{\rho R}{7\text{g cm}^{-2} + \rho R} \tag{1.29}$$

In order to achieve a burn fraction of 1/3, which is considered to represent a successful ignition, the areal density of the compressed hydrogen fuel must be near 3g/cm^2.

Power Plant Fuel Capsules

Currently at Lawrence Livermore National Lab, DT fuel capsules are being designed to produce high enough thermonuclear yield to be considered as useful candidates

Region	Outer Radius cm	Volume cm^3	Density gcm^{-3}	Mass mg
Ablator	0.234	0.0138	1.845	25.46
Main Fuel	0.212	0.0155	0.25	3.875
Spark Gas	0.18	0.0244	3×10^{-4}	7.33×10^{-3}

Table 1.1: Physical parameters for power plant-grade thermonuclear fuel capsules

for HIF power plant capsules. The form of such a capsule is as follows. A spherical ablator shell consisting of a material such as bromine-doped beryllium or a plastic such as 'kapton' ($C_{22}H_{10}N_2O_4$) would be formed containing an even mix of deuterium and tritium vapor. This capsule would be subjected to cryogenic temperatures in such a manner as to cause a layer of frozen DT to form on the inside of the ablator shell. The inner volume of the capsule would be occupied by the remainder of the DT vapor.

The frozen DT shell on the interior of the capsule would constitute the main fuel. The gas in the interior volume would form the 'spark', being heated by the implosion to form a hot spot which initiates thermonuclear burn.

The typical measurements for the regions described for such a capsule configuration are found in Table 1.1. A section of a typical HIF fuel capsule is shown in figure 1.2.

1.2.3 HIF Chambers

The ignition of IFE fuel capsules must be contained in a facility which can both protect the nearby environment from the blast and harness the fusion energy in an economical fashion. Chamber science and engineering is a crucial component to developing realistic fusion power schemes schemes. Several issues must be negotiated by choosing the proper chamber structure. The driver energy must be able to be delivered into the chamber and

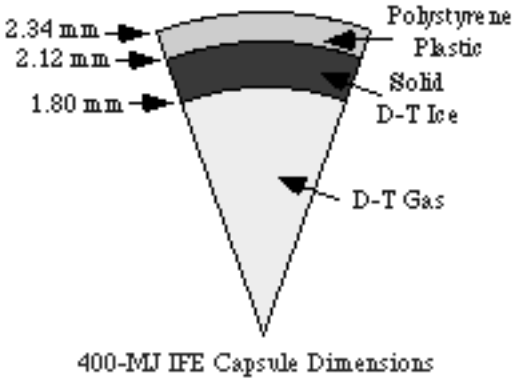

Figure 1.2: Schematic cross section of an HIF fuel capsule

the capsule itself must be able to be injected with precision. The chamber also must offer shielding of the driver and associated diagnostics from the debris and radiation from each thermonuclear shot. After each shot (which consists of hohlraum injection and fuel capsule ignition) it will likely be necessary to to remove the resultant debris from the chamber in preparation for the next shot.

An effective technique for accomplishing these requirements as well as efficiently absorbing the radiative energy for power conversion may be the use of liquid jets of a mixture of beryllium, fluorine and lithium known as *flibe*. Another more recent candidate for the chamber fluid is the beryllium fluoride compound BeF_2. Currently it is expected that in upcoming experiments the fluid will likely not be flibe but BeF_2, omitting the lithium content. As a note, it has become common to refer to any HIF chamber fluid colloquially as 'flibe'. This material could be injected into the chamber in oscillating jets which could perform all of the shielding and thermal hydraulic heat removal.

However necessary, this chamber gas or plasma is also responsible for ionizing the beam, the quantification of which is a major goal of this dissertation. This ionization may

be a problematic process. BeF_2 vapor is likely to be in the path of the beam in varying degrees of density. An average BeF_2 molecular density value near $5 \times 10^{13} cm^{-3}$ is expected to be present in the HIF power plant chamber. Collisions between the beam ions and this BeF_2 result in the removal of electrons from the beam ions. The charge states of the beam ions will increase, possibly complicating beam transport and focusability. However, given the great range of parameters available for variation, it is likely that complications due to BeF_2 ionization can be resolved. However, it is very important for computer modeling of beam transport to be able to calculate the ionization caused by this BeF_2.

Chambers designed presently for HIF power plants are spherical structures with inner radii of several meters. Surrounding this structure would be both appropriate shielding and magnets for focusing the beam into the chamber.

1.2.4 IFE Power Plants

Integrated heavy ion fusion power plant designs incorporating realistic driver, chamber, capsules and energy conversion have been developed extensively. The designs are often modular, allowing for different driver systems to be developed independent of general chamber parameters. An illustration of one such design, the HYLIFE power plant, is shown in figure 1.3. This comprehensive design presents a realistic approach to generating IFE energy. Its name is an acronym for 'High Yield Lithium Injection Fusion Energy'. This name signifies that the chamber fluid which will achieve the neutron, x-ray and blast shielding and absorption is designed to be lithium-based. Other non-lithium chemical compounds can be implemented, like BeF_2 - the important point here is the identification of the power plant components.

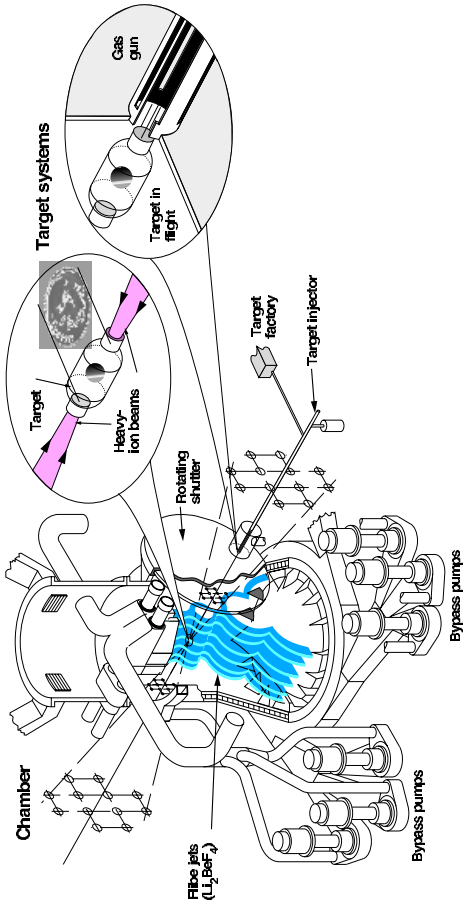

Figure 1.3: Visualization of HYLIFE chamber design

Not shown is the accelerator, which may be a linear accelerator facility producing the beams which would enter into the chamber. The center of the power plant is the fusion capsule target, enclosed in its hohlraum and injected into the protective enclosure generated by the flowing jets of chamber fluid. These targets can be fabricated on-site and sent to the injector as shown.

The target and liquid jets are enclosed by the chamber structure which is surrounded by pumping systems. These systems acts to circulate the chamber fluid and to

generate within the chamber the appropriate vapor pressures. The chamber could be cleared after each shot to a sufficient degree and steady state operation could be achieved. Continued progress on such designs are making an inertial fusion power plant as conceivable as an internal combustion engine.

Final Focus and Chamber

A particular region of current HIF power plants is the site of much of the beam activity addressed in this present work. Along the course of its path through the accelerator systems, the HIF driver beams are focused and adjusted to create the desired beam properties. This focusing is achieved typically by magnetic devices placed along the accelerator channel. However, this focusing can not be performed once the beam enters the chamber in which the fusion target is positioned, where the thermonuclear ignitions occur. Situated before the beam enters the chamber is a final focusing system which performs the last adjustments to the beam before it enters the chamber to be deposited into the target.

It is currently expected that after the final focusing is applied, the beam will travel ballistically into the chamber over a distance of about 300 to 500cm before being deposited into the target. Any beam ionization or other variation in the beam's parameters which occur after the final focus in the chamber can not be corrected. Therefore, the atomic reactions which occur between final focus and deposition into the target are the focus of much attention.

1.2.5 Power Plant Energetics

The ultimate goal of fusion-related research is to facilitate the development of a competitive electric power source. Ideally, an IFE power plant would be developed which could produce about 1000MW of electrical power, comparable to a conventional fission reactor. The generation of such a power supply from individual mini-thermonuclear blasts is outlined below.

The basic energy levels associated with the the implosion and thermonuclear burn of HIF-scale fusion capsules are of the order of megajoules. The total driver energy deposited into the capsule structure could be near 5MJ. The thermonuclear yield of a typical reactor-grade fusion pellet could be of the order of 400MJ, featuring energy gains near 7 to 10. Of this, a fraction would be rendered by the IFE chamber and converted first to thermal and then to electric energy.

Several factors determine the amount of electrical energy produced form a single shot. First, the energetic fusion particles, fragments and radiation must be gathered. This energy, rendered largely into the chamber fluid, becomes thermal energy which, through turbines and generators, is converted into electrical. The turbine or generator efficiency for such a system could at most be 50% [3]. So, a conservative thermonuclear yield of 360MJ from one shot would produce about 180MJ of electrical energy. An appropriate unit to quantify electrical energy in this discussion is the watt-hour. This energy yield per capsule corresponds to about 50kWh. If only one implosion were performed each second, then the power of the plant would be about 180MW. In order to achieve the goal of 1000MW, there should be between 5 and 6 thermonuclear capsule bangs produced in each second.

This shot repetition rate of 5 to 6Hz is typical of the expectations of modern IFE designs. The chamber and beam systems are being designed to handle this ignition repetition rate ('rep-rate') in order to meet the competitive power requirements.

Chapter 2

Atomic Physics and Heavy Ion Fusion

2.1 Introduction

In a commissioned report from 1983, a panel of physicists identified atomic coupling between driver beams and target and chamber materials as an unresolved and potentially problematic phenomenology [15]. Though the uncertainties then were expected to be minimal, it was deemed necessary that further research be conducted into the atomic physics issues of beam-plasma interactions. Most of the uncertainty centered around the calculation of ionization rates associated with the passage of a projectile through a gaseous or rarefied target, particularly an ionized target. Now nearly twenty years later, the atomic processes associated with heavy ion interactions with absorbing media remain popular subjects of experimental and theoretical research. Particularly active is research in the study of the

atomic interactions between ion beams and plasmas. Most of the work has been directed to resolving a particularly perplexing problem, which is the inability to calculate accurately the ionization cross sections for a beam penetrating a plasma.

Over the past decade an extensive experimental effort has validated many trends in beam-plasma interactions such as the general enhancement of beam ionization cross sections in plasmas and the importance of indirect ionization events [17],[60]. However, many empirical results have exposed sometimes-gross shortcomings in theoretical modeling approaches. Specifically, the calculations of the ionization cross sections for beams penetrating plasmas have in general not been consistent with experiment. As a result, the simple and direct approach to calculating ionization rates from discrete cross section formulae has been questioned. This has opened diffuse speculation about the true nature of atomic reactions relevant to HIF such as ionization and plasma energy deposition.

The atomic physics problems associated with the penetration of swift heavy ions through rarefied and solid-density materials constitute a significant set of phenomena. For the heavy ion fusion scientists, the accurate modeling of the behavior of heavy ion beam pulses as they propagate through the conceived power plant chamber plasmas and into target hohlraums is an important component for forming expectations about possible inertial fusion power plant configurations. It is therefore important on a pure atomic science level and on an applied level to be sure that the most up-to-date physics have been developed and incorporated into the modeling efforts. This work presents a thorough investigation of the physics of ion-matter atomic interactions with special focus on HIF-related processes whose quantifications by direct models have been elusive. This dissertation addresses the

majority of those questions providing a new comprehensive modeling scheme for heavy ions penetrating plasmas and gases as well as solid density ionized absorbers.

2.1.1 Plasmas and the Ionization Problem

The process which initiated the renewed interest in beam-target atomic physics is the comparative increase in a projectile's charge state experienced when traversing a plasma target [17]. Beam penetration through plasmas causes enhanced ionization to occur in the projectile ions compared to the penetration through the corresponding cold target with all else held constant. The degree to which this beam ionization may be enhanced has been difficult to quantify, and many experiments have produced results which have been modeled successfully only by mammoth supercomputer runs. Some of the causes for this mismatch were anticipated, but continued investigation of this process has produced data which some have interpreted to indicate that standard ionization cross section calculations are sometimes in error, even in a non-ionized target [18], [19]. Additionally, there have been some observations of enhanced ionization in rarefied non-ionized media [60]. This has generated concern about the validity of even the standard models for ionization in cold, rarefied targets.

Indirect and Multiple Ionizations

Accompanying this beam-plasma activity has been a new interest in the importance of indirect ionization processes which have not been handled traditionally by standard cross section calculations. The standard cross section formulae used to calculate the ionization of a beam typically give the rate of ionization due to a direct collision between an

incident beam ion and a target charge. However, in addition to this direct collisional ionization, a projectile in an excited atomic state can auto-ionize through a number of channels such as Auger cascades. These indirect ionizations have been credited with generating a significant fraction of the anomalously high ionization rates observed in beams penetrating both plasmas and rarefied targets.

Standard direct ionization calculations generally yield a total cross section for ionization of a projectile which is the sum of the cross sections of its individual constituent electrons. This gross ionization cross section can be used to calculate a mean free path for an ionization to occur. However, as re-introduced by Grisham [43], the gross ionization cross section should be considered to represent the grand sum of many types of ionizations which can occur in a collision. In fact, a single collision between a projectile and a target charge may yield multiple ionizations. Incorporation of multiple ionization effects into charge state evolution calculations will not change the average charge state of the beam, but will alter the distribution of charge states within the beam.

2.1.2 Relation to HIF Power Plant Calculations

All of these ionization calculation issues will be addressed in detail in this dissertation. Their roles are important to incorporate into models connected with the two different types of intervening and absorbing materials encountered by heavy ion beams in conceived power plant configurations. These two regimes are (1)chamber rarefied gases and plasmas and (2)target solid-density absorbers. The concerns due to the ionization calculation difficulties are distinguished for each of the two regimes.

2.1.3 Chamber Penetration

A currently-envisioned heavy ion fusion target chamber is expected to contain a rarefied gas or plasma, perhaps consisting of a mixture of lithium, and beryllium fluoride (BeF_2) or just BeF_2 in molecular form with a molecular density near $5 \times 10^{-13}\text{cm}^{-3}$. The incident driver beam ions must propagate through a distance between 300 and 500cm of this chamber ambiance between the last stage of its final focus and the destination fusion target. Along that course, the beam may be ionized to some degree beyond the level with which it entered the chamber. The BeF_2 itself also may be initially ionized or may become ionized during the course of the beam propagation.

The degree of the beam's ionization in this BeF_2 is important to predict. The spot size of each beamlet may need to be sensitively tailored to produce an anticipated volumetric deposition when it reaches the hohlraum. If the spot size of the HIF driver beam should change in the chamber, this will affect the spatial distribution of the beam's energy deposition into the hohlraum target in the chamber's center. This change in volumetric beam deposition into the hohlraum convertor materials will create changes in the geometry of the radiative field created inside the cavity of the hohlraum. The properties of this radiation field are responsible for manner in which the surface of the fusion fuel capsule is ablated. Changes in this field caused by unforeseen changes in the HIF driver beam's volumetric deposition into the hohlraum's radiating materials may have deleterious effects on capsule implosion and thermonuclear yield. The spot size can be strongly affected by the ionization state of the beam's constituent ions. If the charge state should increase, greater Coulomb repulsion may be generated within the beam causing the spot size to increase.

This type of effect due to the Coulomb repulsion among a beam's constituent ions is known as a *space charge* effect.

If any enhanced ionization should occur in the chamber, it can be countered by a number of techniques. The space charge of the beam can be neutralized by adding co-moving free electrons to the beam. Also, the rate of beam ionization can be reduced simply by achieving a lower density of background gas in the HIF chamber. It is important, however, to know what level of beam ionization to expect. If the beam should enter the chamber at an average charge state of +1, what will be its average charge when it reaches the center of the chamber? Will it be +4 or +8? HIF scientists hope to be able to calculate adequately the ionization such that dependable expectations can be formed about what level of countering tactics must be employed, or if any are needed at all.

2.1.4 Target Deposition

The basic cause of the problem associated with the modeling of the deposition of the heavy ion beams into the destination fusion hohlraum is the same as for chamber propagation – uncertainties of charge evolution of beams penetrating absorbers, particularly plasmas. In the case of deposition into the dense plasmas of the fusion targets, the concern of the charge state calculation is not the change in the spot size of the beam but rather the effects on the energy deposition rates.

A charged projectile deposits its energy into a medium primarily by transferring its energy to the constituent electrons in the medium. The rate at which this occurs is a function of many things, chief of which is the square of the charge of the incident projectile. This quadratic dependence of incident ion charge state is a significant factor for deposition

of heavy ionic species. Consider a lead ion beam incident on a target. At an HIF-relevant velocity of $0.2c$, a lead ion's equilibrium charge state while penetrating a cold target (see section 5.1.1) will be near 63+. But, this charge state is expected to be higher if the beam were to penetrate an ionized target. So, will such incident lead ions being deposited into an HIF hohlraum plasma be charged to a state of +63 or +79, for instance? The deposition difference in this hypothetical case is nearly a factor of two, which directly produces a corresponding difference in the range which the projectile ultimately traverses.

Thus, it is important to be able to calculate the charge state evolution of a beam in an ionized target since IFE targets are designed such that the volumetric energy deposition in the hohlraum materials is sensitively tuned. A new understanding of energy deposition in plasmas probably will not threaten any current target designs since the many material and spatial parameters can be adjusted to accommodate beam energy deposition properties. But, it is important to understand beam-plasma interactions and to be able to trust deposition models.

In plasmas, the range of an incident projectile is generally shortened relative to the range in the corresponding cold material. This is due to the enhanced ionization and charge states attained and also to the Coulombic properties of free electrons and their differences with respect to the properties of bound electrons. Now consider that the charge state of an incident heavy ion is also enhanced in a plasma. The combination of these two effects combined may produce a significantly different energy deposition profile in a plasma as compared to the analogous cold target. It is the quantification of this range shortening and deposition profile which is the subject of the study of part of this work.

2.2 Approach

In order to conduct this research, a broad set of basic atomic physics data and modeling must be developed. Then, the actual reactions which determine the charge evolution and energy deposition of a beam must be articulated. In general, all of the reactions addressed are Coulombic in nature, and can be understood as collisions between the beam's shielded nuclear charges and electrons with the penetrated medium's nuclear charge and electrons. The atomic interaction between the beam and any target will be considered to consist basically of two types of processes: (1)ionization and recombination (charge change), and (2)energy deposition. Once the primary problem of charge state determination has been addressed, integrated calculations incorporating energy deposition can be performed. The modeling of charge evolution and the integrated calculations will be applied to resolve the problems of atomic modeling for heavy ion fusion.

Chapter 3

Atomic Principles

3.1 Atomic Data and EOS Modeling

In order to address the complex atomic interactions between a beam and a penetrated material, a suitable atomic modeling suite and data bank must be developed to provide the necessary structural and energetic information for the electrons associated with the atoms and ions involved. This section addresses the various data sources and calculations used to provide the necessary information.

3.1.1 Quantum Numbers

While the electrons within an atom or ion can exist in states characterized by as many as four quantum numbers, the analyses in this dissertation will be sensitive to only two, the principal quantum number n and the angular momentum sub-shell number l. This will be adequate since the variations in an electron's ionization potential with terms beyond l are relatively weak, causing variations of only a few percent at most. This is consistent

with the range of accuracy required for this dissertation, which is near 30% for cross section calculations.

3.1.2 The Bohr Atom

Many useful atomic parameters can be ascertained by scaling of some fundamental values which have been derived from first principles of classical and quantum mechanics. Three constants, the Bohr radius, the fine structure constant and the Rydberg energy will be derived here from a semi-classical analysis of the hydrogen atom. These standard values can be obtained from knowledge of only the electron mass m_e, the electron charge unit e and Planck's constant $\hbar$. Scaling laws for application to other species will also be detailed.

The Bohr radius a_0 can be understood as the radius at which a hydrogenic electron's classical angular momentum ℓ_e equals the lowest value allowed by quantum stipulations, $\hbar$.

$$\ell_e = m_e v_e a_0 = \hbar \tag{3.1}$$

where v_e is the electron's ground state velocity in the hydrogen atom. Since the velocity of the electron is not yet given here, a second equation is needed to solve for a_0. This information can be taken from the electrostatic energy balance of a charge in orbit. Following Bohr and modeling the atom as a planetary-like electron orbiting a solar nucleus, a virial equation relating the electron's energy kinetic and potential energies can be expressed

$$\frac{1}{2} m_e v_e^2 = \frac{1}{2} \frac{e^2}{a_0}. \tag{3.2}$$

Solving for v_e above gives

$$v_e = \sqrt{\frac{e^2}{m_e a_0}} \tag{3.3}$$

Substituting this expression for v_e into the momentum balance equation provides a solution to a_0

$$a_0 = \frac{\hbar^2}{m_e e^2} = 0.529 \times 10^{-8}\text{cm}. \tag{3.4}$$

Note that this result is also obtained from a centrifugal force balance applied to the atomic orbital system.

$$\frac{m_e v_e^2}{a_0} = \frac{e^2}{a_0^2}. \tag{3.5}$$

The fine structure constant can be understood as being the ratio of the electron's orbital velocity to the speed of light c. Solving for the orbital velocity in the above derivations give the simple value

$$v_e = \frac{e^2}{\hbar} \tag{3.6}$$

or

$$\alpha \equiv \frac{v_e}{c} = \frac{e^2}{\hbar c} \approx \frac{1}{137}. \tag{3.7}$$

The Rydberg energy is the ground state binding energy of hydrogen's electron, being approximately 13.6eV. This can be obtained from the above by a simple non-relativistic expression for the kinetic energy of the electron. Using a classical virial relationship between the hydrogenic electron's potential and kinetic energies,

$$\text{Ry} = \frac{1}{2} m_e v_e^2 = \frac{m e^4}{2\hbar^2}. \tag{3.8}$$

Two important scaling relationships are required for applying these basic values to to more complex species: scaling with variable effective nuclear charge $\overline{Z}e$ and scaling with a change in principal quantum number n. With knowledge of quantum mechanics, inserting an arbitrary charge factor $\overline{Z}$ into the balance equations of the Bohr atom provides

the following relationships for charge and n. The binding energy I_n for an electron in shell n sensing an average nuclear charge $\overline{Z}$ scales as

$$I_n(\overline{Z}) \approx \frac{\overline{Z}^2 \mathrm{Ry}}{n^2} \tag{3.9}$$

The radius a_n scales as

$$a_n(\overline{Z}) = \frac{n^2 a_0}{\overline{Z}} \tag{3.10}$$

The orbital velocity of an electron in shell n perceiving a screened nuclear charge $\overline{Z}$, $v_n(\overline{Z})$, scales as the square root of the energy

$$v_n(\overline{Z}) = \frac{\overline{Z}\alpha}{n}. \tag{3.11}$$

The value of the effective charge $\overline{Z}$ can be determined either from screening constants or from the atomic electron distribution analysis of section 3.1.5.

Relativistic Effects

For high-Z atomic species, the strength of the associated Coulomb binding potential may be such that the subsequent motions of the inner electrons may be relativistic. In such cases the classical Bohr scaling laws may require correction. The hydrogen K-shell orbital velocity $\beta c = \alpha c \approx 0.0073c$ is not relativistic, but the K-shell electrons in a uranium atom or ion have a Bohr-scaled velocity of $\beta c \approx 92\alpha c \approx 0.67$ which is certainly relativistic, giving a γ value of 1.35.

The relativistic scaling of the binding energy is given by [25]

$$I_n = (1 - s)m_e c^2 \tag{3.12}$$

in which

$$s^2 = 1 - \beta_n^2, \tag{3.13}$$

β_n being the Bohr-scaled orbital velocity

$$\beta_n = \frac{\alpha \overline{Z}_n}{n^2}. \tag{3.14}$$

While important in principle, this effect is not huge, even for the largest ions considered here. For example, the fully relativistic K-shell binding energy of uranium is found to be 132keV. The analogous non-relativistic value from the classical Bohr scaling would be 115keV. The classical result in this case differs by only about 13% from the correct relativistic value.

Thomas-Fermi Scaling

The Bohr atom is an atom of shells and orbitals with direct analogs to virial systems. The Thomas-Fermi (TF) view of the atom is one of a locally degenerate electron fluid with no distinctions between bound or free or between shells and continuum. Many useful atomic properties can be discerned by treating the electrons associated with each nucleus, bound or free, as a Fermi-degenerate electron gas. This is similar in principle to the analysis of section 1.2.2 in which the macro degeneracy of all of the electrons in a material is considered.

Two values from Thomas-Fermi analysis are useful to consider. The first is the characteristic atomic electron velocity $v_{TF}(Z)$. It is given by

$$v_{TF}(Z) = Z^{2/3} \alpha c \tag{3.15}$$

in which α here is the fine structure constant. It represents a characteristic velocity of the average electron in the atomic Fermi gas. The second TF value relevant to this dissertation

is the TF radius, $r_{TF}(Z)$ which gives a scaling of the radius within which nearly 80% of the electrons of a given atom or ion are located. It is given by

$$r_{TF}(Z) = Z^{-1/3} a_0 \tag{3.16}$$

in which a_0 is the Bohr radius.

3.1.3 Impact Parameters

Many of the calculations in this study will performed to simulate the collision between a projectile or a projectile's constituent electrons and a target charge, either a nucleus or electron. An important consideration in quantifying such collisions is the possible scale of collisional impact parameters b. The characteristic interaction time associated with a projectile with velocity v passing a stationary target charge at a distance b is of the order of b/v. Limitations on this impact parameter and its associated interaction time form the criterion by which the maximum and minimum impact parameters of many atomic reactions are determined.

The maximum sensible impact parameter for a charge in collision with an atom or ion with some bound electrons is related to a distance called the *Bohr adiabat*. Its value is determined by the time interval associated with the characteristic quantum period of an electron around a target atom or ion. This period is expressed by

$$\tau = 1/\omega = \hbar/\overline{I}. \tag{3.17}$$

In this formula, $\overline{I}$ is the average ionization potential of the atom or ion in question (see section 3.1.8).

When the time interval of impact is greater than the associated quantum oscillation period of a typical target electron, no significant energy transfer will occur between the projectile and target electron. This is true because in collisions with greater characteristic times, the passing of the projectile by the target happens adiabatically in the sense that, relative to the target electron's oscillatory motions, the projectile would be proceed very slowly. The distance beyond which this condition is met is the maximum impact parameter. It is determined by

$$\frac{b_{max}}{v} \approx \frac{\hbar}{\overline{I}} \tag{3.18}$$

$$b_{max} \approx \frac{v\hbar}{\overline{I}}. \tag{3.19}$$

The minimum impact parameter in a collision between two charges has at least two possible manifestations. From principles of quantum mechanics, a limitation is imposed on the minimum relative angular momentum between two particles. This minimum value of $\hbar$, when equated to the classical relative angular momentum between the colliding particles gives the following limiting relationship

$$\mu v r = \hbar \tag{3.20}$$

where μ is the reduced mass of the colliding system. If one of the colliding particles should be an electron and the other a nucleus, the reduced mass would be very nearly m_e, the electron mass. The radius r at which this is satisfied is the quantum-determined minimum impact parameter, which sets an approximate lower boundary on the length scale of any interaction

$$b_{min} \approx \frac{\hbar}{m_e v}. \tag{3.21}$$

Another possible limitation exists, however. Suppose that an electron in a target material, bound or free, should be in the vicinity of a passing projectile nucleus of atomic number Z. The kinetic energy of that target electron in the frame of the projectile would be just $\frac{1}{2}m_e v^2$, where v is the projectile's speed. The electrostatic potential energy between the two, with the projectile nucleus shielded to $\overline{Z}$, would be $\overline{Z}e^2/r$. The maximum possible energy transfer in such a Coulomb collision is $2m_e v^2$. The impact parameter at which this energy transfer is achieved (see section 4.2) presents a classical limitation on the minimum impact parameter. The relationship between impact parameter b and energy transfer ΔE at a given collision velocity v will be shown in equation 4.3 to be

$$\Delta E(b) = \frac{(\Delta p)^2}{2m_e} = \frac{2Q^2e^4}{m_e v^2}\frac{1}{b^2} \tag{3.22}$$

where Q is the effective charge of the projectile which interacts with the electron. The impact parameter at which this energy transfer equals the maximum allowable value is

$$b = \frac{Qe^2}{m_e v^2} \tag{3.23}$$

This classical impact parameter limit will compete with the quantum-limited impact parameter in determining the effective minimum impact parameter of a particular collision.

3.1.4 Electron Binding Energies

For many of the reactant atomic and ionic species involved in the set of interactions examined here, the binding energies of the attendant electrons must be obtained. The binding energies for the valence electrons (simply called the ionization potential) at each charge state for most elements are available. Also, the binding energies of inner electrons for neutral atoms are available from calculations and tables found in the associated literature.

However, this investigation requires knowledge of the binding energies of inner electrons for ionized species. For instance, the binding energy of the $2p$ electrons in neutral gold may be readily found, but what would their binding energy be if the gold should be ionized to a charge state of 12? The most facile and reasonably accurate solution to this issue is to employ the *screening constants* of atomic electrons [29] and the Bohr atom scaling given in section 3.1.2. Any given electron in any atom or ion (except hydrogenic cases) is not attracted by the entire, bare nuclear charge during its averaged orbit. The other electrons in the atom or ion have a probabilistic spatial distribution, a fraction of which occupies the space between the electron in question and the nucleus, screening the nuclear charge. The nuclear charge as perceived by a given electron will be reduced by a certain amount depending on the configuration of the other bound electrons. The degree to which other constituent electrons in an atom or ion shield the nucleus as perceived by a particular electron is that electron's shielding constant. The shielding constant of hydrogen's one electron is zero, since there are no other electrons to come between it and the nucleus.

The screened nuclear charge, $\overline{Z}_{nl}$ which an electron nl in an atom of atomic number Z perceives is

$$\overline{Z}_{nl} = Z - S_{nl} \tag{3.24}$$

where S_{nl} is the screening constant for electron nl. The shielding constants and binding energies for all electrons in all neutral atomic species were acquired from a tabulated data bank [65]. From these two sets of data, ionization potential of neutral atoms and associated screening constants, the binding energies for ionized species can be approximated. The key to transposing from neutral values to ionized requires two simple phenomenological points

of atomic physics. (1) The electronic level population of an atom Z ionized to charge state Q is roughly identical to the electron configuration of the neutral atom having $Z' = (Z - Q)$. (2)The binding energy of an electron scales as $\overline{Z}_{nl}^2$, with $\overline{Z}_{nl}$ being the average shielded nuclear charge which that electron perceives.

So, to determine the inner binding energy $I_{nl}(Z, Q)$ of an electron nl in species Z ionized to Q, one first retrieves the binding energy $I_{nl}(Z', 0)$ and shielding constant of the corresponding electron nl in neutral species $Z' = (Z - Q)$. The nuclear charge which that particular electron perceives in atom Z' is

$$\overline{Z}'_{nl} = Z' - S_{nl}. \tag{3.25}$$

Now, the effective charge that the electron nl would perceive in the associated ionized species Z is similarly

$$\overline{Z}_{nl} = Z - S_{nl}, \tag{3.26}$$

since the shielding constant is not a function of the nuclear charge, but only of the electron configuration, which is roughly identical in species Z ionized to Q and neutral species $Z' = (Z - Q)$.

Thus, the adjusted binding energy of electron nl in the ionized species is determined by scaling the neutral-atom value according to the new effective charge:

$$I_{nl}(Z, Q) = I_{nl}(Z', 0) \left(\frac{\overline{Z}_{nl}}{\overline{Z}'_{nl}} \right)^2 \tag{3.27}$$

3.1.5 Atomic Electron Radial Density Distribution

Just as a bound electron in an atom or ion senses the central nuclear charge screened by other bound electrons, external charges interacting with an atom or ion also

encounter its nuclear charge, though screened to a different degree by the constituent electrons. In any given reaction between a charged particle and an atomic or ionic species, the interacting charge encounters the Coulombic field of the atom or ion's nucleus, but shielded by a certain degree as a function of the impact parameter and the ion's charge distribution. This section addresses the determination and approximation of that density distribution as a function of atomic number, ionization state and density.

Exact calculation of the time-averaged spatial distributions of bound electrons including relativistic effects for the high electron velocities encountered in high-Z atoms is accomplished by solving the associated Dirac-Hartree-Fock-Slater equations. This approach however requires a potentially large calculation requirement. Also, the high level of accuracy produced by such sophisticated models is not required by this work. In general, cross section values for ionization of swift heavy ions with many bound electrons can only be stated within 30% accuracy. So, for the work of this dissertation an approximate analytical model which characterizes the general features of the typical electronic distribution about a nucleus should be adequate.

Exponential Screening Potential Model

An approach detailed by Molière [47] and by Chen *et al.* [28] offers one method to model the radial distribution of each electron shell of an atom. In those works, success was reported in using simplified analytical models to describe the electrostatic potentials and shell-wise electron densities in atoms. The justification for this approach can be traced as follows. In a non-ionized atom, the electrons' electrostatic potential can be modeled as diminishing with the inverse of the distance from the nuclear center while also being

screened by the other electrons in an exponentially-decaying fashion. This is expressed by

$$V(r) = \frac{1}{r} \sum_i \sum_{j=1}^{m_i} N_i A_{ij} \exp\left[-B_{ij} r\right] \tag{3.28}$$

in which the summations are over i for the orbitals and over j for the m_i moments in each shell. N_i is the number of electrons in each orbital. The coefficients A_{ij} and B_{ij} are parameters to be determined according to the specific case.

By Poisson's theorem this potential is related to the the total bound electron density $n(r)$ by

$$\nabla^2 V(r) = -4\pi e n(r). \tag{3.29}$$

Substituting into this the expression for the potential $V(r)$ produces

$$n(r) = \frac{Z}{4\pi r^2}\delta(r) - \sum_i \sum_{j=1}^{m_i} \frac{N_i}{4\pi r} A_{ij} \exp[-B_{ij} r] \tag{3.30}$$

with the $\delta(r)$ term added to account for the contribution of the nucleons at $r = 0$. Notice that the ∇^2 operator applied to the potential produces a density of the same general form. This term is the electronic charge density term and it expresses that the density in each shell should be distributed as

$$n_i(r) \propto \sum_{j=1}^{m_i} \frac{N_i}{4\pi r} A_{ij} \exp[-B_{ij} r] \tag{3.31}$$

where $n_i(r)$ is defined as the bound electron density of shell i.

This model, though reported to be quite successful, requires a significant assortment of associated constants. Can it be simplified? The following analysis presents a new and simplified approach to obtaining reasonably accurate electronic density distributions. Suppose each shell n could be modeled by just two constants, C_n and a re-defined B_n whose

units are of length.

$$n_n(r) = \frac{C_n}{r} \exp[-r/B_n] \tag{3.32}$$

With the appropriate C_n and B_n values, this equation should provide a reasonably accurate model of atomic or ionic shell-wise electron distribution. With some additional stipulations and boundary conditions the new parameters C_n and B_n can be determined for each shell n. First, charge neutrality must be maintained. Integration of the density of a shell over the spherical volume produces the charge enclosed $q_n(r)$ at a given radius

$$q_n(r) = 4\pi C_n B_n^2 \left[1 - \left(1 + \frac{r}{B_n}\right) \exp[-r/B_n]\right]. \tag{3.33}$$

For a free atom or ion, as $r \to \infty$ the enclosed charge must approach the total number of electrons in shell n, N_n. Calculating that limit in the above expression gives

$$N_n = 4\pi C_n B_n^2 \tag{3.34}$$

or

$$C_n = \frac{N_n}{4\pi B_n^2} \tag{3.35}$$

One more condition is required to specify the two unknown constants. This is provided by examining the areal charge density, being $4\pi r^2$ times the density expression of equation 3.32. An examination of the plot of exact calculations of the total atomic electron density shows clear phenomenological trends [71]. The function $r^2 n(r)$, where $n(r)$ is the total electron density, features a clear shell structure. The areal density function for each shell features a maximum at a radius whose value increases with increasing n. The density function of equation 3.32 reaches a maximum at $r = B_n$, where the enclosed charge is

$$q_n(B_n) \approx 0.264 N_n. \tag{3.36}$$

The value of B_n can then be interpreted as the median radius of a given shell n. If the B_n value could be determined for each shell then the entire electron density could be modeled.

This radius, which represents the average position of an electron in a given shell n, can be approximated from the ramifications of this model. Given that the shell-wise distributions were approximated by an exponentially screened $1/r$ variation as in equation 3.32, the properties of the peak can be used to determine the peak radius value. It was just demonstrated that within the peak radius B_n, about 26.4% of the shell's charge is contained. Also contained within a radius B_n of shell n are a fraction of the electrons contained in inner shells whose principal quantum number is less than n. Additionally, a smaller fraction of the electrons from outer shells will also contribute to the screening. Combining these electrons, a model-based screening value can be determined

$$S_n \approx f_i N_i - 0.264 N_n - f_o N_o \tag{3.37}$$

in which f_i is the fraction of inner electrons N_i enclosed within B_n and f_o and N_o are the corresponding values for the outer electrons. From inspection of the actual Hartree-Fock-Dirac integrations [71], it can be approximated that about 80% of the inner electrons in shells $n_i < n$ are enclosed within a given shell n and about 15% of the outer electrons in shells $n_0 > n$. N_n is the number of electrons in the shell n. Using this model-based value, the peak radius position can be ascertained from

$$B_n = \frac{n^2 a_0}{Z - S_n} \tag{3.38}$$

With that approach to calculating the peak radii, being the B_n values for each

shell, the total electronic density for a free atom is given by

$$n(r) = \sum_n \frac{C_n}{r} \exp[-r/B_n]. \tag{3.39}$$

An important situation must be addressed here. The above analysis applies to a free atom or ion whose electron distribution extends, in principle, to infinity. An atom or ion bound in a material experiences inter-atomic forces which cause its distribution to change. According to Zel'dovich and Raizer [70] the first-order effect of compressing the electronic distribution is that the density near the cell boundary increases to accommodate the relocated charge. The relative change in the inner region is much less.

These effects can be replicated analytically with a simple heuristic argument. In the previous free-atom formulation, the shell-wise density was normalized such that when integrated over all space, the enclosed charge would be the number of electrons in the shell. In an actual bound atom or ion, the normalization should be performed with an integration only from $r = 0$ to $r = r_0$ where

$$r_0 = \left(\frac{3}{4\pi n_i}\right)^{1/3}; \tag{3.40}$$

n_i is the ionic density in the material. The value r_0 is usually called the *atomic cell radius*, defining a 'cell' in which the electrons of each atom or ion in a material are generally confined. The charge $q_n(r)$ of shell n enclosed within $r = r_0$ is

$$q_n(r_0) = 4\pi C_n B_n^2 \left[1 - \left(1 + \frac{r_0}{B_n}\right) \exp[-r_0/B_n]\right] \tag{3.41}$$

Setting this equal to the number of electrons N_n in shell n, the value of C_n would be

$$C_n = \frac{N_n}{4\pi B_n^2 \left[1 - \left(1 + \frac{r_0}{B_n}\right) \exp[-r_0/B_n]\right]} \tag{3.42}$$

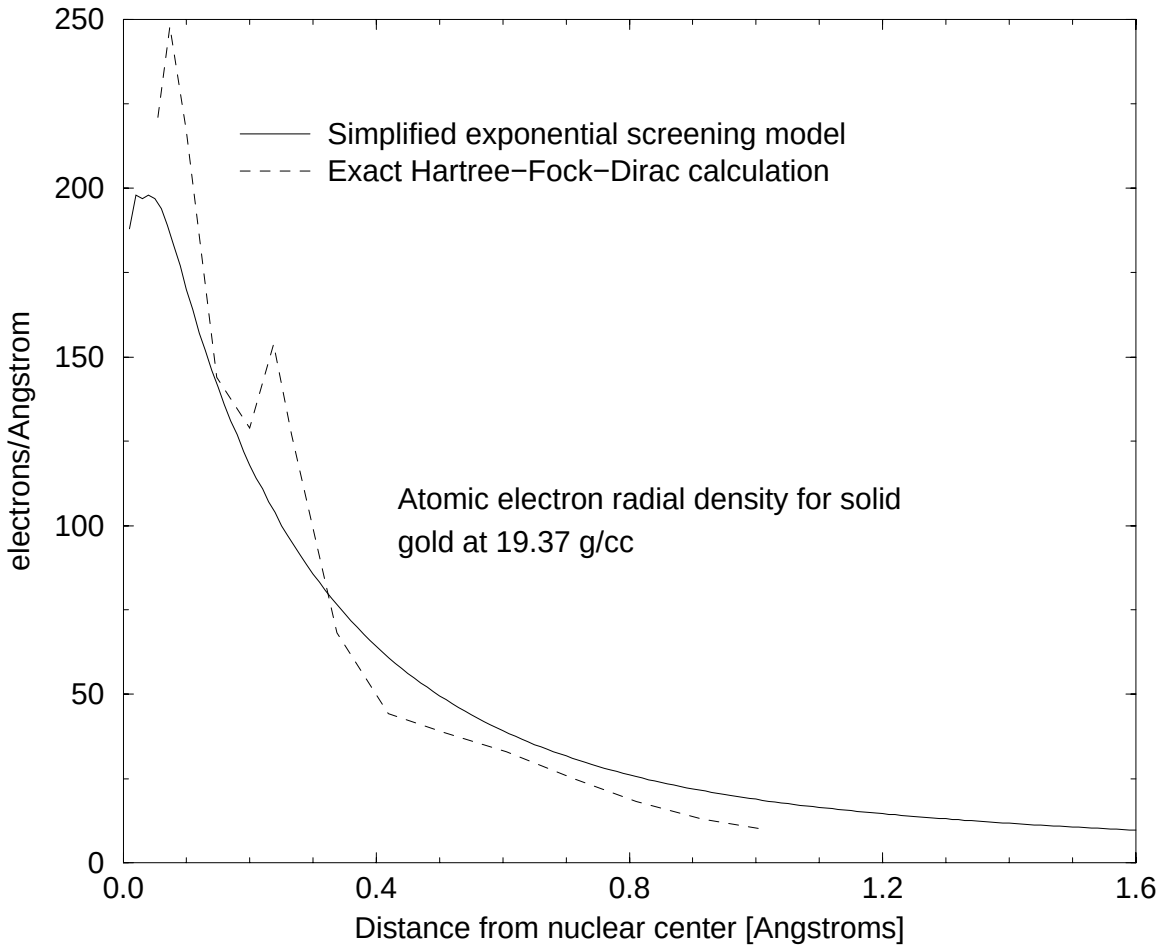

Figure 3.1: Atomic electron radial distribution for gold at solid density and room temperature

An example calculation using this method appears in figure 3.1, which shows the calculated radial density of a gold atom's electrons. The profile compares very well with the actual density distribution calculated from extensive Dirac-Hartree-Fock integrations which are also shown, taken from reference [71]. While the nuances of the shell structure are not followed, the averaged electron distribution behavior is captured. It is this averaged behavior which is important for the analysis of this dissertation.

Free Electron Distribution

While the above model handles the bound electron distributions in atoms and ions, the density profile of the free electrons associated with an ion in a material must also be addressed. The QEOS model of More *et al.* presents a Thomas-Fermi analysis in which the electron density at the cell boundary is related to the charge state Q of the ion by

$$n_f = Q n_i \tag{3.43}$$

where n_i is the ionic density. This is equivalent to expressing that the free electrons distribute themselves over the atomic cell with a flat density distribution. This neglects some shielding behavior but is a good first approximation and will be used throughout this analysis.

3.1.6 Material Charge State

The astrophysical conditions achieved in inertial fusion scenarios require consideration of extensive ionization of materials involved. The degree to which a modeled material is ionized and the ion population distribution are important considerations in the radial electron density profile determination of the previous section and will be seen to be an important component to ion deposition calculations.

If the target material should be in a rarefied state of density n less than about $10^{17}/\mathrm{cm}^3$ then it is generally possible to use the Saha equation to determine the average charge state and charge state distribution of the ionic species in the target. This equation expressing the ratio of the number densities of a species of charge state $i+1$ to its progenitor

at charge state i is [11]

$$\frac{n_{i+1}n_e}{n_i} = \frac{m_e k_B T}{2\pi\hbar^2}^{3/2} \exp[-I_i/k_B T] \tag{3.44}$$

in which n_e is the free electron density and T is the electron temperature. The challenge in using this formula is that the density of the state i and the electron density must be known in order to calculate the density of state $i+1$. This can be solved by an iterative solution converging on the correct distribution of densities.

A solid-density material can not be modeled efficiently by a Saha equation. Hot, dense materials exhibit complicated equations of state and must be handled by sophisticated coding. A very successful model for determining atomic properties of hot, dense materials has been the quotidian equation of state (QEOS) model of More *et al.* [57]. This modeling system has been incorporated into the two-dimensional, radiation-hydrodynamics code LASNEX of Lawrence Livermore National Lab. Values for this work which require more elaborate EOS calculations are taken from the QEOS model as kindly provided by Debbie Callahan Miller and Manoj Prasad of LLNL.

3.1.7 Oscillator Strengths

The oscillator strength for an electronic transition from principle quantum shell n to shell n' is a measure of the energetic and quantal likelihood of an electronic transition. The oscillator strength is a unit-less term which appears in several different forms, all related by specifying the degeneracy of the transition. For a transition between two 'full' shells each having $N = 2n^2$ electrons, the oscillator strength is

$$f_{nn'} = \frac{2^6}{3\pi\sqrt{3}} \left[\frac{\mathrm{Ry}}{E_n - E_{n'}}\right]^3 (nn')^{-3} \tag{3.45}$$

In many applications other factors are introduced depending on the nature of the transition. For instance, it is customary to articulate the oscillator strength of a single electron's transition from shell n to a partially-filled shell n'. This is expressed by dividing the full-shell expression by $2n^2$ and by multiplying by the availability fraction of shell n'

$$\frac{2n'^2 - N_n}{2n'^2} \tag{3.46}$$

producing

$$f_{nn'} = \frac{2n'^2 - N_n}{2n'^2} \frac{2^5}{3\pi\sqrt{3}} \left[\frac{\mathrm{Ry}}{E_n - E_{n'}}\right]^3 n^{-5} n'^{-3}. \tag{3.47}$$

3.1.8 Average Ionization Potential

An important term in equations quantifying the energy transfer from a projectile to the bound electrons in a material is the average ionization potential of the absorbing material $\overline{I}$. For a species of atomic number Z it is defined as

$$\ln\left[\overline{I}\right] = \frac{1}{Z} \sum_{nn'} f_{nn'} \ln[E_{ik}] \tag{3.48}$$

with the summation being over all inner-atomic transitions nn' of energy $E_{nn'}$ and oscillator strength $f_{nn'}$.

The expression for $\overline{I}$ is complex to calculate explicitly. Its values for all of the neutral atoms have been determined theoretically and experimentally [71]. However, in the case of an ionized target, the ionization potential must be adjusted from its neutral atom value to accommodate the new electronic structure of the ionized species. Mehlhorn [45] presented a useful method for adjusting the non-ionized $\overline{I}$ to that for an arbitrary level of target ionization. The adjusted ionization potential $\overline{I}(Z, Q)$ for a target of species Z at a

charge state Q can be approximated by

$$\overline{I}(Z,Q) \simeq \frac{\overline{I}(Z-Q,0)Z^2}{(Z-Q)^2} \tag{3.49}$$

in which $\overline{I}(Z-Q,0)$ is the neutral ionization potential for species $Z-Q$.

While the Mehlhorn scaling is reasonable, values for this analysis will be provided from QEOS calculations, with generous cooperation from Manoj Prasad and Debbie Callahan Miller.

3.1.9 Plasmas and Atomic Effects

While classic beam-plasma interactions such as two-stream instabilities and neutralization are not addressed in this present work, some other important plasma physics must be considered. First it may be useful to introduce a few standard expressions of plasma characterization.

The plasma frequency represents the rate at which free electrons in a plasma exhibit characteristic oscillatory motions. Its value is defined as

$$\omega_p = \sqrt{\frac{4\pi e^2 n_e}{m_e}} \tag{3.50}$$

in which n_e is the plasma's free electron density.

The Debye length of a plasma is the scale of the shielding layer which the free electrons create around a positive charge or potential. This distance represents the length beyond which the charge or potential is effectively screened by the plasma. The Debye length value is

$$\Lambda_D = \sqrt{\frac{k_B T_e}{4\pi e^2 n_e}} \tag{3.51}$$

in which T_e is the electron temperature of the plasma. Note that the product $\Lambda_D \omega_p$ gives the characteristic electron thermal velocity in the plasma.

The plasma parameter is a quantification of the number of electrons contained within a sphere whose radius is the Debye length. The plasma parameter is thus defined

$$N_D = \frac{4}{3}\pi \Lambda_D^3 n_e \,. \tag{3.52}$$

With increasing plasma parameter, the more effectively a charge or potential is screened beyond the Debye length.

The physical consequences of the plasma condition which are germaine to this work involve the effects on the target material's atomic properties. These atomic plasma effects may then effect a change in the incident beam's charge state evolution and energy deposition into the target. A primary manifestation of target ionization level in its atomic properties is the reduction of the binding energy of its electrons due to nuclear shielding. In a plasma, the liberated electrons, though not in a bound state, are still distributed throughout the atomic cells with a certain fraction in the vicinity of the target nuclei. Their presence about the nuclear center can act to shield the target's bound electrons from the nuclear charge. This reduction in effective nuclear charge causes a reduction in the ionization potential of the shielded electrons. This effect becomes important if the Debye length of the plasma Λ_D should be near or less than the characteristic atomic radius $r_a \approx Z^{-1/3} a_0$, where the Thomas-Fermi scaling of the atomic radius is employed.

The effect and its quantification are known as Debye-Hückle shielding. The specific criterion required for this situation to become important is

$$\Lambda_D < r_a \,. \tag{3.53}$$

The largest characteristic atomic radius encountered is typically 1.5Å. In this investigation, the solid-density target materials constituting the HIF hohlraums will exhibit Debye lengths ranging from tens to a fraction of an Angstrom (see section 3.1.10). Therefore, some accounting must be made of this shielding effect.

To first order, the effect of Debye-Hückle shielding on outer electrons can be approximated by quantifying the screening electrons within the atomic radius. If the characteristic ionic radius should be greater than the Debye length, the usual screened nuclear charge value sensed by the target's valence electrons can be considered to be reduced by the plasma parameter. For ionic radii much less than the Debye length, the screening effect can be considered to be negligible.

For intermediate values, the number of plasma screening electrons within the radius of electron in shell n, r_n, can be approximated as

$$S_D \approx \frac{4}{3}\pi r_n^3 n_e = N_D \left(\frac{r_n}{\Lambda_D}\right)^3. \tag{3.54}$$

This is consistent with the free electron distribution modeling described in section 3.1.5. The binding energy will be reduced according to section 3.1.4 by adding this additional plasma screening term to the usual screening term due to bound electrons.

In addition to acting to shield the materials own nuclei, the free electrons in a heated material can dynamically shield the nucleus of an incident ion. This effect is much weaker than the ordinary Debye-Hückle shielding due to the velocity of the projectile.

3.1.10 Tabulated Atomic EOS Properties

As indicated in sections 3.1.6 and 3.1.8, the characterization of the atomic properties of dense plasmas can be difficult to establish. Such atomic properties are necessary for the calculations of this dissertation in that the average charge state and average ionization potential of a target material affect the charge- changing cross sections and the energy deposition of an incident beam. The development of appropriate atomic equation of state models for such purposes has not been included in the efforts of this dissertation. Thus, existing atomic codes were used to provide the necessary atomic parameters for the calculations of this work. The QEOS (quotidian equation of state) model [57] was used by Manoj Prasad of LLNL to provide the following tabulated data. In the following tables the average charge states $\overline{Q}$, average ionization potential $\overline{I}$ and Debye lengths Λ_D are given for several different materials over a range of temperatures T and densities ρ. The range of materials, densities and temperatures covers most of the range of material properties associated with current HIF hohlraum designs.

3.2 Reaction Rates, Density Regimes and Charge Equilibrium

In discussing the theory of projectile-target reactions, it is useful to employ a standard vocabulary of terms characterizing the rates and time scales of the reactions involved. Consider a beam of identical particles with a certain intensity $I(t)$ and velocity v. Incident into a reaction-inducing material the beam's constituent particles will incur reactions. For a reaction cross section σ and a target density n, the rate of reduction in unreacted beam

ρ	T	$\overline{Q}$	$\overline{I}$	Λ_D
1	300	5.55	519	2.44
1	200	5.31	408	2.03
1	100	4.60	266	1.55
1	10	1.98	115	0.745
0.1	300	5.77	729	7.56
0.1	200	5.62	568	6.25
0.1	100	5.14	358	4.62
0.1	10	1.99	115	2.35
0.01	300	5.88	1024	23.7
0.01	200	5.79	782	19.5
0.01	100	5.49	479	14.1
0.01	10	2.45	131	6.7

Table 3.1: EOS properties for carbon with ρ in g/cm^3, T in eV, $\overline{I}$ in eV and Λ_D in Å

ρ	T	$\overline{Q}$	$\overline{I}$	Λ_D
1	300	11.0	736	2.6
1	200	9.92	573	2.23
1	100	7.71	392	1.79
1	10	2.51	201	0.992
0.1	300	11.8	994	7.93
0.1	200	11.0	759	6.69
0.1	100	9.12	489	5.21
0.1	10	2.58	203	3.10
0.01	300	12.3	1342	24.6
0.01	200	11.8	994	20.5
0.01	100	10.3	621	15.5
0.01	10	3.2	217	8.79

Table 3.2: EOS properties for aluminum with ρ in g/cm^3, T in eV, $\overline{I}$ in eV and Λ_D in Å

ρ	T	$\overline{Q}$	$\overline{I}$	Λ_D
1	300	15.4	782	1.0
1	200	13.0	660	0.89
1	100	9.47	524	0.737
1	10	5.07	400	0.320
0.1	300	18.3	994	2.90
0.1	200	15.7	798	2.56
0.1	100	11.2	585	2.14
0.1	10	2.96	355	1.32
0.01	300	20.7	1264	8.62
0.01	200	18.3	984	7.50
0.01	100	13.7	687	6.12
0.01	10	3.22	358	4.00

Table 3.3: EOS properties for iron with ρ in g/cm^3, T in eV, $\overline{I}$ in eV and Λ_D in Å

ρ	T	$\overline{Q}$	$\overline{I}$	Λ_D
1	300	27.4	1560	1.41
1	200	21.4	1369	1.30
1	100	14.0	1190	1.14
1	10	5.29	994	0.691
0.1	300	33.9	1775	4.00
0.1	200	26.5	1528	3.69
0.1	100	16.8	1251	3.28
0.1	10	4.05	965	2.11
0.01	300	40.8	2062	11.5
0.01	200	32.4	1723	10.6
0.01	100	20.9	1369	9.29
0.01	10	4.87	984	6.10

Table 3.4: EOS properties for gold with ρ in g/cm^3, T in eV, $\overline{I}$ in eV and Λ_D in Å

intensity is given by the usual relation

$$\frac{dI(t)}{dt} = -n\sigma v I(t) \tag{3.55}$$

Defining the reaction rate at a given time α as $n\sigma v(t)$, the expression is solved by the common exponential formula

$$\frac{dI(t)}{dt} = -\alpha I(t) \tag{3.56}$$

$$I(t) = I_0 \exp[-\alpha t]. \tag{3.57}$$

Another important relationship can be derived from these equations. The reaction rate α is seen to represent the differential probability per unit time of sustaining a reaction,

$$\frac{-dI(t)/I(t)}{dt} = \alpha \tag{3.58}$$

$$dP(t) = \alpha dt. \tag{3.59}$$

From these probabilistic reaction attrition relationships the probability for a constituent particle to sustain a reaction over a certain time period t can be derived. The differential probability of witnessing a single particle's first reaction in a time increment dt at a time t is given by the fraction of unreacted beam remaining at time t times the differential probability

$$\frac{dP(t)}{dt} = \alpha \exp[-\alpha t] \tag{3.60}$$

The total probability for sustaining a single reaction anywhere in a time interval t is given by integrating the above probability

$$P(t) = \int_0^t \alpha \exp[-\alpha\tau] d\tau \tag{3.61}$$

$$P(t) = 1 - \exp[-\alpha t] \tag{3.62}$$

Note that for a small time $t = dt$, the total reaction probability reduces to the differential probability

$$P(dt) = 1 - \exp[-\alpha dt] \approx 1 - (1 - \alpha dt) \approx \alpha dt \tag{3.63}$$

The *mean free path* (m.f.p.) is defined using this probability expression as the averaged distance $\overline{x}$ a beam particle will travel into a target before sustaining a reaction. This is expressed by weighting each penetration depth x according to the probability of finding unreacted beam at that distance. Switching from time to position differentials,

$$dt = dx/v, \tag{3.64}$$

this integral expression is

$$\overline{x} = \int_0^\infty x P(x) dx = n\sigma \int_0^\infty x \exp[-n\sigma x] dx. \tag{3.65}$$

It's solution is

$$\overline{x} \equiv l = \frac{1}{n\sigma} \tag{3.66}$$

where l is customary notation for the mean free path. The characteristic time τ for a reaction to be induced in the beam is similarly defined as

$$\tau = \frac{1}{n\sigma v} \equiv \frac{1}{\alpha} \tag{3.67}$$

The beam-target interactions investigated here can be expressed using of these standard reaction terms.

3.2.1 Densities and Reaction Rates

The distinction between the penetration of solid-density media and rarefied gaseous media is important because the difference in the associated densities creates different em-

phases on two types of reactions rates. Charge change and energy deposition each have characteristic cross sections and in different density regimes the resultant mean free paths for each may change the relative scale of each. In solid-density targets, the charge state of an incident beam ion is usually assumed to be in an instantaneous equilibrium. An incident ion reaches charge equilibrium when it achieves a charge state at which the net ionizing reaction rates balance the net electron capture reaction rates at a given velocity. The assumption of instantaneous charge equilibrium implies that the time scale for changing from an arbitrary initial charge state to the equilibrium charge is much smaller than the time scale of the typical incremental change in energy.

This can be justified by a rough analysis of the reaction rates involved in typical scenarios. Many electronic reactions participate in the ionization and recombination process as an ion penetrates a material. Near equilibrium, when the ionization and capture rates are nearly equal, the projectile will be ionized roughly to the point at which the outer electron's orbital velocity is equal to the projectile's velocity (see §5.1.1). At this peak in ionization, the ionization cross section will be shown in section 5.4.4 to be given by

$$\sigma \approx 6.5 \times 10^{-14} \mathrm{cm}^2 \mathrm{eV}^2 \frac{\overline{Z_t}^2}{I^2} \times 0.7 \tag{3.68}$$

where I is the instantaneous orbital binding energy and $\overline{Z_t}$ is the screened nuclear charge of the target. Given the equilibrium velocity matching criterion, this would be given by

$$I \approx \frac{1}{2} m_e v^2. \tag{3.69}$$

The velocities of interest to this study are $v \approx 0.2c$. At this velocity, using the above relation, the valence ionization potential at the beam's charge equilibrium should be near

10keV. Using an effective screened target charge of $\overline{Z_t} \approx 10$, the ionization cross section of the beam ion at its charge equilibrium would have an approximate value of

$$\sigma \approx 10^{-21}\text{cm}^2. \tag{3.70}$$

An analogous cross section can be developed for an incremental energy loss reaction. The rate of energy loss of a beam penetrating a target material can be quantified as a function of the beam's velocity v, its average charge state Q, the target ionic density n and target atomic number Z. According to the theory of Bethe [5] (which will be discussed in section 4.3), the energy deposition rate is expressed as

$$\left(\frac{dE}{dx}\right) = \frac{4\pi e^4 Z n}{m_e}\left(\frac{Q}{v}\right)^2 \ln\left[\Lambda_c\right] \tag{3.71}$$

in which the logarithmic term Λ_c is a function of the projectile velocity and atomic properties of the target. Multiplying both sides by the projectile instantaneous velocity v converts the spatial differential to a temporal rate. Dividing by the non-relativistic projectile kinetic energy $E = \frac{1}{2}Am_u v^2$ produces a fractional energy reduction rate

$$v\frac{1}{E}\left(\frac{dE}{dx}\right) = v\frac{8\pi e^4 Q^2 Z n}{A m_u m_e v^4}\ln\left[\Lambda_c\right]. \tag{3.72}$$

Isolating the density and velocity terms, this expression can be interpreted as a reaction rate for fractional energy loss

$$\alpha_E = v\frac{1}{E}\left(\frac{dE}{dx}\right) = n\left(\frac{8\pi e^4 Q^2 Z}{A m_u m_e v^4}\ln\left[\Lambda_c\right]\right)v. \tag{3.73}$$

The quantity in parenthesis represents an effective energy loss cross section σ_E. It can be reduced and quantified as follows:

$$\sigma_E = \frac{8\pi e^4 Q^2}{A m_u m_e v^4}\ln\left[\Lambda_c\right] \tag{3.74}$$

$$\sigma_E = \frac{8\pi e^4 Q^2}{A(m_u/m_e)m_e^2 c^4 \beta_p^4} \ln\left[\Lambda_c\right] \tag{3.75}$$

$$\sigma_E \approx \frac{8\pi r_e^2 Q^2}{1837 A \beta^4} \ln\left[\Lambda_c\right] \tag{3.76}$$

where r_e is the classical electron radius

$$r_e = \frac{e^2}{m_e c^2} = 2.818 \times 10^{-13}\text{cm}. \tag{3.77}$$

For typical cases of importance to this dissertation, swift heavy ions such as lead at a velocity of $\beta = 0.2$ are simulated to penetrate a target material. In a cold target, the effective charge Q of the lead at that velocity is near 63+ and will be near 11+ when the projectile has slowed to a velocity of $v = 0.02c$ (this will be discussed in section 5.1.1). The logarithmic term can be taken from the tables in section 3.1.10. Its values are of the order of just a few. These typical values generate an equivalent energy loss cross section of

$$\sigma_E \approx 10^{-25}\text{cm}^2. \tag{3.78}$$

This is several orders of magnitude smaller than the smallest charge-changing reaction cross section of 10^{-21}. Thus, the mean free path for an incremental energy change should be much greater than the charge-changing mean free path in a dense target. This means that the time interval necessary to achieve charge equilibrium will be much smaller than the time interval necessary to cause a fractional reduction in beam energy since the time interval τ for a given reaction is given by $1/(n\sigma v)$ (see section 3.2) for a given target density n and projectile velocity v. So, it should be the case that the incident projectile ion will be in instantaneous charge state equilibrium as it penetrates a dense material.

In dense materials, the scale of the target usually contains many energy loss and charge-change mean free paths. Therefore the propagation of a beam projectile through

a dense material requires integrated charge evolution and energy deposition calculations, usually employing an instantaneous charge equilibrium model for the projectile's charge state. In rarefied plasmas or gases of $n < 10^{17}\text{cm}^{-3}$, however, the typical situation is that the reduced density extends the energy reduction mean free path and the charge-equilibrium m.f.p. to beyond the scale length of the system. Therefore the time interval for reaching charge equilibrium may exceed the magnitude of the total time to traverse the target system. In this case, the charge may not be able to be considered in instantaneous equilibrium. If the charge state evolution of a projectile ion penetrating such a material must be calculated, then the actual set of charge-changing reaction cross sections must be identified and quantified. The evolution of the charge state can then be calculated using a total reaction rate representing the sum of significant atomic reaction rates for the given beam and target configuration.

These two target regimes, solid-density and rarefied, play out rather illustratively in a putative heavy ion fusion power plant scenario. In the power plant chamber after the final focusing system, the driver beam must penetrate a rarefied plasma whose density may be about $n = 10^{14}\text{cm}^{-3}$. In that regime energy deposition should not be significant, but charge-changing reactions may occur over the expected 300 to 500cm chamber radius. After penetrating the chamber plasma, the ions enter the HIF target, a solid-density material into which the beams deposit their energy. In that solid-density regime, instantaneous charge equilibrium is likely to be achieved and significant energy deposition will occur.

There does exist a mesochoric regime of plasmas and gases whose densities range from about 10^{17}cm^{-3} to 10^{20}cm^{-3} in which ionization and energy deposition occur on a

comparable scale. In this regime, the time evolution of the beam's charge state must be incorporated into energy deposition calculations since both would occur on a comparable time scale.

Other non-equilibrium beam charge evolution may occur in plasmas, even in dense plasma targets [14]. In cold targets, the equilibrium charge state of an incident beam is determined by the balance between competing ionization and capture reactions. Charge transfer of bound electrons in the target to the beam ions dominates the capture reaction rate providing that enough bound electrons are present in the target to cause charge transfer (see section 5.5.1). When the dominant target charge transfer reactions are eliminated due to target ionization, the remaining capture processes are reduced and the charge of an incident ion may take more time to reach equilibrium [14]. This can also result in significant beam energy deposition before equilibrium is reached.

3.3 Quantum Scattering and The Born Approximation

Central to many analyses of atomic scattering reactions is a quantum mechanical perturbation technique known as the *Born Approximation*. More specifically, Born's First Approximation forms the basis of much of stopping power theory and electron ionization theory. It is therefore important to develop an understanding of the approximation itself and its limitations.

Consider the scattering of an incoming beam of particles from a Coulombic potential $V(\vec{r})$ localized to a field. In the case of atomic scattering, the incident particles would be ions of mass M and charge state Q with a mean velocity v. The scattering field would

be the atomic cell of radius r_0 centered on a nucleus of charge Ze. The potential of the incident ion within this localized field would be of the order of QZe^2/r_0.

The first issue to address is the determination of the degree to which classical and quantum models should be applied. If the de Broglie wavelength of the incident particle is much smaller than the scale of the field then the situation can be described classically. This condition is expressed as

$$\lambda_i = \frac{h}{Mv} \ll r_0. \tag{3.79}$$

This is roughly equivalent to requiring that the uncertainties in the incident particle's angular momentum about the field's center be much greater than $\hbar$:

$$Mvr_0 \gg \hbar. \tag{3.80}$$

Note that relativistic effects are considered to be negligible here. At $\beta = 0.2$, this is not a bad approximation. This first requirement places limits on the velocity (momentum) of the incident particle. With r_0 typically equal to a Bohr radius, the requirement becomes

$$v \gg \frac{\hbar}{M\hbar^2/(m_e e^2)} \tag{3.81}$$

$$\beta \gg \left(\frac{m_e}{m_p}\right)\frac{\alpha}{A} \tag{3.82}$$

where A is the incident ion's atomic mass. For $A \simeq 200$ and with $m_p \simeq 1836 m_e$, this becomes

$$\beta \gg 2 \times 10^{-8}, \tag{3.83}$$

which will be satisfied in the range of interest of current applications.

Since the mechanics of the collision are very nearly classical, the quantum effects on the scattering process can be treated effectively by a perturbation technique. The incident

particle's waveform can be represented as a plane wave whose form is simply

$$\Psi_i(\vec{r}) = Ae^{ikz} \tag{3.84}$$

where A is some amplitude which will be taken as real for this analysis. The wave number k is the modulus of a wave vector $\vec{k}_i$ which is prescribed to be along the z-axis for simplicity. This incoming wave would scatter from the localized atomic potential confined to a volume of characteristic dimension a_0. Each differential volume element d^3r within the field scatters this incoming wave as a distinct point source.

The asymptotic behavior of the scattered wave function Ψ_s at $r \gg a_0$ can be expected to be of the form

$$\Psi_s(\vec{r}) = f(\theta, \phi)\frac{Ae^{ikr}}{r} \tag{3.85}$$

where the scattered wave function approaches that of a spherically propagating wave from a point source. The wave number k is used here also as the modulus of the implied wave number of the scattered wave $\vec{k}_s$. This equivalence can be stated since elastic Coulombic scattering is being modeled here. While the scattered wave vector $\vec{k}_s$ would indeed vary in the field of the potential, this analysis is meant to address the behavior well beyond the localized field. The scattered wave vector may indeed be aligned differently than the incident wave vector and the two will satisfy the relationship

$$\vec{k}_i + \vec{k}_x = \vec{k}_s \tag{3.86}$$

where $\vec{k}_x$ represents the phase transfer in the scattering.

The radial functionality of the scattered wave function is that of a standard spherical wave whose amplitude varies as the inverse-square of the radius. The function $f(\theta, \phi)$

contains the angular dependence of the scattering reaction. It also is related to the scattering cross section by

$$\sigma(\theta,\phi) = |f(\theta,\phi)|^2. \tag{3.87}$$

The net stationary state wave function $\phi(\vec{r})$ of the system would be the sum of the incident planar wave function and the scattered spherical wave function

$$\phi(\vec{r}) = \Psi_i(\vec{r}) + \Psi_s(\vec{r}). \tag{3.88}$$

It is this total wave function which is found by solving the wave equation of the system

$$\left[-\frac{\hbar^2}{2\mu}\nabla^2 + V(r)\right]\phi(\vec{r}) = E\phi(\vec{r}) \tag{3.89}$$

where μ is the reduced mass of the projectile-target system

$$\mu = \frac{m_i m_t}{m_i + m_t}. \tag{3.90}$$

This can be reduced by knowing that the total energy of the scattered wave is given by $E = \hbar^2 k^2/(2\mu)$ and by using the substitution

$$U(\vec{r}) = V(\vec{r})2\mu/\hbar^2. \tag{3.91}$$

The wave equation for the scattering system then can be written as

$$\left[-\nabla^2 + U(\vec{r})\right]\phi(\vec{r}) = k^2\phi(\vec{r}) \tag{3.92}$$

This can also be written in a form more suggestive of a solution by Green's function analysis:

$$\left[\nabla^2 + k^2\right]\phi(\vec{r}) = U(\vec{r})\phi(\vec{r}) \tag{3.93}$$

in which $\phi(\vec{r})$ can be solved by a Fourier superposition of the associated Green's functions which satisfy

$$\left[\nabla^2 + k^2\right] G(\vec{r}) = \delta(\vec{r}). \tag{3.94}$$

The solution to $\phi(\vec{r})$ with the function $G(\vec{r})$ is accomplished by integrating over the potential field

$$\phi(\vec{r}) = \phi_0(\vec{r}) + \int G(\vec{r} - \vec{r}')U(\vec{r}')\phi(\vec{r'})d^3r' \tag{3.95}$$

with the function $\phi_0(\vec{r})$ being the solution to the homogeneous equation

$$\left[\nabla^2 + k_s^2\right] \phi_0(\vec{r}) = 0. \tag{3.96}$$

The Green's functional form which satisfies this equation is

$$G(\vec{r}) = -\frac{1}{4\pi}\frac{e^{ikr}}{r}. \tag{3.97}$$

In the integral of equation 3.95 the operand of Green's function is $\vec{r} - \vec{r}'$ where $\vec{r}$ is the position vector of the observation point at $r \gg a_0$ and $\vec{r}'$ is the position of a point within the field $r' < a_0$. The two are related by

$$|\vec{r} - \vec{r}'| = r - \hat{r} \cdot \vec{r}' \tag{3.98}$$

Note that at large r this difference approaches r. It is only significant if it appears in a harmonic function, *i.e.* in the complex exponential where the periodicity makes preservation of terms important.

With this modulus of the difference in radii inserted into the operand in the Green's function of equation 3.97, the form becomes

$$G(|\vec{r} - \vec{r}'|) = -\frac{1}{4\pi}\frac{e^{ik(r - \hat{r}\cdot\vec{r}')}}{r} \tag{3.99}$$

Substituting this approximated far-field Green's function into equation 3.95, the expression for the Green's solution to $\phi(\vec{r})$ becomes

$$\phi(\vec{r}) = \phi_0(\vec{r}) + -\frac{1}{4\pi}\frac{e^{ikr}}{r}\int e^{-ik\hat{r}\cdot\vec{r'}}U(\vec{r'})\phi(\vec{r'})d^3r' \tag{3.100}$$

Comparing this to the expected solution to $\phi(\vec{r})$ in equation 3.88, the significance of the terms can be understood. The solution $\phi_0(\vec{r})$ to the homogeneous wave equation is understood to represent the incident waveform e^{ikz}. The angular dependence of the scattered wave $f(\theta,\phi)$ is shown to correspond to

$$f(\theta,\phi) = -\frac{1}{4\pi}\int e^{-ik\hat{r}\cdot\vec{r'}}U(r')\phi(\vec{r'})d^3r' \tag{3.101}$$

The recursivity of the above system of equations emerges upon a simple inspection. The integral solution to $\phi(\vec{r})$ (more specifically its angular dependence) is a function of itself. This is addressed through an iterative technique known as the *Born Expansion*. However, if the interaction should be sufficiently weak then the total wave function $\phi(\vec{r'})$ in the integrand on the right can be approximated as being simply the original incident planar wave function

$$\phi(\vec{r}) = e^{ikr'}. \tag{3.102}$$

In other words, the effect of the interaction with the potential field is approximated as creating only a negligible perturbation to the original wave function in the integration. This is the essence of the Born Approximation. The limitations of the conditions on which this approximation is based are discussed in the following subsection.

When this approximation substitution is made, the angular function $f(\theta,\phi)$ be-

comes

$$f(\theta,\phi) = \int e^{ik\hat{r}\cdot\vec{r}'} U(r') e^{ikz'} \tag{3.103}$$

From the vector relationships of the radii vectors and wave vectors the following reductions can be made.

$$kz' = \vec{k}_i \cdot \vec{r}' \tag{3.104}$$

$$k\hat{r}\cdot\vec{r}' = \vec{k}_s \cdot \hat{r} \tag{3.105}$$

With these substitutions, the argument of the complex exponential is simplified and the scattering angular dependence becomes

$$f(\theta,\phi) = -\frac{1}{4\pi}\int e^{i\vec{k}_x\cdot\vec{r}'} U(r') d^3r' \tag{3.106}$$

Substituting back into this the expression for the actual Coulombic potential V gives the final form

$$f(\theta,\phi) = -\frac{\mu}{2\pi\hbar^2}\int e^{i\vec{k}_x\cdot\vec{r}'} V(r') d^3r' \tag{3.107}$$

The scattering cross section which results from this scattered wave functionality can be obtained.

3.3.1 Limitations of the Born Approximation

The stipulation that the scattering interaction be so weak that the total wave function at large distances be comparable to the incident wave function can be articulated as follows. The potential of interaction is roughly

$$V(r) = \frac{ZQe^2}{r} \tag{3.108}$$

To say that the effect of scattering from this potential is weak is to say that classical action of an incident particle's impact with the field be small relative to the Planckian value. The action of the potential field is taken as the product of the energy of the field and the time increment of collision.

$$\hbar \gg V(a_0)dt \tag{3.109}$$

With $V(r)$ as above and $dt = a_0/v$ this becomes

$$\hbar \gg \frac{ZQe^2}{v}. \tag{3.110}$$

Using the definition of the fine structure constant $\alpha = e^2/(\hbar c)$ this condition can be expressed in its most frequently cited form

$$\beta \gg ZQ\alpha \tag{3.111}$$

or

$$v \gg ZQ\alpha c \tag{3.112}$$

The implications of this are quite serious, in principle, for heavy ion applications. A typical heavy ion to be modeled in this work is lead, whose atomic charge is 82. Therefore, in order for the Born approximation to be strictly valid, even in collision with a test charge of $Q = 1$, the velocity of the ion must be much greater than $0.6c$. Typical fusion power plant driver beam velocities will probably not be over $0.2c$. However, it will be shown that the Born approximation and its daughter expressions reproduce results quite well over many of the regimes of concern to this work.

3.4 Effective Charge

In many atomic reaction cross section calculations it is important to quantify the effective screened nuclear charge which an incident electron senses upon a collision with an atom or ion of atomic number Z and charge state Q. An electron, either free or bound to an atom, does not necessarily interact with the entire unscreened Coulomb field of the nuclear charge of the colliding atom or ion, unless the incident ion should be fully stripped. Any electrons bound to the target nucleus contribute to the screening of the nuclear charge as perceived by a passing electron. The degree to which that screening occurs is a function of the energy of the incident electron and the electron distribution of the bound electrons of the target atom or ion.

An electron, bound with energy I to a projectile atom or ion, will sense a screened nuclear charge in a target atom or ion which satisfies the following classical balance [54]:

$$I = \frac{(Z - S(b))e^2}{b} \tag{3.113}$$

where b is the impact parameter of the collision and $S(b)$ is the number of screening electrons within a radius of b centered at the target's atomic center. It is given by

$$S(b) = \int_0^b n_e(r) dr^3 \tag{3.114}$$

where $n_e(r)$ is the electronic distribution function characteristic to the atom or ion in question. This electron density distribution can be quantified using the simplified analytical model detailed in section 3.1.5. This balance is related to the *Bohr adiabat* stipulation. At points within the radius b, the target's bound electrons must be characterized by an orbital velocity higher than that of the probing projectile electron. In that case, the characteristic

motions of the incident electron at its binding energy of I will seem relatively slower. Thus the orbital motions of the electrons within b will effectively shield the target nucleus.

Determination of the impact parameter b and the screening levels can be performed by an iterative calculation. This impact radius will be shown to be the basis for an ionization cross section calculation.

Chapter 4

Stopping Power

4.1 Introduction

A projectile atom or ion penetrating a medium transfers its energy to the constituent electrons and nuclei within the medium almost entirely through Coulombic interactions. The projectile ions can transfer energy to both the nuclei and electrons within a target. Since the masses of nuclei are so much greater than the electrons mass, energy transfer to target electrons will dominate by several orders of magnitude [45]. Note that this applies only to collisional energies below which nuclear reactions are induced. At energies much higher than those being addressed here, nuclear reactions can contribute significantly and atomic processes are incidental. The typical HIF beam energy of this examination is near tens of MeV per atomic unit. The energies at which nuclear reactions begin to become significant are above hundreds of MeV/u.

A given material's capacity to receive the energy of a projectile particle through electronic interactions is known as its *stopping power*. These interactions depend on the

equation of state of the material and the electronic characteristics of the projectile. This section outlines a comprehensive study of stopping power theory. Information about target equation of state and electronic distribution was addressed in the previous section. Determination of the projectile's charge state will be addressed in the next.

The stopping power of a target with respect to a given projectile can be determined by quantifying the complete set of energy transfer reactions which may occur between incident charges and the constituent electrons of the penetrated medium. This analysis has been performed extensively over the past century. The resultant stopping power formulae can be investigated best as categorized into four basic types of interactions, which are *bound electron stopping*, *free electron stopping*, *ionic stopping* and *low-velocity stopping*.

4.2 General Electron Stopping

In order to understand the various terms in some of the electron stopping power expressions, it is useful to consider briefly a physical model of projectile-electron energy deposition, from which the exact stopping power expressions are derived. In general, the rate of energy transfer to bound or free electrons within a material from a projectile can be developed from a Coulombic collisional model[38].

Consider an incident charge of mass m_i, charge Q penetrating a material with a velocity v. The net set of Coulombic collisions can be built in terms of an average binary collision between an incident beam particle and the electrons in the target material. As the incident particle passes a target electron at an impact parameter b, they both experience an electric field. This field would have components aligned and anti-aligned to the direction

of motion and transverse to the direction of motion. The net effect of the components parallel to the beam's direction of motion is vanishing since, integrated over the time of the impact, they contribute oppositely on either side of the electron. The transverse field however imparts a non-zero momentum transfer to the system.

The fully-relativistic form of the transverse field generated by the moving incident charge at the position of the electron is given by [38]

$$E_{\perp}(b,t) = \frac{\gamma Q b}{(b^2 + \gamma^2 v^2 t^2)^{3/2}}. \tag{4.1}$$

Here, b is the impact parameter, t is the time measure which is defined to vanish at closest approach and v is the projectile of velocity with γ having its usual relativistic definition. In the present investigation relativistic effects will be considered to be small since the projectile velocity range will be near $0.2c$, so γ will be taken to be unity. The time dependence is arranged such that at $t = 0$ the particles are at closest approach with the modulus of their separation vector $\vec{r}$ equal to b. The momentum transfer from the beam ion to the electron is calculated by integrating the mutual transverse force of the collision over all time:

$$\Delta p = \int_{-\infty}^{\infty} e E_{\perp}(b,t) dt = \frac{2Qe^2}{bv} \tag{4.2}$$

The energy transfered from the incident particle to the electron is then

$$\Delta E(b) = \frac{(\Delta p)^2}{2m_e} = \frac{2Q^2 e^4}{m_e v^2} \frac{1}{b^2}. \tag{4.3}$$

The net energy transfer rate to the electrons in the material is obtained from integrating this individual transfer calculation over all of the encountered electrons. If the atomic number of the material be Z and the ionic density be n then there will be Zn electrons per unit volume. In an incremental beam position advancement of dx the incident

particle encounters a certain number of electrons in the ring formed about the impact parameter:

$$dN = (nZ)2\pi b db dx. \tag{4.4}$$

The total energy transfer per incremental step dx is calculated by integrating over all electrons encountered

$$\frac{dE}{dx} = \int_N \Delta E \frac{dN}{dx} \tag{4.5}$$

which entails an integration of all of impact parameter space:

$$\frac{dE}{dx} = nZ2\pi \frac{2Q^2e^4}{m_e v^2} \int_{b_{min}}^{b_{max}} \frac{1}{b^2} b db. \tag{4.6}$$

The limits of integration, b_{min} and b_{max}, represent the minimum and maximum impact parameters of the collision. This then forms a general expression for the energy transfer of an incident ion to the electrons in a material

$$\frac{dE}{dx} = \frac{4\pi nZQ^2e^4}{m_e v^2} \ln\left[\frac{b_{max}}{b_{min}}\right] \tag{4.7}$$

The specification of minimum and maximum impact parameters is not just a formality. Clearly the natural limits of 0 to ∞ result in a divergent calculation. Limits on the impact parameters must be developed based on physical arguments. Also, so far, the state of the electron receiving the transfered energy has not been addressed. The analysis has assumed that it is stationary. An actual electron in a material will be either bound or free and will be characterized by an energy and velocity. These considerations will be important in determining the impact parameters and will accompany the discussion on the specific forms of the stopping power.

Note that the ratio of maximum to minimum impact parameters is also known as the *Coulomb logarithm* Λ_c. Its value forms a primary distinction among the various stopping power expressions for both bound and free electrons.

4.3 Bound Electron Stopping

The two principle exact forms of bound electron stopping power formulae are due to Bethe [5] and Bohr [9]. These two expressions represent different regimes of applicability and are closely related to the general form derived above. They are distinguished chiefly in their respective choices of collision impact parameter formulation.

The Bohr formula for bound electron stopping power is based on a semi-classical formulation. Its full form is [8]

$$\left(\frac{dE}{dx}\right)_B = \frac{4\pi e^4 n_b}{m_e}\left(\frac{Q}{v}\right)^2 \ln\left[\frac{1.1229 m_e v^3}{Z_p e^2 \omega}\right] \tag{4.8}$$

with n_b being the number density of bound electrons in the target absorbing medium, v is the incident ion's velocity and Q is its charge or ionic charge state. The term ω is the characteristic frequency of the bound target electrons

$$\omega = \overline{I}/\hbar \tag{4.9}$$

in which $\overline{I}$ represents the average ionization potential of the target atomic electrons detailed in section 3.1.8.

Bethe's formulation, on the other hand, is fully quantum mechanical. The full expression for Bethe's version of the stopping power is

$$\left(\frac{dE}{dx}\right)_B = \frac{4\pi e^4 n_b}{m_e}\left(\frac{Q}{v}\right)^2 \left\{\ln\left[\frac{2m_e\gamma^2 v^2}{\overline{I}}\right] - \beta^2\right\} \tag{4.10}$$

in which β and γ have their usual relativistic meanings

$$\beta = \frac{v}{c}, \tag{4.11}$$

$$\gamma = \left(1 - \beta^2\right)^{-\frac{1}{2}}. \tag{4.12}$$

Neglecting the relativistic and higher-order terms, the Bethe form appears simply as

$$\left(\frac{dE}{dx}\right)_B = \frac{4\pi e^4 n_b}{m_e}\left(\frac{Q}{v}\right)^2 \ln\left[\frac{2m_e v^2}{\overline{I}}\right] \tag{4.13}$$

4.3.1 Differences and Limitations on Bohr and Bethe

The Bohr and Bethe stopping power formulae form the foundation for most ion-matter interactions. Implementation of these expressions for energy deposition calculations requires an understanding of their respective differences and regimes of applicability.

Logarithmic Differences

In simplified form, these two standard energy deposition formulae differ only in their respective logarithmic terms. Both match the general form of equation 4.7. An examination of their associated Coulomb logarithms provides important insight into the nature of these two standard formulae and their application to the purposes of this work.

The logarithmic term in the stopping power formulae, which originated in the solution of an integral equation, can be understood in terms of the impact parameters discussed in §3.1.3. In the Bethe form, which is based on quantum theory, the logarithmic term is nearly the ratio of the maximum impact parameter to the quantum-limited minimum impact parameter

$$\Lambda_q \approx \frac{v\hbar\overline{I}}{\hbar/m_e v} \tag{4.14}$$

$$= \frac{m_e v^2}{\overline{I}}. \tag{4.15}$$

Aside from a factor of 2, this is the Bethe stopping power logarithm. The Bohr logarithm term, having been derived from a classical theory, is the ratio of the adiabatic maximum to the classically-limited parameter.

$$\Lambda_c = \frac{v\hbar\overline{I}}{Z_p e^2/(m_e v^2)} \tag{4.16}$$

$$= \frac{m_e v^3}{Z_p e^2 \omega}. \tag{4.17}$$

Velocity and Applicability

The larger of the two minimum impact parameters for the given beam-target scenario in principle determines whether the Bohr or Bethe logarithm is appropriate to the calculation. The Bethe formula is meant to be applied when the quantum minimum impact parameter b_q exceeds the classically-limited value b_c. The Bohr model conversely is intended to be applicable when the classical minimum impact parameter is largest. The theoretical point of transition between the two models occurs when the two possible impact parameters are equal. This is solved by equating

$$b_c = b_q \tag{4.18}$$

where the left and right sides are expressed as in section 3.1.3

$$\frac{Z_p e^2}{m_e v^2} = \frac{\hbar}{m_e v} \tag{4.19}$$

$$v = \frac{Z_p e^2}{\hbar}. \tag{4.20}$$

Using the definition of the fine structure constant, this condition becomes

$$v = Z_p \alpha c \tag{4.21}$$

Note that this is the same criterion for the application of the Born approximation found in formula 3.112. This makes sense, since outside of the Born approximation, the Bethe formula in principle breaks down into the regime in which the Bohr model is meant to address. This rough analysis is also consistent with Sigmund's exact calculations [61] of the point of transition between the two models being

$$v < 2.25 Z_p v_0 \tag{4.22}$$

with $v_0 = \alpha c$.

Note that there is a certain value of Z_p beyond which the Bethe stopping power formula is always technically invalid due to the criterion for satisfying the Born approximation on which it is based. In order for the Born approximation and thus, technically, the Bethe stopping formula to be valid, the beam velocity must satisfy

$$v > 2.25 Z_p \alpha c \tag{4.23}$$

However, there exists an atomic number Z_p beyond which the projectile velocity v would need to be greater than the speed of light in order to satisfy the Born criterion:

$$Z_p > \frac{1}{2.25\alpha} \tag{4.24}$$

or,

$$Z_p > 61. \tag{4.25}$$

This limitation is not commonly acknowledged in the literature and many papers refer to calculations which employ the Bethe stopping power for high-Z projectiles and for velocities well below the quantum-limited values. The remarkable fact is, though, that the Bethe

model reproduces data very well even in classically-limited situations [61]. The reason why the Bethe expression operates beyond its theoretical regime of application is not well understood [61].

Functional Limitations

There are more limitations in addition to these theoretical ones. Catastrophic failure of Bohr and Bethe models occur when the logarithmic term is less than unity. For the Bethe logarithm, this occurs when

$$2m_e v^2 < \overline{I} \tag{4.26}$$

or,

$$2m_e c^2 \beta^2 < \overline{I}. \tag{4.27}$$

A simple approximation for $\overline{I}$ developed by Bloch [7] can be used

$$\overline{I} \approx Z_t 10\text{eV}. \tag{4.28}$$

The logarithmic failure condition for the Bethe expression then becomes

$$2m_e c^2 \beta^2 < Z_t 10\text{eV} \tag{4.29}$$

$$\beta < \sqrt{Z_t} 3.13 \times 10^{-3} \tag{4.30}$$

Velocities below this value produce a meaningless logarithm in the Bethe stopping power expression. This limitation probably will not effect the calculations in this study since these low cut-off speeds represent the very tail of the range of a $\beta = 0.2$ heavy ion. Note that this condition is not dependent upon the projectile atomic number as the impact parameter is.

When the Bethe expression becomes invalid in this manner, accommodations must be made to form a transition into another stopping power expression applicable at low-velocities. In theory the Bohr expression could be implemented here, but this choice is not empirically supported [61].

The Bohr stopping power formula also features a catastrophic failure condition when its logarithmic term is less than 1. This occurs when

$$m_e v^3 < Z_p e^2 \overline{I}/\hbar \tag{4.31}$$

$$v^3 < Z_p e^2 Z_t 0.735 \frac{2\pi^2 e^4}{\hbar^3} \tag{4.32}$$

$$v^3 < 1.47\pi^2 Z_p Z_t \frac{e^6}{\hbar^3} \tag{4.33}$$

$$v < 1.665(Z_p Z_t)^{1/3} \alpha c \tag{4.34}$$

This failure condition is close to the condition specified for the transition into the low-velocity stopping power formulation described in section 4.6.

4.4 Free Electron Stopping

In addition to collisions with bound electrons in the target, a beam ion being deposited into a plasma can collide with free electrons if the target should be ionized to any significant degree. Free electrons in the target behave differently in collisions with beam ions and must be addressed by a separate stopping power expression. The free electron stopping power has appeared in various incarnations throughout the associated literature. Like the bound electron formula it can be expressed in a form with a logarithmic term whose argument represents a ratio of impact parameters.

Mehlhorn [45] following Jackson [38] gives a free electron stopping expression in this manner which is

$$\left(\frac{dE}{dx}\right)_f = \frac{4\pi e^4 n_f}{m_e}\left(\frac{Q}{v}\right)^2 \ln\left[\frac{0.764v}{b_{min}\omega_p}\right] \tag{4.35}$$

Here, b_{min} represents the same quantum or classical minimum impact parameter as in the previous analysis for bound electrons. However, free electrons do not exhibit the same adiabatic maximum impact parameter as bound electrons. Recall that the bound electron maximum parameter is chosen such that at distances $b > b_{max}$, the impact time given by b/v is greater than the quantum orbital oscillations of the target bound electrons. In a plasma, free electrons exhibit a different oscillation period characterized by their associated plasma frequency

$$\omega_p = \left(\frac{4\pi n_e e^2}{m_e}\right)^{1/2} \tag{4.36}$$

in which n_e is the free electron density. In the plasma case, the maximum impact parameter is that distance beyond which the plasma electrons will perform many oscillations in the collision time, causing an adiabatic collision.

Peter and Meyer-ter-Vehn [55] have developed a comprehensive expression for the free electron stopping based on linear and non-linear Vlasov theory. They found for an electron plasma at temperature T a free electron stopping power of

$$\left(\frac{dE}{dx}\right)_{FE} = -\left(\frac{Qe\omega_p}{v}\right)^2 \left\{ \mathrm{G}\left[\frac{v}{v_{th}}\right] \ln[k_{max}\lambda_D] + \mathrm{H}\left[\frac{v}{\sqrt{k_B T/m_e}}\right] \ln\left[\frac{v}{\sqrt{k_B T/m_e}}\right] \right\} \tag{4.37}$$

in which

$$\mathrm{G}(x) \equiv \mathrm{erf}[x] - \frac{2}{\sqrt{\pi}} x \exp[-x^2] \tag{4.38}$$

and

$$\mathrm{H}(x) \equiv \frac{-x^3 \exp\left[-\frac{x^2}{2}\right]}{3\sqrt{2\pi}\ln x} + \frac{x^4}{(x^4+12)}, \tag{4.39}$$

$\mathrm{G}(x)$ being the Chandrasekhar velocity matching function and $\mathrm{H}(x)$ being an additional matching function developed by Peter and Meyer-ter-Vehn. These terms both approach unity for large v/v_{th}.

In the above expressions $\mathrm{erf}(x)$ is the usual *error function*, v_{th} is the plasma electron thermal velocity $\sqrt{2k_BT/m_e}$ and λ_D is the Debye length of the plasma. This form of the stopping power was developed not in terms of impact parameters but in terms of wave numbers k representing momentum transfer

$$p = \hbar k. \tag{4.40}$$

The wavenumber cut-off for collisional momentum transfer, k_{max}, is determined by the lesser of the quantum and classical momentum transfer wavenumbers:

$$k_{max} = \text{minimum}\left\{\frac{m_e v_r^2}{Qe^2}; \frac{2m_e v_r}{\hbar}\right\} \tag{4.41}$$

In the above, $v_r = \sqrt{v^2 + v_{th}^2}$ represents the effective velocity of the thermal electrons in the projectile's rest frame, being a quadrature addition of the projectile and thermal velocities. In references [55] and [54] the authors chose to use just v in the quantum constraint in equation (4.41) instead of the full quadrature velocity. This seems to be inconsistent, and this analysis will employ the quadrature velocity in the quantum impact constraint. The expression as it appears in reference [45] concurs and uses the full quadrature velocity. Note that this k_{max} parameter is simply the inverse of the minimum impact parameter in the logarithm of equation (4.7).

The two functions G($\frac{v}{v_{th}}$) and H($\frac{v}{\sqrt{k_B T/m_e}}$) both approach unity for projectile velocities much greater than the plasma electron thermal velocity. In this case, equation (4.37) may be simplified as follows:

$$\left(\frac{dE}{dx}\right)_{FE} = -\left(\frac{Qe\omega_p}{v}\right)^2 \mathrm{G}\left[\frac{v}{v_{th}}\right] \ln\left[k_{max}\lambda_D \frac{v}{\sqrt{k_B T/m_e}}\right], \tag{4.42}$$

$$\left(\frac{dE}{dx}\right)_{FE} = -\left(\frac{Qe\omega_p}{v}\right)^2 \mathrm{G}\left[\frac{v}{v_{th}}\right] \ln\left[\frac{\sqrt{m_e}k_{max}v}{\sqrt{4\pi n_e e^2}}\right], \tag{4.43}$$

which is just

$$\left(\frac{dE}{dx}\right)_{FE} = -\left(\frac{Qe\omega_p}{v}\right)^2 \mathrm{G}\left[\frac{v}{v_{th}}\right] \ln\left[\frac{k_{max}v}{\omega_p}\right]. \tag{4.44}$$

Recalling the interpretation of k_{max} as the inverse of the minimum impact parameter, the above expression becomes nearly identical to the Jackson free electron stopping expression in equation 4.35:

$$\left(\frac{dE}{dx}\right)_{FE} = -\left(\frac{Qe\omega_p}{v}\right)^2 \mathrm{G}\left[\frac{v}{v_{th}}\right] \ln\left[\frac{\lambda v}{b_{min}\omega_p}\right] \tag{4.45}$$

in which λ is a factor near unity. If the classical condition should determine k_{max} and $v \gg v_{th}$ then the expression reduces to the classic Bohr formula [9]

$$\left(\frac{dE}{dx}\right)_{FE} = -\left(\frac{Qe\omega_p}{v}\right)^2 \ln\left[\frac{m_e v^3}{Q_p e^2 \omega_p}\right] \tag{4.46}$$

This analysis establishes a good correspondence among the various plasma electron stopping power formulae.

Incidentally, the term v/ω_p has the unit of length. Recalling the form of equation (4.7), one should expect that it would be analogous to a maximum impact parameter. The expression can be written as

$$\frac{v}{\omega_p} = b \tag{4.47}$$

$$\frac{1}{\omega_p} = \frac{b}{v}. \tag{4.48}$$

This equates the electron's plasma period to the collision time at a certain distance, b. Thus this distance would indeed be a maximum impact parameter, beyond which the electron would begin to exhibit many plasma oscillations during the collision time. This is the plasma analog of the Bohr adiabat condition.

4.5 Nuclear Stopping Power

Although their contribution is usually negligible, the screened nuclei within the target are able to receive energy from a penetrating projectile through Coulombic interactions analogous to those with electrons. The form for this component of the stopping power is [45]

$$\left(\frac{dE}{dx}\right)_i = -\left(\frac{Qe\omega_{p_i}}{v}\right)^2 \mathrm{G}\left[\frac{v}{v_{th_i}}\right] \ln\left[\frac{\lambda_D}{b_{min}}\right] \tag{4.49}$$

in which ω_{p_i} is the ion plasma frequency defined by

$$\omega_{p_i} = \left(\frac{4\pi n_i e^2}{m_i}\right)^{1/2} \tag{4.50}$$

with n_i and m_i being the ionic number density and mass and v_{th_i} is the ionic thermal velocity.

The Debye length acts as a maximum impact parameter beyond which electron shielding will negate any ionic charge. The minimum impact parameter is just the classical value, given by

$$b_{min} = \frac{Q_p Q_t e^2}{m_\mu (v + v_{th_i})^2} \tag{4.51}$$

in which Q_t is the target ionization state and m_μ is the reduced mass of the binary system $m_1 m_2/(m_1 + m_2)$.

Since the ionic thermal velocities are much less than the electron thermal velocities, the velocity ratio in the G function will be greater and thus the matching will be better for ions. However, the m_i term in the denominator means that the ionic stopping power will be typically a factor of 10^3 smaller than electron stopping terms.

4.6 Low-Velocity Stopping

When the beam velocity is reduced to that of the characteristic Thomas-Fermi orbital velocity of the beam's constituent atomic species (see section 3.1.2),

$$v \leq Z_p^{2/3} \alpha c, \tag{4.52}$$

the previous stopping power expressions become inadequate. In this case, the incident beam ion does not appear as a distinct charge to the target electrons since the motion of the projectile's orbital electrons would be screen its nucleus. This screening of the projectile's nucleus occurs since the collision time would be slow compared to the characteristic orbital time of the projectile's electrons. Also, below this velocity, the equilibrium charge state of the beam as given by Bohr's formula (see section 5.1.1) is not well defined.

Note that this transition velocity might not be 'low' by some standards. For a lead beam ion, the characteristic Thomas-Fermi velocity is approximately $v_{TF} \approx 0.14c$. If the initial lead beam velocity should be $0.2c$ then this transition velocity is reached when the beam energy is still about 1/4 of its initial value.

The quantification of the energy deposition of beams whose velocities are in this

regime is known as 'low velocity stopping' (though this is often a misnomer). For calculations of beam energy deposition in this regime, a theory was developed by Linhard, Scharff and Schiøtt [37]. This form of the stopping power is known as the *LSS model*[37], [45]. Note that this low velocity stopping is sometimes called 'nuclear stopping'. This is also a misnomer, as this energy deposition characterization is not a function of actual nuclear collisions but rather atomic collisions.

The LSS stopping power formula treats the energy deposition of the beam as if ti were caused by a velocity-proportional friction force between the beam and target. The LSS stopping power expression is given as

$$\left(\frac{dE}{dx}\right)_{LSS} = C_{LSS}\sqrt{E} \tag{4.53}$$

in which

$$C_{LSS} = \frac{K\sqrt{E_L}}{R_L} \tag{4.54}$$

with

$$K = Z_p^{1/6}\frac{0.0793 Z_p^{1/2} Z_t^{1/2}(A_p + A_t)^{3/2}}{(Z_p^{2/3} + Z_t^{2/3})^{3/4} A_p^{3/2} A_t^{1/2}}, \tag{4.55}$$

$$E_L = (A_p + A_t) Z_p Z_t E^2 A_t a \tag{4.56}$$

and

$$R_L = \frac{(1 + \frac{A_t}{A_p})^2}{4\pi \frac{A_t}{A_p} N_t a^2}. \tag{4.57}$$

In the above expressions, a is a screened-potential radius term given by $a = a_0 0.8853(Z_p^{2/3} + Z_t^{2/3})^{-1/2}$ with a_0 being the Bohr radius, 0.529×10^{-8}cm.

4.7 Transitions Among Stopping Power Forms

Several clarifications need to be made regarding the choice of energy deposition modeling appropriate for a given beam, velocity and target configuration. Several different stopping power expressions have been presented for different beam velocities. However, as the beam deposits it energy into the target, its velocity decreases and the transition among the various energy deposition models needs to be addressed.

In the analysis of section 4.3 it was shown that the correct choice of stopping power model for beam deposition into bound electrons in principle will vary with the projectile ion's atomic number and velocity. No rigorous formalism yet exists for determining the exact dependence of stopping power model on projectile velocity. However, some empirical trends have been identified in the literature which will be employed in this present work. The goal of this dissertation is not to correct or improve the physics of stopping power but rather to use the best stopping power models to examine the effects of beam charge state evolution changes on energy deposition into various targets.

4.7.1 Bethe *vs.* Bohr

Suppose the beam velocity v is greater than its associated Thomas-Fermi atomic orbital velocity

$$v > v_{TF} = Z_p^{2/3} \alpha c \tag{4.58}$$

where Z_p is the beam species atomic number. At such beam velocities, either the Bohr stopping power formula or the Bethe version is meant to model correctly the beam's energy deposition into the target bound electrons. In principle, when the Born approximation

validity is established

$$v > 2Z_p \alpha c \tag{4.59}$$

the Bethe model is meant to be used. At velocities lower than the Born criterion velocity, but greater than $Z_p^{2/3}\alpha c$, the Bohr stopping power formula is meant to apply. When the beam velocity drops below its associated Thomas-Fermi scaled velocity v_{TF}, the LSS stopping model is appropriate.

However, a curious trend has been noted by Sigmund and others [61]. For velocities greater than the low-velocity stopping power limit, being the Thomas-Fermi velocity v_{TF}, the Bethe stopping power model is more reliable than the Bohr model. This is true even if the Born approximation criterion is not satisfied. The Bohr model is simply not empirically valid in most applications. The Bethe stopping power formula is found to be useful even beyond the technical limitations of the Born approximation. *Therefore in this work, only the Bethe stopping power formula will be employed for projectile velocities v greater than v_{TF}.*

4.7.2 Low Velocity Transition

In principle, if a projectile should enter an absorbing medium at a velocity greater than its Thomas-Fermi velocity, it should eventually be slowed to the point at which a transition should be made to the regime in which the low-velocity stopping power should be used to model its energy deposition. However, the LSS stopping power value is not in principle equal to that of the Bethe model at the point of transition,

$$v = v_{TF}. \tag{4.60}$$

Empirically, ion beams do not exhibit a sharp change in energy deposition rate at the transition point [71]. The transition from logarithmic Bethe stopping to LSS low-velocity stopping must be modeled in a continuous manner, representing the natural behavior of ions stopping in an absorbing material.

In order to achieve a continuous connection between the Bethe and LSS stopping power formulae at and around the velocity at which a transition between the two should occur, a variety of functional smoothing techniques have been proposed. Peter and Meyer-ter-Vehn [54] have suggested that the two expressions be joined quadratically such that the lesser dominates by

$$\left(\frac{dE}{dx}\right)_{B,LSS} = \frac{\left(\frac{dE}{dx}\right)_B}{(1 + \left(\frac{dE}{dx}\right)_B^2 / \left(\frac{dE}{dx}\right)_{LSS}^2)^{1/2}} \tag{4.61}$$

Others such as Mehlhorn [45] and Varelas and Biersack [67] have simply considered the smallest value of either the Bethe/Bohr or LSS models to be the appropriate one at each point. As it happens, the manner in which the low-velocity stopping and logarithmic are merged does indeed affect the deposition profile and range calculation. *Based on the recommendations in references [54] and [71], the LSS velocity dependence will be engaged by the quadratic transition detailed above.*

If the velocity should be low enough to cause a negative logarithmic stopping in either the Bethe model then the bound electron term may be considered to have vanished. In this case the combined stopping power above would be just the LSS stopping contribution.

Both of these bound electron stopping power applicability issues, the choice of Bethe's formula over Bohr's and the transition into LSS application, deserve a designated theoretical review. But, the detailed justification of these issues is not the task at hand.

The purpose here is to employ the most reliable energy deposition scheme since the focus of the original work of this dissertation is comprehensive beam charge evolution modeling in targets while leaving energy deposition questions to another student.

4.8 Complete Stopping Power Form

Given the different stopping power physics presented in sections 4.2 through 4.6 a comprehensive energy deposition formulation applicable to any beam-target configuration can be developed. This complete form represents the sum of the stopping power contributions from collisions with target bound electrons and a transition to the low-velocity LSS formula $\left(\frac{dE}{dx}\right)_{B,LSS}$, free electron stopping $\left(\frac{dE}{dx}\right)_{FE}$ and energy transfer to target nuclear charges $\left(\frac{dE}{dx}\right)_i$. These were each addressed in the previous analysis.

A total comprehensive stopping power expression can be stated as a linear combination of the stopping power expressions due to each separate process:

$$\left(\frac{dE}{dx}\right) = \left(\frac{dE}{dx}\right)_{B,LSS} + \left(\frac{dE}{dx}\right)_{FE} + \left(\frac{dE}{dx}\right)_i . \tag{4.62}$$

This follows the stopping power formulation presented in reference [54].

Chapter 5

Projectile Charge State Calculations

In the energy deposition discussion of the preceding chapter, all of the terms in the beam stopping power formulae were quantified except for Q, being the charge state of the incident ion. The determination of the beam charge state to be used in stopping power formulae and the abstracted determination of the charge state of any projectile traversing a material represents a formidable problem. It constitutes the primary motivation of this dissertation and of many modern atomic physics research endeavors. While some physical uncertainties exist in energy deposition schemes [61], the most perennially difficult issue is the understanding of the reactions which cause the charge of a projectile to change along its course through an absorber. For the HIF scientist this issue has posed an uncertainty about atomic interactions whose resolution is desired.

The following sections detail the approaches to calculating the atomic processes

responsible for effecting a change in the charge state of ions penetrating a given material. Also presented is a context of previously-employed methods and problems motivating a closer investigation of current methods.

5.1 Current Understanding of Charge State Evolution

In general, two approaches exist for determining the charge state evolution of an ion penetrating a target: (1)equilibrium charge state equations, (2)discrete reaction calculations. Historically the most useful technique for addressing projectile charge state values for energy deposition calculations is the former method. Semi-empirical fits for determination of the equilibrium charge states attained by projectiles penetrating cold, solid-density target materials have been exceptionally successful [25]. At a given velocity an ion penetrating a material will eventually reach an equilibrium charge state at which the ionization of the projectile by collisions the target is balanced by the capture of electrons from the target onto the projectile. In cases in which the path length required for reaching charge equilibrium is less than the scale of the target itself (see section 3.2.1) and much less than the distance required for a small incremental change in projectile energy, the charge state can be assumed to be in instantaneous equilibrium throughout its propagation. The time dependence of the charge state evolution in that case would not be an issue.

In more rarefied targets with densities less than about 10^{17}cm^{-3} or in targets having a low areal density nx where n is the number density of the target and x is its thickness, charge equilibrium may not be attained within a depth small compared to the scale of the system. In such cases the time-evolution of the charge state must be addressed. There is

thus a need for quantifying the cross section for ionization by collision with target atoms and any free electrons. Also, beam propagation through plasmas has not been studied to the extent to enable a semi-empirical fit for ion deposition into plasma targets. Thus, discrete models have been proposed to be used to model the charge evolution of ions penetrating plasmas [54].

In the HIF chamber, the density of the ambient gas or plasma is such that charge equilibrium is not likely to be achieved along the 300 to 500cm path length between the designed chamber entrance and target location. Thus, determination of the beam charge evolution in the chamber can not be addressed by a formula providing equilibrium charge states. In that case, discrete cross sections calculations must be employed to determine the charge state evolution of a beam in the HIF chamber. In the target, however, the beam will be deposited into a solid target material which will rapidly be heated to form a dense plasma. The nature of the charge evolution of a beam penetrating such a target plasma has not yet been determined. Regardless, discrete ionization and capture reactions will be useful in forming preliminary expectations about the nature of the charge evolution of beams in dense plasma targets.

While a simple formula providing the charge evolution of an HIF-related beam scenario does not yet exist (but will be developed in this work), the concept of equilibrium charge expressions will be examined. The nature of such approaches to charge evolution calculations can provide useful insight into beam-target atomic interactions.

5.1.1 Equilibrium Charge

The original ansatz which serves as the basis for early equilibrium charge state formula was given by Bohr [8]. He surmised that the equilibrium charge state Q_E of an ion penetrating a given non-ionized material at a velocity v would be the one at which the characteristic valence electron orbital velocity $v_v(Z_p, Q_E)$ equals the projectile velocity. This criterion can be understood better in the frame of the incident projectile, in which observers would see the target constituents rushing past at velocity v. If an orbital electron should be moving in its shell less swiftly than the passing nuclei and electrons, it will be removed. This is to say that unless its binding energy, which is related to its velocity, is greater than its kinetic energy at the beam velocity, it will be removed from the projectile. Alternatively, this condition relates that capture of an electron from the target onto the projectile ion will occur if the binding energy of the next available shell in the projectile's electronic structure should be greater than the kinetic energy of an electron approaching with the projectile velocity v. Note that this implicitly requires that the target should possess some loosely-bound valance electrons with energy I_t such that

$$I_t \ll \frac{1}{2} m_e v^2. \tag{5.1}$$

Thus, the projectile will be in charge equilibrium Q_E if the following energy balance is established

$$\frac{1}{2} m_e v^2 \approx I_v(Z_p, Q_E) \tag{5.2}$$

or

$$v \approx v_v(Z_p, Q_E). \tag{5.3}$$

Many techniques have been offered to quantify this relationship. Betz presents a comprehensive overview of the various charge state equilibrium models [6]. The form which has appeared most frequently in the literature and which appears to have enjoyed more examination and fine tuning is the exponential model due to Bohr, Betz and Brown and Moak [10]. With amazing simplicity it relates the equilibrium charge state Q_E of a projectile of atomic number Z to its velocity v.

$$Q_E = Z(1 - \exp[-v/v_1]) \tag{5.4}$$

where v_1 is the characteristic Thomas-Fermi velocity of an orbital electron in the projectile

$$v_1 = Z^{2/3}\alpha c. \tag{5.5}$$

This expression has been adjusted slightly in various papers by variations in the associated constants for comparison to experimental data [1]. For this present purpose the original form is acceptable for analysis.

What is most amazing is that the model requires no information about the medium being penetrated. The equilibrium charge state achieved in the beam, which is known to represent the balance point of the ionization and recombination rates, is not a function of the material properties. This amazing result actually contains some implicit assumptions. The principal approximation is that the material being penetrated contains electrons which are very loosely bound with respect to an electron's kinetic energy of relative motion in the system

$$E_k = \frac{1}{2} m_e v^2. \tag{5.6}$$

For most atoms, the outer-most electrons are typically bound by just a few electron-volts. The relative energy of motion in electron-volts for non-relativistic beam velocities is obtained

by

$$E_k = \frac{1}{2} m_e c^2 \beta^2 \tag{5.7}$$

$$E_k = (0.5)511\text{keV}\beta^2 \tag{5.8}$$

Assuming a target valence electron binding energy of 10eV, the equilibrium fit should be valid when

$$E_k > 10\text{eV} \tag{5.9}$$

which is to say

$$255\text{keV}\beta^2 > 10\text{eV} \tag{5.10}$$

or

$$\beta > 0.01 \tag{5.11}$$

Since this analysis is meant to address swift ions of $\beta \sim 0.2$, that velocity limitation will not present a problem.

Another beam velocity limitation on this semi-empirical fit is that in principle it is meant to be applied when $v > v_1$. Note that this velocity restriction is also the velocity criterion for validity of the LSS stopping power formulation of section 4.6. However, it is noted that the Bohr fit for the equilibrium charge state of a projectile in a target is valid even for beam velocities v well below the beam's Thomas-Fermi orbital velocity [71].

Several general target properties can cause this beam equilibrium charge state formula to be invalid. It is well known that the equilibrium charge state of an ion penetrating a gas is lower than the corresponding charge state in a solid target [20]. The semi-empirical fit detailed above is relevant to deposition studies of beams in solid targets. Also, this equilibrium formulation is not yet applicable to ionized targets. Both experimental and

theoretical investigations of the charge state equilibria achieved by ions in plasmas indicate that the equilibrium charge state in plasmas is higher than the equilibrium charge given by the traditional Bohr-based fit. This inability to address plasma charge evolution has motivated much of the ion-plasma atomic physics research of late. The goal of developing a model and a new fit to be applicable in plasmas is addressed in this dissertation.

Physics of the Semi-empirical Fit

A consideration of the physical basis of the semi-empirical fit can provide a better understanding of the fit itself and important atomic physics properties. Since the equilibrium condition requires that the outer electron velocity at the equilibrium charge state should be equal to the projectile velocity, a useful relationship can be developed by inverting the Bohr equilibrium charge state equation. Substituting in the valence electron velocity $v_v(Z,Q)$ of an atomic species Z charged to Q for the projectile velocity $v = \beta c$, the semi-empirical fit can be shown to be identical to an expression relating the valence electron orbital velocity of an ionized projectile to its charge state. The following analysis will employ the notation Q for projectile charge state in place of equilibrium charge Q_E.

$$Q = Z(1 - \exp[-v_v(Z,Q)/v_1]) \tag{5.12}$$

$$\frac{Z-Q}{Z} = \exp[-v_v(Z,Q)/v_1] \tag{5.13}$$

$$\ln\left[\frac{Z-Q}{Z}\right] = -v_v(Z,Q)/v_1 \tag{5.14}$$

which gives a final useful form of

$$v_v(Z,Q) = v_1 \ln\left[\frac{Z}{Z-Q}\right]. \tag{5.15}$$

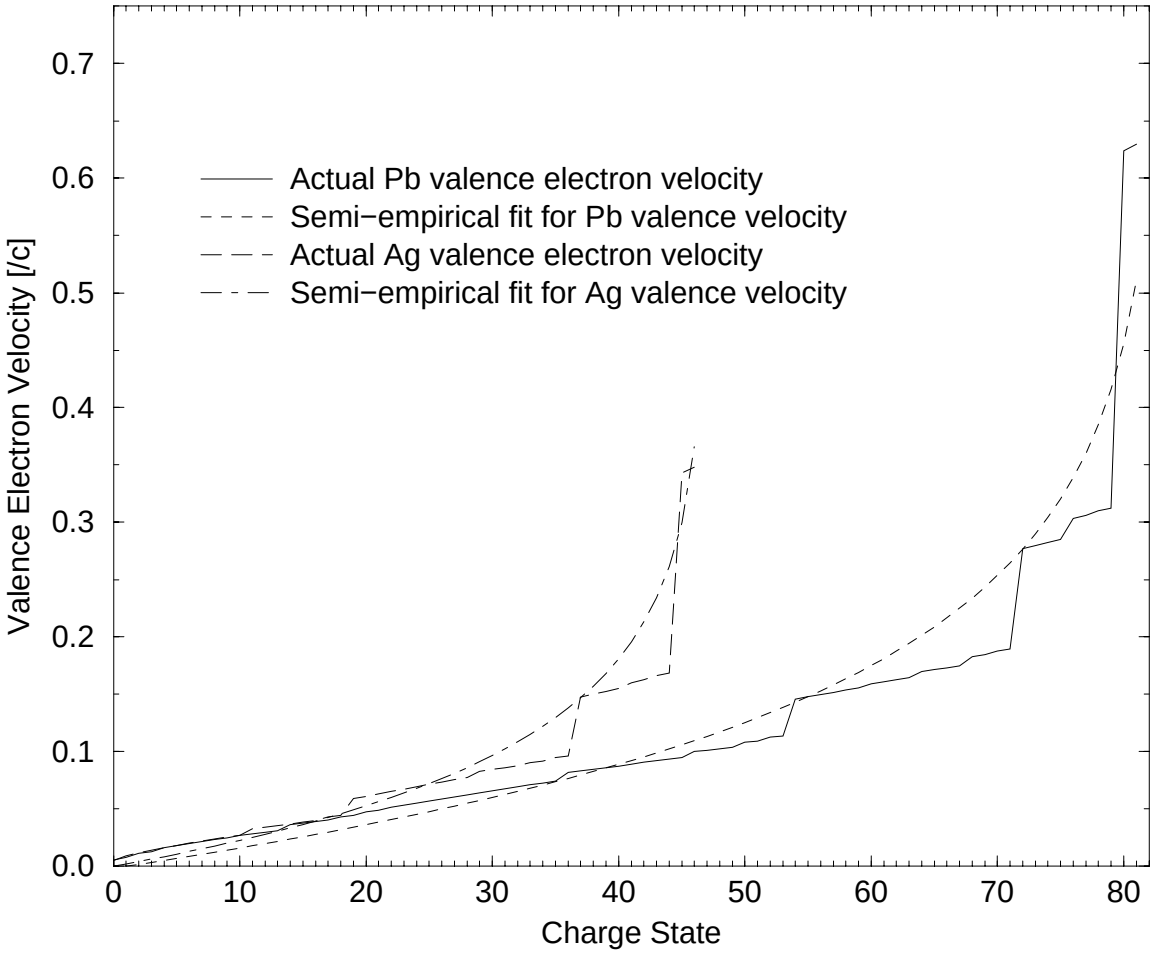

Figure 5.1: Valence electron velocities for all charge states of Pb and Ag, empirical and calculated from inverted Bohr formula

This actually is an accurate representation of the charge state dependence of a charged species' valence electron velocity. Figure 5.1 plots this function for the valence velocities of lead and for silver at all charge states Q (except for the fully-stripped cases, for which there are no valence electrons). Agreement is excellent, within about 25% over all charge states.

Note that a check for consistency can be made with the hydrogenic state of any ion. From the basic Bohr atom scaling, the velocity of the one electron in a hydrogenic ion with charge state $Q = Z - 1$, $v_v(Z, Q = Z-1)$, is given by (see section 3.1.2)

$$v_v(Z, Q = Z-1) = Z\alpha c. \tag{5.16}$$

But, from the above analysis this value should also be given by

$$v_v(Z, Q = Z-1) = v_1 \ln[Z]. \tag{5.17}$$

Substituting the explicit form of the Thomas-Fermi velocity v_1 gives

$$v_v(Z, Q = Z-1) = Z^{2/3}\alpha c \ln[Z]. \tag{5.18}$$

If the orbital velocity of a hydrogenic ion obtained from Bohr scaling should be equal to the value obtained from this new scaling, then the following identity can be stated:

$$Z^{2/3}\alpha \ln[Z] \approx Z\alpha \tag{5.19}$$

Is this observed to be true? Figure 5.2 displays the hydrogenic ion electron velocities for every species (excluding hydrogen) as calculated from the Rydberg scaling and the Thomas-Fermi logarithmic scaling which is produced from the semi-empirical fit. The agreement is

excellent. Note that this relationship is actually demonstrating that for Z values in this range,

$$\ln[Z] \approx Z^{1/3}. \tag{5.20}$$

Appendix B provides a brief analysis of the validity of this approximation in the regime of interest to this dissertation.

This valence electron velocity scaling will be employed later to develop a new semi-empirical fit for charge evolution of ions in partially-ionized targets.

5.1.2 Discrete Calculations

The primary goal of this dissertation involves the quantification of the charge-changing reactions which a projectile sustains while penetrating a variety of target types. These reactions can be divided into two categories:(1)ionization and (2)capture. In general, the atomic properties of a projectile species and penetrated medium are accounted and the various reaction rates are formulated based on a number of atomic theories. Ionization can result from collisions between a projectile's electrons and the target's nuclei, bound electrons and free electrons. Capture (or recombination) can occur by the transfer of electrons from the target atoms or ions onto the projectile or by the capture by the projectile of a free electron in the target.

The first discrete cross section developed was the ionization cross section for collision between an incident ion and a target nucleus. This was accomplished early on by Thomson [66] and then by Bohr [8]. After the revolution of quantum mechanics, Bethe reformulated ionization theory along with energy deposition theory [5]. Since that time, many

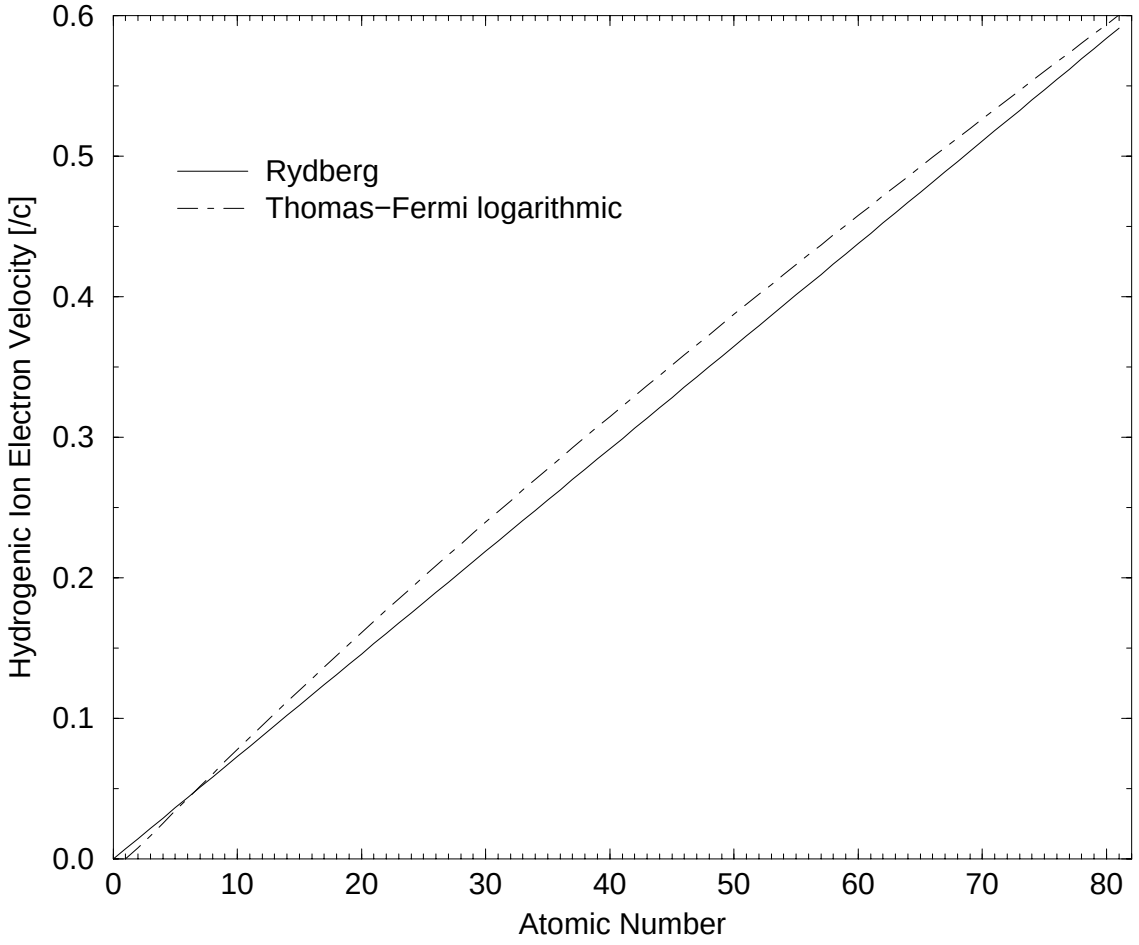

Figure 5.2: Electron velocities for hydrogenic ions of each species

other quantum and semi-classical approaches have been developed producing many associated ionization cross sections. Despite these decades of attention, no consistent formalism presently exists for a robust ionization model. The Bohr formula has been out-dated by principles of quantum mechanics. The Bethe expression was left in a form which included several terms which are difficult to calculate. The currently employed quantum and semi-classical models were once regarded as quite successful [54], but have been couched in doubt with the rebirth of interest in beam-plasma interactions.

This doubt about the modern approaches to calculating ionization cross sections has generated concern among HIF scientists and atomic physicists about the accuracy of the cross sections which they traditionally use for ionization calculations. Recent experiments have produced data which some have interpreted as indicating that one type of popular cross section model, the binary encounter model (BEM), underestimates by a factor of 2 or more the ionization cross section of beams penetrating plasmas [19]. An important component of this work is to investigate this issue and to develop a reliable ionization scheme.

5.2 The Ionization Problem and Indirect Ionizations

Over the past decade much attention in atomic physics, plasma physics and HIF circles has been directed to the problem of enhanced ionization of projectiles penetrating absorbing media. For regimes in which equilibrium charge state fits aren't applicable, individual cross sections have been assembled to form *ab initio* models for calculations of the charge state evolution of beams penetrating targets. What has been observed is that empirical ionization rates are often inconsistent with the reaction rates being predicted by

current models.

The problem in calculating ionization cross sections for ion beams incident on targets is due to a number of issues. First, the appropriate choice for an ionization model for a particular beam-target arrangement is not well defined. A wide array of ionization formulae have been developed since the time of Thomson. Today, it seems that every one which has ever been developed is still being cited. Moreover, it seems that every formula cited in one reference is elsewhere shown to be faulty. Compounding this is the re-emergence of a sensitivity to effects which change beam ionization rates even given a robust nominal ionization model. Even if an ionization formulation could be found which is reliable for a certain projectile-target configuration, changes in target ionization state or density introduce changes in the observed ionization cross sections which sometimes defy theoretical modeling. The ionization problem has manifested in at least two regimes which are of direct concern to HIF scientists.

5.2.1 Plasma Enhancement

Plasmas and cold targets each require their own associated set of ionization or recombination cross sections for incident ion beams. Enhanced ionization cross sections for beams penetrating plasma targets compared to the cross sections in the analogous cold gas targets were forecast by Nardi and Zinamon in 1982 [17]. This phenomenon has since been experimentally validated to an extensive degree. Comparing the energy deposition and charge state of an ion beam in a cold gas to the same gas in an ionized state reveals that the charge state of the incident beam is in general increased in the latter case [36]. Also, direct measurement of the charge states attained by beams penetrating plasmas has confirmed

that ionized targets induce greater beam ionization rates than non-ionized targets[19].

The reason for the enhanced charge states is understood as being due to several atomic processes. First, the charge transfer of bound electrons from the target to the incident ion which ordinarily serves to neutralize the projectile can be significantly reduced, particularly for nearly fully-stripped plasmas. Also, the reaction rates for free electrons in the target to recombine with the projectile are in general much lower than the rates for charge transfer of bound target electrons to the projectile. Another cause is due to the change in nuclear screening of the target constituents. Many ionization reactions will be shown to be a function of the square of the effective target nuclear charge sensed by the incident beam's electrons. If the target should be ionized, its nuclear charge may be screened less effectively and may contribute more to ionizing an incident ion.

However, even though considerable theoretical effort has been directed to develop a comprehensive modeling scheme to simulate this enhancement, some observed ionization cross sections baffle the atomic physics community. Ionization rates of beams penetrating plasmas have been shown to exceed that which the best models predict – sometimes by a factor of 2 to 3 [18], other times by a factor of over 10 [19]. These deviant ionization enhancements have been observed at projectile velocities near $\beta = 0.13$, which is close to the proposed HIF beam velocities of $\beta = 0.2$.

5.2.2 Enhanced Ionization in Cold Matter

Even when the target is not ionized, observed ionization cross section of incident beams can confound calculation. Shevelko *et al.* have investigated the cross sections for total ionization of a variety of species of projectile in a rarefied gas target [60]. They reported

that standard cross sections underestimate the actual ionization rates of ions penetrating cold gas targets whose density was near $10^6 cm^{-3}$. It was shown that the direct models often accounted for only about 70% of the total observed ionization. This underestimation is less severe than that of some plasma cases, but it merits attention nonetheless.

Similar calculations of the ionization of swift projectiles in dense foils have been performed and compared to experiment with no reports of significant problems [59],[32]. In some cases, second-order enhancement has been observed to occur in solid-density foils [27], but the total ionization cross section has not deviated from theory in a problematic way. The reason why rarefied gases (or plasmas) are more prone to enhanced ionization than dense targets is linked to the indirect ionization mechanism which is believed to be responsible. This is discussed in the following section and in section 7.1.3. The important point now is that rarefied gas targets, a characterization which may include HIF chambers, exhibit a particular type ionization enhancement.

5.2.3 Indirect Ionization Events

The observed levels of enhanced ionization in both plasmas and rarefied gas targets have been attributed to shortcomings in the simple direct ionization approach. The problem is that most ionization models are useful in calculating only the direct ionization of an electron from its ground state in the projectile. This does not address many of the other processes which can contribute to the total ionization rate of a beam penetrating a target.

Instead of simply causing ionization, an encounter between a beam projectile and a target particle can cause the projectile to form an excited electronic state. From this excited state, the projectile may execute either a direct ionization in a subsequent collision

with the target or an *auto-ionization*. These auto-ionization processes are also categorized generally as *indirect ionizations*. An auto-ionization or indirect ionization is the collisionless removal of an electron caused by energy transfer from an electron transition within the projectile. It is analyzed further in more detail in sections 5.5.3 and 7.1.3 [52],[60].

This complex behavior is not addressed in the standard direct ionization models. The problem is that in order to calculate these ionizations from excited projectile states, the electronic configuration of the excited state must be known. In a given collision causing excitation, a wide array of electronic arrangements may result. In order to quantify such processes it becomes necessary to employ more sophisticated computational techniques.

Monte Carlo Approaches

In an effort designed to address these indirect ionizations from excited states, advanced simulations have been undertaken by Olson *et al.* [52]. These calculations, known as CTMC for *computed trajectory Monte Carlo*, aim to solve the total Hamiltonian equations of the electrons of an atom or ion in collision. It, like the other atomic reaction models used here, is an independent particle model (IPM) in which each electron is treated separately with no collective effects. These calculations have been shown to agree well with the experimental results in some cases [19]. However, the CTMC results have been shown to underestimate severely the cross sections in a regime very close to that of HIF. Matsuo *et al.* [26] have performed calculations and measurements of ionization of several noble gases by impact with a 6MeV/u bare nucleus. The ionization of xenon predicted by the CTMC method is lower than experiment consistently by a factor of 2 to 4. The Monte Carlo methods currently employed do not enable a facile, desk-top calculation of charge state evolution

and energy deposition which is needed for many applications. The codes require months of operating time on parallel computing facilities. There is great motivation to develop a rapid and reasonably accurate desk-top approach to ionization calculations.

5.3 The Role of This Investigation

This dissertation explores the possibilities of vindicating the discrete cross section approach to calculating beam ionization cross sections. This will be accomplished by correcting problems in previous direct ionization cross section models and by establishing trends in enhanced ionization which can be adapted into new semi-empirical adjustive factors. The goal is the development of a quick and versatile charge evolution and energy deposition modeling system. The data suggesting that discrete ionization cross sections are in error will be re-examined also in order to ascertain the cause of enhanced ionization. The key component is a study of the set of reactions which characterize ionization or recombination in a projectile.

5.4 Ionization Reactions

By the same Coulomb collisions which are responsible for transfer of energy from a beam into an absorbing medium, attendant electrons may be removed from a traveling ion as it collides with the nuclei and electrons in a target material. This section outlines several standard ionization models and provides an analysis of their differences and applicability. The existence of such a variety of ionization models is testimony to the uncertainty associated with such a basic calculation as collisional ionization.

5.4.1 The Bohr Ionization Model

The Bohr ionization cross section was developed in 1948 in connection with Bohr's treatise on the interaction of particles and matter[9]. It is closely connected to the Thomson model [66]. It is based on classical collisional theory and therefore inherits the weakness of neglecting a full quantum mechanical treatment. However, it still enjoys some recent application [31]. It is instructive to re-derive the simplest form of the Bohr-Thomson formula from first principles. The energy transfer expression of equation 4.3 relates the impact parameter of a collision between a moving charge with an electron to the energy transferred to that electron. If the energy transferred is equated to the binding energy I_{nl} of a reactant electron of quantum numbers nl, then the associated impact parameter is that which achieves ionization.

$$\Delta E = I_{nl} = \frac{2Q^2e^4}{m_e v^2}\frac{1}{b^2}. \tag{5.21}$$

Interpreted as the radius of collision, that ionization impact parameter can be used to generate an equivalent ionization area, or cross section

$$\sigma = \pi b^2 = \frac{2\pi Q^2 e^4}{v^2 I_{nl} m_e} \tag{5.22}$$

Another, more complete form of the classical ionization cross section is derived from an integration of the differential cross section

$$d\sigma = \frac{2\pi Q_t^2 e^4}{m_e v^2}\frac{dT}{T^2} \tag{5.23}$$

in which T represents the energy transfer in a collision between the target charge and a projectile electron. Integration is performed over the maximum energy transfer $2m_e v^2$ and the minimum energy transfer necessary to achieve ionization of electron nl, I_{nl}. This

produces, with some substitutions from the Bohr atom vocabulary,

$$\sigma_B = 4\pi a_0^2 Q_t^2 \left[\frac{\alpha}{\beta}\right]^2 \sum_{nl} \left[\frac{\mathrm{Ry}}{I_{nl}} - \frac{1}{2\beta^2}\right]. \tag{5.24}$$

In the Bohr ionization formula above, a_0 is the Bohr radius, α is the fine structure constant and β is the projectile speed divided by c. The total cross section is given as the sum of those of the individual electrons.

5.4.2 Bethe Ionization

The ionization cross section due to Bethe is from his classic 1930 work [5] and was based on the Born approximation (see §3.3). It is closely related to the Bethe stopping power theory, but with the frames of the projectile and absorbing material reversed. In ionization, a projectile electron receives energy from the target nuclear charges and electrons into which it is advancing. The cross section for a projectile electron nl to be ionized is given by the Bethe form as

$$\sigma_{nl} = 4\pi a_0^2 \left(\frac{\alpha}{\beta}\right)^2 \frac{\mathrm{Ry}}{I_{nl}} Z_t^2 f_{nl} \ln\left[\frac{4\beta^2\gamma^2/\alpha^2}{C_{nl} I_{nl}/\mathrm{Ry}}\right] \tag{5.25}$$

where $C_{nl} \approx 0.048$ for the hydrogenic case [32]. The f_{nl} term is related to the oscillator strength of the bound-free transition from shell n to the continuum (see section 3.1.7).

The problem with applying this formulation is the large degree of uncertainty associated with the factors f_n and C_n. Bethe himself in the classic 1930 work was only able to express the C_n term to '*etwa Zehnerpotenz kleiner*', or about a factor of 10 smaller than the respective binding energy for multiple-electron systems. Tabulations have been made of some values of the associated terms, but a simple formalism does not exist for broad application over different projectile species and ionization states.

5.4.3 PWBA Models

Based on calculations similar to that of the Bethe expression is a class of ionization models known as PWBA (plane wave Born approximation) models. They treat the wave function of the incident and scattered waves in a simplified manner as described in section 3.3. Some prominent PWBA models are due to Merzbacher and Lewis [46] in 1958 and by Hansteen *et al.* in 1975. Many other analyses of this model have been conducted and the literature is replete with references.

The seminal equation of PWBA models is the Born integral expression for the ionization cross section of an electron nl in a projectile ion [25]

$$\sigma_{nl} = \frac{8\pi a_0^2 \overline{Z}_t^2 \alpha^2}{\beta^2} \int_0^\infty d\epsilon \int_{q_0}^\infty \frac{dq}{q^3} |F(q)|^2 \tag{5.26}$$

in which ϵ represents the kinetic energy of the ionized electron and and q is the momentum transfer of the collision. $\overline{Z}_t$ has its usual meaning as the target nuclear charge and β is the projectile velocity divided by c. The form factor $F(q)$ is the inner product of

$$<\vec{\epsilon}| \exp(i\overline{q} \cdot \overline{r})|\vec{nl}> \tag{5.27}$$

where $\vec{\epsilon}$ and $\vec{nl}$ represent the wave functions of the ionized continuum electron and the initial bound electron nl respectively. This expression is often parameterized more conveniently as

$$\sigma_{nl} = 4\pi a_0^2 \alpha^2 \overline{Z}_t^2 \frac{1}{\beta^2} \frac{1}{\overline{Z}_{nl}^2} f(\eta_{nl}, \theta_{nl}). \tag{5.28}$$

In the above form η_{nl} is the square of the ratio of the projectile velocity v to the orbital velocity of the electron to be ionized v_{nl}

$$\eta_{nl} = \frac{v^2}{v_{nl}^2}, \tag{5.29}$$

and θ_{nl} is a measure of the screening constant for a particular electron, representing the ratio of the actual ionization potential to the value calculated by scaling the Rydberg value using the bare nuclear charge. $\overline{Z}_{nl}$ is the screened nuclear charge of the projectile atom or ion as perceived by electron nl.

The values of the function $f(\eta_{nl}, \theta_{nl})$ which are the solutions to this integration have been tabulated in various references [35]. The PWBA models are then implemented by selecting the appropriate tabulated value for the particular electron nl to be ionized. Note that such PWBA approaches are not simply functions of the ratio of the projectile velocity v to the orbital velocity v_{nl}. Like the Bethe formula, the PWBA cross sections require particular values for each different shell for different species.

5.4.4 Binary Encounter Models

A semi-classical alternative approach to the Born-based calculations has been developed which offers a simplified application. These schemes are known as *binary encounter models* (BEM) and were articulated first by Gryzinski [34] and Garcia [30] in the late 1960s. Additional lasting work towards their development was performed by Vriens [68]. Calculations based on this model employ a simplified two-body Coulomb scattering cross section for the target charge's collision with the projectile electrons. The exact analytical form of the binary encounter models will be derived. The most general form will then be analyzed qualitatively to develop an understanding of the origin and scaling of the terms involved.

BEM Form and Velocity Matching

The exact form of the binary encounter model formula has appeared in several manifestations. They are distinguished by their different functional dependences on the velocity of the projectile and the orbital velocities of its electrons. The nature of the velocity dependence and the exact BEM ionization cross section formula itself are derived as follows.

The differential binary Coulomb cross section on which the BEMs are based is most generally expressed as $d\sigma_C(v, v_2, dE)$. In this, v is the incident velocity of the ionizing agent, v_2 is the instantaneous velocity of the projectile's orbital electron to be ionized and dE is the energy transfer in the collision. While the electrons in an atom or ion are generally treated as having one characteristic velocity v_{nl}, they indeed can exhibit a spread in velocity distribution. This velocity distribution function is expressed by $\rho(v_2, v_{nl})$ such that

$$\int_0^\infty 4\pi v_2^2 \rho(v_2, v_{nl}) dv_2 = 1. \tag{5.30}$$

The total cross section is generated by integrating over the range of electron velocities and energy transfer values

$$\sigma(v, v_{nl}) = \int_0^\infty \int_{E_{min}}^{E_{max}} 4\pi v_2^2 \rho(v_2, v_{nl}) \sigma_C(v, v_2, dE) dv_2 dE \tag{5.31}$$

in which E_{min} is the binding energy I_{nl} of the electron in question and E_{max} is the kinetic energy of the ionizing agent in the frame of the projectile atom or ion.

The choice of projectile electron velocity distribution distinguishes among the different models. Several analytical expressions have been used and success has even been reported using a δ distribution for the projectile's electrons' velocities [40]. The first use-

ful algebraic solution to this integration was performed by Gryzinski using a hydrogenic velocity distribution [34]

$$\rho(v_2, v_{nl}) = \frac{8}{\pi^2}\frac{v_{nl}^5}{(v_{nl}^2 + v_2^2)^4}. \tag{5.32}$$

The resultant cross section for the ionization of electron nl in the projectile appears as

$$\sigma(V) = \pi e^4 \overline{Z_t}^2 \frac{1}{I_{nl}^2} \mathrm{G}[V] \tag{5.33}$$

in which G$[V]$ is a function of the scaled velocity $V = v/v_{nl}$. The algebraic form of this velocity function is as follows [34]. If $V = \frac{v}{v_n} > 0.206$ the value is given by:

$$\mathrm{G}[V] = \frac{\alpha^{3/2}}{V^2}\left\{\alpha + \frac{2}{3}(1+\beta)\ln[2.7+V]\right\} \times (1-\beta)(1+\beta^{1+V^2}) \tag{5.34}$$

with

$$\alpha = \frac{V^2}{1+V^2} \tag{5.35}$$

and

$$\beta = \frac{1}{4V(1+V)}; \tag{5.36}$$

for $V < 0.206$ the velocity-matching function is simply

$$\mathrm{G}[V] = \frac{4V^4}{15}. \tag{5.37}$$

This function is plotted in figure 5.3. Note that the maximum occurs at a scaled velocity of $V = 1$. This indicates that maximum ionization of an electron nl is achieved at a collision velocity equal to v_{nl}.

The term $\overline{Z_t}^2$ is the effective screened target nuclear charge perceived by the individual electron nl. Its determination is discussed in the following section. The power this type of cross section expression is that it does not in principle depend explicitly on

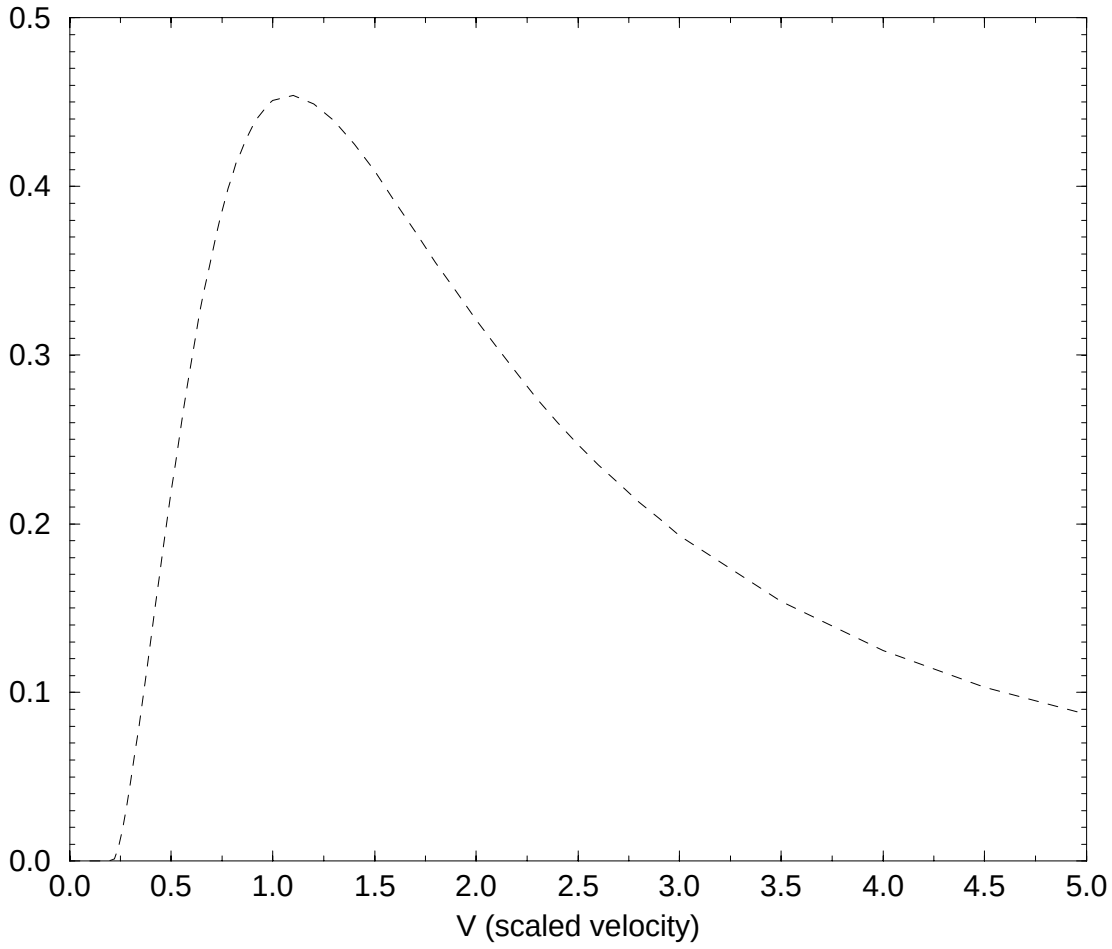

Figure 5.3: The Gryzinski velocity function

the individual velocities of the projectile and electrons, but only on their ratios. Therefore, regardless of the quantum numbers or screening constant of the projectile electron to be ionized, the ionization cross section is sensitive only to the ratio of the projectile velocity v to the orbital velocity v_{nl} of the electron to be ionized. This presents a significant advantage to the PWBA models which require adjustments for individual shells and sub-shells incorporating tabulated values.

Screened Impact Parameter

The final form of the BEM cross section generated by Gryzinski

$$\sigma(V) = \pi e^4 \overline{Z_t^2} \frac{1}{I_{nl}^2} \mathrm{G}[V] \tag{5.38}$$

requires accounting of the screening of the ionizing target charge by its bound electrons. The nature of this screened charge term can be understood through a qualitative examination of the binary encounter ionization cross section.

In a Coulomb collision between an electron nl and a charge Z_t, the energy transfer is given by equation 4.3. The maximum energy transfer allowable by collisional mechanics is

$$\Delta E_{max} = 2 m_e v^2. \tag{5.39}$$

Classically, the cross section for removing a projectile electron nl scales as the area generated by the impact parameter at which this maximum energy transfer equals the binding energy of the electron I_{nl}. Using equation 4.3 explicitly, this is expressed as

$$\Delta E_{max} = 2 m_e v^2 = \frac{2 Z_t^2 e^4}{m_e v^2} \frac{1}{b_{min}^2} \tag{5.40}$$

where b_{min} is the impact parameter of the collision at which this maximum energy transfer occurs. Equating $2m_e v^2$ to I_{nl} and solving for b_{min} gives

$$b_{min} = \frac{2Z_t e^2}{I_{nl}}. \tag{5.41}$$

This analysis, which ignores dependence on the collision velocity, actually provides insight to the scaling of the Gryzinski form. The cross section given by this model would be $\sigma \approx \pi b_{min}^2$. Using the above form of the impact parameter gives a cross section very similar to the exact BEM form

$$\sigma \propto \pi e^4 \frac{Z_t^2}{I_{nl}^2}. \tag{5.42}$$

Velocity matching is not included, of course. This also is the general scaling of the PWBA ionization cross section as presented in reference [59].

The effective target charge term in the actual BEM cross section formula is solved simultaneously with the impact parameter as the solution to a classical Coulomb balance. The impact parameter for electron nl is given by

$$I_{nl} = \frac{\overline{Z}_t(b_{nl})e^2}{b_{nl}}. \tag{5.43}$$

Solving for b_{nl},

$$b_{nl} = \frac{\overline{Z}_t(b_{nl})e^2}{I_{nl}}. \tag{5.44}$$

The impact parameter b_{nl} is measured from the center of the target nucleus. $\overline{Z}_t(b_{nl})$ is the effective screened charge of the target nucleus experienced by the projectile electron in nl as it penetrates the electron distribution of the target atoms and ions. It is a function of the amount of screening of the target's nuclear charge by the electronic density within a

sphere defined by radius b_{nl}.

$$\overline{Z}_t(b_{nl}) = Z_t - \int_0^{b_{nl}} n(r) d^3r \tag{5.45}$$

in which $n(r)$ is the electron density about the typical target nucleus. This density is calculated according to the approach outlined in section 3.1.5. The simplified exponential screening model developed there will be used to generate all of the target electron density distributions required for the cross section calculations.

5.4.5 Ionization Adjustments

The performance of the ionization models will be analyzed in section 5.7, but some important preliminary issues are addressed here.

Ionization Potential Correction

It has been noted that even for the most simple example of hydrogen ionization by proton impact, the BEM and PWBA models fail to model the ionization cross section [25],[40]. The cross section peak predicted by the BEM velocity matching at $V = 1$ is not experimentally observed. The idealized proton energy which would produce the maximum cross section is $E_p = (m_p/m_e)13.6\text{eV} \approx 25\text{keV}$. What is observed is a maximum near 50keV. The same misalignment occurs even for higher-Z hydrogenic ionizations. Anholt *et al.* reported that the peak in the ionization of hydrogenic xenon occurs near a value of twice the expected value in collisions with gaseous xenon.

The reason for this apparent miserable failure is the nuclear charge enhancement due to the presence of the incident proton [40],[69]. In the course of a close collision, such

as those involved in K-shell ionization, the ionizing charge (here a proton) may actually pass within an approximate sphere defined by the ionized electron's orbital radius. The presence of the ionizing charge near the nuclear center of the ionized atom or ion actually temporarily increases the effective nuclear charge perceived by the electron to be ionized. In this case, the total effective charge Z' perceived by the electron would be

$$Z' = Z - S_{nl} + f Z_t \tag{5.46}$$

in which Z is the ionized ion's nuclear charge, S_{nl} is the screening constant for the electron and Z_t is the nuclear charge of the ionizing agent. f is an occupation fraction representing the fraction of the collision for which the nuclear superposition occurs. Given that the close K-shell collision can occur with equal probability on either side of the electron (nuclear side or continuum side), a value of $f = 0.5$ is reasonable.

This change in effective charge results in a change in the effective orbital velocity of the electron. Using the Bohr velocity scaling for the adjusted orbital velocity of a K-shell ($n = 1$) electron gives

$$v' = Z'\alpha. \tag{5.47}$$

This will cause an increase in effective velocity of the ionized electron which causes the peak to shift to a value higher than the actual orbital velocity. Using this adjustment, K-shell ionization can be calculated and matched to experimental data [40].

Note that this effect should only be an issue for ions in which the K-shell ionization cross sections dominate the total cross section. Since this dissertation is focused on the atomic physics of heavy ions with many electrons, this effect will not be important. It is important to address to demonstrate that some of the apparent glaring problems of the

BEM formulae are actually well understood and correctable.

Non-ideal Target Charge Dependence

Another important adjustment is due to non-ideal functionality of the target effective charge. In all of the ionization cross sections presented here the effective charge of the ionizing agent has appeared in quadratic dependence, $\overline{Z}_t^2$. However, in the ionization formulae based directly on the Born approximation, such as the Bethe and PWBA expressions, this behavior is found not to represent nature well in some cases [26]. The breakdown point is linked to the breakdown of the Born approximation as applied to the ionizing system. As discussed in section 3.3 and following Matsuo *et al.*, the criterion for PWBA applicability to collision between a bound electron and an ionizing charge q at velocity v is

$$v > 2q\alpha c. \tag{5.48}$$

When the velocity is lower than this value for a given charge q, the perturbation technique on which the Born-type analyses are made is violated. In this scenario the Born violation manifests as a deviation of the functionality of the ionizing charge from the ideal q^2 behavior.

In experiments investigating this effect, Matsuo and his colleagues studied the ionization of various neutral atoms by impact with bare nuclei with energies of $6\mathrm{MeV}/u$. The nuclei ranged from helium to argon. In their analysis they parameterized the functionality of the ionizing charge as $\overline{Z}_t^{\mu}$, where $\mu = 2$ in the ideal cross section behavior. It was observed that as the charge of the bare nucleus increased to argon, the observed value of the exponent μ changed from near 2 for helium to 1.88 for argon. A recommendation for correcting for this effect is given in reference [26].

5.4.6 Free Electron Ionization

While the bound electrons and target nuclei ionize a beam as detailed in section 5.4, any free electrons in the target contribute to the ionization in a different manner. This is due to the different kinematic properties which free electrons exhibit in collisions. Since the electron mass is much less than that of a nucleus, the velocity dependence of the ionization cross section due to free electron impact will exhibit a different functionality.

This free electron ionization may be particularly important to study since the greatest levels of enhanced ionization have been observed in plasmas [19]. The only significant difference between cold target ionization and plasma ionization aside from the differently-screened target nuclei and remaining bound electrons should, in principle, be the free electron contribution.

For most modeling efforts of swift, non-relativistic heavy ions penetrating plasmas, the Lotz free electron ionization formulation has been employed [54]. The Lotz expression is basically identical to the original Bethe ionization cross section. The ansatz which Lotz followed is that the ionization caused by an electron impact exhibits a functionality similar to ionization by a collision with a nuclear charge. An important kinematic distinction must be made, however. A free plasma electron in the target, by conservation of momentum, is only able to ionize an electron in the projectile whose orbital velocity is less than the projectile velocity, which is approximately equal to the velocity of the incoming plasma electron in the projectile's frame. A target nucleus, being at least 1837 times heavier than an electron, is able to ionize even at velocities lower than the collision velocity.

Lotz extracted from the Bethe formulation a simplified functional dependence of

projectile velocity and ionization potential which features a cut-off at $v = v_{nl}$. The resultant expression is

$$\sigma_{nl} \approx \frac{a_1}{E_k I_{nl}} \ln[E_k/I_{nl}] \tag{5.49}$$

in which a_1 represents the unknown structural and empirical term. The maximum of the Lotz function occurs at $E_k = eI_{nl}$ where e here is Euler's constant.

Experimental data were used to determine the appropriate semi-empirical terms. This is essential since the Bethe ionization equation and thus the Lotz formula are formulated chiefly for hydrogenic ions. For ions of other species, the atom-specific terms are uncertain. The fitted terms in the Lotz or Bethe equations are not just some arbitrary factors introduced to compensate for poor modeling. They represent a determination of at least two unknown parameters which are inherent in the formulation and which represent important electronic structural information. The fitted terms may also be used to incorporate extra indirect ionization processes. This cross section is versatile enough to accommodate them and its semi-empirical nature reasonably allows such fitting.

In Lotz' work, experimental data from the ionization of many neutral atomic species by electron impact were analyzed. Additionally, ionization cross sections were obtained from species ionized to a charge state of +1. This ionization of already-charged species exhibited a functionality consistent with that of the neutral species. A general cross section was thus developed with the following constant:

$$\sigma_{nl} \approx \frac{4.0 \times 10^{-14}\text{cm}^2\text{eV}^2}{E_k I_{nl}} \ln[E_k/I_{nl}] \tag{5.50}$$

This form of the Lotz formula and in particular this constant value of 4.0×10^{-14} has been cited widely.

Deviations in Highly-Charged Ions

As is often the case with semi-empirical physics, a formula such as the Lotz expression is tested in a few cases and its success is extrapolated to others. While the Lotz formula is valid for ionization of neutral or +1 species, experimental studies have since demonstrated a deviation which was not foreseen by Lotz or by those who have implemented his formula. The Lotz ionization cross section formula (equation 5.50) deviates quite significantly from experiment when applied to ionization of more highly-charged ions.

Stenke *et al.* reported measurements and analysis of the electron impact ionization of W^{q+}, where $q = 1...10$ [50]. This is especially relevant to this HIF study since the atomic number of tungsten is near to those being considered for driver beam ions. For most every charge state q examined the observed cross sections are significantly higher than those predicted by the original Lotz fit at certain electron velocities. Specifically, the measured cross sections deviate from theory most prominently at electron velocities near or below the theoretical cross section function's peak at

$$V = v/v_{nl} \tag{5.51}$$

where v is the electron velocity and v_{nl} is the orbital velocity of the electron in the tungsten to be ionized. At velocities such that $V < \sqrt{e}$, the observed cross sections are larger than the respective theoretical values by a factor typically between 8 and 16. Around the peak at $V \approx \sqrt{e}$ the data can exceed theory by about a factor of 2. At velocities much larger than the peak velocity the agreement improves and observed cross sections match those given by the Lotz formula.

Gregory and Crandall [33] have provided similar measurements of the ionization

of Xe^{6+}. Their data reveal a total electron impact ionization, including ionization from excited states, which is at times a factor of 10 higher than the Lotz value at low collision velocities and as much as a factor of 4 higher at the peak of the velocity dependence $V \approx 1$.

The net effect of these deviations in many instances is to reduce the value of the energy at which the Lotz function attains a maximum and to increase the value of that maximum cross section.

The cause for this deviation is likely to be ionizations from excited states and indirect auto-ionizations. Neither are addressed in the Lotz formula which calculates only direct ionization from ground state. As is evident, the Lotz formula can *not* be simply used as it has been, as a universal ionization formula for all projectile species and charge states. It must be adjusted for each charge state and to include accounting of ionization from excited states. *This adjustment has not previously been incorporated in beam charge state evolution studies relevant to HIF.*

This error alone could be responsible for many of the miscalculations of enhanced ionization in plasmas. This analysis will be pursued further in Chapter 7. In the experiments producing anomalously high ionization data, primarily at GSI, the projectiles have been generated with initial charge states ranging from +10 to +40 [19]. The Lotz formula as presented was not empirically calibrated for such high ionization states, but in most recent applications the specifically-generated empirical term of 4.0×10^{-14} of equation 5.50 has been used as a universally applicable constant [54]. Additionally, since the experiments have involved highly charged heavy ions at energies of several MeV/u, the gross ionization cross sections are dominated by individual electron cross sections near the peak of the

Lotz function where deviations have been observed. For instance, in the GSI experiment involving Au^{28+} at $8.6\text{MeV}/u$ [19], the ratio of the projectile velocity to the electrons' orbital velocities ranges from 0.25 to 2.5.

5.4.7 Lotz, Gryzinski and High V

The Bohr, Bethe, PWBA, BEM and Lotz formulae each bear their own functional dependence on the projectile and electron orbital velocities. However, independent of all modeling, one empirical point remains solid. It is observed and supported analytically that at beam-target collision velocities much higher than the beam projectile's orbital velocities, the dependence of the ionization cross section on velocity approaches a uniform ionization energy and velocity functionality [24]. This behavior is identical for all ionizing agents, whether they be electrons or screened atomic nuclei. The unified cross section functionality at high scaled velocities $V \equiv v/v_{nl}$ is typically expressed as

$$\sigma_{nl} \propto \frac{1}{I_{nl}} \frac{\ln[E]}{E} \tag{5.52}$$

where E is the kinetic energy of an electron traveling at the same speed as the projectile (or incident ionizing agent in the reversed frame) and I_{nl} is the ionization potential of the electron to be ionized in the projectile.

This expression is actually just a high-velocity approximation of the actual Bethe-type logarithmic dependence

$$\sigma \propto \frac{\ln[E/I_{nl}]}{EI_{nl}}. \tag{5.53}$$

For $E \gg I_{nl}$, which to say $v \gg v_{nl}$, this can be reduced by

$$\frac{\ln[E/I_{nl}]}{EI_{nl}} = \frac{(\ln[E] - \ln[I_{nl}])}{EI_{nl}} \approx \frac{\ln[E]}{EI_{nl}}. \tag{5.54}$$

In this non-reduced form, this functionality is seen to be identical to the Lotz ionization formula. Indeed, it was this behavior which Lotz guessed would model electron ionization properly.

The original non-reduced functionality and the Lotz function itself can be re-expressed in another useful way using the scaled velocity $V \equiv v/v_{nl}$, or $V^2 = E/I_{nl}$ as

$$\frac{\ln[E/I_{nl}]}{E\,I_{nl}} = \frac{1}{I_{nl}^2}\frac{\ln[E/I_{nl}]}{E/I_{nl}} \tag{5.55}$$

or,

$$\sigma_{nl} \propto \frac{1}{I_{nl}^2}\frac{\ln[V^2]}{V^2} \tag{5.56}$$

Note that from this analysis, the high-velocity dependence and thus the Lotz ionization function can be expressed in the same simple terms as the BEM formula. The functionality of the scaled velocity can be separated from the inverse-square ionization potential term producing a cross section of the form

$$\sigma_{nl} \propto \frac{1}{I_{nl}^2} f(V). \tag{5.57}$$

Let us explore this BEM-Lotz similarity a bit further. The general form of the BEM ionization cross sections were shown to be (see equation 5.33)

$$\sigma(V) = \pi e^4 \overline{Z_t^2}\frac{1}{I_{nl}^2}\mathrm{G}[V] \tag{5.58}$$

The constant πe^4 can be rewritten by using some Bohr-atom substitutions:

$$\pi e^4 = \pi \left(\frac{e^2}{a_0}\right)^2 a_0^2 \tag{5.59}$$

and

$$\mathrm{Ry} = \frac{e^2}{2a_0} \tag{5.60}$$

give

$$\pi e^4 = 4\pi a_0^2 \mathrm{Ry}^2 \approx 6.5 \times 10^{-14} \mathrm{cm}^2 \mathrm{eV}^2 \tag{5.61}$$

Compare this to the Lotz function

$$\sigma_{nl} = 4.5 \times 10^{-14} \mathrm{cm}^2 \mathrm{eV}^2 \frac{1}{I_{nl}^2} \frac{\ln[V^2]}{V^2}. \tag{5.62}$$

The general forms of these two functions differ only by a factor of 0.615. In other words, the Lotz function can be written in the same general form as the BEM function

$$\sigma_{nl} = \pi e^4 \left[0.615 \frac{\ln[V^2]}{V^2} \right]. \tag{5.63}$$

The only difference in the two is presumably their V functions.

This can be examined further. Given that at high velocities the behavior of the models all should merge, it may be illuminating to compare the Lotz cross section and the BEM cross section to examine the nature of their behaviors at high V. Figure 5.4 displays the Gryzinski velocity dependence function and the Lotz velocity dependence extracted from the form above. Indeed, at high scaled velocities the two functions merge. The primary difference is the location of their respective peaks and cut-off values. The Lotz function exhibits a cut-off at $V = 1$. This is expected from conservation of momentum. A target electron can only ionize a bound projectile electron if its velocity relative to the projectile is greater than the bound electron's orbital velocity. However, the Gryzinski model is meant to be applied to nuclei which, by virtue of their larger mass, can ionize below this cut-off.

This type of ionization functionality is powerful in its simplicity It requires no shell-by-shell adjustments as the PWBA models do. The cross section for ionization of electron nl is a function only of the relative velocity v between the projectile and target

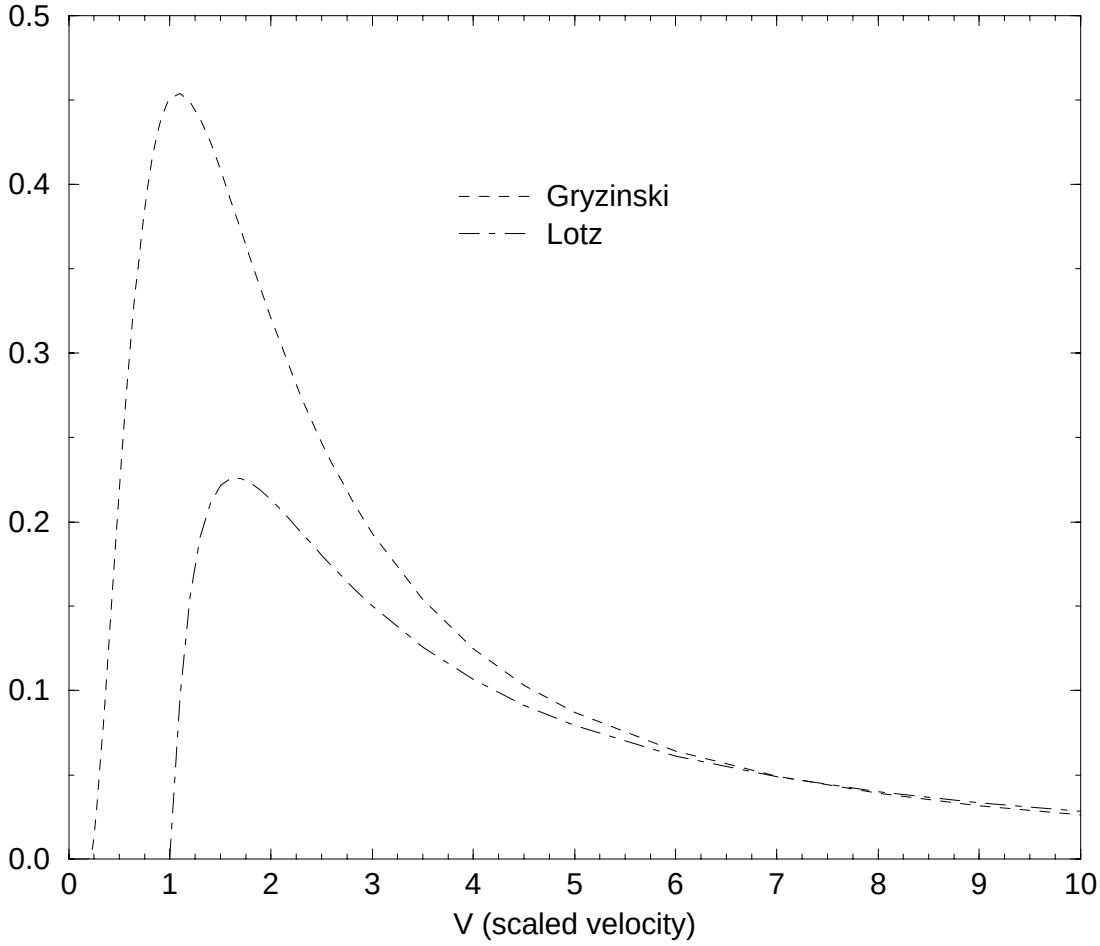

Figure 5.4: Unified scaled velocity functionalities for Gryzinski and Lotz ionization cross section models; $V \equiv v/v_{nl}$

and the orbital velocity of the electron to be ionized v_{nl}. The performance of these models will be examined more in section 5.7.

5.4.8 Ionization by Bound Electrons

The above ionization expressions addressed only the target nuclear charge contribution and the free electron contribution to the ionizing collision. However, the bound electrons of a target atom or ion also contribute to the ionization cross section. What is the associated velocity dependence of the ionization caused by bound electron impact?

Following Bethe [5] and Scheidenberger *et al.* [59], the contribution of target bound electrons to the total ionization cross section can be incorporated by replacing the effective target nuclear charge $\overline{Z}_t^2$ with

$$\overline{Z}_t^2 + (Z_t - Q_t) \tag{5.64}$$

where Q_t is the average charge of a target ion and $Z_t - Q_t$ is the number of bound electrons remaining on the target ion.

The physical reason for this can be understood from the scaling behavior of the ionization cross sections. They each are functions of the square of the ionizing charge. The square of the electron's charge is unity, but it contributes $(Z_t - Q_t)$ times to the cross section. The total bound electron contribution is just $(Z_t - Q_t)$ times this cross section and is added to the nuclear term with the $\overline{Z}_t^2$ coefficient.

However, a subtlety must be addressed here. Do bound electrons ionize as free electrons or as a massive nuclei? Does the fact that they are bound alter the properties of their ionizing cross sections? Including them with the target term as indicated above

suggests that they generate the same ionization cross section as the target, aside from the squared charged factor.

The issue is not clearly resolved. For instance, why is beam ionization in hydrogen plasmas so different from the ionization in cold hydrogen gas? The free plasma electrons certainly behave differently than when bound. In this analysis the bound electrons will be included in the total charge in the manner following Bethe, though the issue merits some future development beyond the scope of this dissertation.

5.4.9 Addressing Indirect Ionization

So far, all of the discrete ionization models described have been direct ionization models and have not addressed the ionization problem described in section 5.2. The challenge is to determine trends in data to establish an understanding of when the indirect processes are important. If they should be determined to be important for this present study then a semi-empirical adjustment will be sought to avoid the need for time-consuming and costly Monte Carlo calculations.

The preceding investigation of the Lotz ionization problem helps to clarify the state of affairs. Also, the extensive work of Shevelko finding enhanced ionization in rarefied gases establishes the general magnitude of the non-plasma ionization effects.

Cold Gases

Shevelko *et al.* reported ionization cross sections of beams penetrating extremely rarefied cold targets with density $n \approx 10^6 \text{cm}^{-3}$. Measurements were taken with a beam ion species range from magnesium to uranium and over initial charge states ranging from

1+ to 29+. The conclusions suggest that the indirect ionization contribution to the total ionization cross section is consistently near 40% of the direct ionization contribution for charges greater than 1+ (meaning that the direct contribution is only 70% of the total). The total is then near a factor of 1.4 greater than the direct value. Ionization cross sections for electron impact of singly-ionized species exhibited no noticeable deviation from direct modeling according to the Lotz formula. This factor of indirect ionization contribution of 1.4 seems to be consistent across a wide range of beam energies, from 0.2MeV/u to 12MeV/u.

A sensible approach would be then to multiply the direct ionization cross section by a factor of 1.4 for projectile ions whose charge state is greater than 1+ when penetrating a gas.

Plasmas

Indirect ionization contributions to the total ionization cross sections of beams penetrating plasmas, however, can not be approximated with such facility. The departure of empirical ionization cross sections from the Lotz formula does seem to begin at charges greater than 1+, but the nature of the departure is more complex. Enhancements as high as a factor of 6 or 10 have been reported, combined with a change in the velocity-dependence of the ionization. Also, at beam-target collisional velocities high relative to the beam's electron orbital velocities the enhancement is reduced and the Lotz theory begins to match experiment.

Rather than attempting to fit all of the diffuse empirical data of electron impact ionization cross sections for multiply-charged ions, a simple empirical approach can be em-

ployed. A general trend can be developed in the deviations of the experimentally determined cross sections from the Lotz formula (see section 5.4.6). First of all, the deviations from ionization cross sections predicted by the Lotz formula were only noted in target species (corresponding to beam species in the usual frame of reference) with charge states greater than 1. The enhancement of Lotz ionization was observed in these charged ions at electron beam energies near or lower than the valence energies of the ion. This energy range corresponds to a range of scaled velocity $V \equiv v/v_{nl} \leq \sqrt{e}$, where v_{nl} is the orbital velocities of the valence electrons of the species to be ionized. Recall that the value $\sqrt{e}$ originates as the maximum of the function $\ln[V^2]/V^2$, which is the velocity dependence of the free electron ionization cross section. Ionization by collision with a heavy nucleus has a peak in its cross section at $V = 1$.

In this regime, the observed ionization cross sections due to electron beam impact exceeded the Lotz cross section by near a factor of 2 at beam energies such that $V \approx \sqrt{e}$ and by a factor of over 10 when $V \ll \sqrt{e}$. Note that these trends are certainly not uniform and have been observed to vary for different target ions and charge states [50],[33]. But, these empirical factors can be used as a starting point for an attempt to adjust the Lotz formula to achieve better agreement with experiment. This empirical adjustment scheme will be applied in section 5.7.1.

5.4.10 Multiple Ionizations

In the ionization models detailed above, each individual electron on an incident ion is treated independently and each electron is characterized by its own ionization cross section. Given all of the N electrons' cross sections, a total cross section can be generated

by summation

$$\sigma_T = \sum_{i=1}^{N} \sigma_i. \tag{5.65}$$

This total cross section is useful in forming a net mean free path for an incremental charge change to occur

$$\ell = \frac{1}{n\sigma_T}. \tag{5.66}$$

But, the collision between an incident ion and a target particle may produce not just one incremental ionization but several in one collision. This is distinct from enhanced ionization; it is a probabilistic and collisional issue inherent to all ionization reactions in atoms or ions with more than one electron. Imagine the incident ion to be represented by a geometrical area defined by the maximum likely impact parameter. This collisional impact parameter is related to the orbital radii of the individual electrons. A colliding charge will penetrate this area, reacting with any number of bound electrons. The gross probability P of any reaction to occur in a single collision with an atom or ion can be interpreted as the cross section for the reaction σ divided by the impact area of the collision πb^2

$$P \approx \frac{\sigma}{\pi b^2} \tag{5.67}$$

This quantification can be understood by visualizing a target particle passing through the incident ion's impact area. If the cross section for ionization be very small relative to the impact area, an ionization event is not very likely in a single collision. If the cross section is near the size of the impact area then each collision will be more likely to produce an ionization.

For an atom or ion containing more than one electron, a collision with a target charge may induce an ionization of more than one electron. The degree to which this

can occur is roughly related to the probability defined above. The probability of a double ionization is proportional to P^2, the square of the ionization probability. A probability for triple ionization should be near P^3, and so forth.

A detailed analysis can be used to formulate a more rigorous treatment of multiple ionizations. Each electron i in a beam projectile has an associated reaction probability defined by its impact parameter and its cross section for ionization. This probability is a function of the impact parameter of collision. Imagining the atom or ion as an impact area defined roughly by its constituent electrons' orbital radii, a collision probability will be highest within each electron's individual area, but will vanish far beyond it. A useful approximation given by Kessel [39] is to treat the distribution of reaction probability as a step function, with a constant value within some scaled impact parameter and zero outside of it. A useful scaled maximum impact parameter b_i for a given electron was found by Kessel [39] to be

$$b_i = \sqrt{2} r_i \tag{5.68}$$

where r_i is the electron's scaled Bohr radius. With this value for the maximum parameter, the step-approximated ionization probability would be

$$P_i(b) \approx \frac{\sigma_i}{\pi b_i^2} \tag{5.69}$$

for $b \leq b_i$ and zero for $b > b_i$.

In order to calculate the single and multiple ionization probabilities, a combinatorical assessment must be made of the ensemble. The probability that *only* electron i will

be ionized at a certain impact parameter is

$$ {}^{i}P(b) = P_i(b) \prod_{j \neq i} (1 - P_j(b)) \tag{5.70} $$

The probability ${}^{I}P(b)$ that only one, but any one electron will be ionized in a collision is

$$ {}^{I}P(b) = \sum_i P_i(b) \prod_{j \neq i} (1 - P_j(b)). \tag{5.71} $$

The probability that two electrons i and j will be ionized at a certain impact parameter is similarly given by

$$ {}^{ij}P(b) = P_i(b) P_j(b) \prod_{k \neq i,j} (1 - P_k(b)) \tag{5.72} $$

with a summation over i and j providing the total double ionization probability.

In order to convert these probabilities into a cross section, an integration must be performed over all possible impact parameters. For a particular multiple probabilistic configuration ${}^{m}P$ the associated cross section is expressed by

$$ {}^{m}\sigma = \int_0^\infty 2\pi \, {}^{m}P(b) b db. \tag{5.73} $$

Employing the step-function characterization of the individual probabilities, this integration can be performed easily.

Cross section values for each multiple ionization process can be determined from this detailed analysis or by a simple scaling from the average probability of equation 5.67. For cases of large, many-electron ions such as those considered in this dissertation, multiple electron probabilities can be calculated generally only to within a factor of 2 or 3 certainty [51]. This is due to the fact that indirect ionization effects, though not always significant in total ionization cross section calculations, are usually important to consider in multiple ionization analyses [27]. The values presented using the simplified analysis described here are

similarly only intended to represent a rough estimate. However, these values are still useful for calculations and are as reliable as other estimates, within the associated uncertainties.

Using the approximate analysis, the average probability can be used to generate multiple probabilities ${}^{m}P$ of order m by:

$$ {}^{m}P \approx P^{m}. \tag{5.74} $$

This can be re-expressed as a cross section as follows. The gross ionization cross section σ_T, being the sum of the individual electrons' cross sections, actually must represent the sum of all of the multiple ionization cross sections according to [26]

$$ \sigma_T = 1^{1}\sigma + 2^{2}\sigma + 3^{3}\sigma + ... \tag{5.75} $$

The multiple ionization cross sections can be expressed in terms of the single ionization cross section by the ratio

$$ \frac{{}^{m}\sigma}{{}^{1}\sigma} \approx P_T^{(m-1)}. \tag{5.76} $$

The decomposition of the gross ionization cross section can be reduced by this substitution to

$$ \sigma_T = {}^{1}\sigma(1 + 2P_T + 3P_T^2 + ...). \tag{5.77} $$

From this, the cross sections for multiple ionization can be approximated by

$$ {}^{m}\sigma = {}^{1}\sigma P_T^{(}m - 1) \tag{5.78} $$

In this way the cross section for single ionization can be determined and the multiple ionization cross sections can be obtained.

Some important trends for multiple ionization can be ascertained from this analysis. For a given projectile and velocity, the total ionization cross section per collision with

an target atom or ion increases with target atomic number. Therefore, since the projectile's own geometrical impact parameter remains the same regardless of the target identity, the probability for multiple ionization should increase with target atomic number. This has been verified by Meyerhof *et al.* [27]. Also, for a given target, the multiple ionization probability is maximized at a velocity corresponding to the maximum cross section. Note that for near-neutral atoms this may occur at a low velocity near αc, much lower than the $0.2c$ expected for heavy ion fusion drivers.

5.5 Electron Capture Reactions

Now are described the set of reactions which can cause an electron to be added to the incoming beam ion, reducing its charge state. These reactions and their associated cross sections will be used to complement the ionization calculations to develop a total charge evolution model. As in the study of ionization reactions, plasma targets induce their own particular set of capture reactions due to the behavior of free electrons. Thus, the capture reactions can be categorized into those concerning bound electrons and those concerning free electrons.

5.5.1 Charge Transfer

The capture of an electron in a target material by an incident projectile ion can occur in general by either a reaction in which radiation is emited or by a non-radiative reaction. Due to the absence of the requirement of a photon, non-radiative processes are characterized by a greater reaction cross section than radiative processes for a given target

electron. The only significant non-radiative mechanism for target electron capture by a projectile is the *charge transfer* reaction. It is due originally to Oppenheimer [53] and was refined with later work by Brinkman and Kramers. The final form is known as the OBK model honoring its three developers. If the target should not be fully-stripped, the incoming projectile may acquire electrons originally bound to the target atoms or ions. This charge transfer reaction rate depends on the initial energy E_i of the bound electron in the target and its final energy E_f in the beam ion. Its cross section is expressed by

$$\sigma_{ct} = 4.1 \times 10^4 \sum_{n_i} \sum_{n_f} N_i a_{eik} \times \frac{Q_p^2 e^4 E_i^{5/2} E_f^{3/2} E_k^4}{[E_k^2 + 2E_k(E_i + E_f) + (E_i - E_f)^2]^5} \tag{5.79}$$

in which $E_k = m_e v^2/2$ and N_i is the number of electrons in the original target shell. The eikonal factor a_{eik} accounts for reduction in this reaction with increased deviation from the Born approximation on which it is based. It is expressed as

$$a_{eik} = \frac{\pi \eta v_i}{\sinh(\pi \eta v_i)} \exp\left[-2\eta v_i \arctan\left(\frac{v/2 - \epsilon\eta}{v_i}\right)\right] \tag{5.80}$$

where $\eta = \alpha c/v$, $\epsilon = (E_f - E_i)/1\text{Ry}$ and $v_i = \sqrt{E_i/1\text{Ry}}$. The total charge transfer reaction rate is obtained by summing over all initial electron bound states in the target and all final captured states in the projectile.

5.5.2 Radiative Capture

While the charge transfer reaction described above involves no photon emission, two types of capture reactions can occur which are accompanied by a radiative emission. Radiative capture reactions can be induced both by free plasma electrons and in some cases by bound target electrons.

The transition of a free plasma electron in the target medium to a bound state of principal quantum number n in a moving beam ion is known as *radiative electron capture*. It is more accurately described as *free electron radiative capture* to distinguish it from radiative capture of a bound electron. Its cross section is given by Spitzer [62] as

$$\sigma_n = 2.1 \times 10^{-22} \frac{E_b^2}{E_r(E_r + E_b)} \mathrm{cm}^2 \tag{5.81}$$

in which E_b is the binding energy of the final state and E_r is given by

$$E_r = \frac{1}{2} m_e \sqrt{v^2 + v_{th}^2}, \tag{5.82}$$

v_{th} being the plasma electron thermal velocity. The total radiative capture reaction rate is found by summing over all possible n receiving shells in the projectile:

$$\alpha_{REC} = \left\{ 1 - \frac{N_{n_g}}{2n_g^2} \right\} \alpha_{n_g} + \sum_{n=n_g+1}^{\infty} \alpha_n. \tag{5.83}$$

In low-Z targets containing bound electrons, the second type of radiative capture can be important to consider. Bound electrons in the target atoms or ions can also radiatively recombine with the incoming projectile. Quantification of this process is due to Stobbe [63] and is performed according to a non-relativistic dipole model. Its formula, for capture into shell n of the projectile, appears as

$$\sigma_n = (9165\mathrm{b}) Z_t \left(\frac{\kappa^3}{1 + \kappa^2} \right) \frac{\exp(-4\kappa \arctan[\kappa^{-1}]}{1 - \exp[-2\pi\kappa]} \tag{5.84}$$

in which $\kappa = v_n / v$. Scheidenberger *et al.* present an excellent overview of this process as well [59].

5.5.3 Dielectronic Recombination

Another important electron capture reaction for ions penetrating a plasma is *dielectronic recombination*. This process plays a special role in the recent history of beam charge state calculation. For years it was neglected, until it was demonstrated by Peter and Meyer-ter-Vehn to be a potentially dominating process [54]. The effect of this improved understanding is that the expected augmentation of the projectile charge state in plasmas, according to theory such as that of Nardi and Zinamon [17], is countered by dielectronic recombination, reducing the beam charge state enhancement.

In this process, a recombining electron joining a beam ion in shell n, whose binding energy is E_n, transfers some of its total energy to an electron in shell i of binding energy E_i, which is consequently excited to shell j, bound by E_j. The angular momentum l of the captured electron can be specified as well. Electrons excited by this process will eventually either auto-ionize or radiatively de-excite. The auto-ionization proceeds at a rate given by an Einstein coefficient [54]:

$$A_a(jnl \rightarrow iE_k l \pm 1) = \frac{8}{\sqrt{3}} \frac{1\mathrm{Ry}}{\hbar} \frac{Z_p^2}{n^3} \frac{1\mathrm{Ry}}{(E_i - E_j)} \frac{1}{(2l+1)} f(i \rightarrow j) G_l(k, k'). \tag{5.85}$$

$G_l(k, k')$ is the partial *Kramers-Gaunt factor* for the bound-free transition of the captured plasma electron back into the continuum by auto-ionization. It quantifies deviations of the process from the classical regime. k and k' indicate the momentum vectors of the reactant plasma electron before the collision with the projectile and after, respectively. See references [54] and [4] for an analysis of this factor and its values. The radiative de-excitation of the

captured electron occurs at a rate of

$$A_r(j \to i) = \frac{1\mathrm{Ry}}{\hbar}\alpha^3 \left[\frac{(E_j - E_i)}{1\mathrm{Ry}}\right]^2 f(j \to i). \tag{5.86}$$

Using the above Einstein coefficients, the formulation of the dielectronic recombination cross section is as follows [54].

$$\alpha_{dr} = \frac{h^3 n_f}{(2\pi k_B m_e T)^{3/2}} \sum_i \sum_j \sum_{n,l} N_i \frac{g_j - N_j}{g_j}(2l+1)\frac{A_r A_a}{A_r + A_a}\mathrm{F}(s,t) \tag{5.87}$$

in which $\mathrm{F}(s,t)$ is a resonance function matching the projectile velocity with the plasma electron velocity:

$$\mathrm{F}(s,t) = \frac{e^{-(s-t)^2} - e^{-(s+t)^2}}{4st}, \tag{5.88}$$

with

$$s = \left[\frac{E_j - E_i + E_{nl}}{k_B T}\right]^{1/2} \tag{5.89}$$

and

$$t = \left[\frac{m_e v^2}{2k_B T}\right]^{1/2}. \tag{5.90}$$

5.5.4 Three-body Recombination

A related but rarely significant reaction is the *three-body recombination* reaction in which a radiative recombination occurs and excess energy of the recombining electron is transfered to another plasma electron. The reaction rate for this process is given by Zel'dovich and Raizer [70] as

$$\alpha_{3br} = 2.92 \times 10^{-31}\mathrm{cm}^3\,\mathrm{s}^{-1}\frac{Q_p^3 n_f}{(v_r/\alpha c)} \tag{5.91}$$

in which Q_p is the projectile charge and α is the fine structure constant.

5.5.5 Capture Density Effects

In order for a projectile to capture an electron from the continuum or from a target atom or ion, the captured electron initially may exist in a bound state in the projectile with a very large principal quantum number n. Subsequently the electron may reach its destination in a ground level in the projectile by radiative cascading decays. Alternatively, the electron may be ionized by a number of processes before it reaches the ground state. The probability that this newly captured electron would be ionized before maintaining residency in a ground state in the projectile increases with the density of the target n_t and the velocity of the projectile v. This is because the competition between cascading decay and collisional re-ionization is biased towards re-ionization with increasing direct collisional reaction rate α

$$\alpha = n_t \sigma v \tag{5.92}$$

given the same radiative decay rate. The net result is the suppression of capture reactions with increasing density and velocity. This is the cause of the effect mentioned at the end of section 5.1.1.

Peter and Meyer-ter-Vehn have quantified this effect as a function of the system's parameters including the principal quantum numbers nl of the shell into which the capture has occurred. The suppression is presented as an approximate unit-less factor P by which the individual capture cross section should be reduced. This factor is given as

$$P = 1/(1 + 5 \times 10^{-18} \frac{Z_t^2 n_t 1\mathrm{cm}^3}{Z_p^6 v/\alpha c} l^2 n^5). \tag{5.93}$$

It is meant in this form to be applicable for large v and large n [54]. Some adjustments may be required in order to make it broadly employable.

The effects of this electron capture suppression in an incident beam due to high target density are believed to cause an increase in the equilibrium charge states in a solid target *versus* in a gas target. While in principle this effect is present, the degree of change will be considered small, particularly for a heavy ion's charge state, and this effect will be largely be ignored. This is the case since the charge-changing cross sections for a given element at a given velocity vary over many orders of magnitude with changes in projectile charge state (see section 5.7). The goal of developing reliable capture reactions is primarily to combine them with ionization models to establish the balance point in a given scenario. This balance point at which capture and ionization rates are equal represents charge equilibrium. Given that the capture and ionization cross sections vary so strongly over the range of projectile charge states for a system, changes in a cross section of even 50% to 100% could be tolerated since they would not change the equilibrium charge value significantly. However, if a more detailed analysis should be needed, this term can be implemented.

5.6 Roles of Cross Sections

The ionization and capture cross section models discussed in sections 5.4 and 5.5 can be assembled to form a comprehensive charge changing rate for a given beam penetrating a target. The roles of individual cross sections can be understood in terms of the two main objectives of this dissertation. The two processes which need to be addressed are the ionization of a heavy ion beam penetrating a rarefied medium and the charge evolution and energy deposition of a beam directed into a dense plasma.

For the study of beam ionization in HIF chambers, the electron capture reactions

will not be important since the driver beam's charge state will be low and ionization reactions will dominate the charge evolution. For a heavy ion such as lead at velocities typical of HIF scenarios, $v = 0.2c$, the equilibrium charge state would be at least 63 (see section 5.1.1). At charge states greater than this equilibrium value, charge transfer will dominate. At lower charge states ionization will dominate. For HIF chamber applications, the maximum charge of the beam ions encountered will be of the order of 10+ to 15+. At these charge states, ionization will dominate the reaction rate by many orders of magnitude. This will be seen in more detail in section 5.7.

For the studies of the deposition of beams into dense target materials, it is hoped that the beam's actual charge state evolution will be characterized by instantaneous charge equilibrium as in the case of deposition into cold targets. In this situation, the charge state of the beam at each velocity as it slows will be that charge at which the total ionization reaction rate is equal to the total capture rate. It is not yet known when and if this will be the case for a heavy ion beam penetrating a dense plasma. It is well known (see section 5.1.1) that ions reach equilibrium charge states in cold targets. However, the entire ensemble of capture and ionization rates have not yet been analyzed sufficiently to establish whether or not equilibrium charge evolution can be expected in beams penetrating HIF hohlraum materials heated to hundreds of eV. Ideally, if the charge evolution of a heavy ion in a dense plasma target should be characterized by an equilibrium value, that will be one which is eventually expressible by a new, simple equation analogous to the old semi-empirical fit for cold target deposition. For this purpose, all of the capture and ionization reactions will be required, as well as the physics of energy deposition.

5.7 Experimental Validation of Cross Sections

The variety of theoretical and semi-empirical models developed in sections 5.4 and 5.5 can be checked against measured ionization rates in order to determine their validity. In order to perform these calculations in a comprehensive manner, a computer code suite was developed incorporating the cross section models of the previous sections. This will allow calculation of ionization and capture cross sections for a user-specified beam species penetrating a user- specified target. Appendix C contains information about the specific details of these and codes and other codes used in this dissertation.

One code is called **x** and is used in the following analyses to generate all ionization and capture cross sections. Another code called **zstopx** calculates and gives as an output the relevant cross sections, but also computes the evolution of the beam's average charge state as a function of time and distance of penetration through the specified target. In the following calculations and comparisons to experimental data, the energy deposition of the beam into the target will not be significant at all. The **zstopx** code is also equipped with the capability to calculate the energy deposition of the beam into a target, but that function is not useful here (see Chapter 6). The **zstopx** code is useful here to calculate the average charge state evolution of a beam penetrating a plasma target (see section 5.7.1), which is a function of the relevant beam charge-changing cross sections. Most experimental data regarding the ionization cross sections for beams penetrating plasmas is found in the form of a measured average change in the incident beam's charge state after penetrating a plasma. This requires a simple beam evolution routine which advances the beam in mean

free path steps ℓ according to

$$\ell = \frac{v}{\alpha_{tot}} \tag{5.94}$$

where v is the beam's velocity and α_{tot} is the total charge-changing reaction rate. It is defined by

$$\alpha_{tot} = |\alpha_I - \alpha_C| \tag{5.95}$$

where α_I is the total reaction rate for beam ionization and α_C is the reaction rate for electron capture onto the beam. After each step ℓ, the average charge state of the beam is considered to have changed, either by $+1$ if the ionization reaction rate α_I should be greater than the capture rate α_C or by -1 if the capture rate should be the larger of the two. This is discussed in more detail in Chapter 6.

5.7.1 Ionization Comparisons

The expanse of functions intended to model beam ionization cross sections remains an unconquered landscape. Even in the past decades both the Bohr and Bethe models have been used [31],[32]. Meanwhile, the PWBA and BEM models have also enjoyed application [59],[54]. As yet, no clear consensus exists on when each is applicable and why they differ so significantly [25].

The differences among the values predicted by the various expressions are not just cosmetic. The ionization cross section models all exhibit the same general scaling for target ionizing charge, but exhibit different functional dependence on the projectile velocity v and orbital electron velocities v_{nl}. Some models such as the PWBA formulae require articulation of terms for each shell and sub-shell, where the BEM expressions are independent of such

terms.

Though the situation seems to be obscured by the variety of possible models, progress can be made on the issues at hand. The primary objective is to address two regimes of ionization involving the penetration of swift heavy ions through HIF-relevant materials. The first is the study of the ionization of near-neutral ions penetrating a gaseous and possibly ionized medium. The second is the charge evolution calculation of the ions as they are deposited into a solid-density material.

Based on the simplicity of the binary encounter models and their asserted effectiveness, they will serve as the primary ionization model to be examined in the following analysis. If shown to be faulty then the other models can be implemented. However, a goal of this work is to determine if the BEMs can be used effectively. They will therefore serve as the first-test calculation.

Ionization Velocity Regimes

The two main ionization scenarios considered here, ionization of near-neutral beams in a rarefied target and charge evolution of beams in dense targets, actually form a convenient dialectic of the two different projectile-electron velocity space regimes of ionization. These are (1)high scaled velocity ($V \gg 1$) and (2) near-peak velocity ($V \approx 1$), where V is the scaled velocity being v/v_{nl} for each projectile electron nl which may be ionized. The latter is called 'near peak' ionization since the maximum value of the ionization function for a given electron ionization potential occurs at $V = 1$. The penetration of an HIF chamber gas by heavy ions with charge states ranging from 1+ to 10+ represents the former and the charge evolution of ions, perhaps near charge equilibrium, while deposited

in solids represents the second case. The following sections address these two cases.

Ionization of Swift Near-Neutrals

Ideally, the ionization cross section of a heavy ion driver beam at all likely beam charge states would be determined experimentally. However, heavy ion fusion scientists now are forced to rely on calculations with no direct empirical data in the regime of interest. The problem is that it is not yet possible to generate beams of high-Z projectiles at tens of MeV/u at low charge states. This situation is a concern to the HIF community since this is exactly the case desired to be understood for chamber transport calculations for HIF power plants. It is quite easy to create beams of even higher energy, but with greater initial charge state, but studying the prototypical 20MeV/u Pb^{1+} beam is not possible *per se*. However, consider reversing the frame of this collision. If the projectile became a target, a charge could be driven against it while measuring the ionization of the target. This is exactly the technique employed by Lotz and others investigating free electron-induced ionization.

Such data have been gathered in a parameter space of immediate interest to HIF. Matsuo *et al.* have gathered data from the ionization of several species by collision with bare nuclei. The beam energy of the experiment was 6MeV/u, which gives $\beta = 0.11$. This data is useful since the velocity range is near that of putative HIF beams, the species being ionized is neutral, and the charges of the ionizing agents examined included those very close to the chamber constituents.

In the ionization of swift, near-neutral high-Z species, the cross sections are dominated by the removal of the outer valence electrons, being very weakly bound. For binding energies of a few eV, the associated orbital velocities are near αc. Therefore, the ratio of the

frame velocity to the orbital velocity can be near 10. This fact is of tremendous significance. At such scaled velocities many of the troubling distinctions among the different ionization cross section models become independent of the mass of the ionizing agent. In this regime even electrons ionize exactly as protons [24]. The analysis of section 5.4.7 demonstrated the merging of the Gryzinski BEM and the Lotz formulae in this regime.

Note also that this is the same experiment which demonstrated deviation from q^2 ionizing charge dependence for high-Z ionizers (see section 5.4.5). In the following analysis the corrections for such effects will not have been included.

The performance of the BEM/Lotz functions at these high velocities will be examined with respect to the data and to each other. Using the Gryzinski velocity dependence of equations 5.34 and 5.37, the binary encounter model was employed to model the Matsuo data. Also used was a hybrid model consisting of the Gryzinski velocity function below $V = 7.3$ and the Lotz form for $V \geq 7.3$ (the two meet near $V = 7.3$).

Representative experimental cross sections taken from Matsuo and his colleagues appear in table 5.1. The values modeled using both the straight BEM formula and the hybrid BEM-Lotz model are also included for comparison. In general, both models provide cross section values of which the majority are within 15% of the experimentally determined cross sections. The average error in for the four cross sections measurements for the xenon target is 23.8% for the BEM model and 20.4% for the hybrid model. The greatest disparity observed between theory and experiment is about 40% for the ionization of xenon by helium as calculated by the BEM cross section. The hybrid model here gives a value within 33.2% of the experimental cross section. The experimental uncertainty was estimated to be near

	Ar			Kr			Xe		
	Exp	Gry	Hyb	Exp	Gry	Hyb	Exp	Gry	Hyb
He	1.27	1.06	1.20	1.90	1.40	1.57	2.98	1.77	1.99
C	10.6	9.57	10.8	15.9	12.6	14.1	23.7	16.0	17.9
Ne	26.8	26.6	30.0	39.3	35.0	39.2	56.8	44.3	49.8
Ar	70.0	86.1	97.3	98.3	114	127	144	144	161

Table 5.1: Measured cross sections [$/10^{-16}\text{cm}^2$] for ionization by collision with a 6MeV/u beam of bare nuclei [26]. The column headers list target type and designate 'Exp' for experiment, 'BEM' for BEM calculations and 'Hyb' for hybrid calculations; rows designate the incident ionizing nuclei

8.4% [26].

No clear over-calculation of cross sections are observed with increasing beam q value as expected from section 5.4.5. This is probably the case since the problem was expected based on analysis of the PWBA cross section – the BEM and hybrid models used here may not be vulnerable to that particular error. Also, the effect may be small compared to the $\approx 20\%$ error of the calculations.

The case above which is most relevant to HIF chamber ionization calculations is the ionization of xenon and argon by a charge of $q = 2$ (a helium nucleus). This is true even though the gas through which the HIF beams will propagate will likely consist of $Z = 9$ fluorine. Due to screening, the net effective charge sensed by the projectile electrons most likely to be ionized is near 1.5 [51]. The cases more relevant to cross section calculations for beams being deposited into dense targets are the ones involving the higher q beams. This is true since in the dense solids, higher beam charge states will be achieved and the valence electrons at those states will be more strongly bound and will sense a higher effective target screened nuclear charge as detailed in section 5.4.4.

The comparisons conducted above for both the near-peak ionization and the ion-

ization of swift neutrals span the ranges of both atomic number and velocities relevant to HIF while confirming the cross section values to be within useful tolerances.

Ionization Near Peak

As discussed in section 5.1.1, the charge state of an ion penetrating a sufficiently dense absorber rapidly reaches an equilibrium value. This value is the charge state for which the orbital velocities of the valence electrons are comparable to the projectile velocity itself. In terms of the ionization cross section modeling parameters, this is a regime in which $V \equiv v/v_{nl} \approx 1$. This is also the scaled velocity regime at which the cross section velocity-dependence reaches a maximum.

Some discrete cross sections are available for testing cross section theory for this case. A fundamental test would be to compare the measured and calculated cross sections for a very simple ionization system: ionization of a light ion by proton impact with a proton beam energy such that the ionization cross section is maximized. Rudd *et al.* reported the cross sections for the ionization of helium by proton impact. The effective nuclear charge enhancement by incident charge superposition (see section 5.4.5) and resultant effective increase in the ionization potential of the K-shell electrons will be considered. The effect of this process is that the peak occurs with a proton beam energy near 80keV. The measured cross section value at this energy is approximately $9 \times 10^{-17}\text{cm}^2$. The value given by the BEM calculation is $9.6 \times 10^{-17}\text{cm}^2$. The experimental uncertainty in the measurements were not stated as the data points were compiled from many sources.

A similar calculation for a high-Z ion was provided by Anholt and his colleagues [25]. They reported the cross sections of hydrogenic xenon (Xe^{53+}) penetrating a range of

targets. At a beam energy of 200MeV, which corresponds to the velocity of the one K-shell electron, the cross section measured for penetration a xenon gas is near $4.8 \times 10^{-20}\text{cm}^2$. The corresponding value calculated by the BEM formula is $5.16 \times 10^{-20}\text{cm}^2$. The uncertainty in the experimental cross section is near 30%.

Meyerhof and his coworkers examined the near-peak ionization of highly ionized ions of even larger atomic number at collisional energies of several hundred MeV/u [27]. In principle, since the BEM formula is a function of only the ratio of projectile to orbital velocities, the cross section modeling should be addressed adequately. Indeed, the BEM calculation proved successful in even this regime. For a uranium ion at a charge state of 83+, the total measured cross section for ionization in a gold foil at an energy of 430MeV/u was near $1 \times 10^{-18}\text{cm}^2$, with an uncertainty of approximately 15%. The corresponding BEM value is $1.06 \times 10^{-18}\text{cm}^2$. For penetration of a carbon foil at the same velocity, the total cross section was reported to be near $8 \times 10^{-21}\text{cm}^2$. The BEM calculation produces a value of $8.5 \times 10^{-21}\text{cm}^2$. Note that this set of comparisons addresses not just a hydrogenic ion, but a more complex ion containing 9 electrons, which is fluorine-like.

Another set of useful measurements from an unpublished GSI experiment have been presented by Olson [51]. The work reported measurements of the cross sections of xenon ions at 1.4MeV/u penetrating a nitrogen target. At a charge state of 24+, the total ionization cross section was reported to be near $1.85 \times 10^{-17}\text{cm}^2$. The corresponding BEM value is found to be $2.14 \times 10^{-17}\text{cm}^2$. The uncertainty in the empirical value is about 20%. This result, again, represents ionization near the peak of the velocity dependence of the cross section formula. Since the atomic number of the target is greater than 1, screening

effects were important for the calculation, as they were for the other non-hydrogenic targets. This reinforces the reliability of the modeling detailed in section 5.4.4.

Plasma Ionization

The comparisons between experimental data ionization models of the ionization of ionic species by electron impact requires special attention. This is because free electrons, whether in a beam or in a plasma target, collisionally ionize in a different manner from screened nuclei as discussed in section 5.4.6. Also, the magnitude of enhancement of electron impact ionization rates due to indirect ionization processes is generally greater than the magnitude of the indirect enhancements of ionization by beam collision with a screened target nuclear charge.

A semi-empirical method for quantifying the deviations of observed ionization rates from the Lotz ionization formula was proposed in section 5.4.9. In this section, that new empirical adjustment will be employed in comparisons with electron impact ionization cross sections.

Dietrich *et al.* [18] conducted the first measurements of the charge state of a swift heavy ion through a plasma. This first work also established that the body of physical models was not adequate to wrestle the surprise exhibition of the data. Dietrich and his colleagues were forced to employ a corrective factor to adjust the models in order to agree with the experimental date. The BEM ionization cross section was multiplied by a factor of 2.5 in order to achieve agreement between the calculated beam ionization and the observed beam ionization. Analysis here has shown (see also section 7.1.2) that the BEM cross section should not be totally to blame for the plasma ionization. Upon close inspection the Lotz

formula emerges as the most likely source of the miscalculation.

In the GSI experiment [18], a xenon beam initially charged to 37+ at an energy of 5.9MeV/u was observed to be ionized to an average charge state near 42+ after traversing 20cm of hydrogen plasma whose density was near $4 \times 10^{18}\text{cm}^{-3}$. The models employed here forecast an average emerging charge of only 40. This is not an alarming shortfall. It can indeed be corrected by multiplying the BEM cross section by 2.5, which reproduces the observed final charge state. However, the atomic processes which dominate this charge evolution involve ionization of electrons whose orbital velocities are near or less than the projectile velocity. In such cases in which the scaled velocity $V \equiv v/v_{nl} \leq 1$ significant ionization enhancements were observed in electron beam ionization of highly-charged ions (see section 5.4.6). The GSI beam-plasma experiment of Dietrich and his colleagues was actually just another form of the experiments in which an electron beam was used to ionize a target species. The GSI experiment was simply a frame-reversal of the Lotz-type electron beam experiments, with the roles of the targets and beams reversed. But, instead of just causing ionization by electron impact, a hydrogen plasma also generates ionization in an incident beam through collisions with the protons. Thus two cross sections must be employed to characterize the total ionization : the BEM cross section for ionization by proton impact and the Lotz cross section for ionization by free electron impact.

However, in the analysis of the experimental data, only the BEM cross section was adjusted by a corrective factor. It has been shown here that the Lotz formula can underestimate electron ionization cross sections significantly. Therefore, it should be expected that the Lotz cross section – not just the BEM cross section – should be augmented by a

corrective factor. Given that Shevelko's analysis indicated a consistent need for a factor of 1.4 for nuclear ionization, this factor could be applied to the BEM cross section in this analysis instead of the 2.5. The rest of the necessary adjustments should be applied to the Lotz formula. Given this arrangement, the corrective factor to the Lotz formula needed to reproduce the data, along with the factor of 1.4 applied to the BEM values, is near 12. This is sensible since the magnitude of deviation from Lotz in this velocity range for other high-Z ions is on the order of 10 [50]. This enhancement by 12 is within the observed levels of experimental deviation from the Lotz formula and was it is near the factor proposed in section 5.4.9.

In another experiment, Stöckl *et al.* have measured the ionization of gold beams penetrating hydrogen plasmas. Their results were surprising because the enhancement they observed was not able to be corrected by a factor of 2.5 applied to the BEM cross section. It was concluded then that a corrective factor approach would not work to model ionization in plasmas, and that the BEM formula in general was not reliable. No mention was made of the deviations of the Lotz formula from observed electron ionization values. In light of the present work, this conclusion is re-examined. Again, this is a regime in which many of the electrons have orbital velocities near or less than the projectile velocity. Following the previous re-analysis, which was based on the conclusions of section 5.4.6, the Lotz free electron ionization cross section was multiplied by a factor of 12. That approach here also provides a close replication of the empirical data. Through 20cm of hydrogen plasma at $5 \times 10^{17}\text{cm}^{-3}$, a gold ion initially charged to 28+ at 8.6MeV/u was found to reach a final average charge state of 42 ± 2. Using the corrected Lotz formula and the 1.4 factor on the

BEM value, the final charge is 42.5. If the density should be reduced to $2 \times 10^{16}\text{cm}^{-3}$, the final measured charge was 33 ± 2. The modeled average charge state, using the corrected Lotz cross section, was found to be 30 for the same beam and target parameters.

While no analytic representation of the observed deviations from the Lotz formula have been developed, good consistent agreement has been achieved here by quantifying to first-order the observed enhancements in both the BEM and Lotz ionization formulae. This is a new result in that it is the first analysis which has identified and corrected the Lotz problem for beam-plasma interactions. This supports the corrective approach outlined in section 5.4.9.

5.7.2 Capture Comparisons

The cross section calculations associated with the capture of an electron by a penetrating projectile are not as controversial as those of ionization. However, it is important to be sure that proper modeling has been achieved particularly since the cross section calculations depend not only on the explicit cross section formula itself but also on atomic values such as binding energies and radial density distributions.

Some capture cross section values from a GSI experiment were reported by Olson [51]. For the same 1.4MeV/u xenon collisions in nitrogen, capture cross section measurements were made for a variety of charge states ranging from 24 to 33. These results along with the theoretical values are presented in figure 5.5. The uncertainties in the GSI measurements are near 20%. The total capture cross section is the sum of the non-radiative charge transfer reaction and the radiative capture of bound electrons according to models of section 5.5.1 and 5.5.2.

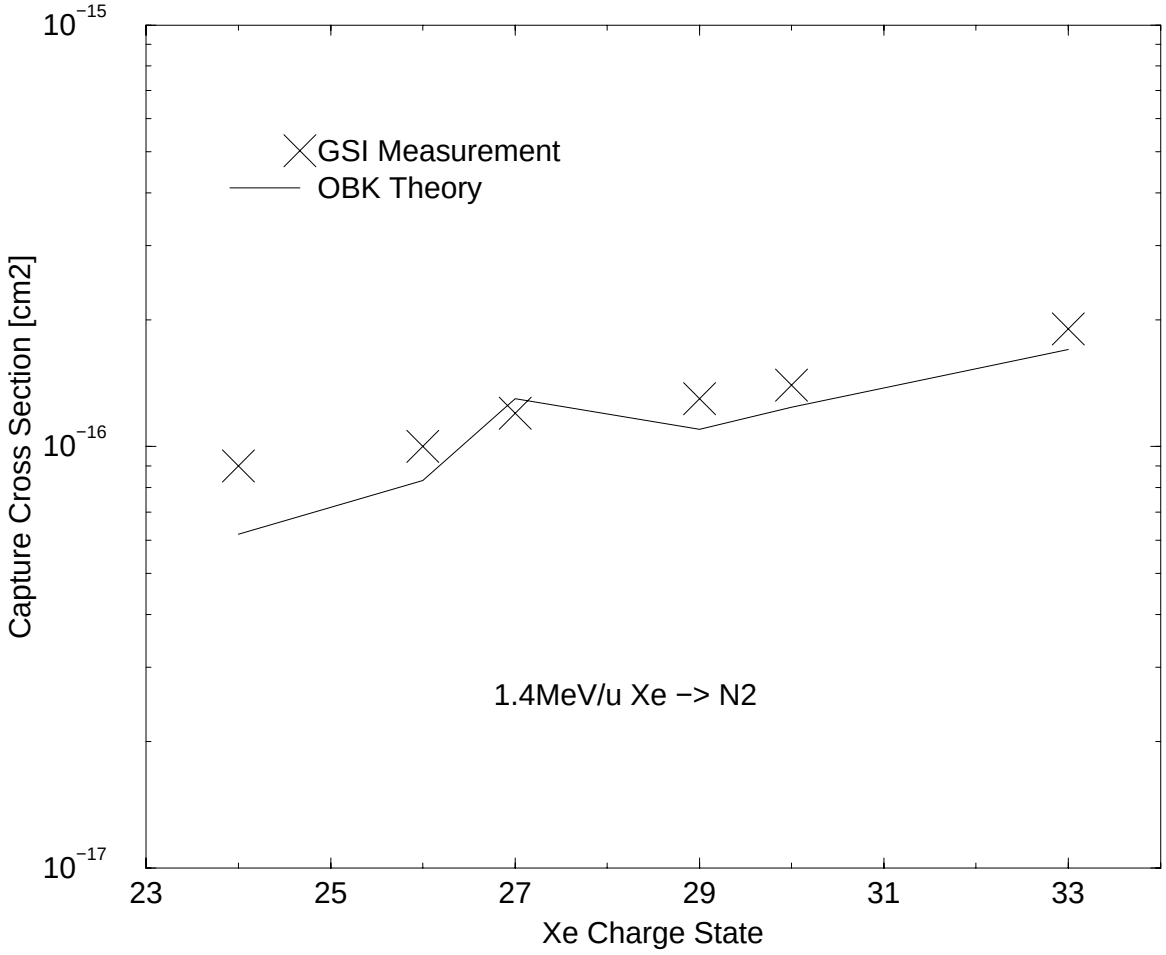

Figure 5.5: Total capture cross sections for $1.4\mathrm{MeV}/u$ xenon penetrating a nitrogen target, experiment and theory; experimental uncertainty is near 20%

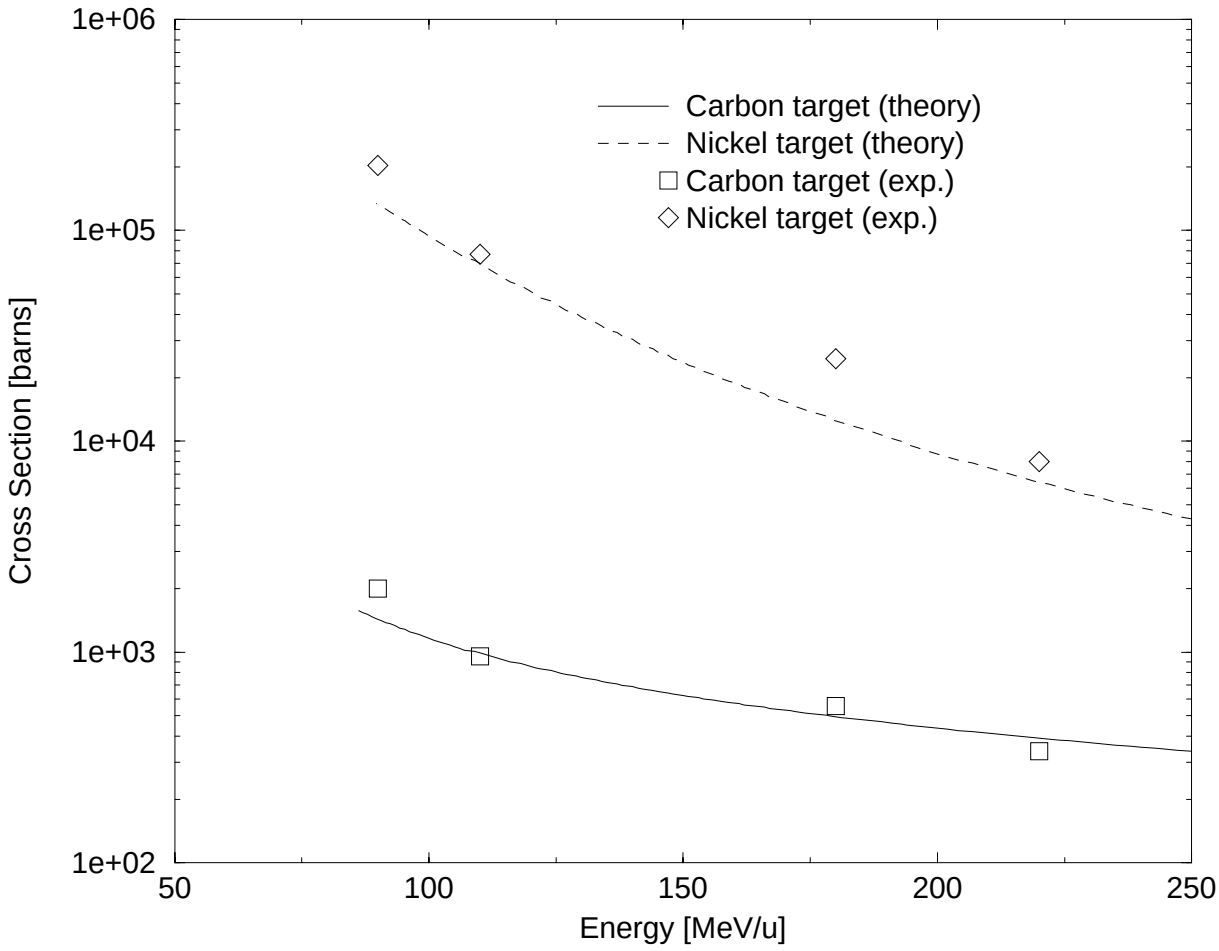

Figure 5.6: Total capture cross sections for Au^{78+} penetrating carbon and nickel targets, experiment and theory; experimental uncertainty is near 40%

Some other useful capture cross sections have been reported by Scheidenberger *et al.* [59]. They presented capture rates for hydrogenic gold penetrating nickel and carbon targets. Figure 5.6 shows the theoretical and experimental values of the total recombination cross sections of Au^{78+} penetrating both nickel and carbon targets. The uncertainties in the capture cross section measurements are given to be near 40%. This seems relatively large, but note that the capture rates vary over many orders of magnitude over the energy range examined here. Agreement between theory and experiment is within error.

These results validate the OBK capture model in non-ionized targets over a range of velocities and atomic numbers of both target and projectile. As with the ionization cross section comparisons, an even stronger validation can be made by using the Bohr semi-empirical fit. Note that the density suppression factor detailed in section 5.5.5 was not required in the above comparisons. In the low density of the target in the gas measurements is such that the effects are not significant. Also, the effect is not important in thin foils.

5.7.3 Comparison to Bohr Equilibrium

While experimental cross section values have been found for comparison with calculated values from the ionization and capture formulae, another comparison is available without new experimental apparati. Recall the semi-empirical fit for the equilibrium charge state of a projectile in any given medium as discussed in section 5.1.1. Aside from density effects, the approximate average value of the equilibrium charge state exhibited by a beam penetrating a target can be determined knowing only the beam velocity and atomic number.

Encoded in this assertion is an implicit statement about cross sections. At the equilibrium charge state predicted by the semi-empirical fit, the discrete ionization and capture cross sections should be nearly equal, independent of the target material. The magnitude of the respective cross sections will certainly vary over the range of projectiles and targets, but the charge state at which they intersect should occur near the expected equilibrium charge state value. So, given a set of recombination and ionization reaction formulae, a definitive check can be made of their accuracy in cold matter calculations by comparing the equilibrium which they collectively forecast to that empirically determined to be the correct value. Validations can thus be established for the entire set of reaction

rates for desired scenarios. At a given velocity, the ionization and capture cross sections for a beam of atomic number Z can be calculated for each charge state Q from $Q = 0$ to $Q = Z$. They should intersect at the equilibrium charge state.

It is important to note that some variations have been employed in the equilibrium fit formula to achieve an exact match to data for different beam-target set-ups [1]. In the following analysis, only the most general form of the semi-empirical fit

$$Z_{eq} = Z(1 - \exp[-\beta/(Z^{2/3}\alpha)]) \tag{5.96}$$

will be used. This form of the expression is still very useful and accurate for the purposes here. The variations employed in the literature to fine-tune this fit consist of minor adjustments such as replacing the $Z^{2/3}$ with $Z^{0.667}$ or the 1 with 1.034 [45]. The differences between the current models and the semi-empirical fit may be in part due to failure to account for such adjustments, but their relative effects will be considered to be small.

Also, the effects due to density suppression may be addressed. In the following analysis the cross sections will be employed without the density correction suggested by Peter and Meyer-ter-Vehn (see section 5.5.5). The effect of density suppression of capture reactions is only responsible for a change in equilibrium charge state of a few for a high-Z beam [20]. An error due to the exclusion of these effects will thus be relatively small. The equilibrium charge state values predicted using the unadjusted cross sections may therefore be consistently lower than those which would be expected in a solid target. However, the validation achieved by this analysis will still be very useful, particularly since this comparison between discrete cross section values and the semi-empirical fit for charge equilibrium has not been conducted before.

Consider a lead projectile penetrating a gold target. A useful energy range to examine for the purposes of this work is from 100MeV/u to about 1MeV/u. The total ionization and capture cross sections were calculated for this beam, target and velocity range. The cross section values can be viewed graphically in figure 5.7 for an incident energy of 20MeV/u. The dashed line on the plot represents the value forecast by the semi-empirical fit formula, which is 63 for this case. Agreement between the equilibrium charge state calculated by the Bohr semi-empirical fit and the equilibrium charge states determined by intersection of the capture and ionization cross sections is nearly precise at this velocity.

Figure 5.8 displays the lead ion equilibrium values given by the intersections of ionization and capture as in figure 5.7 but for a range of velocities, including the 20MeV/u value above, for the gold target. The agreement between the reaction rate model developed here and the empirical data represented by the Bohr equilibrium charge formula is excellent over the entire velocity range. The equilibrium charge states calculated by the cross section intersection method are within about 15% of the semi-empirical fit value consistently. As expected, the data are systematically low, probably due to exclusion of capture suppression in dense targets.

This test can be repeated for other targets establishing the validity of the cross sections calculated in other target atomic numbers. This is an important step. The equilibrium charge state of a beam is largely independent of the target being penetrated, so this procedure of comparing ionization to capture should give the same charge states in any target.

The equilibrium values calculated for penetration into a carbon targets over the

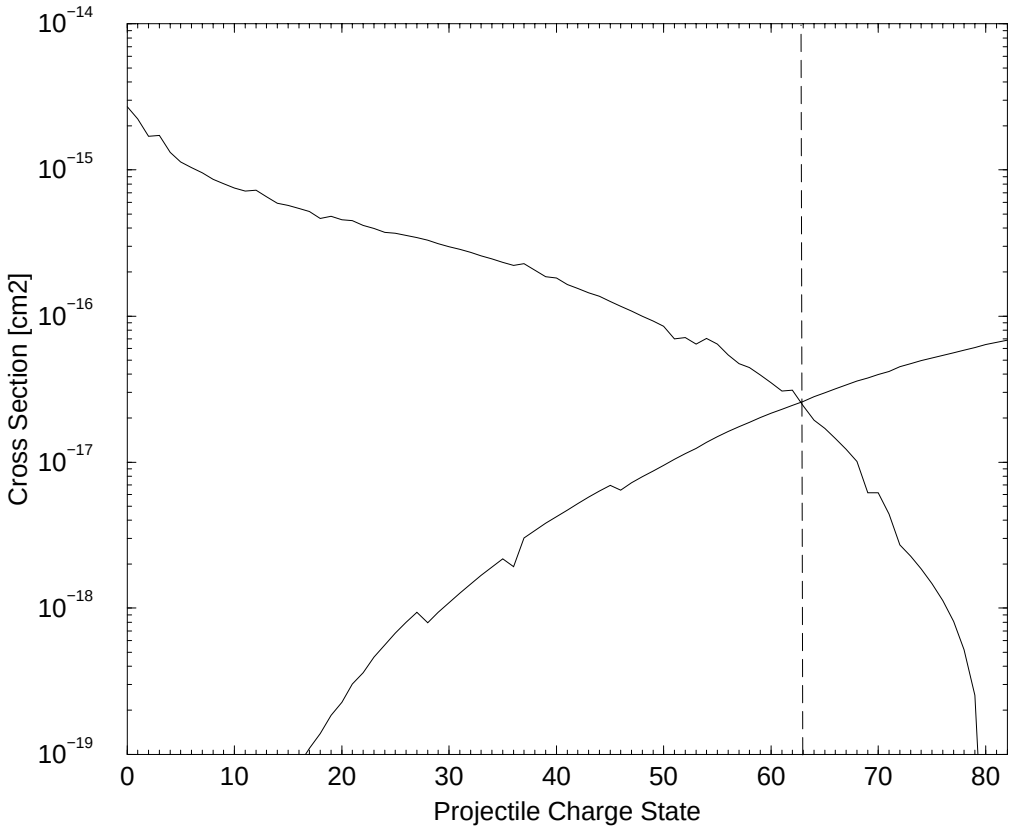

Figure 5.7: Total recombination and ionization cross sections for 20MeV/u Pb penetrating a cold solid gold target; Expected equilibrium charge is shown by the dashed line

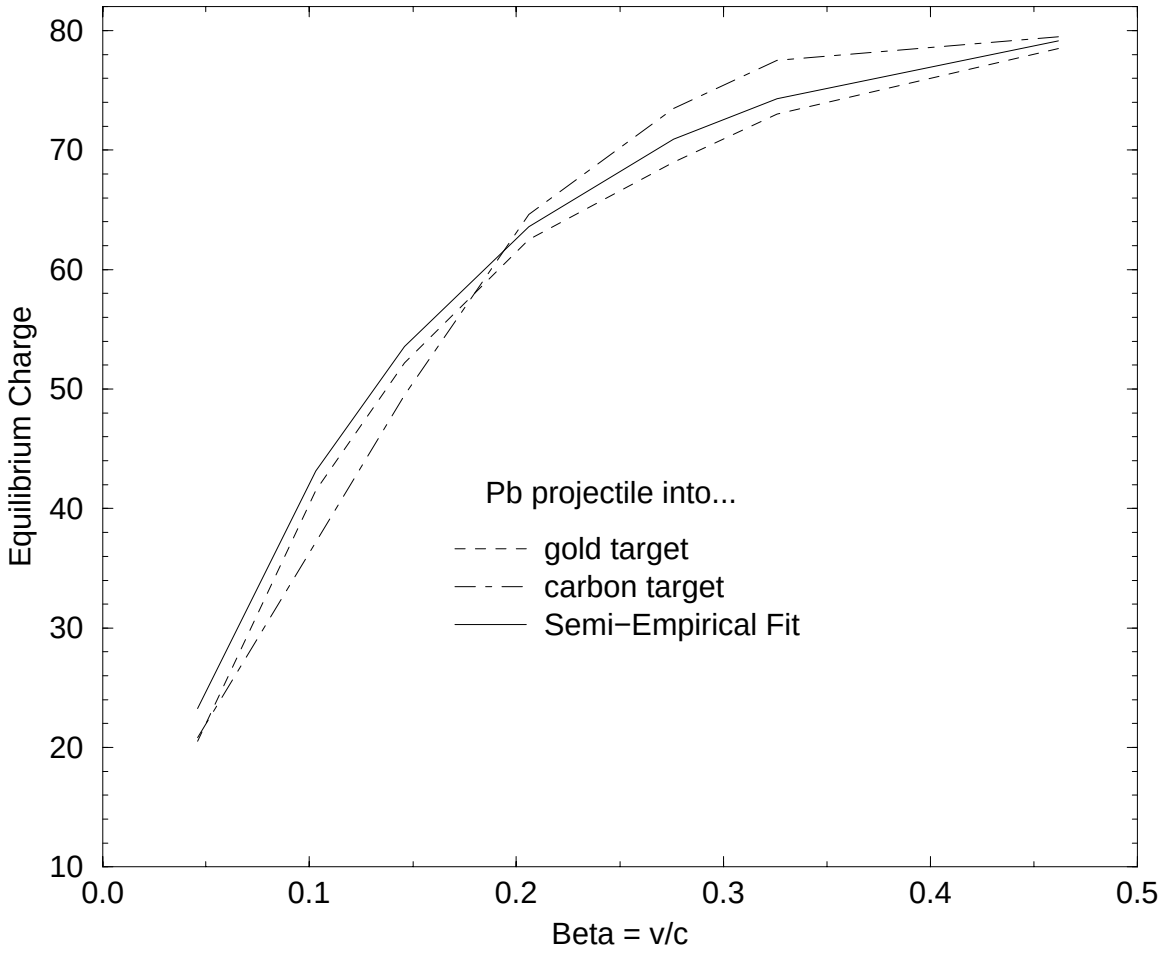

Figure 5.8: Modeled equilibrium charge state values with corresponding values given by the semi-empirical fit for lead penetrating gold and carbon targets

range of velocities appear with those in the gold target in figure 5.8. In the carbon target as in the gold target, agreement between the cross section-determined equilibrium charge state and that given by the traditional fit are within about 15%.

The above examinations were performed for a lead projectile penetrating both high-Z and low-Z targets. An analogous systematic study was performed for a potassium ion penetrating both gold and carbon targets. The potassium beam velocity range considered was lower since the relevant range scales as $Z^{2/3}$. In figure 5.9 are displayed the equilibrium

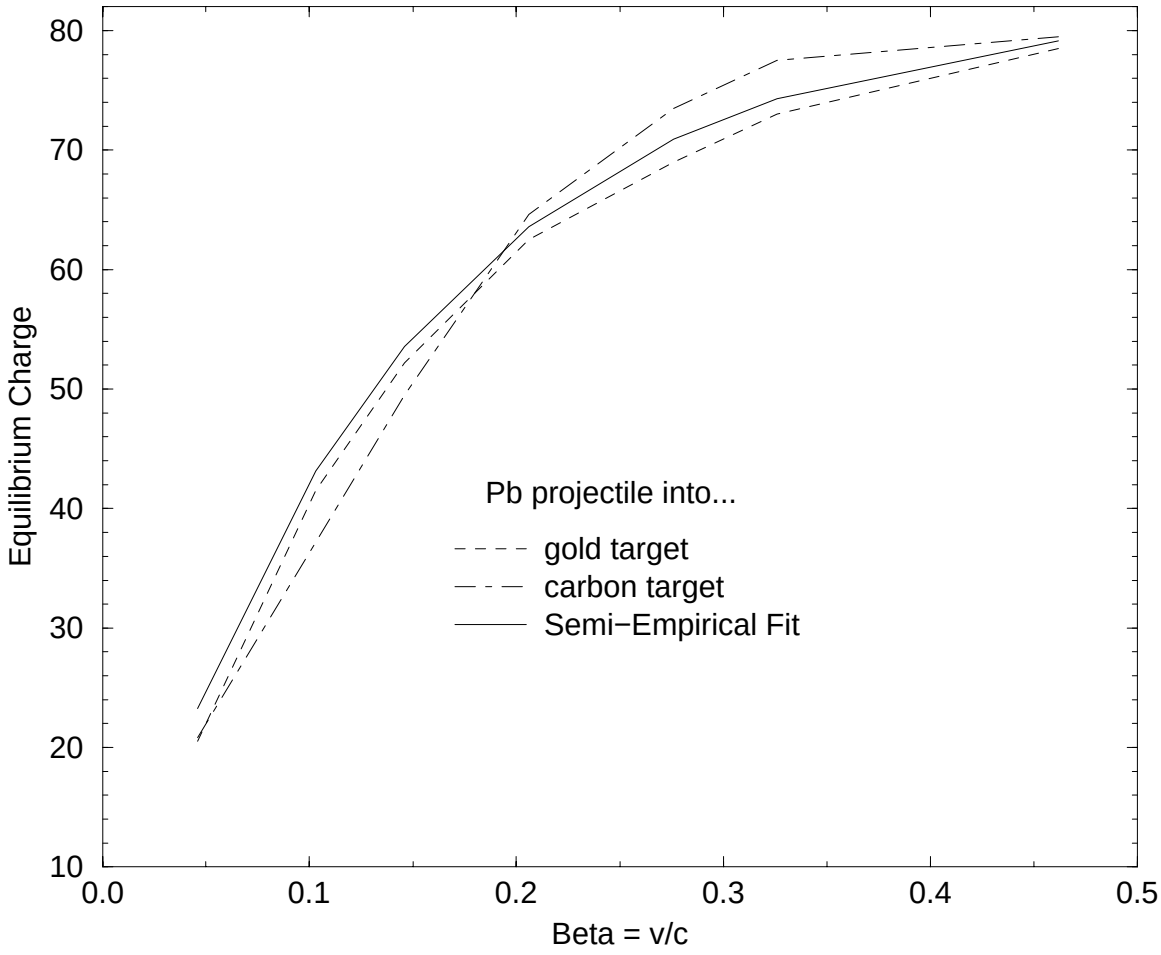

Figure 5.9: Modeled equilibrium charge state values with corresponding values given by the semi-empirical fit for potassium penetrating gold and carbon targets

charge states as calculated by the current modeling suite along with the corresponding semi-empirical values. Again, the agreement is excellent, within approximately 15% of the values given by the Bohr semi-empirical fit.

This equilibrium charge method of checking charge-changing cross sections is significant in that, even ignoring density effects, the general values against which the comparison is made are known to be reliable from the extensive history of reliability of the semi-empirical fit. The close validation over a wide projectile velocity range in targets

spanning the periodic table establishes the broad success of the ionization and capture models to be able to provide equilibrium charge information. The comparison with the results taken in the carbon target establish that this method is reliable for low-Z targets such as the HIF chamber gas and some of the hohlraum materials. The gold test demonstrates model reliability in high-Z hohlraum materials.

This comparison is the first time that the semi-empirical equilibrium charge formula has been reproduced from first-principle atomic reactions. Its success supports the reliability of the models used in this dissertation and conclusions drawn from them. It could be explored in more detail here, but the purpose of this present work requires only a simple validation.

Chapter 6

Integrated Deposition Calculations

The first major goal of this dissertation has been the calculation of the charge-changing reactions in beams penetrating rarefied gases or plasmas into which the beam deposited an insignificant amount of energy. These calculations are useful, for instance, for determining the charge evolution of an HIF driver beam penetrating the gas or plasma which may be contained in the HIF power plant chamber. The second major goal addresses the final destination of the beams in the hohlraum fusion targets. The heavy ion driver beams will deposit their energy into the targets positioned at the center of the HIF power plant chamber, heating the targets during the course of the deposition.

This chapter presents the methods by which the charge evolution physics of beam energy deposition presented in Chapter 4 can be integrated with the charge-changing reaction formulations discussed in Chapter 5. These integrated calculations will be used to model the charge evolution of an ion or beam as it deposits its energy into a target material. These calculations will first be performed for beams penetrating cold target materials

and will later be used to model beam deposition into plasmas. The calculations will be compared to some actual experimental measurements of beam ranges in solid, cold targets.

While the physics of energy deposition into cold, non-ionized solid targets has been understood for most of the 20th century, the physics of beam energy deposition into dense plasma targets has not been resolved. The charge evolution and deposition behavior of beams in dense plasmas will be analyzed using the charge-changing reaction formulae and energy deposition models developed and outlined in previous sections and the computational tools developed here. The eventual objective is a new, comprehensive understanding of the physics of beam deposition into dense plasmas.

A computer code suite was developed to model the charge evolution and energy deposition of a given projectile ion into a specified target material. The code suite consists of two programs called **zstop** and **zstopx** . The former is equipped only to treat the beam as if it were in instantaneous charge equilibrium throughout its deposition into the target. It uses the Bohr equilibrium formula (equation 5.4) to determine the instantaneous beam charge state at each given velocity. That beam charge state is used with the energy deposition physics of Chapter 4 to perform energy deposition calculations. The second code, **zstopx** , incorporates beam charge state calculations from the ionization and capture cross sections discussed in Chapter 5 as well as energy deposition models of Chapter 4. It does not treat the beam as necessarily in charge state equilibrium, but tracks the evolution of the beam's charge state according to the associated capture and ionization reaction rates. This code requires much more time to run since for each step in the calculation new ionization and capture rates are calculated for the beam, rather than just using a simple formula to

give beam charge state at each point.

Appendix C contains information on the use these two codes as well as the other computer programs developed for this dissertation.

Note that the calculations of this chapter do not yet constitute a useful final computational tool. These calculations are now performed only to validate the charge evolution models in conjunction with energy deposition physics. This work does not benefit calculations of charge changing rates of beams traversing chambers, since those calculations do not require consideration of the energy deposition of the incident beam. The **zstop** code as yet does nothing which has not been done many times before, which is the calculation of the beam deposition into a target using an old formula for the calculation of the beam's equilibrium charge state. The calculations performed by the **zstopx** code using the actual charge-changing reactions are indeed original. But, the code's modeling routines will be too slow to be used in a serious target deposition calculation code such as the LASNEX code of Lawrence Livermore National Lab since the charge evolution calculations are too time consuming.

However, these calculations will eventually be used to demonstrate that (1)the physics of beam charge evolution and energy deposition are clearly understood and (2)that understanding can be used to develop a useful new result, which is a simple and fast equation giving equilibrium charge state for a beam in a dense plasma.

The **zstop** and **zstopx** codes model the average charge state and energy evolution of an ion penetrating a material, not a distribution of different beam evolutions. This averaged evolution can be considered to represent the average behavior of a beam being

deposited. The energy and charge state of the average ion is tracked in numerical steps representing incremental advancements of the beam in space in time. Each incremental calculation step is determined by the smaller of two mean free path lengths: the m.f.p. for an integer or fractional charge change of the beam or the distance required for a small incremental reduction in beam energy. The integrated charge and energy evolution calculations will be performed by a Runga-Kutta method.

6.1 Numerical Beam Evolution

The method of numerically integrating the differential beam energy loss and charge-changing rates in a target are described below. They are different for each code, zstop and zstopx, representing beam charge evolution calculation by discrete reaction rates or by instantaneous equilibrium formula.

6.1.1 Discrete Cross Section Approach

Consider the use of the zstopx code which employs discrete charge-changing reactions rather than an equilibrium formula to determine the incident beam's charge evolution while penetrating a target. The mean free path for a single charge change of a beam's average ion is determined as follows. All relevant capture and ionization rates affecting the beam's charge state are calculated for the average beam ion at its current charge state Q_1 and velocity v_1. This is accomplished using the models of Chapter 5. Then, a net reaction rate is stated, being the total reaction rate for a charge change in the beam. This net charge-changing reaction rate α_{tot} is given as the absolute value of the difference between

capture and ionization reaction rates α_C and α_I respectively,

$$\alpha_{tot} = |\alpha_I - \alpha_C| \tag{6.1}$$

This difference between charge-increasing and charge-decreasing reactions achieves the desired result of a vanishing total reaction rate when the α_I and α_C terms are equivalent. In other words, when the capture and ionization reactions balance, there will be no net charge-changing reaction. The m.f.p. distance ℓ_q associated with this charge-changing reaction rate is given by the relation

$$\ell_q = \frac{1}{\alpha_{tot}} v_1 \tag{6.2}$$

where v_1 is the velocity of the beam at the start of each incremental calculation step. This interval can also be expressed as a time increment dt_q for a change in beam charge state,

$$dt_q = 1/\alpha_{tot}. \tag{6.3}$$

The competing beam evolution process is the reduction in the beam's energy by transferring energy to the target as described in Chapter 4. The mean free path for a small, incremental reduction in beam energy is calculated as follows. The m.f.p. for reduction in beam energy will be chosen such that the incremental integration step causes the beam's energy to be reduced by a small fractional amount ϵ. Typically, an ϵ value of 1% will be used in these calculations. This level of accuracy should be more than adequate for the modeling in this dissertation. This incremental time advancement dt_e for a fractional beam energy loss ϵ is specified by

$$\Delta E = \left(\frac{dE}{dx}\right)_1 v_1 dt_e = \epsilon E_1 \tag{6.4}$$

where E_1 is the beam's energy at the start of the integration step and $(dE/dx)_1$ is the energy loss rate (stopping power). This time increment over which the beam's energy would be reduced by this incremental amount is

$$dt_e = \epsilon E_1 v_1 \left(\frac{dE}{dx}\right)_1^{-1} \tag{6.5}$$

This can be expressed as a distance ℓ_e by

$$\ell_e = v_1 dt_e. \tag{6.6}$$

The smaller of the two mean free paths, ℓ_q and ℓ_e, will determine the size of the integration step taken, ℓ. The time increment dt over which this incremental beam advancement occurs is just

$$dt = \frac{\ell}{v_1}. \tag{6.7}$$

If the incremental step for achieving a unit charge change ℓ_q should be the smaller of the two mean free paths then a beam advancement will occur accompanied by a charge change. The associated change in beam energy will be less than the fractional change ϵ. It will be given instead by

$$\Delta E = \left(\frac{dE}{dx}\right)_1 dt \tag{6.8}$$

where dt would be less than dt_e.

If, conversely, the incremental energy loss step ℓ_e should be smaller than the charge-changing m.f.p. then the advancement would occur but not accompanied an integer change in the beam's average charge state. The energy of the beam would be reduced by a fractional amount ϵ. The advancement would contribute to the evolving charge state, but only in a probabilistic way. Recall from the analysis of section 3.2 equation 3.62 which expresses the

nature of the time-evolution of the probability of a reaction characterized by a reaction rate α:

$$P(t) = 1 - \exp[-\alpha t]. \tag{6.9}$$

The time increment t associated with the mean free path is defined as $t = 1/\alpha$, producing a reaction probability of about 0.632. Consider the case of a reaction rate given by the total charge-changing reaction rate α_{tot} of equation 6.1. If the time should advance in increments smaller than $dt_q = 1/\alpha_{tot}$ then according to this mean free path model, the charge state of the beam will not have changed. However, there will have been some probability for a charge-changing reaction accrued over the time interval. This probability will be less than $1 - 1/e \simeq 0.632$ which defines the mean free path for a reaction, but it will contribute to the beam's charge evolution as follows.

After a time $dt < 1/\alpha_{tot}$, the probability of sustaining a reaction of rate α_{tot} is

$$P(dt) = 1 - \exp[-\alpha_{tot} dt]. \tag{6.10}$$

After this first step, which is smaller than that needed to achieve a charge-changing reaction, the charge-changing time increment for the subsequent step will be reduced. After the first time increment of dt, a subsequent time increment dt' necessary to cause a charge change would be that which would satisfy

$$\frac{1}{\alpha_{tot}} = dt + dt' \tag{6.11}$$

or

$$dt' = \frac{1}{\alpha_{tot}} - dt \tag{6.12}$$

where dt is the value of the first time step taken which did not result in a charge-change. Thus, in the next iterative beam advancement step, it will be this increment dt' which is compared to the next energy reduction time increment dt_e.

Typically, if the incident beam has not reached its equilibrium charge state, the charge-changing time increment determines the integration steps. When the beam charge state is near or equal to the equilibrium value, the energy deposition time increment will likely be smaller since the net charge-changing reaction rate will then be low.

The path of only one particle is followed per run, representing the average beam particle's charge and energy evolution. The energy and charge of this ion are evolved as detailed above until the point at which the energy has been reduced to 1% of the initial ion energy. Note that this type of modeling will produce a beam charge evolution which may oscillate between at least two integer values. This will thus produce a jagged energy deposition rate profile, with the energy deposition changing with the square of the oscillating charge. This is actually physical since an actual ion in a beam will not exist in a single charge state but will oscillate among several at each beam velocity as it traverses a medium.

6.1.2 Using Charge Equilibrium Formulae

Suppose alternatively that the zstop code should be run which uses a simple formula such as the Bohr equilibrium formula (equation 5.4) to provide the beam's charge state. In that code, the beam's charge state will always be considered to be at its equilibrium value Q_E for a given velocity v_1. The mean free path for a charge change would be linked to the beam energy more directly than in the previous approach since the instantaneous equilibrium charge state is an explicit function of the beam energy. Numerical integration in this

case is more simple since the charge state and energy are already functionally linked.

A incremental beam time advancement for this case can be selected as follows. At an initial beam velocity v_1 and resultant equilibrium charge state $Q_1 = Q_E(v_1)$, the beam's differential energy deposition rate into the target is determined according to the physics of Chapter 4. A time step is calculated which would achieve a fractional beam energy loss ϵ_E

$$dt = \frac{1}{v_1}\epsilon_E E_1 \left(\frac{dE}{dx}\right)_1^{-1}. \tag{6.13}$$

where $(dE/dx)_1$ represents the initial energy deposition rate of the beam. No separate charge-changing m.f.p. is needed to be expressed in this case since the charge state is a function of the energy. This time increment dt will be used to perform the subsequent step of numerical integration.

6.1.3 Runga-Kutta Integration

At each point in the simulated evolution of the beam deposition, regardless of the manner in which the charge evolution is calculated, a suitable incremental time step dt is chosen as detailed above. This time step represents an advancement over which the beam's energy and charge state will change in a small, integrable manner. The initial beam parameters before the incremental advancement is made are Q_1, E_1, and v_1 which represent the beam's charge state, energy and velocity respectively.

A second set of values Q_2, E_2 and v_2 are formed according to the choice of charge evolution calculation and the nature of the time steps as described in the previous sections. The energy E_2 is given by

$$E_2 = E_1 + v_1 dt \left(\frac{dE}{dx}\right)_1 \tag{6.14}$$

The second beam velocity value v_2 is taken from the new energy (non-relativistically) to be

$$v_2 = \sqrt{\frac{2E_2}{A_p m_u}} \tag{6.15}$$

in which A_p is the projectile's atomic mass number and m_u is the atomic mass unit. The new charge value depends on the charge evolution model employed. A new energy deposition rate is then calculated for the new beam parameters

$$\left(\frac{dE}{dx}\right)_2. \tag{6.16}$$

This represents the energy deposition rate which the beam would exhibit if it had been advanced to the new energy and charge state values signified with a subscript of 2.

The actual energy decrement over the specified time increment is considered to be an average of the deposition rate as a function of the the original beam parameters (with subscript 1) and the deposition rate which is a function of the new values (with subscript 2). This is performed by a first-order Runga-Kutta method. It is first-order in the sense that the beam's energy deposition rate over the interval dt is considered to vary linearly from the initial value to the rate at the end of the interval. This is expressed by

$$\frac{dE}{dx} = 0.5\left\{\left(\frac{dE}{dx}\right)_1 + \left(\frac{dE}{dx}\right)_2\right\}. \tag{6.17}$$

The actual change in the beam's energy ΔE over the increment is given by

$$\Delta E = 0.5\left\{v_1\left(\frac{dE}{dx}\right)_1 + v_2\left(\frac{dE}{dx}\right)_2\right\} dt. \tag{6.18}$$

A new beam energy is formed $E' = E_1 + \Delta E$ and from it a new velocity v'. The averaged distance which the beam progressed in the incremental step is taken as

$$dx = 0.5(v_1 + v')dt. \tag{6.19}$$

A new beam charge state Q' is determined as well, either due to any integer change which may have occurred or a new value from an equilibrium charge state formula, depending on the model being used.

6.2 Demonstration of Modeling

The objective here is to demonstrate that the charge evolution models and energy deposition formulae can be integrated using the above numerical formulation to produce meaningful beam deposition calculations. These will be used later as tools to analyze the effects of target ionization levels on an incident beam's charge state evolution and energy deposition. In order to validate the accuracy of the calculations employed in the zstopx and zstop codes, experimental and proven semi-empirical results were collected which present data against which the results of the code could be compared. Verification of the calculations is demonstrated with particular focus on beam and target regimes of interest to HIF scenarios.

While the charge-changing reactions which alter the beam's average charge state have been validated in Chapter 5, a significant test is to use those charge evolution models to produce the charge state value of an incident particle to be used in energy deposition calculations. In Chapter 4 it was shown that the energy deposition of a charged particle into a target varies as the square of the incident particle's charge. Energy deposition and range calculations are therefore sensitive to the charge evolution calculations. A validation of the zstopx code by comparing its deposition profiles and ranges to experimentally and semi-empirically determined ones would be a strong endorsement that both beam charge

Energy [MeV/u]	zstopx	zstop	Exprmnt
114.09	867	862	861.8
50.56	307	302	301.7
20.68	122	116	117.0
10.08	71.9	67.0	67.1

Table 6.1: Ranges [mg/cm^2] in plastic of gold beams at different initial energies in gold targets, calculated and measured; Experimental uncertainty is near 0.2%.

evolution and energy deposition can be calculated individually and integrated successfully.

An excellent source for experimental data regarding heavy ion deposition into cold, solid density targets is found in Heckman *et al.*'s work [21]. That reference presents measurements of the deposition range of gold beams whose initial energies vary from 151MeV/u to 7.65MeV/u, covering well the range of interest of HIF and current atomic physics interest. Two targets were chosen for the experiments in that work, plastic and gold, with the expressed intent of investigating materials relevant to HIF research.

Table 6.1 lists the ranges of gold ion beams being penetrated into gold targets for a variety of initial beam energies. Presented are both experimental ranges and ranges produced from calculations of the codes developed in this dissertation. Note that the ranges as calculated from the zstopx codes are consistently longer than the measured range. This is most likely due to the fact that the cross section for charge transfer from the target onto the incident ion was not corrected for suppression due to target density effects. This was discussed in section 5.5.5. The ranges calculated according to the zstop code, which employs the Bohr equilibrium charge state formula for beam charge state, are nearly exactly matched to the experimental ranges.

Calculating the range of energy deposition of a beam into a target using a beam charge state value given from a semi-empirical fit for beam charge state is not a new result,

but merely confirms that the basic energy deposition modeling employed here is reliable. However, the use of discrete ionization and capture reactions to calculate the charge state of a beam as it is deposited into a target is a new result. These calculations are the first ever to calculate the range of a high-Z beam penetrating solid target, using a projectile charge state calculated from first principle without the benefit of a semi-empirical fit. The integrated modeling scheme outlined here as well as the physics of charge evolution and energy deposition will be used to draw new conclusions about the deposition of beams into dense, plasma targets.

The success of the modeling scheme employed in the zstopx code could be explored further in future work. The goal of this present work is only to establish that integrated charge evolution and energy deposition calculations can be performed using individual cross sections to calculate a beam's charge evolution in a target. This success will be extended in the following chapter to analyze the deposition of heavy ion beams penetrating a dense plasma target.

Chapter 7

Analysis and Results

The investigations of this work enable useful new conclusions to be formed for atomic physics in general and for heavy ion fusion applications. First, an improved understanding of the enhanced ionization rates observed in beams traversing rarefied gases and plasmas has been developed. Based on the details of this new understanding, conclusions can be formulated about the occurrences of anomalous ionization and new experiments can be recommended which would better address the remaining uncertainties in ionization cross sections for HIF. The comprehensive charge evolution modeling scheme developed here in Chapter 5 and the energy deposition models and calculations outlined in Chapters 4 and 6 will be used to perform calculations relevant to HIF beam penetration of two types of media. The two principle beam-target interactions which will be examined are (1)the ionization of ion beams incurred while traversing a rarefied gas or plasma (with ionic density near 10^{14}cm^{-3}) with no significant energy loss and (2)the energy deposition of ion beams into dense plasma targets. Also, based on the physical trends in the charge evolution of

beams penetrating dense plasmas, a new formula is developed enabling the calculation of the equilibrium charge state of a beam ion penetrating dense, partially ionized plasma targets such as those which may exist in HIF hohlraums as they are heated by the incident driver beams.

7.1 The Enhanced Ionization Problem

The foremost issue to be addressed is the problem of unexpectedly high ionization cross sections observed for beams penetrating both cold and ionized absorbers. This previous confusion about the shortcomings of ionization models has induced doubt about many beam-plasma interaction calculations and even about calculating atomic interactions of beams with neutral gases. This work has identified several problems with previously-employed cross section calculations which, if corrected, can appropriately address the situation. Also, by identifying the nature of the problem, expectations can be formed about regimes in which anomalously high ionization should be a concern in HIF and where it should not. Most important for the HIF applications is that an improved understanding of the ionization problem has shown that calculation of the ionization cross sections for beams penetrating rarefied gases or plasmas can be performed with confidence by using standard direct ionization models if appropriate attention is given to the types of indirect ionizations which can be expected.

7.1.1 Types of Indirect Ionization

Two distinct types of indirect ionization enhancements of direct ionization cross sections have been identified in incident ion beams corresponding to two basic targets regimes. These are (1)ionization enhancement by free electron impact and (2)beam ionization enhancement in cold gas targets. The former, due chiefly to deviations from the expected Lotz-type free electron ionization function (see section 5.4.6) has been shown to produce more extreme enhancements than ionization enhancement in cold targets. Enhancement of beam ionization rates in cold gases have been shown to increase the direct ionization cross section only by a factor of about 1.4. This distinction and its implications for previously-held views on ionization enhancement and cross section problems are discussed below.

7.1.2 The Plasma Distinction

Through the differences in beam ionization observed in the creation of a plasma state in targets, an understanding can be developed of the nature of the ionization problem. As yet, only one possibility had been seriously considered for explaining anomalously high beam ionization cross sections: inefficacy of the nuclear ionization models (usually the BEM discussed in section 5.4.4) to address auto-ionization from excited projectile atomic states. These indirect ionization cascades are currently considered to be the likely, yet onerously calculated, cause of the ionization cross section enhancements in beams penetrating plasmas and gases. The correction factor which Dietrich *et al.* employed to account for indirect ionization enhancement of direct ionization [18] was applied to the Gryzinski BEM collisional

ionization cross section. The factor which they chose was shown in later experiments not to be sufficient to account for all of the enhanced ionization [19]. It was then assumed that even the corrected cross section approach was not useful and that the BEM cross section was irreparably wrong in many cases.

However, the problematically high beam ionization rates reported by Dietrich and Hoffmann in particular were observed in a beam penetrating a hydrogen plasma target. From the physics of the BEM model, nuclear ionization in a cold hydrogen target is nearly identical to nuclear ionization in a hydrogen plasma since in both cases the screening of the nucleus is negligible and the incident ion's electrons would sense the entire unscreened proton charge in ionizing collisions. *So, enhanced ionization in plasmas should only be attributed to BEM shortcomings insofar as ionization in cold gas targets is underestimated by it.* In this case, the truly anomalous ionization occurred only in the plasma target and should then clearly not be attributed to BEM cross section problems alone.

Furthermore, this dissertation has shown that in fact the cross section responsible for the calculation of ionization due to free electron impact does require extensive correction. This correction was required, but not applied, in the experiments in which the BEM was blamed for under-calculation of observed cross sections [19], [18] (See section 5.4.6 for this analysis). Shortcomings in this free electron ionization cross section (the Lotz formula) have not yet been identified as a cause of under-estimation of ionization rates of beams penetrating plasmas. Analysis here has shown that its current use in its original form is guaranteed to under-estimate electron impact ionization cross sections significantly in some cases, particularly for ionization of highly charged heavy ions penetrating hydrogen plasmas.

In section 5.7 were presented extensive comparisons which demonstrate that the BEM cross section accurately models ionization cross sections of beams penetrating cold matter, both in solid targets and in gases. Experimental data quantifying the ionization of neutral atoms by collisions with bare nuclei was reproduced within about 30% tolerance with direct BEM cross sections (see section 5.7.1).

Though some indirect ionization processes are likely to have contributed in the observed beam ionization enhancement in cold targets, their magnitudes and degree of deviation from direct ionization theory have been observed to be consistent and consistently less than the deviations from theory found in plasmas [60]. The problem particular to cold gas enhancement can be addressed separately. For many applications, such as those analyzed by Dietrich and Hoffmann, both the enhancement in plasmas and the enhancement in cold targets were certainly present. The approach of applying a correction factor to the BEM ionization cross section is indeed a sensible approach to handling the indirect ionization for collisions with nuclei. But, the free electron contribution to indirect ionization must be addressed and it must be quantified by a separate corrective factor in future works.

7.1.3 Target Density and Indirect Ionization

Enhancement of direct ionization reactions by indirect phenomena has been shown to be a significant effect in some cases of beam interactions in which either the target is a gas or rarefied plasma. The manifestation of indirect ionization contributions to direct ionization may be linked to the density of the target into which a beam is penetrating. For effects similar to those causing the suppression of electron capture reactions in beams penetrating dense targets, these indirect ionization phenomena which involve electronic

activity in the incident beam's outer principal quantum shells may be suppressed as well.

A proposed formalism for determining the target density regime in which indirect processes such as auto-ionization become important can be developed. This is not an effect due to changes in the target equation of state but rather to changes in the direct ionization reaction rates relative to the indirect ionization rates. A direct ionization of a beam by collision with a target occurs at a rate which is a function of the direct reaction cross section σ_d, target density n_t and the projectile velocity v

$$\alpha_d = n_t \sigma_d v. \tag{7.1}$$

The rate for a typical indirect ionization process in an excited atomic state is a function of the auto-ionization rate A_a, which in isolation does not depend on target density. It is a property of the atomic structure of the excited projectile atom or ion. Following the formulation used in the dielectronic recombination analysis of section 5.5.3, the auto ionization rate for an excited atom or ion can be calculated by [54]

$$A_a(jnl \rightarrow iE_k l \pm 1) = \frac{8}{\sqrt{3}} \frac{1\text{Ry}}{\hbar} \frac{Z_p^2}{n^3} \frac{1\text{Ry}}{(E_i - E_j)} \frac{1}{(2l+1)} f(i \rightarrow j) G_l(k, k'). \tag{7.2}$$

In this form, n is the original excited shell of the electron which is ejected and j and i are the initial and final states of the de-exciting electron.

This expression can be reduced to a characteristic value for HIF applications by some simple scaling. A relevant case to consider would be for a high-Z ion with an electron excited to a state $n \approx 10$ followed by a dominant transition from a valence electron $j \approx 5$ to a hole in the inner shell $i = 1$ [54]. Using typical values for oscillator strengths and the Kramers-Gaunt factor summed over l, 0.01 and 0.2 respectively, the auto-ionization rate

becomes approximately

$$A_a \approx 10^{14} \frac{Z_p^2}{n^3} \frac{1\mathrm{Ry}}{(E_i - E_j)} \mathrm{s}^{-1}. \tag{7.3}$$

Using Bohr-like binding energy scaling for the various shells, this becomes

$$A_a \approx 10^{11} \mathrm{s}^{-1}. \tag{7.4}$$

The criterion for establishing the density regime near which these indirect ionizations become important is

$$A_a > \alpha_d. \tag{7.5}$$

This condition states that indirect auto-ionization events proceed at a rate greater than direct collision ionizations in the target. This can be expressed in more detail as

$$10^{11} \mathrm{s}^{-1} > n_t \sigma_d v. \tag{7.6}$$

Using a typical geometrical value of the direct ionization cross section $10^{-16}\mathrm{cm}^2$ and a projectile velocity near $\beta = 0.1$ this gives

$$n_t < 10^{17} \mathrm{cm}^{-3}. \tag{7.7}$$

This simple analysis can actually support some meaningful interpretations. First, this justifies that calculations of beam penetration into dense targets should not require consideration of indirect ionization processes, since the densities of the solids considered are at least several orders of magnitude larger then this approximate critical density of $10^{17}\mathrm{cm}^{-3}$. Also, this explains why the plasmas studied in the GSI experiments [19], [18], [36], whose densities were near or lower than this density, exhibited the indirect ionization cross section enhancements. In the Shevelko experiment examining beam ionization in

targets of a density near 10^6cm^{-3} [60], the density criterion of equation 7.7 is met within a margin of many orders of magnitude. Thus, the presence of enhanced beam ionization rates due to indirect processes can be understood.

Note that the HIF chamber densities in IFE power plant designs are expected to be of the order of 10^{14}cm^{-3}. According to this analysis, that chamber density may be rarefied enough to allow indirect processes to be important for incident heavy ion beams.

7.1.4 New Semi-empirical Accounting for Enhanced Ionization

Given that the enhancements of beam ionization in plasma targets and in cold targets can be distinguished, more sensible semi-empirical adjustment factors can be used to modify direct nuclear ionization cross sections. For ionization of beams penetrating plasmas it has been shown that amplification of the direct free electron ionization cross section is by as much as a factor near 10 for highly charged projectiles with $V \equiv v/v_{nl}$ lower than the ionization peak which occurs near $V = \sqrt{e} \approx 1.65$. Near the peak and for velocities such that $1 < V < 2$ the deviation is typically by a factor of 2. For $V \gg 1$ the indirect phenomena do not contribute and the Lotz expression agrees well with observed data [50].

For ionization by collision between a projectile electron and a target atom or ion's shielded nucleus, the Shevelko results show a consistent trend in ionization cross section enhancement [60]. The results indicate that the amplification of direct ionization is by a factor near 1.4 over a wide range of projectiles, charge states and energies. This factor can be used with reasonable reliability as a correction factor for direct ionization calculations for ions penetrating gaseous targets.

These two schemes can be used to formulate a more thorough semi-empirical scheme for quantifying indirect ionization phenomena.

7.1.5 Recommendations For Future Experiments

Based on the preceding delineation of the ionization problem, a clear and simple experimental program can be outlined to address any remaining uncertainties in ionization cross sections for HIF purposes. The following recommendations are based on a standard experimental technique of shifting the frame of reference from the target to the beam. In other words, just as in the experimental work of Stenke [50] and Matsuo [26], ionization cross sections for a heavy ion beam species X can be determined by directing a beam of charged particles, either ions or electrons, against a target of atomic number X. Also, measurements of the ionization cross sections of species X at charge states $Q > 0$ can be performed by using a crossed beam technique [33],[50].

Since the velocity dependence of nuclear collision ionization and electron impact ionization are different, complete examination of the problem will be accomplished by two types of experiments.

Electron Impact Ionization

First, electron impact ionization should be studied for a wide range of energies from cut-off to near-relativistic for each relevant charge state of a given ion. Once the dependence of indirect ionization events on charge state and energy are gathered empirically a complete semi-empirical fit can be drawn.

Several semi-empirical adjustments need to be made to the original Lotz ionization

formula in order to fit it to the body of experimental data. The observed electron impact ionization cross section is shown to deviate from the Lotz cross section when the species to be ionized is charged to an initial charge state greater than 1+. The magnitude of the cross section, particularly at electron impact energies near or lower than the ionized species' valence electron energies, is found to deviate from the magnitude of the cross section predicted by the Lotz formula. Also, the electron beam energy (or projectile velocity in another frame of reference) at which the electron ionization cross section reaches a maximum is different from that value expected from the Lotz formula. The following formulation is recommended to accommodate an eventual new fitting of the Lotz formula to the data. For ionization of an ion of species Z charged to $+Q$ by electron impact, the following general cross section formula is proposed

$$\sigma_{nl}(Z,Q) = \frac{a_{nl}(Z,Q)}{f_{nl} E_k I_{nl}} \ln[E_k/I_{nl}]. \tag{7.8}$$

The term f_{nl} will shift the peak of the electron impact ionization cross section, an effect which was observed in the empirical data.

Ionization by Screened Nuclear Charge

Ionization cross sections due to collisions with screened nuclei in the target exhibit their own particular behaviors with regard to indirect ionization events. The behaviors of these indirect ionization enhancements can be addressed by a simple and thorough proton or bare nucleus impact ionization study. This recommended experimental battery would be analogous to the work of Matsuo *et al.* but with collision energies of 20MeV/u. Since the BEM-type ionization cross sections scale with the square of the charge of the ionizer, the

results from such a study can be used and scaled for broad application. Protons or other bare nuclei can easily be accelerated to nearly any regime of interest required, particularly those of heavy ion fusion. Trends in indirect ionization and their deviations from direct calculations can be evaluated over the energy range and initial ionization recipient's initial charge state forming a complete data set. This set can be used, as in the case for electron ionization, to form a semi-empirical data bank.

This type of experiment could be improved by using a crossed beam technique as in the experiments of Stenke [50] and Gregory [33]. This could be used to study the ionization of more highly-charged ions by collision with bare nuclei, specifically quantifying the cross section values needed for current HIF studies. Measurement of ionization by proton or helium nucleus impact should be adequate to address current HIF chamber ionization concerns since the screened charge of the BeF_2 perceived by the incident lead ion at $20\text{MeV}/u$ is near 1.5 [51].

7.1.6 Optimal Direct Ionization Cross Section

Based on both empirical comparison and theoretical justification, an improved direct ionization modeling scheme was developed to be used to model ionization of a beam ion's electrons by impact with screened nuclear charges in the target. The BEM ionization cross section and its 'universal curve' velocity dependence (see figure 5.3) were used in this dissertation to provide excellent agreement with experimental data.

However, the expected form of the ionization cross section at high beam velocities relative to projectile electron orbital velocities is not exactly represented by the Gryzinski model's energy functionality. The Gryzinski values for $V \gg 1$ deviate, though not catas-

trophically, from the expected and experimentally-supported (see reference [24]) behavior given by

$$\sigma_{nl} \propto \frac{1}{E I_{nl}} \ln[E/I_{nl}]. \tag{7.9}$$

A hybrid model was therefore proposed which consists of the Gryzinski velocity function from section 5.4.4 for velocities less than approximately 7.3 and the idealized logarithmic behavior for higher velocities. This hybrid model was detailed in section 5.4.7. It was shown to model accurately ionization of neutral species by nuclear collision in section 5.7.1.

7.2 Heavy Ion Propagation Through Rarefied Targets

This section features calculations and discussions regarding the ionization of beams penetrating rarefied gases and plasmas associated with HIF power plant chambers and related experiments. The ionic density of the material in the chambers and vessels which the beams will traverse (BeF_2 or nitrogen in some upcoming experiments) is expected to be near 10^{14}cm^{-3}. Thus, according to the analysis of section 7.1.3, indirect processes can be expected to contribute to ionization rates. The roles of indirect ionization and direct ionization of beams in HIF-related rarefied targets will be examined in the following studies. Note that energy deposition calculations will not be considered in the following studies since the targets being considered are rarefied and no significant energy transfer is expected between the beam and gaseous target.

7.2.1 HIF Chamber Propagation

A specific scenario which is representative of an HIF power plant driver and chamber configuration is an initially singly-ionized beam of 20MeV/u lead ions penetrating a BeF_2 ambient gas or plasma at molecular densities near $5 \times 10^{13}\text{cm}^{-3}$. The degree to which the BeF_2 will be ionized is not certain at this point. Even if the chamber gas should initially be non-ionized, it may become ionized during the course of the beam's penetration due to photo-ionization by the radiation generated by the heating HIF hohlraum. Also, the beam itself will cause ionization in the chamber ambient through the same collisions which cause ionization in the beam itself. Given that the chamber BeF_2 may exist in a plasma state, calculations of beam ionization will be performed for penetration of both a cold, non-ionized gas and for BeF_2 ionized to varying degrees.

Since the density of the ambient gas or plasma in the HIF chamber will be much lower than 10^{17}cm^{-3} (see section 7.1.3), and since a plasma state in the BeF_2 may be encountered, indirect beam ionization processes must be addressed. Of the two types of direct ionization reactions, screened nuclear impact and free electron impact ionization, only the former is expected to be enhanced by any indirect ionization augmentation in HIF power plant chambers. This expectation is understood by examining the relative velocities of the beam and its ions' valence orbital velocities. The HIF driver beam velocity is expected to be near $0.2c$. The initial charge of the beam upon entering the chamber should be near 1+. Conservative expectations indicate that a significant fraction of the beam could be ionized to charge states as high as 12+ after traversing 300cm of the BeF_2. The valence electron velocity of a lead beam at this charge state can be calculated according to equation 5.15

to be approximately $0.02c$. Thus, the scaled velocity $V \equiv v/v_{nl}$ where v_{nl} is the beam's valence orbital velocity should be near10 for the highest beam charge state and greater than 10 for the lower charge states. In this regime of $V \gg 1$, the Lotz formula for electron impact ionization was shown to model the experimentally observed ionization cross sections well. Indirect processes did not contribute to the total ionization in this regime.

Furthermore, even if the chamber should be in a plasma state, the ionization by collision with the BeF_2 nuclei and their remaining bound electrons will be much larger than even an enhanced free electron contribution. This will be demonstrated by examining the associated cross sections. Therefore, the only ionization cross section which will be increased by indirect contributions would be the BEM cross section. The enhancements to the BEM formula due to these indirect processes will be applied as outlined in section 7.1.4.

First consider penetration of a cold, non-ionized HIF chamber gas by a beam of lead ions. The calculated ionization cross sections for lead ions at $0.2c$ penetrating BeF_2 over a range of charge states is presented in table 7.1. They also are shown graphically in figure 7.1. The values presented there have not been modified by any ionization enhancement factors and have been generated by the BEM formula. Note also that these represent ionization cross sections *per BeF_2 molecule*. The value is therefore the sum of the cross sections due individually to two fluorine atoms and one beryllium.

Using those values the average charge evolution of the beam can be calculated as it penetrates the chamber. Two computations were made for penetration of this cold BeF_2 chamber, one with no ionization enhancement and one with the factor of 1.4 applied to the ionization cross sections. At the charge states involved here, electron capture reactions are

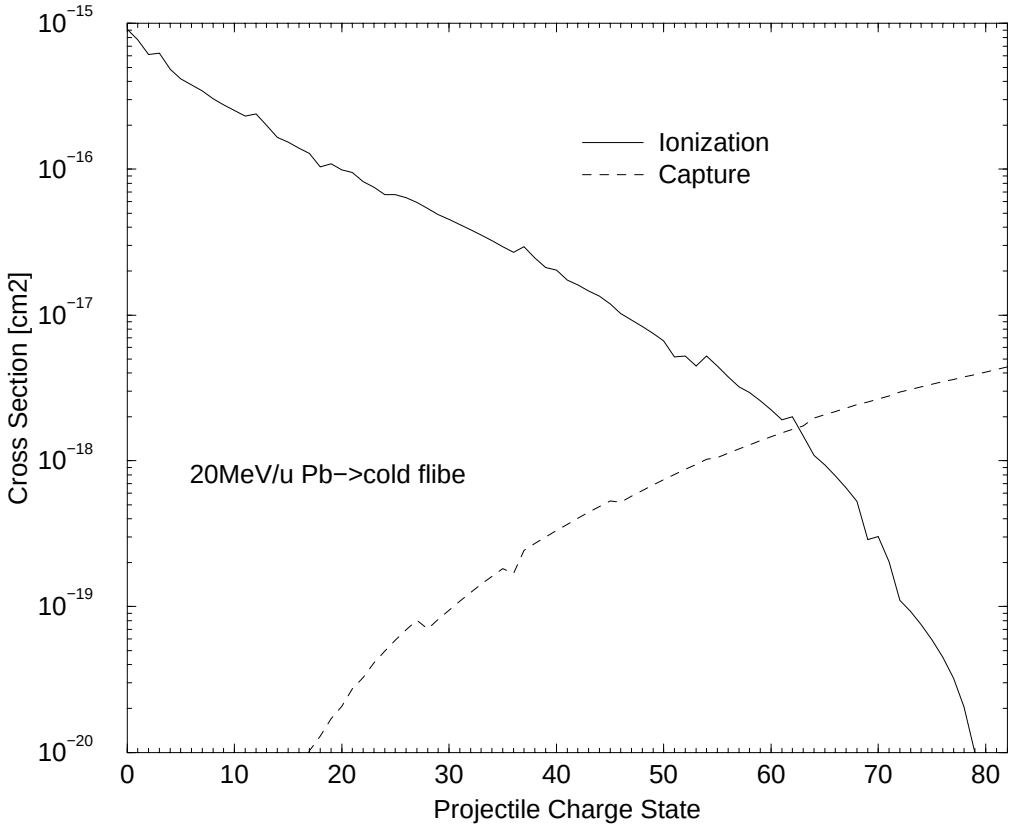

Figure 7.1: Cross sections for direct ionization and capture for 20MeV/u Pb beam penetrating an HIF chamber gas of $5 \times 10^{13}\mathrm{cm}^{-3}$ BeF_2 calculated by BEM

Charge State	Cross Section [$/10^{-16}\mathrm{cm}^2$]
0	9.12
1	7.74
2	6.12
3	6.24
4	4.83
5	4.17
6	3.78
7	3.45
8	3.03
9	2.77
10	2.53
11	2.32
12	2.40

Table 7.1: Cross sections for direct ionization of 20MeV/u Pb beam penetrating an HIF chamber gas of $5 \times 10^{13}\mathrm{cm}^{-3}$ BeF_2 calculated by BEM

inconsiderable. Figure 7.2 displays the calculated average charge evolutions of the beam as it penetrates the chamber for these and other cases.

Calculations without the enhancement indicate that the average charge state of a 20MeV/u lead beam initially charged to +1 entering a typical HIF chamber containing the cold BeF_2 at $5 \times 10^{13}\mathrm{cm}^{-3}$ would be between 6 and 7 after traversing 300cm and between 9 and 10 after 500cm. With the enhancement factor included the average beam charge states are between 8 and 9 after traversing 300cm and between 11 and 12 after 500cm.

Now consider the calculation of the ionization cross sections for the above case but supposing the BeF_2 were ionized to some degree. Table 7.2 displays the ionization cross sections generated by three separate arbitrary target ionization levels. They are (1)F ionized to 2+ and the Be to 1+; (2)F ionized to 4+ and the Be to 2+; (3)F ionized to 8+ and the Be to 4+; The free electrons were given a temperature of 20eV in all cases. The value of this

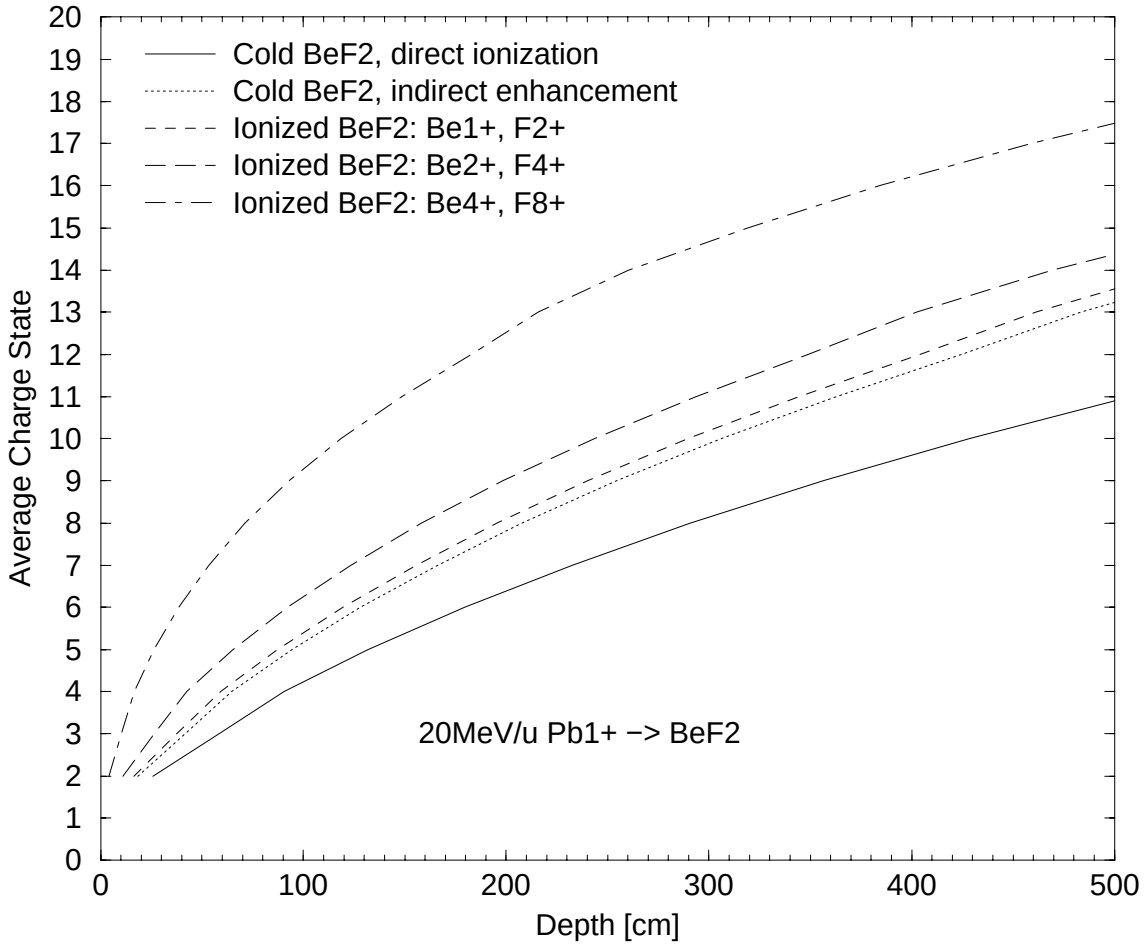

Figure 7.2: Various charge evolution calculations for a 20MeV/u Pb beam penetrating HIF chamber plasma of $5 \times 10^{13}\mathrm{cm}^{-3}$ BeF_2; dotted line shows results using cross sections multiplied by 1.4 and dashed line shows case of ionized BeF_2 (see text)

temperature does not affect the cross sections and is arbitrary. In these calculations note that indirect ionization enhancement was included both in the free electron component and the BEM component to the cross section as in section 7.1.4. This is a conservative approach but is consistent with the approach which was employed in section 5.7 to model the GSI plasma data. But, as discussed earlier, due to the relative velocities of the beam and its valence electrons, the free electron impact ionization is expected to behave as predicted by the Lotz formula. The corrective factors are only engaged at lower beam velocities or at much higher beam charge states which correspond to a smaller scaled velocity V.

Figure 7.3 displays the ionization and capture cross sections for a lead beam at $v = 0.2c$ penetrating the BeF_2 ionized as in case (3) above. Note that the ionization cross section due to plasma electron impact ionization is consistently smaller than the total ionization cross section (consisting mainly of the BEM ionization cross section) by about a factor of 10.

The charge evolutions of an HIF driver beam in each of those ionized BeF_2 cases are also shown in figure 7.2. Notice that the case with the lowest ionization (including indirect enhancements) does not cause a significantly higher charge evolution than the case calculated using BEM enhancement in a non-ionized chamber. This is expected since the BEM nuclear ionization dominates due to the fact that the square of the screened nuclear charge of the target constituents will cause that contribution to exceed even the enhanced free electron contribution. The BEM contribution is indeed a bit higher also here because the screening of the BeF_2 nuclei is reduced, but also reduced are the number of bound electrons which ionize. For instance, the outer valence electrons which dominate the total

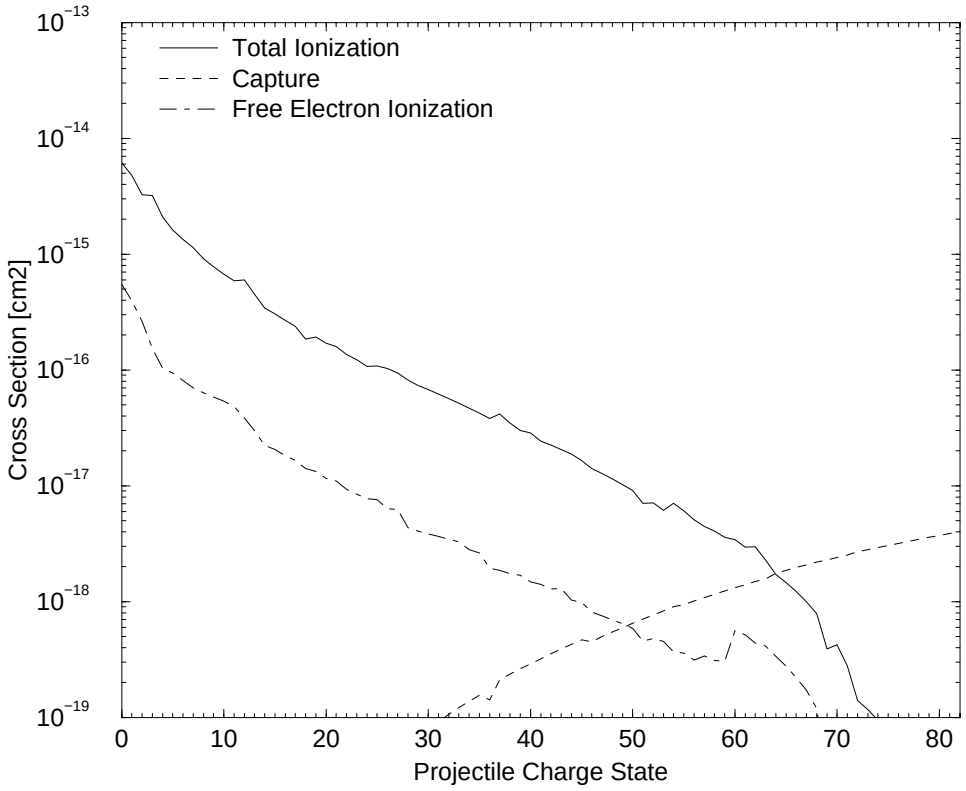

Figure 7.3: Cross sections for ionization and capture for 20MeV/u Pb beam penetrating an HIF chamber plasma of $5 \times 10^{13}\mathrm{cm}^{-3}$ BeF_2 with Be^{4+} and Fe^{8+}

Charge State	Cross Section (1)	(2)	(3)
0	14.7	22.8	61.3
1	12.2	18.1	47.9
2	9.42	12.9	32.5
3	9.30	12.5	32.0
4	7.16	8.91	21.0
5	6.17	7.35	16.2
6	5.55	6.45	13.5
7	5.04	5.73	11.4
8	4.44	4.95	9.11
9	4.03	4.44	7.78
10	3.67	3.99	6.70
11	3.36	3.63	5.86
12	3.46	3.72	5.99
13	2.87	3.01	4.51
14	2.35	2.43	3.41
15	2.17	2.23	3.05
16	1.96	2.01	2.67
17	1.80	1.84	2.39
18	1.46	1.48	1.85
19	1.52	1.54	1.92
20	1.38	1.39	1.71

Table 7.2: Cross sections $/10^{-16}\mathrm{cm}^2$ for ionization of $20\mathrm{MeV}/u$ Pb beam penetrating an HIF chamber gas of $5 \times 10^{13}\mathrm{cm}^{-3}$ BeF_2 with 3 levels of ionization (see text) and correction for BEM enhancement

cross section sense a screened fluorine nuclear charge of 0.768 and 9 bound electrons in the neutral BeF_2 case. In the case of the ionized BeF_2 with F^{2+}, the lead's outer electrons sense a fluorine nuclear charge of about 2 but with only 7 bound electrons. The net result is a target charge term of 9.59 in the neutral case and 11 in the ionized case, only a 16% increase. But, with higher BeF_2 ionization levels, the incident beam's charge evolution does indeed to differ significantly from the charge evolution in cold BeF_2.

Charge State	Total	$m = 1$	$m = 2$	$m = 3$	$m = 4$
0	9.12	4.42	1.36	1.30	0.401
1	7.74	4.11	1.13	0.31	0.085
2	6.12	3.67	0.84	0.19	0.043

Table 7.3: Multiple ionization cross sections $/10^{-16}\text{cm}^2$ for 20MeV/u Pb beam penetrating an HIF chamber gas of $5 \times 10^{13}\text{cm}^{-3}$ BeF_2; no enhancement included

Multiple Ionization Probabilities

The above analysis provides useful average charge state evolution calculations and net charge-changing reaction cross sections for HIF driver beams in power plant chambers. However, detailed HIF beam dynamics calculations require knowledge of the actual distribution of charge states in the beam. This requires an accounting of the multiple ionization probabilities discussed in section 5.4.10.

The multiple ionization cross sections for a multiplicity up to $m = 5$ over a range of charge states for the case of the lead projectile penetrating the cold BeF_2 are presented in table 7.3. The probabilistic technique employed here for the generation of the following data was the most basic approach using the average probability (see section 5.4.10). However, the levels of multiple ionization agree well with similar calculations by Olson [51].

7.2.2 Calculations for Intermediate Experiments

In addition to full-scale power plant scenarios, several other HIF beam experiments may be implemented soon. These intermediate experiments are intended to serve as proof-of-principle steps towards the development of a full scale power plant. The atomic physics issues of two such upcoming experiments are addressed below. For the beam physics parameters discussed here, please see Appendix A.

HCX

The HIF driver beam systems hoped to be employed in imploding reactor-grade fusion fuel capsules will require the delivery of very high currents of ions, near 1Amp, onto a small target. One of the scientific challenges presented by such a scheme is the control of high current beams. While possible in principle, some technological and scientific issues remain to be validated along with some basic engineering questions. A *high current experiment* (HCX) is now being designed by scientists at the Virtual National Laboratory for Heavy Ion Fusion Research to address those issues and to establish confidence in high current beams as driver candidates.

The planned beam parameters of the HCX are as follows. The beam ion will likely be potassium charged initially to 1+. The energy of the ions will be 1.8MeV, which is about 46.2keV/u. This corresponds to a beam velocity near 0.01c. A current between 300 and 800mA will be sought to be generated in the beams. The perveance achieved is hoped to be comparable to that of the planned HIF power plant beams, between 10^{-3} and 10^{-5}. The beam will be directed through a background atmosphere of air (approximated by nitrogen) over a channel distance of about 20m. The pressure of this ambient gas may be between 10^{-6} and 10^{-8}Torr. Ideally, the pressure will not have to be pumped down to the lower end of this range since that poses engineering difficulties. But, if the ionization cross sections should be large for this beam, then low pressures may be needed to avoid ionization.

An important consideration must be made in this case. Due to the low beam velocity in this experiment, the equilibrium charge state Q_E which the potassium beam ions would eventually reach (if the accelerator channel were very long) is quite low. It is

found from the semi-empirical fit to be

$$Q_E = 19(1 - \exp[-0.01/(19^{2/3}\alpha c)]) \approx 3.2 \tag{7.10}$$

While it is certainly not expected that the HCX beam would reach an equilibrium charge state in the rarefied nitrogen ambient gas, conclusions can be formed about the limits of expected ionization of the potassium beam. At this low energy of 46.2keV/u, the potassium will not be ionized beyond about a charge state of 3+. However, it is desired even that this low charge state will not be reached in the HCX accelerator channel. In fact, a successful experiment will be considered to be one in which only a small fraction of beam is ionized beyond 1+.

The ionization and recombination cross sections for potassium at this energy penetrating molecular N_2 for a range of charge states are shown in figure 7.4. Note that equilibrium charge state of the beam as calculated by the Bohr semi-empirical fit (marked by the dashed line) coincides exactly with the charge state at which the capture and ionization cross sections balance. No corrections for indirect ionization enhancement have been incorporated into those cross sections. The ionization cross sections at low charge states are quite high with respect to the other values which have been associated with HIF experiments. The reason for this is the low beam energy. At 1.8MeV, the beam velocity is very near that of its orbital electrons, maximizing the cross section. Note also that as the charge state increases, the cross sections decrease very quickly. This is due to the exponential drop-off in the BEM ionization velocity function for $V < 1$ as in figure 5.3. Also, keep in mind that the values presented in the figure are for molecular nitrogen N_2.

The question is, How rarefied must the HCX channel air be to limit ionization

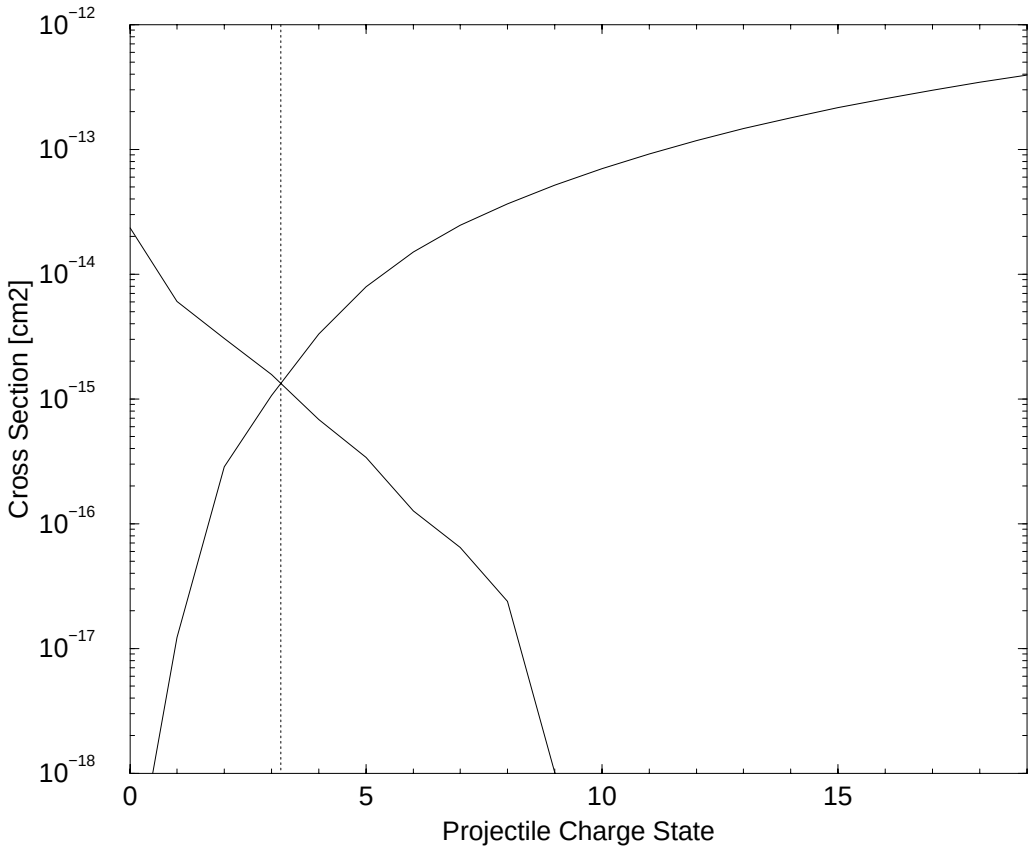

Figure 7.4: Cross sections for direct ionization and capture for 1.8MeV K beam penetrating a nitrogen gas; the dashed line marks the Bohr semi-empirical charge state

to within a specified tolerance? The ionization cross section of K^{1+} by molecular nitrogen at this energy is near $60 \times 10^{-16}\text{cm}^2$. At the highest pressure of 10^{-6}Torr, which gives a molecular density of near $3.5 \times 10^{10}\text{cm}^{-3}$, the fraction of K^{2+} ionized from the K^{1+} is given according to section 3.2 by

$$f(2+) = 1 - \exp[-(3.5 \times 10^{10}\text{cm}^{-3})60 \times 10^{-16}\text{cm}^2(20\text{m})] \tag{7.11}$$

which is about 34%. This may be unacceptably high and pressure reduction may be required for HCX beyond that which was originally anticipated.

If 99% of the beam is to be maintained at the initial charge state of 1+ then the density of the HCX accelerator channel must be near $8 \times 10^8\text{cm}^{-3}$. This corresponds to a pressure near 2.4×10^{-8}Torr.

IRE

Following the HCX, the next intermediate experiment designed to demonstrate confidence in actualizing an HIF power plant is the IRE, or *integrated research experiment*. The success of the IRE would ideally lead to the development of an actual engineering test facility (ETF), the final step before the realization of an IFE power plant. The experiment would incorporate the key elements of accelerator, focusing and chamber technology in a scaled system.

An important proof-of-principle issue for the IRE project is to demonstrate successful final focusing of the driver beam. Currently the crucial aspect of this is the handling of beam's space charge effects. The IRE is being designed to achieve the same space charge properties as those of the possible HIF power plant driver beams. The perveance of the

IRE beam in final focus is therefore desired to be similar to that of the eventual HIF driver beams. This value will be between 10^{-5} and 10^{-3}. Since this perveance represents a unitless quantity of space charge repulsion, its scaling between HIF beams and IRE beams will be examined in terms of ionization created in the respective chambers. This will therefore connect to the cross section analysis developed in this dissertation.

The IRE will not feature, however, a beam identical to the intended HIF driver beam. Currently envisioned for the IRE is a potassium beam with an initial charge state of 1+ at an energy near 400MeV. The current will likely be a fraction of the intended HIF driver beam current. Therefore some scaling factors may need to be considered in order to establish a correlation between HIF and IRE beam perveance values and their respective ionization levels.

The desired equivalence of the perveance of the HIF and IRE beams can be expressed and related to current and charge state as follows. Using the variables with subscript 1 to represent those associated with the IRE and 2 for the HIF values, we can equate the perveances of the two beams

$$Q_1 = Q_2 \tag{7.12}$$

which, using the explicit form, gives

$$\frac{q_1 \lambda_1}{m_1 v_1^2} = \frac{q_2 \lambda_2}{m_2 v_2^2}. \tag{7.13}$$

Re-expressing the linear current density as a current by $\lambda = I/v$ leads to

$$\frac{q_1 I_1}{m_1 v_1^3} = \frac{q_2 I_2}{m_2 v_2^3}. \tag{7.14}$$

The beam ion candidates for an HIF power plant will likely be in the atomic vicinity of lead. The energy of the HIF driver beam will be close to 20MeV/u with $\beta = 0.2$. Given these

typical values and the values of the IRE presented above, the implications of perveance equivalence on beam parameters can be found:

$$\frac{q_2 I_2}{q_1 I_1} = \frac{208}{39}\left(\frac{v_2}{v_1}\right)^3 \tag{7.15}$$

which gives

$$\frac{q_2 I_2}{q_1 I_1} \approx 5.3\left(\frac{v_2}{v_1}\right)^3. \tag{7.16}$$

At an IRE beam energy of 400MeV this ratio becomes

$$\frac{q_2 I_2}{q_1 I_1} \approx 43. \tag{7.17}$$

It is expected that the currents employed in the IRE beamlets should be several factors of ten smaller than the HIF driver beam currents per beamlet [22]. At the highest (and most desirable) IRE beam energy of 400MeV, this current scaling provides direct implications for the charge states of the respective beams, namely

$$q_2 \approx q_1. \tag{7.18}$$

In other words, the charge evolution of the IRE beam should be designed to be similar to the charge evolution of the HIF beam in the chamber.

The cross sections determining the IRE ionization rates will be a function of the ion choice and velocity. The chamber gas through which the beams will propagate will likely be air, which will be treated as molecular nitrogen for the purposes of these calculations. The ionization cross sections for ionization by nitrogen of the beam potassium ion at 100 and 400MeV over a range of possible charge states are listed in table 7.4. The velocities at two these energies are between $0.073c$ and $0.146c$. Note that the cross sections are

Charge State	100MeV	400MeV
0	15.6	5.15
1	7.95	2.74
2	5.90	2.03
3	4.48	1.54
4	3.29	1.14
5	2.50	0.878
6	1.53	0.563
7	1.37	0.520
8	1.00	0.402
9	0.671	0.293
10	0.504	0.230
11	0.369	0.176
12	0.255	0.130

Table 7.4: Cross sections $/10^{-16}\mathrm{cm}^2$ for ionization of potassium beam penetrating a molecular nitrogen gas at two energies with no correction for BEM enhancement

actually larger at the lower energy. This is because the scaled velocity $V = v/v_{nl}$ for the outer dominating electrons is closer to the peak for the lower energy. The velocities of the outer electrons of potassium and its associated ions are typically near $0.01c$, giving a scaled velocity value near 10 for the 100MeV case and near 20 for the 400MeV case.

A useful scaling question can therefore be addressed by selecting the nitrogen (air) density which will induce a charge evolution similar to that of the HIF beam evolution. Figure 7.5 shows the average charge state of a 400MeV IRE beam as a function of two different densities covering a range which should provide an estimate for the appropriate perveance scaling. An IRE chamber density near $5 \times 10^{14}\mathrm{cm}^{-3}$ should provide a charge evolution and perveance closely matched to that of the eventual HIF driver beams.

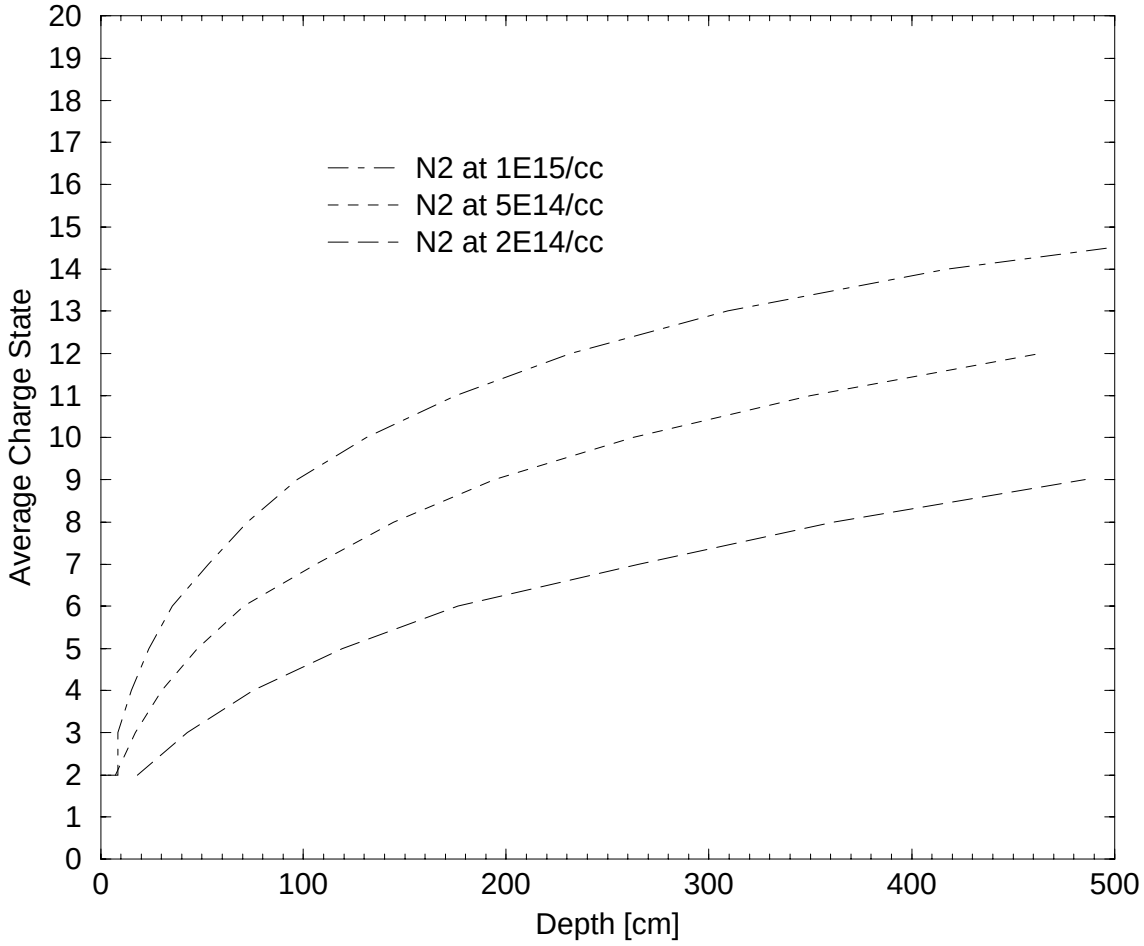

Figure 7.5: Various charge evolution calculations for a 400MeV K^{1+} beam penetrating molecular nitrogen at various densities

7.3 Beam Deposition in Target Materials

The second primary application of the atomic physics models developed and described in the present work is the improved simulation of the deposition of ion beams into dense, ionized solids. Particularly, the scenario of heavy ions penetrating HIF hohlraum plasmas will be examined. Modeling the deposition of heavy ion beams into dense plasmas requires the physics of ion energy deposition of Chapter 4, the charge evolution models of Chapter 5, and the integrated calculation technology of Chapter 6. This section incorporates those bodies of knowledge to perform calculations of heavy ion deposition relevant to HIF target scenarios.

As the hohlraum targets are heated by the incident beam, the nature of the energy deposition of the beam will change due to at least two factors: (1)the free electrons in the plasma target receive an incident beam's energy differently than bound electrons; (2)the equilibrium charge state evolution of the beam in the heated plasma target is expected to be enhanced relative to its charge state evolution in a cold target. Both of these effects will be incorporated in the calculations in this chapter.

The stopping power of ionized targets with respect to a given incident beam is a function of the target's atomic properties and the beam's charge state. The quantification of the target's role in the stopping power, particularly the presence of free electrons and the change in the average ionization potential of its bound electrons, were addressed in section 3.1.8 and in Chapter 4. The atomic properties of several representative target plasmas were tabulated in section 3.1.10. Now, the only undetermined variable in calculating the energy deposition of a beam penetrating a dense plasma target is the charge state evolution

of the incident beam ions. All of the real activity in the following analysis is therefore in connection with the charge state modeling.

Armed now with a good understanding of the nature of the relevant processes, the charge evolution of beams being deposited into dense plasma target material can be modeled with good confidence and the integrated slowing-down calculations can be performed. Additionally, the physics of the preceding analyses will be used to develop a new semi-empirical fit for the equilibrium charge evolution of projectiles in dense target plasmas.

In section 5.7.3 it was demonstrated that the equilibrium charge state values given by the semi-empirical fit could be replicated from the ionization and capture cross sections outlined in this dissertation. In section 6.2 it was shown that energy deposition profiles along with ranges could be calculated with excellent accuracy using the integrated charge evolution and energy deposition calculations. The intent of the analysis in this section is to extend that success to modeling the deposition of beams in ionized targets.

The intended customers of this investigation are those who are interested in modeling the deposition of HIF driver beams into hohlraum convertor materials. But, since the analysis and resultant new semi-empirical fit will be sufficiently general, any calculations of beam interaction with dense, partially-ionized plasmas will benefit.

For the current application, the crucial issue is the determination of the degree to which the ionization state of the target material alters the charge evolution of a penetrating beam. A useful beam-target configuration to consider is that of a proposed HIF driver-hohlraum system. This may consist of a 4GeV lead beam ($\approx 20\text{MeV}/u$) penetrating a material ranging from a high-Z foam to a low-Z hydrocarbon. The densities of these targets

can range from 0.01g/cm^3 to 10g/cm^3. The temperature of the materials in the following analyses will range from cold (room temperature) to 300eV, which is near the maximum temperature achieved in current HIF hohlraum designs. At those high temperatures the target materials feature extensive ionization. The equation of state parameters needed were taken from the tabulated data of section 3.1.10.

The effects of different levels of target ionization on the projectile charge-changing cross sections will be evaluated systematically. The effects of these potential changes in projectile charge evolution on the integrated energy deposition calculations will then be evaluated.

7.3.1 Considerations for Dense Plasma Targets

Some details of charge-changing cross sections and energy deposition in dense plasmas should be addressed before preceding with the analysis proper. Both ionization and capture reactions will require special attention in the case of dense plasma targets. The presence of free electrons due to the target ionicity have been considered in some chamber calculations, but the density of the targets in this application plus the inclusion of energy deposition require some attention.

Since the target materials in which the cross section calculations will be performed are ionized, the problems of beam ionization enhancement due to collisions with target nuclei and with free electrons must be addressed. From the atomic physics investigations of this dissertation, several points emerge which will be useful in the resolution of the ionization enhancement issue in dense HIF plasma targets.

The most important observation is that in dense materials processes of auto- ion-

ization from excited states are suppressed or are not important. This is based both on the analysis of section 7.1.3 and the agreement between equilibrium fits and cross section calculations in section 5.7.3. The calculations in cold targets reproduced semi-empirical values well using only direct ionization cross sections. One can expect the direct ionization calculations in plasma targets to be reliable as well since they differ from the cold matter case only in effective target charge scaling and the addition of the free electron component.

Now, the free electron component has been shown to be responsible for significantly enhanced ionization in some cases. But, recall that those results were observed in a rarefied hydrogen plasma in which the nuclear ionization and free-electron ionization are both induced by a charge of 1. Thus, the effects of the complex free-electron indirect ionization behavior were relatively significant. In the case of higher-Z plasmas, the nuclear charge and bound electron contributions can be expected to be greater than the free electron component. This is due to the $\overline{Z}_t^2 + (Z_t - Q_t)$ target charge dependence of the BEM ionization cross section (see section 5.4.8) as compared to the target charge factor Q_t associated with the free electron ionization cross section. Also, the Lotz free electron cross section velocity dependence is at all values either less than or equal to that of the BEM nuclear ionization functionality. This coupled with the high-density suppression of the indirect ionization effects indicate that enhanced ionization in plasmas should not be an issue for these calculations.

Electron capture processes in hohlraum plasmas will be due to both any bound electrons present and the radiative recombination of free electrons. In general, the charge transfer reaction rates from bound electrons will be far greater than the radiative recom-

bination rates from the free electrons [54]. The eikonal-corrected OBK (Oppenheimer, Brinkman and Kramers) model and the radiative charge transfer model of section 5.5 will be used to calculate the total charge transfer cross sections. This approach was shown to reproduce the average equilibrium charge state of a beam penetrating a cold target within a few charge states. However, the eikonal adjustments may break down at high target ionization levels. This is due to the fact that at high ionization, the initial binding energies of the electrons in the target ions will be larger than the typical energies of a neutral atom's valence electrons. While the adjusted OBK theory works well for near-neutral targets and their associated dominating low valence energies, the theory has not been applied yet to the extreme conditions of the dense plasmas studied here. However, the qualitative and gross trends predicted by the charge transfer models will be useful.

The density corrections for capture reactions also can be employed. This was discussed in section 5.5.5. In section 5.7.3 it was shown that even without such corrective factors the charge-changing models reproduced the equilibrium charge states of beams penetrating a cold target within about 15% of the value given by the semi-empirical fit. Since this error is within the error of the typical cross section value, which is 30%, capture density effects will not be considered to be important.

In the dense target materials simulated here, some consideration must be made for the lowering of the binding energies of the target's valence electrons by plasma shielding. This was discussed in section 3.1.9. This was not an issue in the chamber gases due to the reduced density. However, in the heated hohlraum targets, the Debye length can be of the order or less than the typical ionic radius. Therefore, the valence electron energies will

be reduced roughly according to the reduction in effective target ionicity as described in section 3.1.9.

Another important process in highly-ionized, high-Z plasmas must be addressed which has not yet received much attention in the associated literature. While it is well understood that a projectile can lose electrons due to an ionizing collision with the target, another channel exists for electron loss in certain cases. The charge transfer process which normally acts to reduce the projectile charge can occur in reverse. Instead of receiving a bound electron from the target, a projectile can transfer one of its electrons to an ionized target. This form of electron loss can be important in partially ionized plasmas and will be considered in the following analyses. It will be calculated by the same charge transfer formulas for target-to-projectile charge transfer, but with the roles of the projectile and target reversed.

7.3.2 Charge Equilibrium Evolution in Dense Plasmas

If a quotidian calculation technique is sought to be developed for beam-target deposition, then the integrated energy loss and charge evolution calculations must be rapid. Since energy deposition is easily calculated by a few formulae, the majority of the computation time is due to the iterations associated with the charge evolution calculations. Ideally, some form of a semi-empirical fit would be made available for plasma deposition as in cold targets if the dense plasma charge evolution were equilibrium-dominated and if that equilibrium condition could be formulated.

The first issue to resolve then is whether or not the charge evolution of a projectile in a dense plasma can be considered to be in equilibrium. In dense cold target materials,

a given projectile very rapidly reaches and maintains throughout its range a charge representative of an equilibrium charge state given by the Bohr semi-empirical model. But, it has been established that at least in some beam-plasma deposition scenarios, the projectile charge state at a given velocity is not necessarily the local equilibrium charge state [14],[54]. This is attributed to suppression of capture reactions in highly-ionized plasmas. Radiative free electron recombination generally occurs at a rate lower than charge transfer reactions, so without the benefit of charge transfer, equilibrium charge attainment in a beam penetrating a target plasma may be delayed. The equilibrium condition then may be dependent upon the atomic properties of the target, specifically the availability of bound electrons to generate the stabilizing charge transfer reactions.

It can be demonstrated that in at least certain hypothetical dense target plasmas, the charge of an incident heavy ion will not necessarily attain equilibrium in a time scale small with respect to the characteristic energy deposition time. In this case, the beam's charge state will not change as quickly as the characteristic energy change and the beam ions will not be in charge equilibrium at all points. Consider a beam-target configuration likely to exhibit non-equilibrium charge evolution of an incident beam: heavy ion deposition into a fully-stripped dense plasma. Figure 7.6 shows the charge state as a function of velocity of initially 20MeV/u Pb^{10+} ions penetrating a fully-stripped carbon target at 300eV and 0.01gcm^{-3}. Note that a dense carbon plasma at these conditions, as seen from the tabulated data in section 3.1.10, would not actually be fully-stripped. However, the fully-stripped condition was imposed on the target to illustrate the effects of a complete absence of bound target electrons. The beam charge state encountered at each velocity was taken from

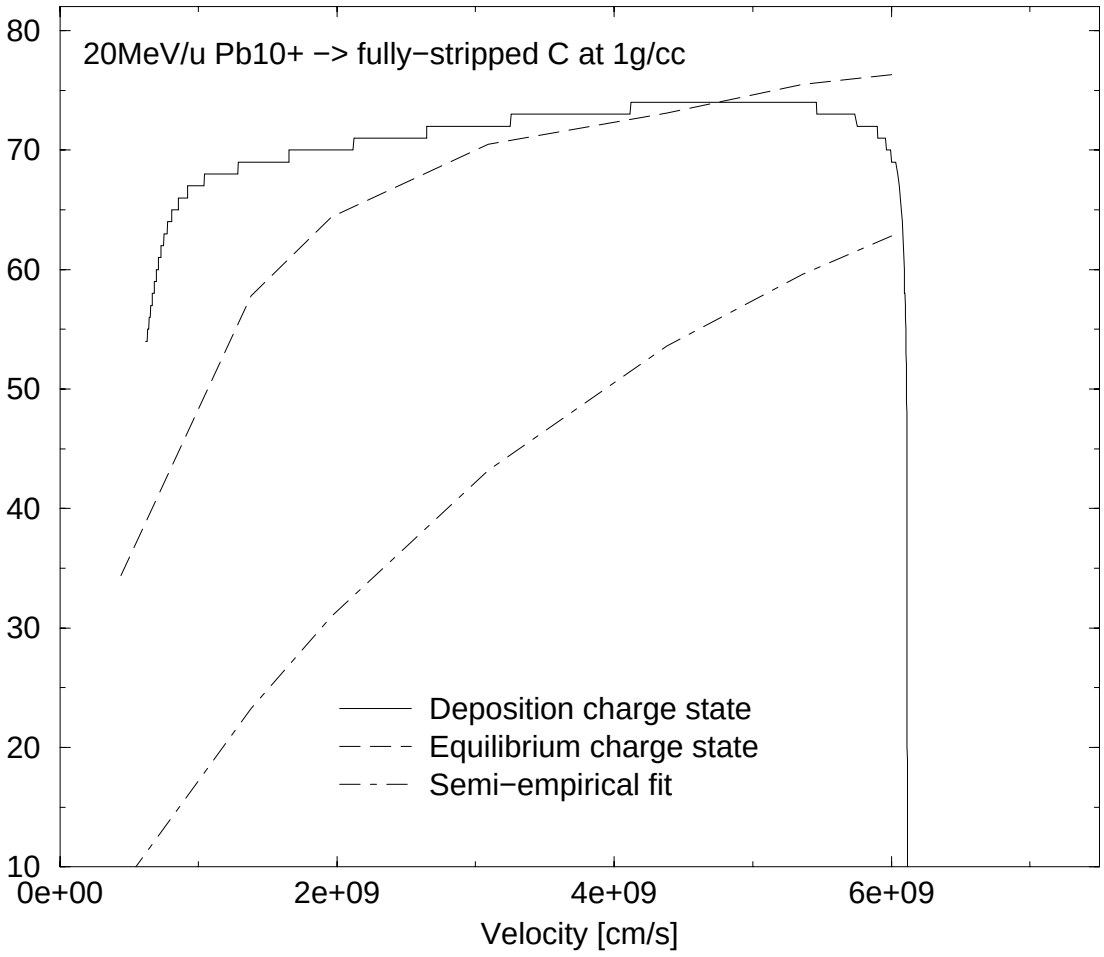

Figure 7.6: Charge evolution of 20MeV/u lead penetrating a fully stripped carbon plasma at 0.01gcm^{-3}

the integrated energy deposition and charge evolution calculations using the **zstopx** code outlined in Chapter 6. Shown for comparison are the equilibrium charge states which a beam would reach at each velocity as calculated by the method of section 5.7.3 and the equilibrium charge states given by the Bohr semi-equilibrium fit for deposition in cold matter.

In this simulation the projectile clearly does not maintain a charge state representative of an equilibrium value. After rising from its initial charge state of 10+, the lead ion lingers in the higher state as it slows, not following the equilibrium value which drops more

swiftly with velocity. This is caused by the reduced capture rate since there are no bound electrons on the carbon ions to support charge transfer. This situation is not likely to be characterized by a simple semi-empirical fit since the charge state at most points along the range depend on the past history of the projectile.

Another useful way to analyze the non-equilibrium behavior is to compare the time scales for incremental charge and energy change at each velocity. If the time scale for charge change should be comparable to or smaller than the time scale for a small incremental change in beam energy, then the beam projectile ions can be considered to be in instantaneous charge equilibrium. If the charge-change times should be larger, the energy will change significantly before charge equilibrium is reached. Figure 7.7 displays the time increments as a function of velocity for the change in charge and a 1% change in beam energy for the lead penetration of the fully-stripped carbon target. The time increments for charge change form a repeating pattern representing the progressive reduction in reaction rate as the projectile approaches each new charge state. The energy deposition time increment appears as a smooth curve. The important feature is that the charge-change time increment is typically several orders of magnitude larger than the incremental energy loss time. This indicates again that charge equilibrium is not achieved. This manifests also in the fact that the change in beam velocity over which the charge change is achieved is considerable. For instance, note that a new charge state is reached near $v = 4 \times 10^9$cm/s and the subsequent new charge state is not obtained until the beam velocity has dropped to approximately 3.5×10^9cm/s.

For comparison, note the analogous values for deposition of the same beam into

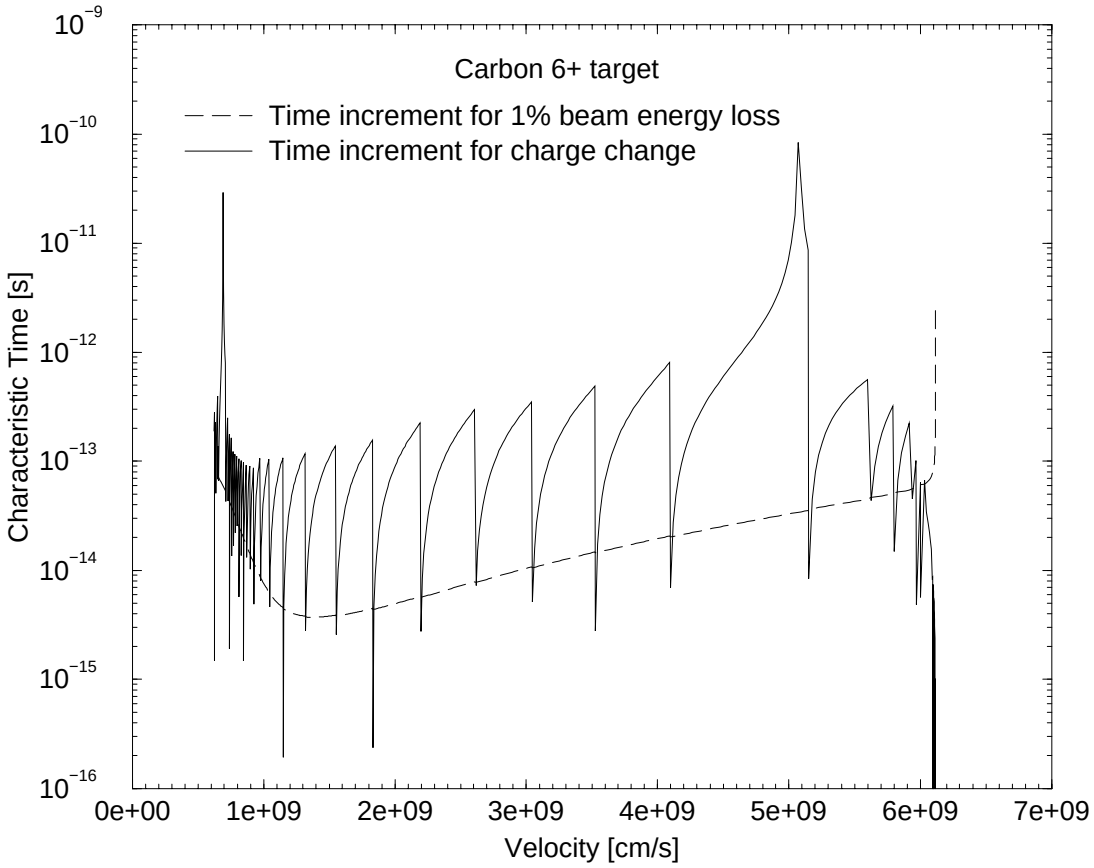

Figure 7.7: Charge change and energy deposition time increments for a 20MeV/u lead projectile penetrating a carbon plasma of average charge 6+ at 0.01gcm^{-3}

a neutral, cold carbon target at $0.01 g/cm^3$ in figure 7.8. In this case, since the charge changing reactions are increased by the presence of charge transfer, the pattern formed by the charge-change times cycles more quickly and less clearly than in the fully-stripped case. The charge-change time values for this case are all well below or are comparable to those of energy deposition. Also note that each charge change, marked by the jagged cycling in the charge time increment, occurs with very little fractional change in beam velocity. In this case charge equilibrium is maintained at virtually every point in the deposition and the actual equilibrium charge state is given approximately by the Bohr semi-equilibrium fit of equation 5.4.

This determination of non-equilibrium beam charge state evolution in the fully-stripped carbon plasma is consistent with the consensus regarding charge evolution in fully-stripped plasmas [14],[54], [17]. When target ionization levels are such that charge transfer is sufficiently suppressed, charge equilibrium is not achieved in a time or deposition distance increment small with respect to the characteristic beam energy loss path length.

For this fusion investigation, the first point to ascertain is whether or not the fully-stripped condition will be achieved in HIF hohlraums. Even if hohlraum materials are not fully-stripped at temperatures as high as 300eV, the levels of ionization will certainly be large. The procedure then is to determine the maximum level of target ionization likely to be achieved in HIF hohlraums and whether or not that level of ionization will induce equilibrium charge evolution in penetrating beams.

According to the material equation of state properties listed in the tables in section 3.1.10, several instances are observed in which the target material becomes nearly-

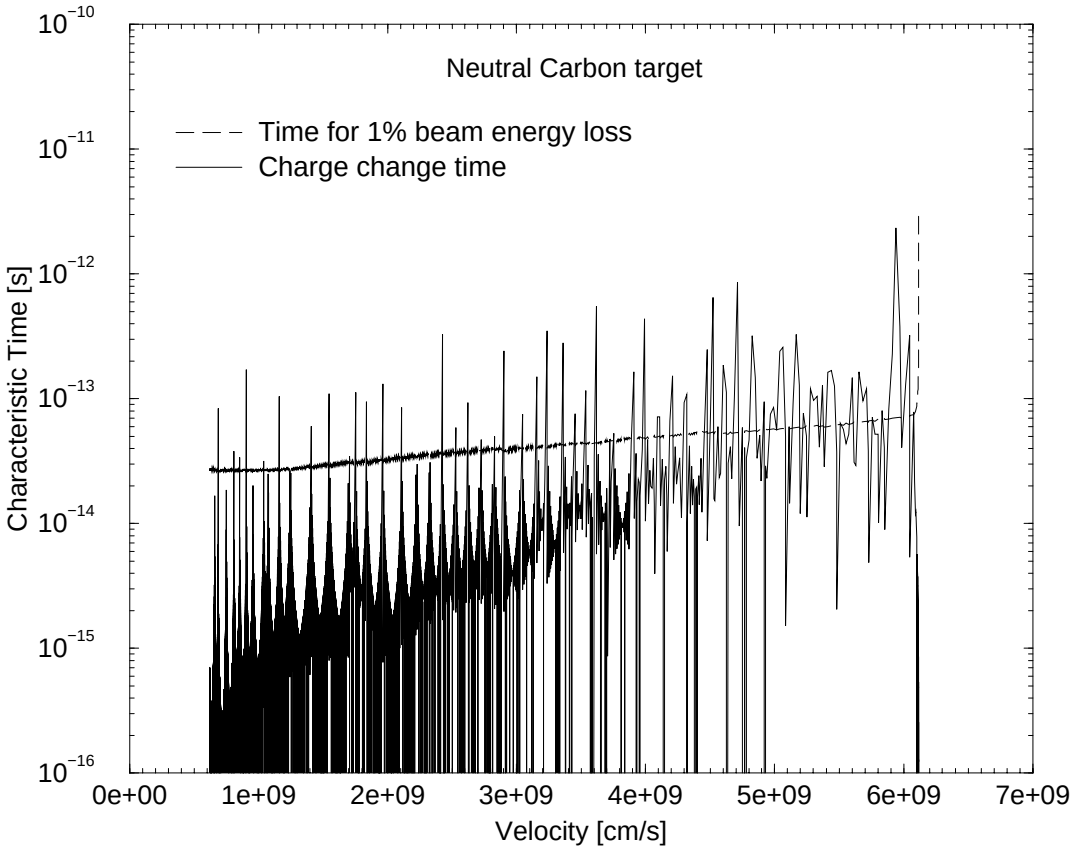

Figure 7.8: Charge change and energy deposition time increments for a 20MeV/u lead projectile penetrating a cold carbon target at 0.01gcm^{-3}

fully-stripped within the range of parameters likely to be encountered in HIF hohlraums. However, none are ever fully-stripped. This happens to be significant. Consider carbon at a density of $0.01 g/cm^3$ at a temperature of 300eV, which exhibits an average ionization level of nearly 5.9. This represents the case most likely to result in non-equilibrium behavior. Does it indeed do so?

Figure 7.9 displays a time increment plot as a function of velocity analogous to figure 7.7 but for the same $20 MeV/u$ Pb $^{10+}$ penetrating a carbon target charged to an average state of 5.9+ at a density of $0.01 gcm^{-3}$. As in the cold carbon target case, the time increment values for charge change are mostly situated well below or close to those of energy deposition. Note also that the rate at which the projectile charge state cycles is rapid with respect to the deposition velocity change as in the case of the cold carbon target and in contrast to the case of the fully-stripped target. The presence of even just one bound electron for every ten carbon ions makes a significant difference.

The fact that this plasma condition does indeed induce equilibrium can be seen most directly by comparing the charge states encountered during the integrated evolution of the particle and the equilibrium charge states calculated by the capture and ionization models at representative velocities. If the projectile's charge state at every velocity during its deposition into the target should be equal to the equilibrium charge state calculated at that velocity then equilibrium charge state evolution would be achieved. Using the **zstopx** code of Chapter 6, the integrated beam charge evolution and energy deposition calculations were performed for this case. The average charge state of the beam ions at each point during the simulated evolution appear in figure 7.10. Also plotted are the equilibrium charge states

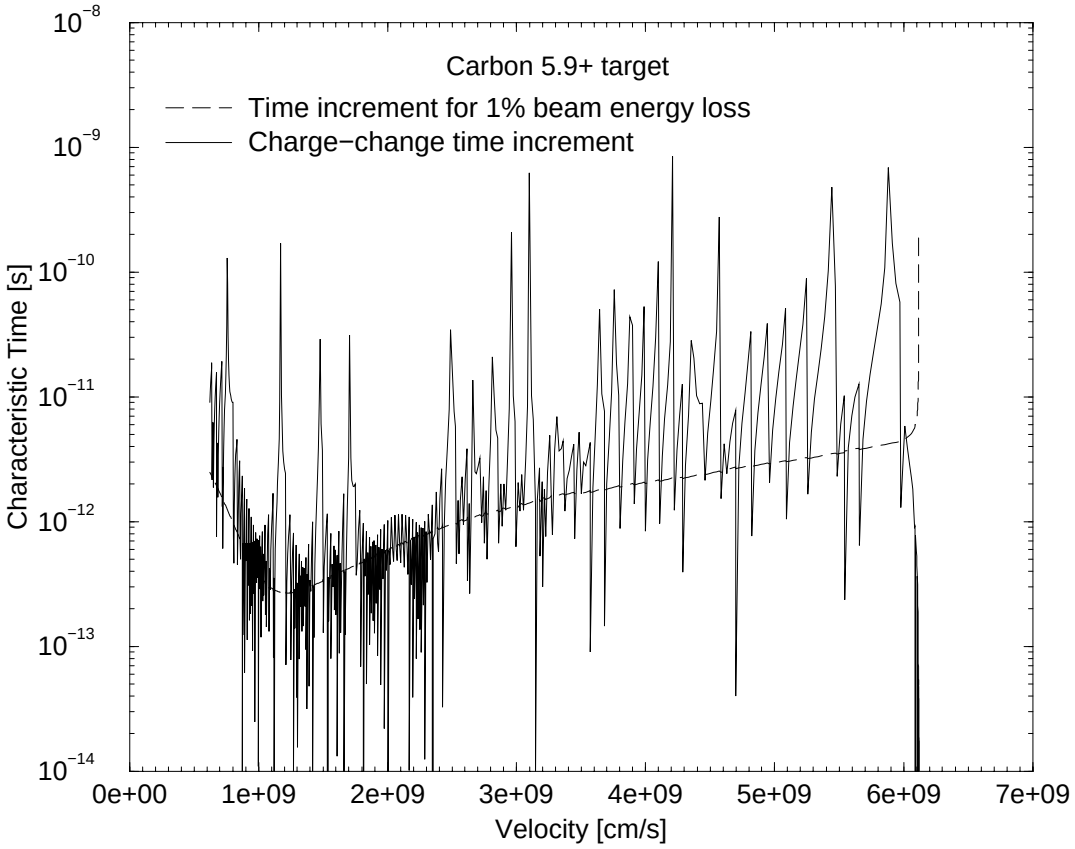

Figure 7.9: Charge change and energy deposition time increments for a 20MeV/u lead projectile penetrating a carbon plasma of average charge 5.9+ at 0.01gcm^{-3}

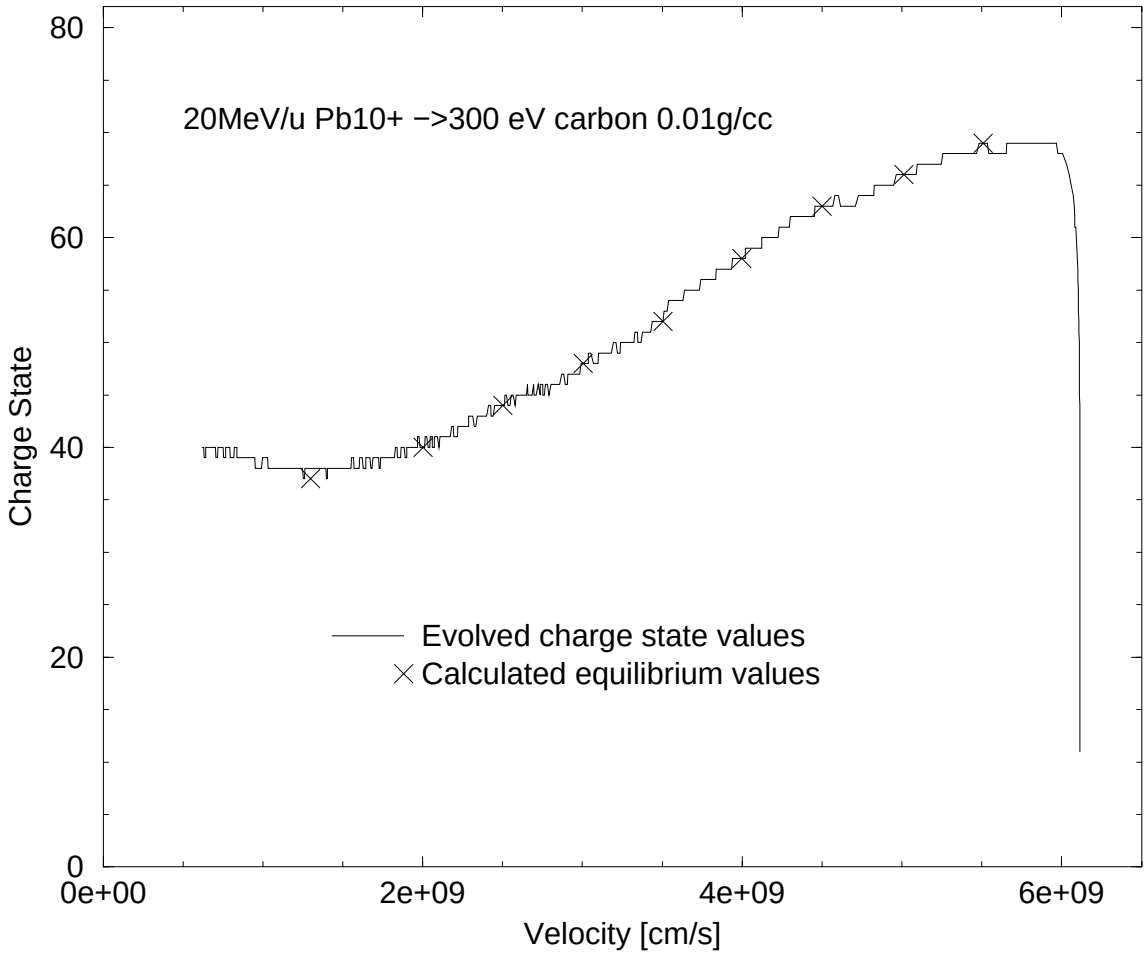

Figure 7.10: Charge states for a 20MeV/u lead projectile penetrating a carbon plasma of average charge 5.9+ at 0.01gcm^{-3}

at representative velocity values as calculated according to section 5.7.3. The lead beam is shown to be in equilibrium throughout its range in this plasma.

This case represents an extremum of material conditions encountered in HIF hohlraum materials heated to 300eV. The fact the electronic properties of the carbon target in this extreme case actually induced equilibrium charge evolution in an incident driver beam indicates that equilibrium evolution should be expected in most other HIF target materials since they will feature less fractional ionization than in this example.

7.3.3 Cross Section and Equilibrium Charge Trends

Given that equilibrium charge attainment can be expected for most hohlraum scenarios considered presently, the exact nature of the charge equilibrium of beams penetrating dense plasma targets will be examined in detail. This examination will be performed with special attention to the actual cross section values which determine the charge state. The goal of this analysis is to establish trends in equilibrium charge evolution which could eventually form the basis for a new semi-empirical fit for charge equilibrium in partially-ionized plasmas.

Charge-change cross sections and equilibrium charge values will be calculated systematically over a range of parameters. The specifics of the cross sections will be discussed and trends in equilibrium behavior will be evaluated. Note that the purpose now is not do develop a library of charge evolution plots to serve as the basis of an approximate fit, but rather to examine representative cases to determine the important processes which influence charge equilibria in dense plasma targets.

Let us first consider the case of a lead projectile simulated to be deposited into a gold plasma at $1 g/cm^3$. The target temperatures examined will range from 10eV to 300eV. The velocity of the lead beam will be varied from $0.2c$ to $0.05c$, covering the range of interest in this study. Figures 7.11 through 7.13 display the ionization and capture cross sections in the 300eV gold target with an average charge state of 33.9, with each figure representing a different lead ion velocity. In each plot, the point at which ionization and capture cross sections meet is the charge equilibrium value and is marked by a line.

Several primary observations should be made here. The cross section for ionization

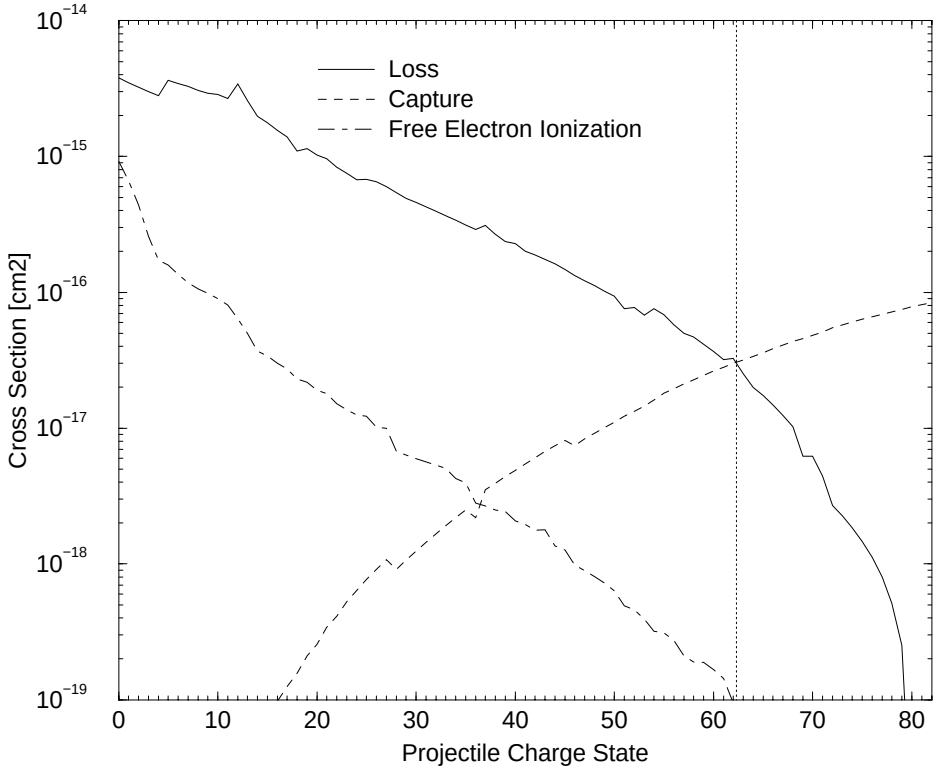

Figure 7.11: Charge-changing cross sections of lead at $v = 0.2c$ penetrating a gold plasma at 1gcm^{-3} and 300eV

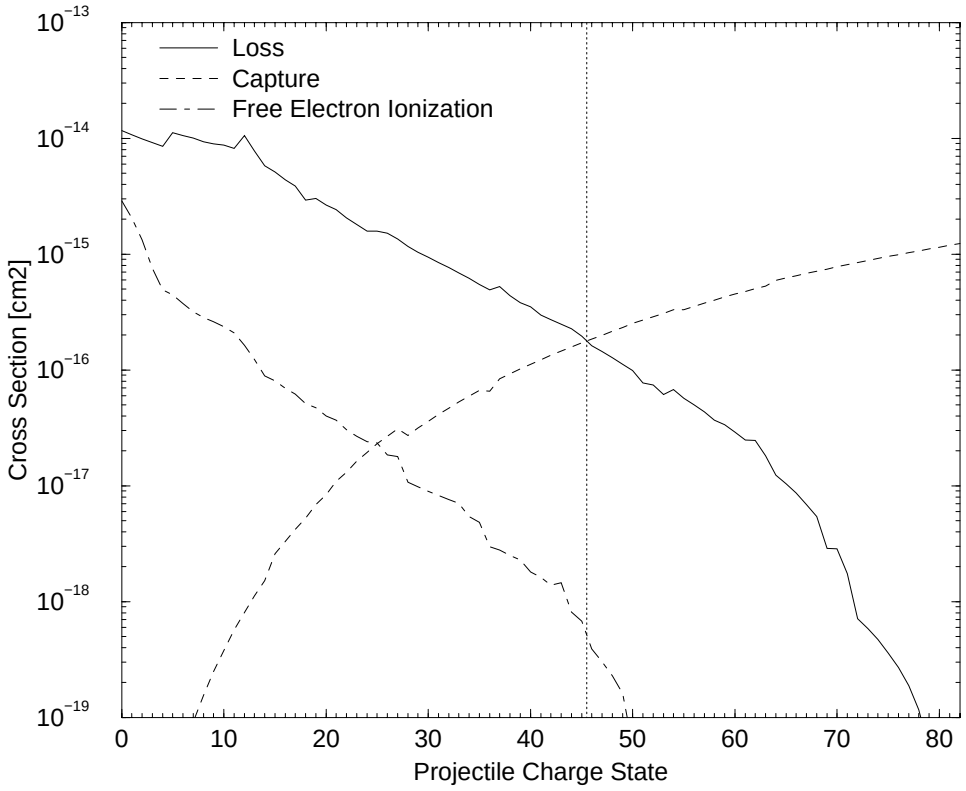

Figure 7.12: Charge-changing cross sections of lead at $v = 0.1c$ penetrating a gold plasma at 1gcm^{-3} and 300eV

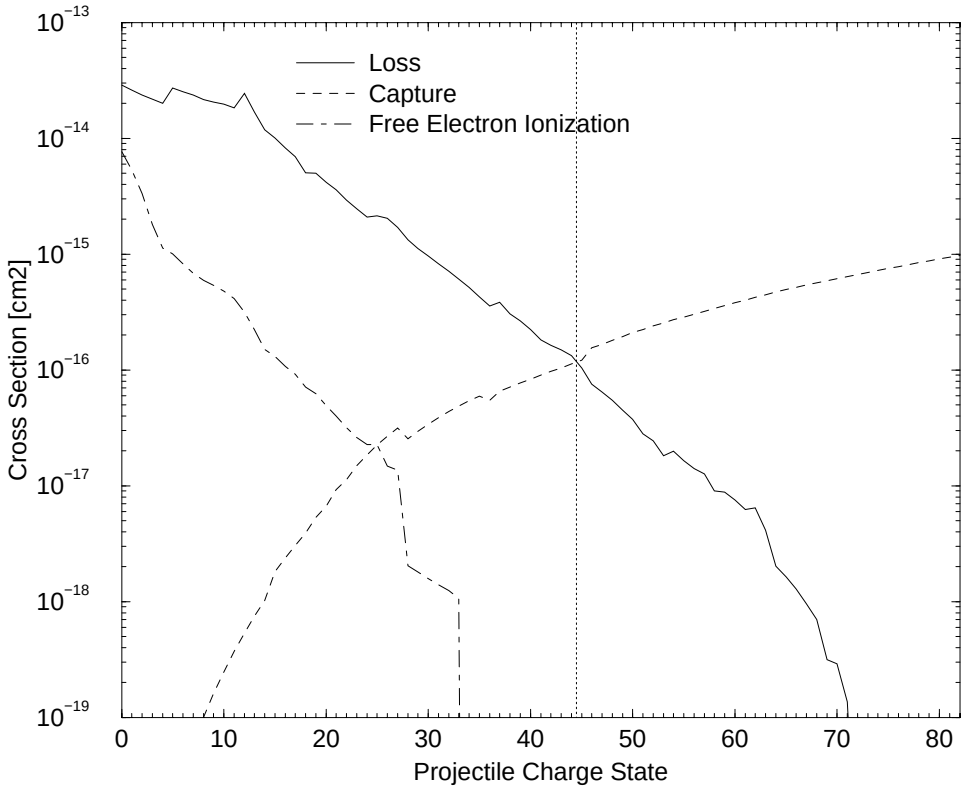

Figure 7.13: Charge-changing cross sections of lead at $v = 0.05c$ penetrating a gold plasma at 1gcm^{-3} and 300eV

due to free electron collision is shown to be small relative to the total electron loss cross section. The cross section for radiative capture of free electrons was included in each case, but was found to be many orders of magnitude lower than the charge transfer cross section. It was plotted on the graphs with the other cross sections, but did not even appear within the scale of the figures. *The free electron contributions to both ionization and capture were shown to be insignificant in each case.* The equilibrium charge value predicted by these calculations as well as for other projectile velocities are plotted in figure 7.14. Included is the charge equilibrium value predicted by the traditional semi-empirical fit for cold matter. The calculations in the gold plasma at 300eV and $1g/cm^3$ show a marked charge state enhancement which increases as the projectile slows.

Before analyzing these trends in more detail, their manifestation in beams penetrating other target materials and ionization levels should be examined. Consider now a low-Z plasma consisting of carbon at $0.1gcm^{-3}$ with a temperature of 100eV. The average charge state of such a target material is 5.14. The loss and capture cross sections were calculated for this case using the same lead projectile and associated velocities. Figures 7.15 through 7.17 display the results.

Note that here again the free electron contribution to the cross sections is minimal. Free electrons contribute neither to loss nor to capture rates in the plasma. Ionization is dominated by the BEM nuclear ionization and capture is dominated by charge transfer.

The equilibrium charge state values for these and other velocities are displayed in figure 7.18. As in the case of the gold plasma, the beam equilibrium charge state in the carbon is close to the charge state it would have in a cold target (according to the Bohr

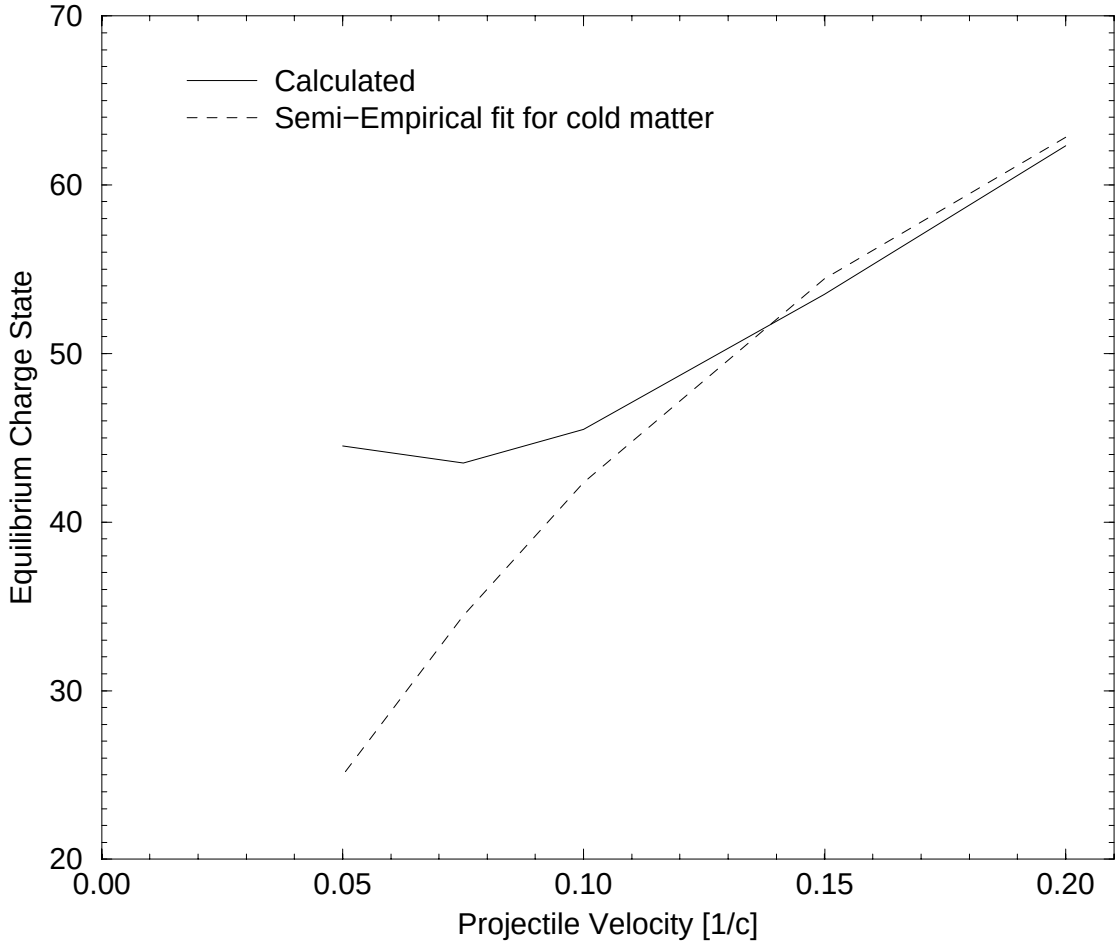

Figure 7.14: Equilibrium charge states of lead ions penetrating a gold plasma at $1\mathrm{gcm}^{-3}$ and 300eV

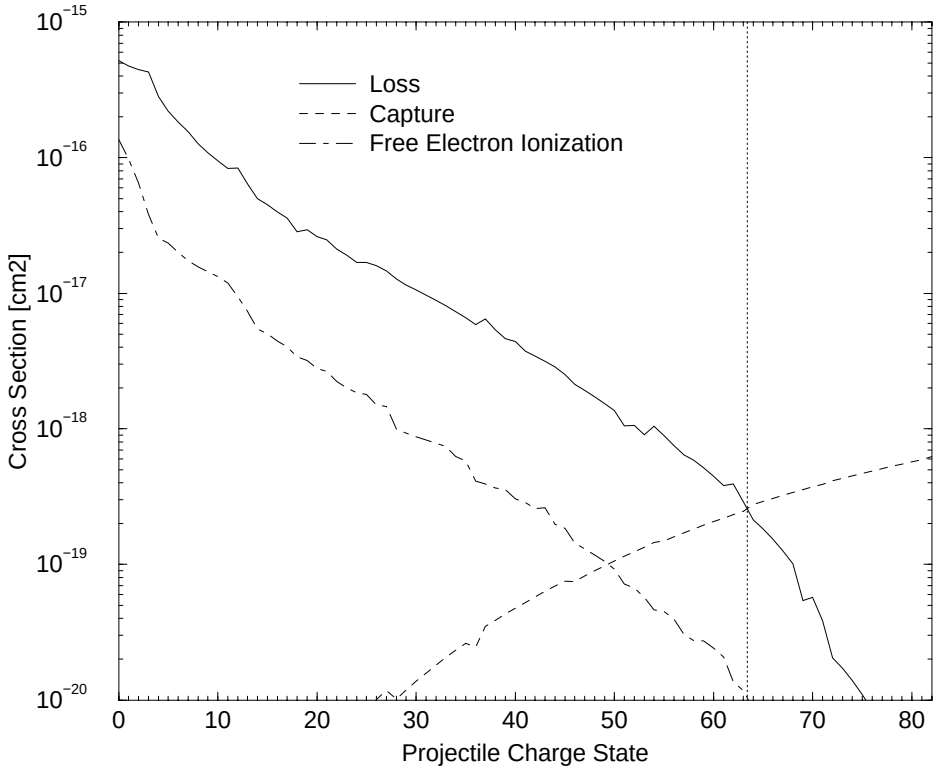

Figure 7.15: Charge-changing cross sections of lead at $v = 0.2c$ penetrating a carbon plasma at 0.1gcm^{-3} and 100eV

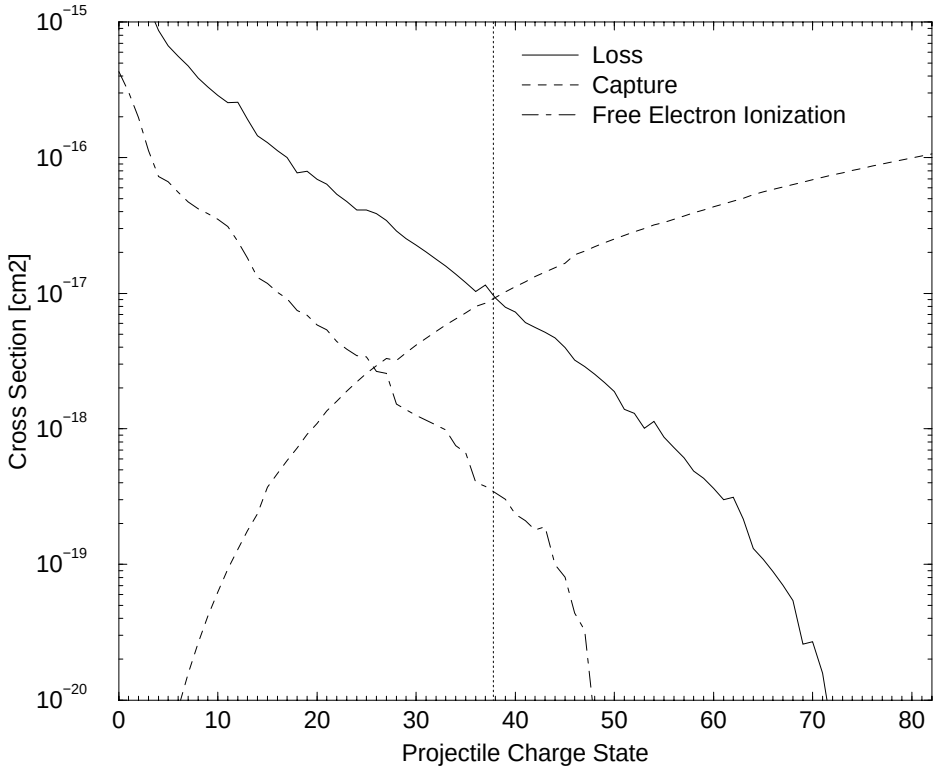

Figure 7.16: Charge-changing cross sections of lead at $v = 0.1c$ penetrating a carbon plasma at 0.1gcm^{-3} and 100eV

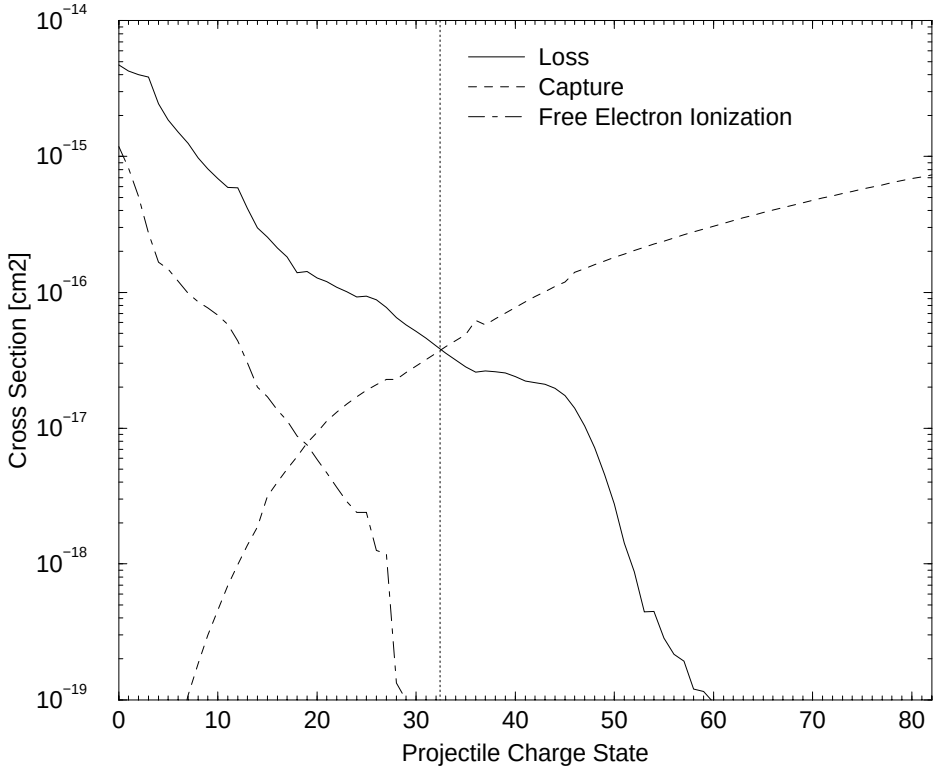

Figure 7.17: Charge-changing cross sections of lead at $v = 0.05c$ penetrating a carbon plasma at 0.06gcm^{-3} and 100eV

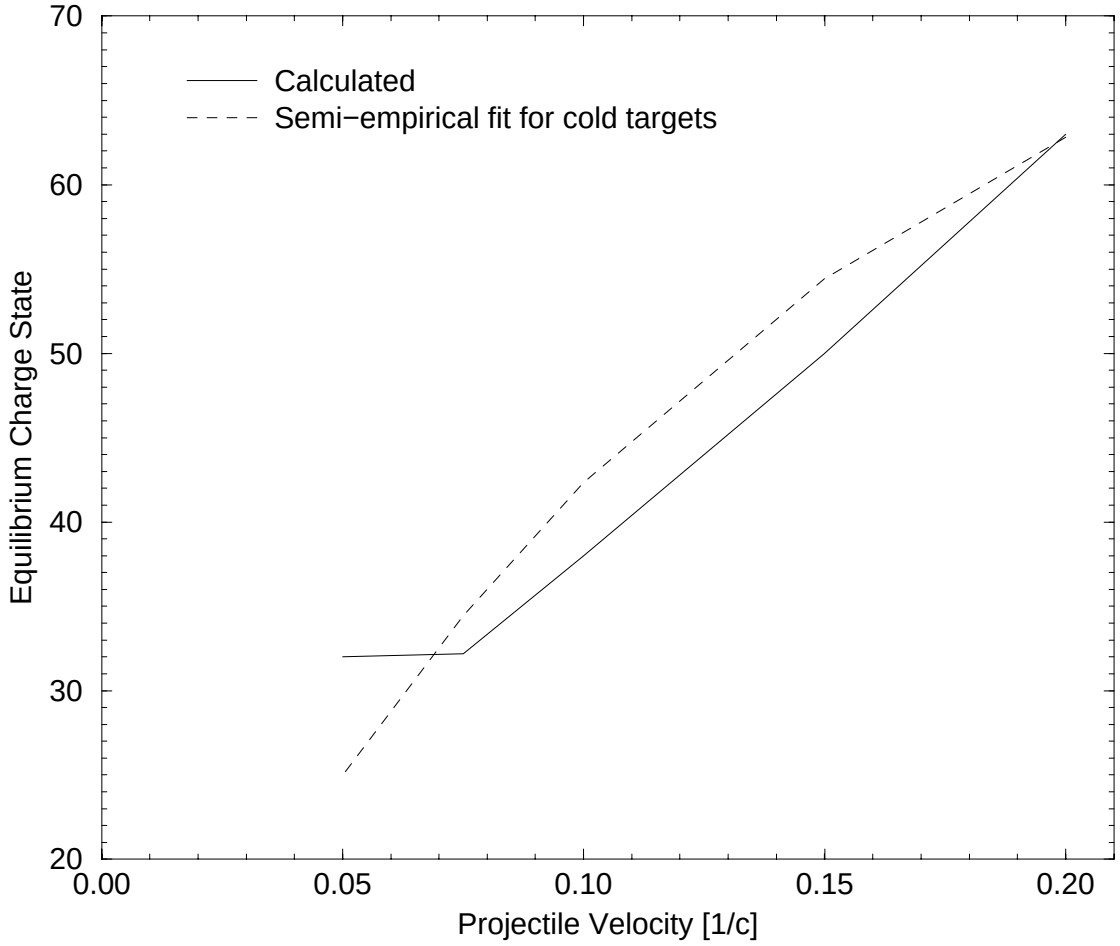

Figure 7.18: Equilibrium charge states of lead ions penetrating a carbon plasma at $0.1\mathrm{gcm}^{-3}$ and 100eV

semi-empirical formula) for high velocities and greater than the Bohr value at low velocities. Note that for intermediate velocities the equilibrium charge state in the plasma is actually lower than the cold target charge state. This is probably just due to inexact modeling and the difference is only by a few charge states, certainly within the uncertainty of the associated cross sections.

Let us examine the reaction rates and equilibrium charge states of a lead beam penetrating a third material. Figure 7.19 shows the equilibrium charge states of lead penetrating an iron plasma of density $0.1 g/cm^3$ whose temperature is 300eV. The average charge state of the iron target under these conditions is 20.72. Again observed is a near coincidence between the lead beam's charge states in the iron plasma and the equilibrium charge states according to the Bohr semi-empirical fit at high velocities. The equilibrium charge state in the plasma is increased relative to the Bohr values with decreasing velocity.

The trends observed in the cross sections and resultant equilibrium charge values can be interpreted to identify the dominant process determining increased charge state levels. It has been shown that the free electron contributions are not significant in any of the cases examined. The primary comparative feature of the charge evolution in dense plasmas is enhancement with respect to the cold matter value which increases as the projectile slows. While the plasma electrons do not appreciably alter the cross sections, the cause for enhanced ionization in the above cases can be identified.

First consider the high-velocity behavior. In all cases, for high velocities, the equilibrium in the partially ionized plasma is close to that of the semi-empirical fit for cold matter charge state equilibrium. This is intuitive. For a swift projectile whose velocity is

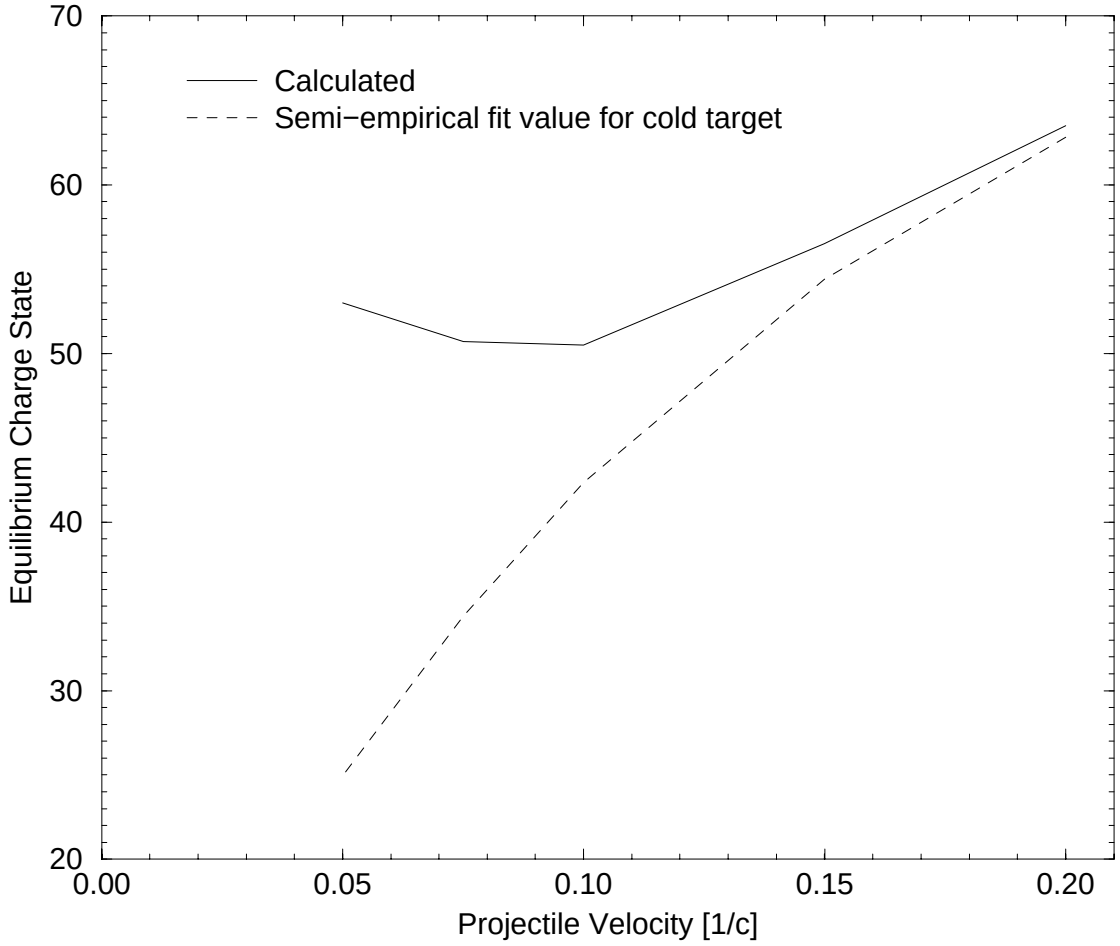

Figure 7.19: Equilibrium charge states of lead at penetrating an iron plasma at $0.1\mathrm{gcm}^{-3}$ and 300eV

much greater than the scaled Thomas-Fermi electron velocity of the target

$$v \gg Z_t^{2/3} \alpha c \tag{7.19}$$

the distinction between bound and free in the target electrons should not be pronounced. This is because the target electrons, bound or free, would appear as a stationary electron fluid to the swift projectile.

As the projectile continues to deposit its energy into the target, slowing down further, the equilibrium charge states in the plasmas begin to exceed the analogous charge states in cold targets. The cause of this trend can be understood from a plot comparing the charge-changing cross sections of the beam in an ionized material to the analogous cross sections in the corresponding cold material. Figure 7.20 displays the total capture and loss cross sections for the case of a lead ion with $v = 0.1c$ penetrating a gold plasma whose density is 1g/cm^3 at both 300eV and room temperature. The comparison reveals that indeed the ionization in the plasma is enhanced relative to the cold target case due to the reduced screening of the target nuclei. However, this effect is not dominant. What most strongly changes the charge state equilibrium value is the relative decrease in charge transfer of electrons onto the beam from the plasma target compared to the transfer from the cold target. This is due to the absence of favored valence electrons with low binding energies which ordinarily dominate the transfer reaction and which are not present in the plasma targets.

A similar comparison can be drawn for the carbon target equilibrium values. Figure 7.21 shows the cross sections for charge change for a lead ion at $v = 0.05c$ penetrating a carbon target of density 0.1g/cm^3 at 100eV and at room temperature. The cause of the

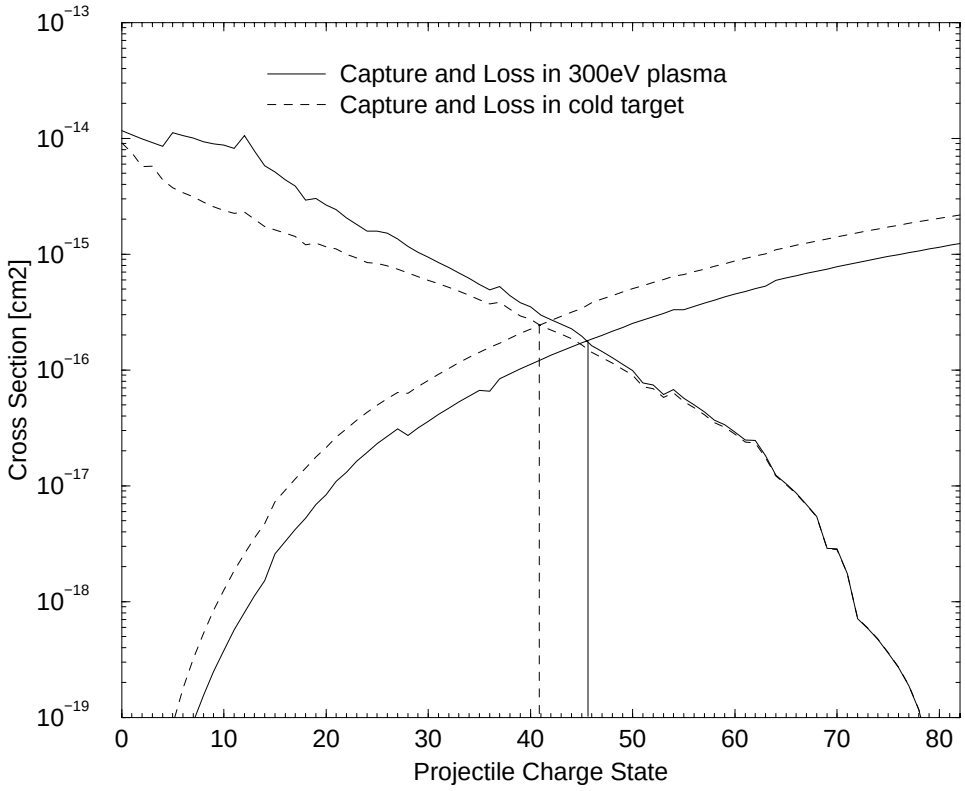

Figure 7.20: Equilibrium charge states for lead at $v = 0.1c$ penetrating a gold plasma at 1gcm^{-3} at room temperature and 300eV

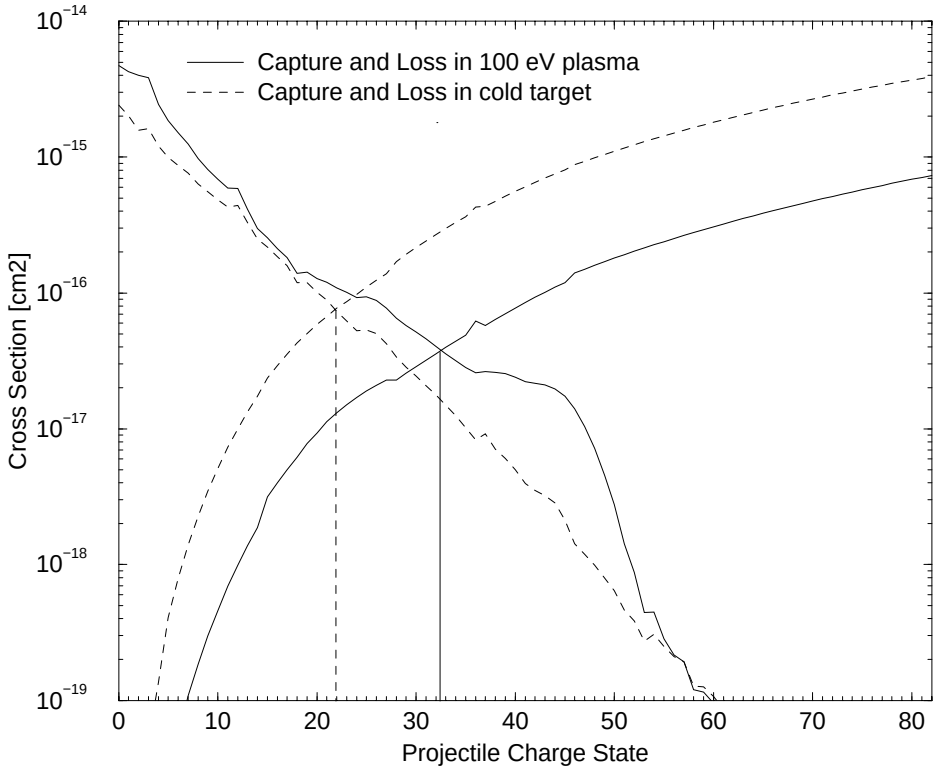

Figure 7.21: Equilibrium charge states for lead at $v = 0.05c$ penetrating a carbon plasma at 0.1gcm^{-3} at room temperature and 100eV

relatively enhanced charge state in the plasma can again be seen to be due primarily to the reduction in charge transfer with the liberation of the target's outer electrons to the plasma. Since radiative recombination occurs at a rate many orders of magnitude lower, the total capture reaction rate decreases substantially with the loss of target valence electrons.

Two pivotal points about cross sections and equilibria in dense plasmas can be taken from the above calculations. (1)The free electrons are roughly transparent to the incident ions. (2)The dominant effect in determining equilibrium is the reduction in the

non-radiative charge transfer cross section due to target ionization levels and corresponding loss of valence electrons.

The identification of these two points provides the understanding necessary to proceed with articulating a new semi-empirical formula for beam equilibrium charge behavior in partially ionized plasmas.

7.3.4 A Semi-Empirical Fit for Charge Equilibrium in Partially-Ionized Plasmas

A desire for calculations of ion beam deposition into dense plasma targets is that they be performed using a beam charge value given by a simple, compact expression rather than by time-consuming discrete cross section calculations. Given the results of the preceding section, basic heuristic conclusions can be drawn regarding the factors determining the charge evolution of ions penetrating plasmas. In this section, those factors are quantified in a way which enables a new semi-empirical fit to be expressed for the charge evolution of beam ions in dense, partially-ionized plasmas.

Such a charge state formula would represent a significant advancement in beam-plasma interaction physics. It has been unclear how target ionization levels effect incident beam charge state and deposition. Some efforts have been made to account for target EOS effects by including the thermal velocity of the target's free electrons in quadrature with the projectile velocity in the cold-matter semi-empirical charge state fit [2]. This is based on the idea that the plasma's free electrons ionize the beam more strongly as a function of their thermal velocities. However, the analysis of this dissertation has shown that the plasma electrons are largely transparent to the beam in the case of dense plasma targets

whose atomic numbers are greater than 6. The above study of ionization and capture cross sections of ions penetrating dense plasma targets has identified the primary cause of enhanced beam ionization levels in dense plasmas. The reduction in charge transfer capture rates in plasmas compared to capture rates in cold targets is several orders of magnitude greater than the corresponding relative increase in beam ionization in plasmas compared to cold targets. The charge state at which capture and ionization rates in plasma targets are balanced, signifying the charge equilibrium, is thus higher. This capture reaction reduction and a simple quantification of it consistent with the previous semi-empirical fit due to Bohr will be developed as follows.

Recall the nature of the previous semi-empirical fit used for cold target calculations (see section 5.1.1). The ansatz which served as its basis was that the equilibrium charge state of an incoming projectile would be that charge state at which the beam's valence electron velocity equals that of the projectile itself. Let us examine this more closely. Implicit in this is actually an assumption about the equation of state of the target. Suppose that the projectile's charge state should increase beyond the equilibrium value Q_E at a given velocity v. The idea is that a capture reaction would rapidly occur to restore the equilibrium charge level. Why? Because there should be, in a cold target, some valence electrons of binding energy $I_v(Z_t, 0)$ which satisfy

$$I_v(Z_t, 0) + \frac{1}{2} m_e v^2 \leq I_v(Z_p, Q_E + 1) \tag{7.20}$$

where $I_v(Z_p, Q_E + 1)$ is the binding energy of the projectile's valence electrons at an equilibrium charge state of Q_E. For high projectile velocities, the neutral target's valence binding energies of typically a few eV would be small relative to the value of $\frac{1}{2} m_e v^2$. This energy

relation could then be re-written approximately as

$$\frac{1}{2}m_e v^2 \leq I_v(Z_p, Q_E + 1). \tag{7.21}$$

This is known to be true since the equilibrium charge value was formed based on the condition

$$\frac{1}{2}m_e v^2 \approx I_v(Z_p, Q_E), \tag{7.22}$$

and in general

$$I_v(Z_p, Q_E) < I_v(Z_p, Q_E + 1). \tag{7.23}$$

The traditional Bohr semi-empirical fit formula can be obtained from equation equation 7.22 by substituting for the valence binding energy $I_v(Z_p, Q_E)$ the virial kinetic energy of the valence electrons $\frac{1}{2}m_e v_v^2(Z_p, Q_E)$. Using equation 5.15 for the valence velocity $v_v^2(Z_p, Q_E)$ and solving for Q_E provides the traditional semi-empirical fit formula.

The significance of this is that at the temporarily higher charge state, the ionization energy of an incoming captured electron would be greater than $I_v(Z_t, 0) + \frac{1}{2}m_e v^2 \approx \frac{1}{2}m_e v^2$. Given this energetic relationship, charge transfer is favored to occur from the target valence electrons to the projectile. This will occur until the energetic balance is achieved at a projectile equilibrium charge state Q_E such that

$$I_v(Z_t, 0) + \frac{1}{2}m_e v^2 \approx I_v(Z_p, Q_E). \tag{7.24}$$

In the case of an ionized target of charge $Q_t > 0$, the valance energy of the target ion $I_v(Z_t, Q_t)$ will begin to exceed the usually negligible values of neutral atoms. As the ionization level increases, a greater projectile equilibrium charge state is required to achieve the energetic balance. Note that this energetic balance is a function of the orbital energies

of the bound target electrons, not the thermal energies of the plasma electrons which do not contribute significantly to beam charge-changing reactions. For a given projectile velocity, the projectile charge state which achieves valence energy balance would be necessarily greater in an ionized target with $Q_t > 0$ than in a non-ionized target. This is true since in general

$$I_v(Z_t, Q_t) > I_v(Z_t, 0), \tag{7.25}$$

which is to say that the ionization potential of an ionized species is greater than the ionization potential of the same neutral species.

This is consistent with both qualitative expectations and with the calculations of the preceding sections. But, how can this relationship be quantified into a rapidly calculated formula? The answer lies in the inversion of the semi-empirical fit itself. As presented in section 5.1.1, the semi-empirical fit is actually based on an inversion of the relationship between an ion's valence electron orbital velocity and its charge state. This relationship is

$$v_v(Z, Q) \approx Z^{2/3} \alpha c \ln\left[\frac{Z}{Z - Q}\right] \tag{7.26}$$

where $v_v(Z, Q)$ is the valence orbital velocity of species Z charged to $Q+$. This velocity can be used to form an energy of both the projectile and target valence electrons. Substituting into the equilibrium condition energy balance gives

$$\frac{1}{2} m_e v_v^2(Z_t, Q_t) + \frac{1}{2} m_e v^2 \approx \frac{1}{2} m_e v_v^2(Z_p, Q_E) \tag{7.27}$$

and using equation 5.15 provides the following relationship

$$\left(Z_t^{2/3} \alpha c \ln\left[\frac{Z_t}{Z_t - Q_t}\right]\right)^2 + v^2 \approx \left(Z_p^{2/3} \alpha c \ln\left[\frac{Z_p}{Z_p - Q_E}\right]\right)^2. \tag{7.28}$$

This equation expresses the energy balance of the valance electrons of an beam at its equilibrium charge state Q_E penetrating a partially ionized dense plasma. Solving this expression for Q_E provides the new equilibrium charge state of a projectile in a partially ionized plasma. This formula, constituting a useful new result, is

$$Q_E(v) = Z_p \left(1 - \exp \left[\frac{-\sqrt{v^2 + (Z_t^{2/3} \alpha c \ln[\frac{Z_t}{Z_t - Q_t}])^2}}{Z_p^{2/3} \alpha c} \right] \right). \tag{7.29}$$

This resultant expression for the equilibrium charge is analogous to the previous cold target fit with a target valence velocity term added in quadrature. Note that for a cold target with $Q_t = 0$, this formula reduces to that of the Bohr semi-empirical value. This formula should not be used for fully-stripped targets with $Q_t = Z_t$, in which case there are no bound target electrons and the function is consequently undefined.

One adjustment needs to be made to make this more broadly applicable. The expression relating an ion's valance velocity to its charge state is valid for situations in which the liberated electrons do not screen the nuclei in the target material. In other words, it applies if the Debye length of the target plasma is greater than the typical ionic radius as discussed in section 3.1.9. However, as indicated by the values of the Debye lengths for HIF-relevant target plasmas in section 3.1.10, this condition will not always be met in the targets simulated here. Thus, the effects of nuclear screening by plasma electrons must be included.

The most facile and reasonably accurate way to address this is by quantifying the number of free electrons within the ionic radius. The effect of these electrons is to reduce the total effective ionic charge, which will produce a corresponding reduction in target valence electron velocity according to the relation in equation 5.15. Thus, the adjusted version of

equation 7.29 can be expressed as

$$Q_E(v) = Z_p \left(1 - \exp \left[\frac{-\sqrt{v^2 + (Z_t^{2/3} \alpha c \ln[\frac{Z_t}{Z_t - Q_t'}])^2}}{Z_p^{2/3} \alpha c} \right] \right) \tag{7.30}$$

with

$$Q_t' = Q_t - \frac{4}{3} \pi r_t^3 n_e \tag{7.31}$$

in which r_t is the ionic radius of the target material. Alternatively, if the Debye length of the plasma should be equal to or smaller than the characteristic ionic radius, the effective target charge can be written simply using the plasma parameter N_D

$$Q_t' = Q_t - N_D \tag{7.32}$$

Calculations Using the New Formula

The equilibrium charge state values which this fit predicts can be examined for lead beam penetration of various dense plasma targets which are also representative of heated hohlraum materials. Consider the scenario of a lead projectile with velocity $v = 0.2c$ penetrating a gold target of density $1 g/cm^3$ at 300eV. Figure 7.22 displays the equilibrium charge states calculated for that case using the Bohr semi-empirical fit for charge equilibria in cold targets and the charge states calculated using the new fit for partially ionized plasma targets. The lead beam's equilibrium charge evolution forecast by the new equilibrium formula agrees well with the trends expected from discrete cross section calculations and with qualitative expectations based on the energetic analysis.

The target valence velocity term added in quadrature in this case is

$$v_v(79, 33.9) = 79^{2/3} \alpha c \ln[79/45.1] \approx 0.0756c \tag{7.33}$$

The new equilibrium charge formula was applied to two other cases examined through analysis by discrete cross sections. Figure 7.22 also shows the equilibrium charge states for a lead beam penetrating an iron plasma at 0.1g/cm^3 and 300eV and a carbon plasma at 0.1g/cm^3 and 100eV. The average charge state of the iron target is 18.3 and the carbon is 5.14. Note that the equilibrium charge states of the lead beam in the iron plasma are similar to those in the gold plasma. This is true because the valance electron orbital velocity of iron at 18.3 is given by equation 5.15 to be

$$v_v(26, 18.3) = 26^{2/3}\alpha c \ln[26/7.7] \approx 0.079c \tag{7.34}$$

which is close to the valence orbital velocity of the gold target charged to 33.9. The valence energy of the carbon target at an average charge state of 5.14 is

$$v_v(6, 5.14) = 6^{2/3}\alpha c \ln[6/0.86] \approx 0.0468c. \tag{7.35}$$

This relatively low carbon target valence velocity results in a less pronounced beam charge state enhancement relative to the equilibrium charge state in the corresponding cold target.

While no empirical data exists against which to compare the new fit, several facts support its reliability. First, the discrete cross sections which provided the justification for the ansatz on which it is based have been shown to be reliable in reproducing known equilibrium values in solids. Though only accurate enough to predict charge equilibrium to within several charge states, the individual cross sections can certainly be trusted to provide reliable estimations of the relative importance of the various ionization and capture reactions. From such an analysis, the reduction in charge transfer clearly distinguishes itself as the process which dominates the ionization enhancement. The new formula was based

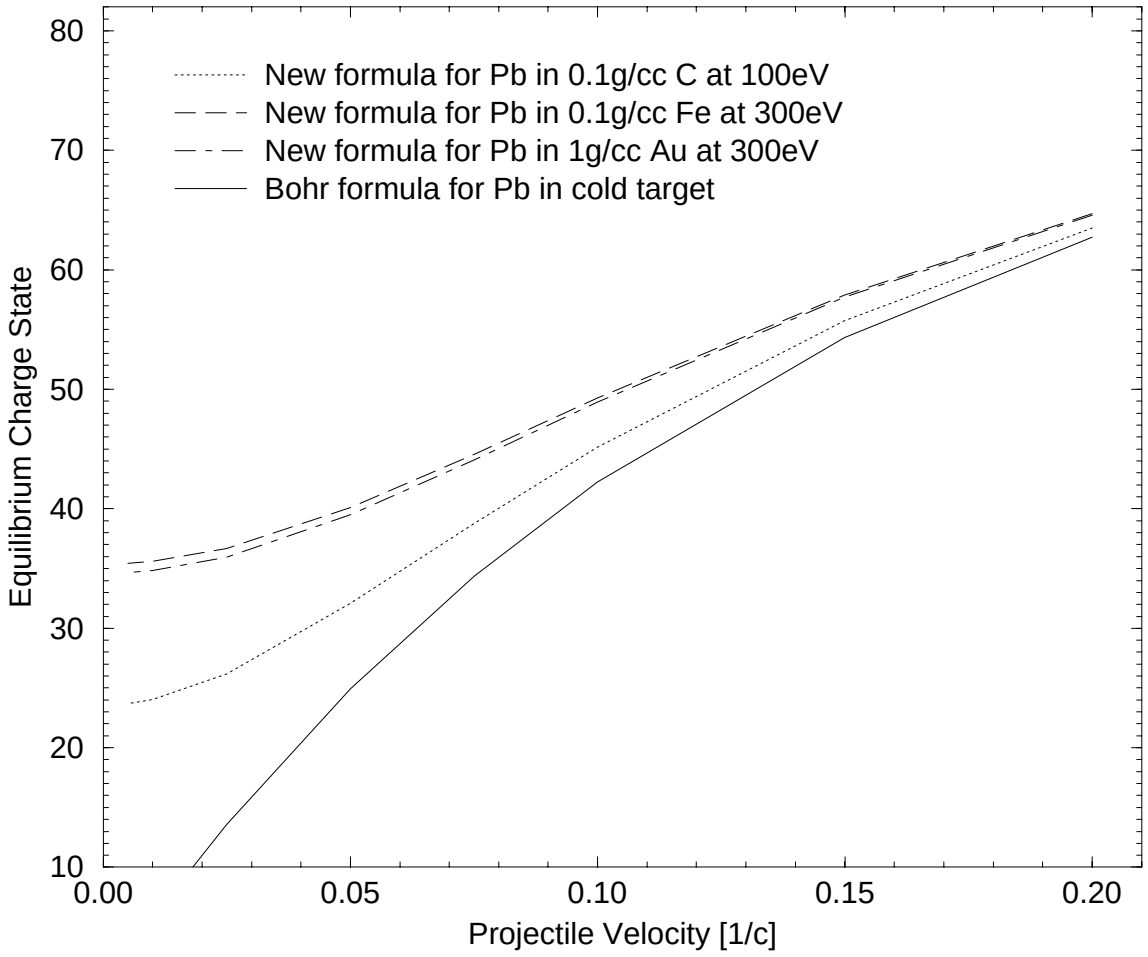

Figure 7.22: Equilibrium charge states of lead ions penetrating various target plasmas

on a sensible extension of the original Bohr semi-empirical fit which has been shown to be successful.

The values predicted both by time-consuming discrete calculation and by the nearly instant application of the new formula provide results which are consistent with each other. The results are also consistent with expectations based on an understanding of the atomic energetics involved and a knowledge of the ionization and capture cross sections which determine the beams equilibrium charge state. The new formula for charge equilibrium in a partially-ionized medium can thus be trusted to provide very sensible and reliable results. Its application to integrated energy deposition calculations will be examined in the following section.

7.3.5 Integrated Calculations for Targets

Using the new charge evolution formula for partially-ionized dense plasma penetration developed above, integrated calculations can be performed evolving both the energy loss and charge evolution simultaneously. The charge state evolution of the projectile which determines the energy deposition will be generated from the new semi-empirical fit. The target equation of state values, average charge state and average ionization potential, will be taken from section 3.1.10. From these systematic runs, new expectations can be formed for beam deposition in ionized target materials for HIF applications.

Consider first the deposition of the prototypical lead beam with $v = 0.2c$ into a gold target of $1 g/cm^3$ at temperatures ranging from 10eV to 300eV. The integrated charge evolution and deposition calculations for these cases are shown in figure 7.23. Included is the profile calculated for a cold gold target at the same density by using the traditional

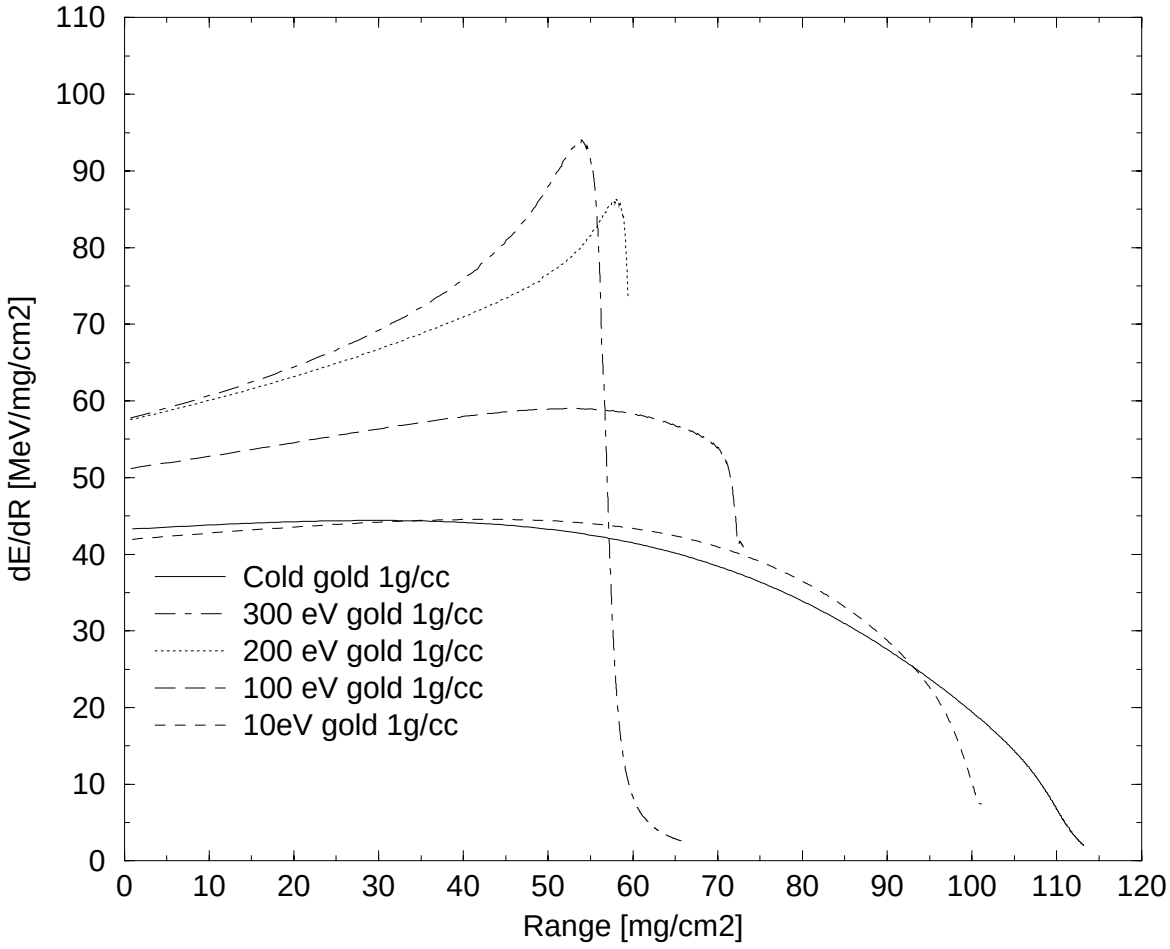

Figure 7.23: Energy deposition profiles for 20MeV/u Pb penetrating a dense gold plasma with $\rho = 1\text{gcm}^{-3}$ at several temperatures

semi-empirical equilibrium charge state for cold matter.

At least two distinctive trends are noted. First, the range of the beam decreases progressively with target ionization levels. Also, the Bragg peak of the deposition profile is more accentuated with increasing target temperature. This behavior is due to two influences. First, aside from beam charge enhancement in plasmas, the stopping power in a plasma target is generally greater than the stopping power in the same cold target. This can be exemplified by comparing the respective logarithmic terms in the stopping power

formulae for both. Neglecting beam charge state dependence, the energy deposition rates of the beam in two targets, gold at 300eV and cold, can be expressed in ratio by

$$\frac{dE/dx(300\text{eV})}{dE/dx(cold)} = \frac{45.07\ln[\Lambda_b(300\text{eV})] + 33.93\ln[\Lambda_f]}{79\ln[\Lambda_b(cold)]} \tag{7.36}$$

At a beam velocity of $0.2c$, this ratio is found to be

$$\frac{45.07 \times 3.20 + 33.92 \times 7.48}{79 \times 4.05} \approx 1.25 \tag{7.37}$$

Thus, even without charge enhancement effects, the energy deposition will be expected to be greater in the plasma. This effect becomes more pronounced as the projectile slows. At a velocity of $0.1c$, this ratio is near 1.37.

The effects of beam charge state enhancement on the deposition in the plasma target can be isolated by comparison. Figure 7.24 displays the deposition profile of the lead beam into the 300eV plasma using both the new equilibrium fit for ionized targets and the old fit for cold targets. The comparison shows that the charge state enhancement is also responsible for a degree of range shortening and Bragg peak enhancement.

Now consider the lead beam deposition into a carbon target at 1g/cm^3. Figure 7.25 displays the associated energy deposition profiles for $20\text{MeV}/u$ lead penetrating the carbon at temperatures ranging from 10eV to 300eV. The trends of Bragg peak enhancement and range shortening are again observed.

The isolated effect of the charge enhancement in the plasma can be examined as in the gold target scenario, by plotting a representative profile using both the new fit and the old charge equilibrium model. Figure 7.26 displays such a comparison for the case of the 300eV carbon plasma. In this instance, the Bragg peak is reduced considerably

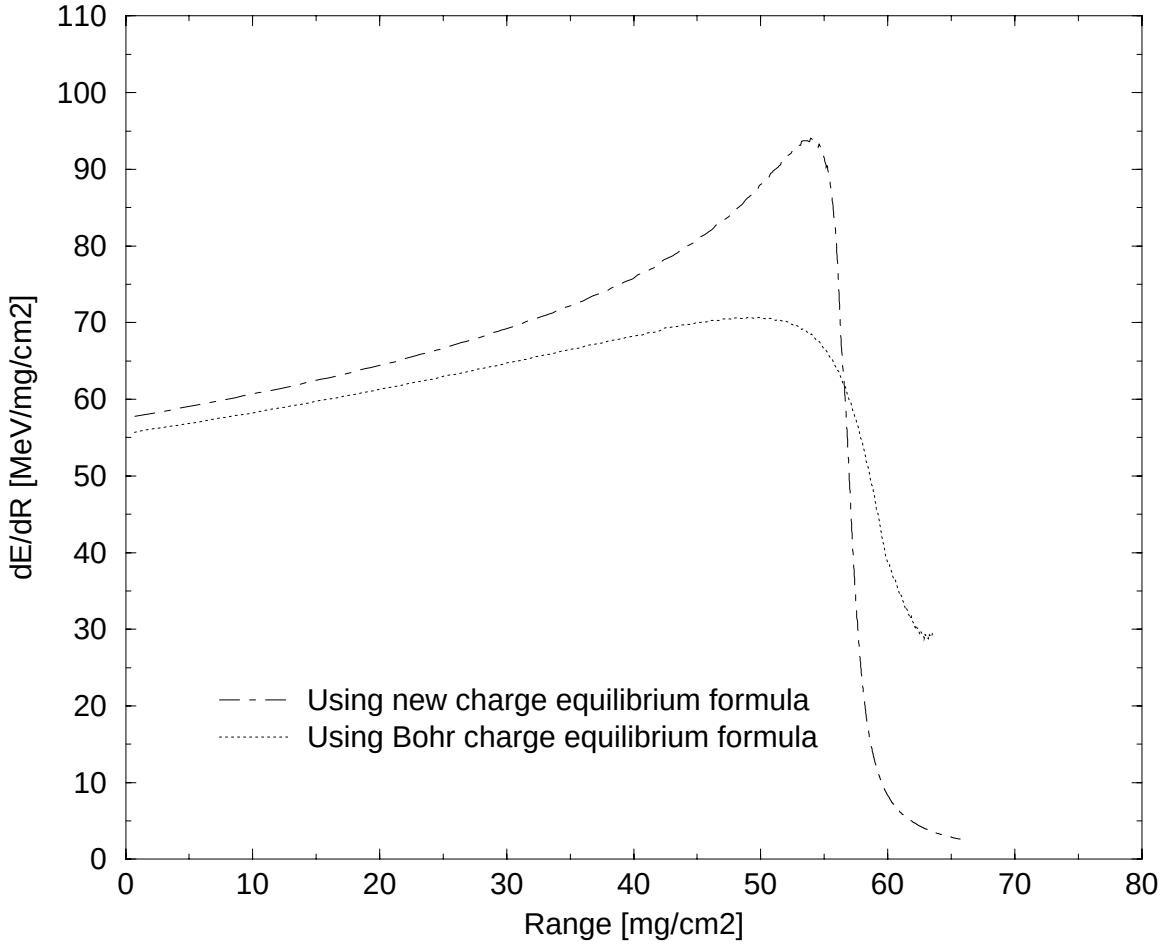

Figure 7.24: Energy deposition profiles for 20MeV/u Pb penetrating a dense gold plasma with $\rho = 1\text{gcm}^{-3}$ at 300eV using old and new charge equilibrium models

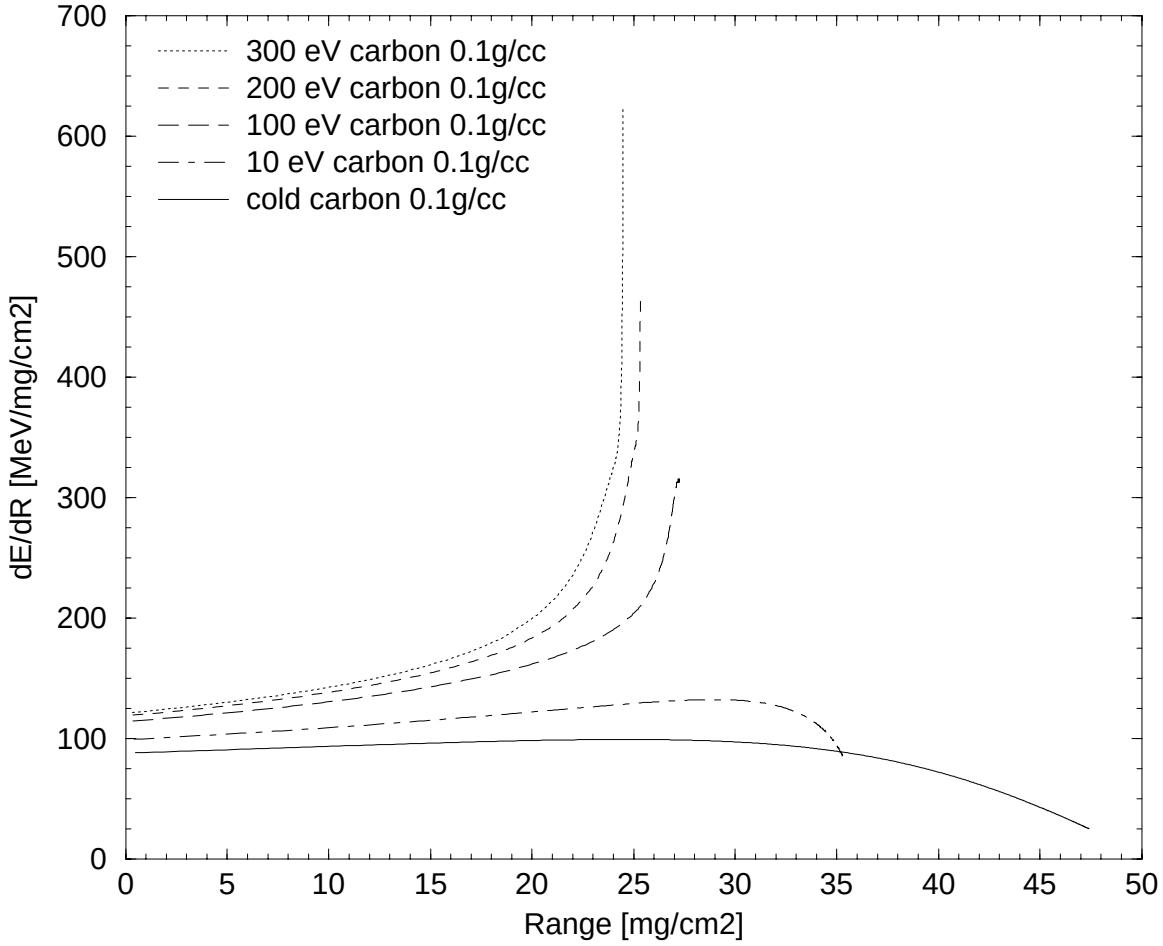

Figure 7.25: Energy deposition profiles for $20\mathrm{MeV}/u$ Pb penetrating a carbon plasma with $\rho = 0.1\mathrm{gcm}^{-3}$ at several temperatures

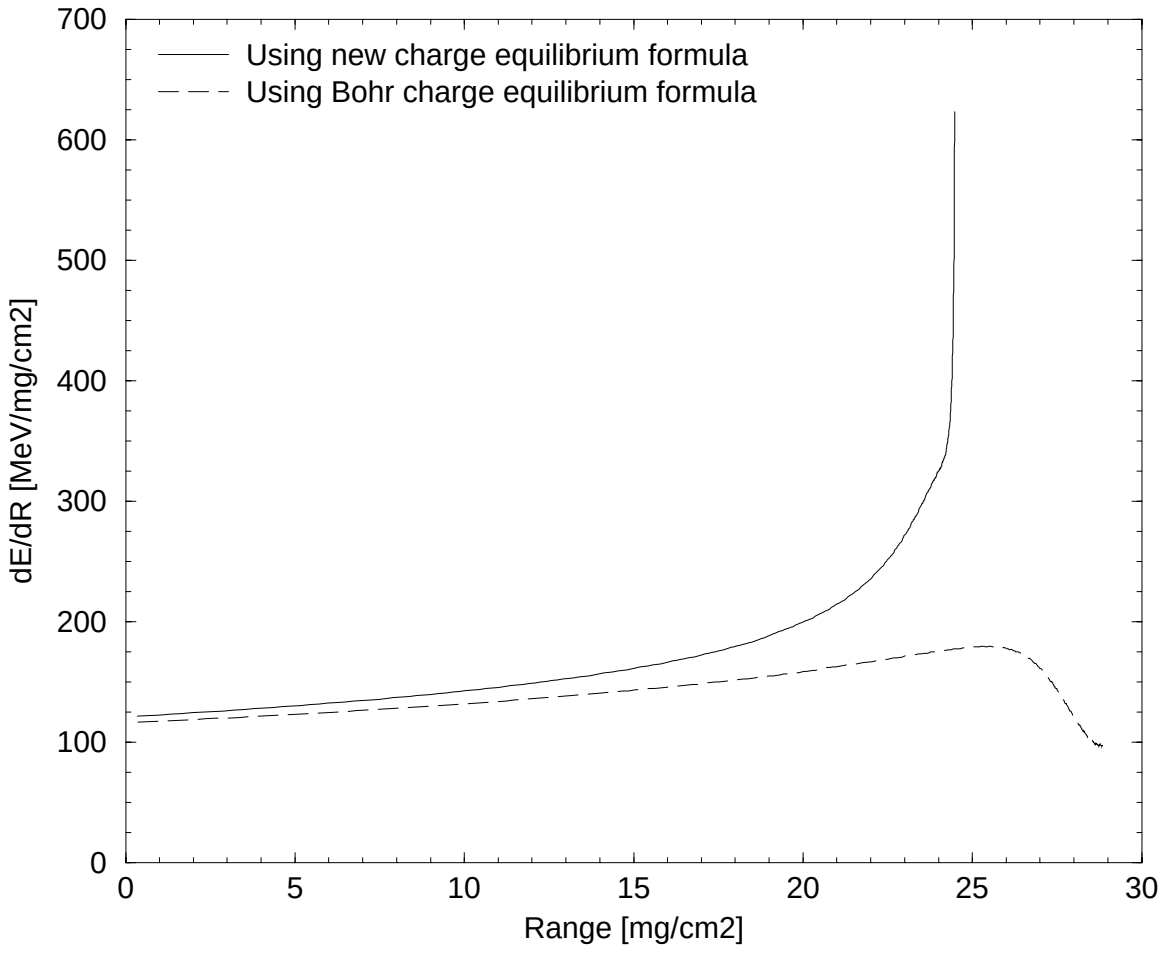

Figure 7.26: Energy deposition profiles for 20MeV/u Pb penetrating a carbon plasma with $\rho = 0.1\text{gcm}^{-3}$ at 300eV using both the new charge equilibrium fit and the cold matter fit

when using the previous equilibrium model for cold target charge state. The effect of the enhancement of charge state is to drive up the equilibrium value as the projectile slows as the projectile velocity becomes close to the velocity of the ionized target's valence electrons. This compounds the energy deposition rate at that regime, acting to create a highly accentuated Bragg peak.

7.4 Summary and Outlook for HIF Atomic Physics

Difficulties and significant uncertainties in calculating charge-changing cross sections and energy deposition of beams penetrating rarefied and dense plasma targets have been addressed in this dissertation. Applications of the improved atomic physics models to HIF chamber and target scenarios enable important new conclusions for HIF and useful new atomic physics information.

This dissertation presents good evidence to support the conclusion that despite recent questions [19], the binary encounter model of Gryzinski can be used to produce reliable beam ionization cross sections, particularly for HIF applications. Unaccountably high ionization levels should not be expected in the HIF chamber and that calculations can be performed with the BEM direct ionization cross section models outlined in section 5.4.4. There should be no need for concern about unknown ionization processes and the HIF community can advance past concerns over ionization uncertainties and proceed with the simple and fast calculation approach outlined here. If experiments should be sought to determine relevant cross sections exactly, reversed-frame or crossed beam techniques are recommended rather than the traditional direct approach of measuring the ionization of a the heavy ion beam penetrating a target. If space charge effects should remain a problem for HIF driver beam propagation in HIF chambers, other system parameters can be varied in the HIF chamber to reduce ionization and to enhance beam neutralization. It is important however to be able to calculate reasonably accurate ionization cross sections for modeling efforts.

Design of indirectly driven HIF targets may benefit if expectations about the

accentuated Bragg peaks of beams penetrating dense plasmas are validated. If beam energy deposition should occur in a more well-defined volume, the materials of the hohlraum can be more accurately adjusted to achieve more subtle changes in the spatial distribution of the radiation field. Also, less energy would be lost to deposition in materials positioned along the beam's path to its intended deposition destination. With evolving laser-generated plasma technology, this deposition issue can be further resolved with experiments in dense, high-Z plasma targets.

The beam charge evolution and energy deposition behaviors calculated using the new equilibrium charge equation presented here certainly beg future verification by a thorough experimental examination. However, just as in the case of the cold matter semi-empirical equilibrium fit, the physical basis on which the model was based is strong enough such that observed deviations from empirica can likely be incorporated by parameterizing one or several terms in equation (equation 7.29) which can be tuned.

The important point is that for HIF chamber and target scenarios, concerns about poorly-understood ionization and other atomic effects can be alleviated by a close examination of atomic processes for heavy ion fusion.

Bibliography

[1] J.M. Anthony and W.A. Lanford. Stopping power and effective charges... *Physical Review A*, 25(4):1868, April 1982.

[2] R.O. Bangerter. Personal communication. February 1997.

[3] R.O. Bangerter. *Phil. Trans. Royal Soc. London A*, 357:575, 1999.

[4] D.R. Bates, editor. *Atomic and Molecular Processes*. Academic, NY, 1962. see section by Bates and Dalgarno.

[5] H. Bethe. *Ann. Phys.*, 6:325, 1930.

[6] H.D. Betz. Charge states and charge-changing cross sections of fast heavy ions. *Rev. of Mod. Phys.*, 44:465, July 1972.

[7] F. Bloch. *Z. Phys.*, 81:363, 1933.

[8] N. Bohr. *Philos. Mag.*, 25(10), 1913.

[9] N. Bohr. *Mat. Fys. Medd. K. Dan. Vidensk. Selsk.*, 18(8), 1948.

[10] M.D. Brown and C.D. Moak. *Phys. Rev. B*, 6(90), 1972.

[11] D.D. Clayton. *Principles of Stellar Evolution and Nucleosynthesis*. The University of Chicago Press, 1983.

[12] G.A. Cowan. *Sci. Am.*, 235(1):36, July 1976.

[13] D.H. Crandall. *Physica Scripta*, 23(2):153–162, Feb. 1981.

[14] Y.T. Lee D. Bailey and R.M. More. *Journal de Physique*, 44(11):C8–149, Novembre 1983.

[15] B. Richter M. Rosenbluth D. Eardley, D. Hammer. Heavy ion fusion. *JASON Committee Report, The MITRE Corporation*, (JSR-82-302), 1983.

[16] J.J. Duderstadt and L.J. Hamilton. *Nuclear Reactor Analysis*. John Wiley and Sons, Inc., 1976.

[17] Z. Zinamon E. Nardi. *Phys. Rev. Lett.*, 49:1251, 1982.

[18] K.G. Dietrich et al. Charge state of fast heavy ions in a hydrogen plasma. *Phys. Rev. Letters*, 69(25):3623–3626, December 1992.

[19] C. Stöckl *et al.* Experiments on the interaction... *Nuc. Inst. Meth. in Phys. Res. A*, 415:558–565, 1998.

[20] H. Geissel *et al. Nuc. Inst. Meth*, 194:21–29, 1982.

[21] H.H. Heckmann *et al. Phys. Rev. A*, 36(8):3654–3669, October 1987.

[22] J.J. Barnard *et al.* Planning for an integrated research experiment. *LBNL internal report*, (ThP.IV-16).

[23] J.M. Hansteen *et al. Atomic Data Nuclear Tables*, 15:305, October 1987.

[24] K. Paludan *et al. J. Phys. B*, 30:3951, 1997.

[25] R. Anholt *et al. Physical Review A*, 32(6):3302, 1985.

[26] T. Matsuo *et al.* Gross ionization cross sections... *Phys. Rev. A*, 60(4):3000–3007, October 1999.

[27] W.E. Meyerhof *et al.* Multiple ionization in... *Phys. Rev. A*, 35(4):1967–1970, February 1987.

[28] Y.F. Chen *et al.* Analytic representation of atomic... *J. Phys. B*, 26:1071–1080, 1993.

[29] C. Fischer. Personal communication. October 1999.

[30] J.D. Garcia. *Phys. Rev. A*, 1:280, October 1970.

[31] H. Gould. *Phys. Rev. A*, 26(2):1134–1137, August 1982.

[32] H. Gould. *Phys. Rev. Letters*, 52(3):180–183, January 1984.

[33] D.C. Gregory. *Phys. Rev. A*, 27(5):2338–2341, May 1983.

[34] M. Gryzinski. *Phys. Rev. A*, 138:305, 1965.

[35] B.H. Choi G.S. Khandelwal and E. Merzbacher. *Atomic Data*, 1:103, 1969.

[36] D.H.H. Hoffmann. Energy loss of heavy ions in a plasma target. *Phys. Rev. A*, 42(4):2313–2321, August 1990.

[37] M. Scharff J. Linhard and H.E. Schiott. Range concepts and heavy ion ranges. *Notes on Atomic Collisions II*, 33(14), 1963.

[38] J.D. Jackson. *Classical Electrodynamics*. John Wiley and Sons, Inc., 1975.

[39] Q.C. Kessel. *Bull. Am. Phys. Soc.*, 14:946, 1969.

[40] A. Kumar. *J. Phys. B*, 11(8):1435, 1977.

[41] E.P. Lee and J.W-K. Mark. Spot heating calculation for a heavy ion driven high temperature experiment. *Lawrence Berkeley Laboratory Report*, 33(LBL-16890 UC-34a), April 1984.

[42] W. Lotz. *Z. Physik*, 206:205, 1967.

[43] D.E. Post et al. L.R. Grisham. *Rev. Sci. Instrum.*, 53:281–284, 1982.

[44] J.H. McGuire and P. Richard. *Phys. Rev. A*, 8(2):1374, September 1973.

[45] Th. A. Mehlhorn. A finite temperature model for ion energy deposition. *J. Appl. Phys.*, 52(11):6522–6532, November 1981.

[46] E. Merzbacher and H.W. Lewis. *Encyclopedia of Physics*, volume 34. Springer, Berlin, 1958.

[47] G. Moliere. *Z. Naturf.*, A2:133.

[48] R. M. More. Personal communication. MArch 1999.

[49] M.Sataka. *Phys. Rev. A*, 39(5):2397–2403, March 1989.

[50] M.Stenke. *Atomic and Plasma Material Interaction Data for Fusion*, 6:51–58, 1995.

[51] R.E. Olson. Stripping cross sections for fast, low charge state ions. *Procedings of the HIF2000 Symposium on Heavy Ion Fusion*, 2000. Conference procedings to be published in Nuclear Instruments and Methods Special Issue.

[52] R.E. Olson, J. Ulrich, and H. Schmidt-Bocking. Multiple-ionization collision dynamics. *Phys. Rev. A*, 39(11):5572, June 1989.

[53] J.R. Oppenheimer. *Phys. Rev.*, 31:349, 1928.

[54] T. Peter and J. Meyer ter Vehn. *Phys. Rev. A*, 43(4):2015–2030, February 1991.

[55] T. Peter and J. Meyer ter Vehn. *Phys. Rev. A*, 43(4):1998–2014, February 1991.

[56] R. Rhodes. *Dark Sun: The making of the hydrogen bomb*. Simon and Schuster, NY, 1995.

[57] D.A. Young R.M. More, K.H. Warren and G.B. Zimmerman. A new quotidian equation of state (qeos) for hot dense matter. *Phys. Fluids*, 31(10):3059–3077, October 1988.

[58] M. Rosen. *Physics of Plasmas*, 6:1690–1699, 1999.

[59] C. Scheidenberger. *N.I.M. Phys. Res. B*, 142:441–462, 1998.

[60] V.P. Shevelko. *N.I.M. Phys. Res. A*, 415:609–613, 1998.

[61] P. Sigmund. Charge-dependent electronic stopping... *Phys. Rev. A*, 56(5):3781–3793, November 1997.

[62] L. Spitzer. *Jr. Astrophysics*, 107(7), November 1948.

[63] M. Stobbe. *Ann. Physik*, 7:661, 1930.

[64] M. Tabak and D. Calllahan-Miller. Design of a distributed radiator target... *Nuclear Instruments and Methods in Physics Research Sec. A*, 415:75–84, 1998.

[65] D. Thomas. Binding energies of electrons in atoms... *http://www.chembio.uoguelph.ca/educmat/atomdata/bindener/ELECBIND.HTM*, 1997.

[66] J.J. Thomson. *Conduction of Electricity Through Gases*. Cambridge University Press, 1906. (out of print).

[67] C. Varelas and J. P. Biersack. *Nuclear Instruments and Methods*, 79:213, 1970.

[68] L. Vriens. *Pro. Royal Soc. London*, 90:935, 1966.

[69] R. Laubert amd I. Sellin W. Brandt. *Phys. Rev.*, 151(90):56–59, 1966.

[70] Zel'dovich and Raizer. *Physics of Shock Waves and High-Temperature Hydrodynamic Phenomena Vol. 1*. Academic Press, 1966. (out of print).

[71] J. F. Ziegler, editor. *Stopping and Ranges of Ions in Matter, Vol. 5*. Pergamon, 1980.

Appendix A

Beam Physics

In addition to the isolated atomic physics of beam ions, the effects of atomic processes on the beam electrodynamics will be considered in this work. In order to address this issue, which is primarily important for chamber ionization and transport, a brief overview of the physics of intense ion beams is presented in this section.

Consider a beam consisting of ions of a particular energy E and velocity v (non-relativistic). In a frame co-moving with the beam, the ions can be considered to occupy a certain averaged volume defined by the beam spot size a and the pulse length l. In this frame the beam ions are characterized by an average number density n, which is just the total number of ions N divided by the volume $\pi a^2 l$.

Charged to a state $+q$, these beam ions constitute a current I given by

$$I = n\pi a^2 v q |e|. \tag{A.1}$$

This current is related to a linear charge density λ by

$$I = \lambda v \tag{A.2}$$

Note that the current varies linearly with the charge of the constituent ion.

Emittance and Perveance

In addition to the net velocity in the of the beam in the direction of propagation, the individual beam ions exhibit individual motions characterized by velocities transverse to the axis of propagation. This velocity spread is quantified by the *emittance* of the beam, which is a measure of the phase-space area of its component ions. This emittance ϵ can be generally expressed as

$$\epsilon^2 \propto < r^2 >< v_r^2 > \tag{A.3}$$

where r is the transverse displacement from the beam center and v_r is the transverse velocity. Note that each of the terms on the right of the equation above have physical interpretations. The average value of the square of the radial displacement is proportional to the beam spot radius a. The average of the square of the velocity is proportional to the ions' average kinetic energy, which is just the temperature.

One of the chief concerns about using intense particle beams as HIF drivers is related to an effect known as space charge. Ignition of reactor-grade fusion hohlraums may require a beam with a spot size of only a few millimeters. When focused to such small radii, the collective Coulomb repulsion of the beam ions may become significant. This repulsion will increase with increasing ion charge state and with decreasing spot radius. A measure of the collective space charge repulsion is the *perveance* Q of the beam. It is a unit-less quantity expressed by

$$Q = \frac{qe}{m_i} \frac{2I}{(\beta\gamma c)^3} \tag{A.4}$$

in which m_i is the beam ion mass, and β and γ have their usual relativistic definitions as a function of the beam velocity v. For a non-relativistic beam scenario, like the ones considered for the IRE and HCX, this perveance can be simplified as

$$Q = \frac{qe}{m_i}\frac{2I}{v^3} \tag{A.5}$$

Rewritten slightly and making the substitution $\lambda = I/v$, a simplified form of the perveance is obtained

$$Q = \frac{qe\lambda}{T} \tag{A.6}$$

where $T = \frac{1}{2}m_i v^2$.

Ion Equations of Motion

In a co-moving frame, the beam system can be seen as an ensemble of ions in a self-induced electric field. An important component of this electric field is in the radial direction and is related to the beam's current density. The radial field $E_r(r,z)$ within the beam is given by

$$E_r(r,z) = \frac{2\lambda r}{a(z)^2} \tag{A.7}$$

where $a(z)$ is the spot radius of the beam as a function of beam transit along z. Note that an ion at the beam's center $r = 0$ experiences no electric field. The radial motion of a beam ion of charge q due to this electric field is given by

$$m_i\frac{d^2r}{dt^2} = qeE_r(r,z). \tag{A.8}$$

Since the ion's position along the direction of propagation z is related to time simply by $z = vt$, the force equation can be written in terms of a spatial differential as

$$\frac{d^2r}{dz^2} = \frac{qe}{m_i v^2} E_r(r, x). \tag{A.9}$$

Substituting into this the expression for the electric field gives

$$\frac{d^2r}{dz^2} = \frac{qe}{m_i v^2} \frac{2\lambda r}{a(z)^2} \tag{A.10}$$

which, recalling the definition of perveance is just

$$\frac{d^2r}{dz^2} = Q \frac{r}{a(z)^2} \tag{A.11}$$

Appendix B

Properties of the Transcendental Function $\ln[\ln[Z]]/\ln[Z]$

Consideration of an interesting logarithmic function has been induced by the assertion of the approximation

$$\ln[Z] \approx Z^{1/3}. \tag{B.1}$$

This seems at first to be a non-intuitive relationship. However, analysis shows that this is indeed a reliable estimation for Z in the domain of atomic numbers. This function can be more generally written

$$\ln[Z] \approx Z^{1/\nu} \tag{B.2}$$

where ν is some real number. One step of logarithmic algebra produces

$$\frac{\ln[\ln[Z]]}{\ln[Z]} \approx \frac{1}{\nu}. \tag{B.3}$$

In order for this approximation to be valid, the derivative with respect to Z of equation B.3 must be vanishing. In other words, at some Z value, will there be a point at

which the value of equation B.3 locally does not vary with Z. Once this regime has been established, the actual constant term representing the value of the function in that region will be shown to be near 1/3.

Taking the derivative of equation B.3 produces

$$\frac{1}{\ln^2[Z]Z} - \frac{\ln[\ln[Z]]}{\ln^2[Z]Z} = 0 \tag{B.4}$$

which is true if

$$\ln[\ln[Z]] = 1 \tag{B.5}$$

which is to say

$$Z = e^e. \tag{B.6}$$

So, the original ansatz that $\ln[Z]$ can be represented by $Z^{1/\nu}$ is indeed true if $Z = e^e \approx 15.15$. This makes sense: the natural logarithm of this value is e and taking the natural logarithm again produces 1. The value of the function in equation B.3 is then $1/e$, which is very close to the presumed value of 1/3.

How good is this approximation over a broad domain covering atomic numbers from 2 to 92? Figure B.1 displays the plot of the left hand side of equation B.3 as a function of Z. note that the function diverges at $Z = 1$. But, the important feature is noted in the proximity to 1/3 of the values of the function for $Z \geq 5$. This shows that the original approximation holds very well for most atomic number values of concern to this dissertation.

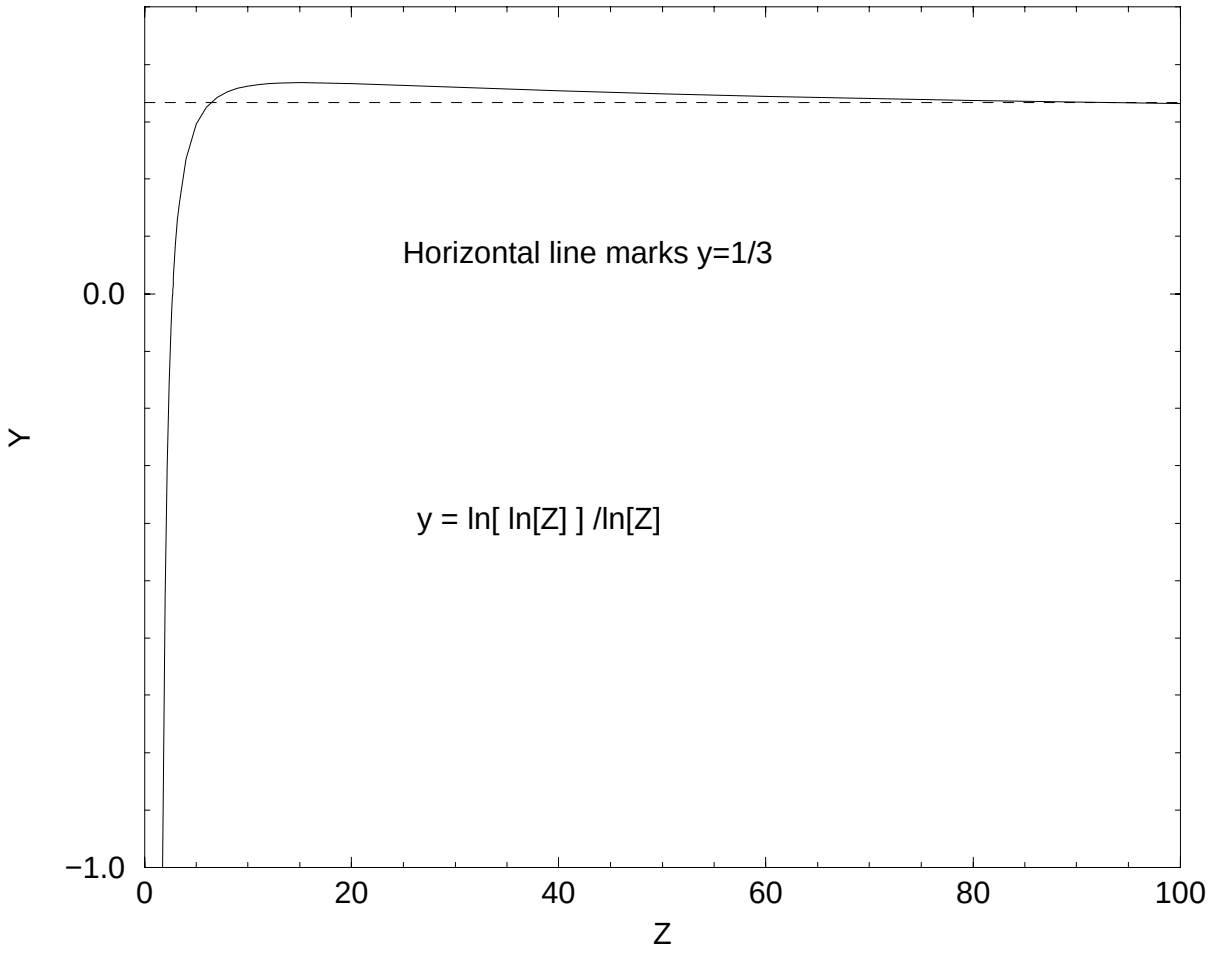

Figure B.1: Values of the transcendental function $\ln[\ln[Z]]/\ln[Z]$

Appendix C

Computer Codes

In this appendix some details are discussed about the computer programs developed to perform the calculations of this dissertation. The primary language used in this work was actually FORTRAN77. Despite its age and growing obscurity, FORTRAN77 is easy to use and well suited for the handling of formulas required by the atomic physics modeling of this research.

Three general codes were developed to perform most of the calculations discussed here. One is used to calculate beam charge-changing cross sections including multiple ionization probabilities. This first code is called simply **x** (representing 'cross section') and is the one most useful for HIF chamber ionization cross section calculation. The second code, **zstop** , features no charge changing cross section calculations but does have an energy deposition routine. This code calculate the energy deposition of a beam into a target. Beam charge state information is provided using an equilibrium charge state formula (either the old Bohr formula of equation 5.4, or the new equation 7.29). The third code, **zstopx** ,

contains both the beam charge changing routines plus the subroutine for calculating beam energy loss into the target. It is used to perform integrated charge evolution and deposition calculations. Since it is used for energy deposition calculations using first-principle charge evolution, it calculates only the average beam charge information and does not employ the multiple ionization calculations.

Of the three primary codes, only the first, x, will be useful in future calculations. Beam charge-change calculations will be needed to be performed regularly for many different upcoming HIF-related experiments. Therefore, a code is sought which can run quickly and can be manipulated easily. The x code accomplishes this. The other two codes will not be a useful product since any future calculations of beam deposition into dense targets will be performed with existing routines. However, those codes would benefit by an update to include the new charge equilibrium formula for beams penetrating dense plasmas (equation 7.29). That update can be made with only a line or two of new code. Thus, the **zstopx** and **zstop** codes developed here will only be useful to provide preliminary results.

All of the codes exist on the 'jess' server in Building 47 of LBNL's AFRD division. Each of them are operated in a similar manner. Each requires two atomic data bank input files which are read by the code automatically. These are (1)'estruct.dat' which contains the shell structures, screening constants and ionization potentials for every electron in every neutral atom from hydrogen to uranium; (2)'ibar.dat' which contains the average ionization potentials for every neutral atom from hydrogen to uranium. These must be included in the same directory as the compiled, executable code. Each code then requires an input file containing the beam and target parameters for the interaction sought to be simulated. The

input file is contained in a subdirectory which is specified below. One or more output files are then generated. The use of each code is demonstrated in the following sections.

C.1 x

The x code exists in a text file containing FORTRAN77 code. This form is called x.f and its compiled form is simply called **x** . The input file specifying the beam and target parameters of the problem is called 'x.inp' and must be placed in a sub-directory called 'xinp'. The complete listing of the FORTRAN source of this code appears at the end of this appendix.

A sample input file x.inp is listed below. It is the input deck which contains the parameters for calculating the charge-changing cross sections for a lead beam penetrating a BeF_2 gas. The first line of the input deck specifies the projectile (beam) atomic number Z_p and its atomic mass number A_p. The values here are 82 and 208 respectively, representing a common lead isotope. The next line specifies the beam energy and initial charge state. When the beam energy is negative, as it is here, the value is interpreted by the code as energy per atomic mass unit. The units of the energy on line 2 are eV, so this beam has an energy of 20MeV/amu. Note that powers of ten are signified using D, since the code uses double precision calculations. The charge state here is given as -1. When the initial charge state is negative, the x code interprets that as an instruction to compute the cross section values for every charge state Q from $Q = 0$ to $Q = Z$.

```
82, 208
-20.0D6, -1
```

```
0.025, -5.D13, 0
2
4,9,1.0,0
9,19,2.0,0
```

The next line, line 3, gives the temperature, density and charge equation of state flag for the target. The units of the temperature value are eV, so the value here of 0.025 represents approximately room temperature. The target density value, here -5×10^{13}, represents number density since it is a negative value. If it were positive, it would be interpreted by the code as mass density in g/cm^3. The last number 0 tells the code to use the average atom model for the charge state of the target. This means that every target species will have the same charge state. The next line, line 4, carries the value 2. This represents the number of atomic or ionic species in the target. Since this input deck simulates a BeF_2 chamber, there are 2 target species. The next two lines give the atomic information for those two species, being beryllium and fluorine. The target species should be listed according to increasing atomic number. The first of the two lines, therefore, is for beryllium. The three values on line 5 represent the first species' atomic number $Z_t(1)$, its atomic mass $A_t(1)$, and its charge state $Q_t(1)$. Here, the first target species is beryllium, with atomic number 4, atomic mass 9 and at a charge state of 0. The next line, line 6 contains the analogous information for fluorine. This completes the input deck requirements for this problem.

The output which this particular file produces consists of two separate files. One is

'xmulti.out' and the other is 'xlist.out'. The first contains more information than the latter, but the latter is more useful to peruse quickly to see the overall cross section values and beam equilibrium charge state for the case at hand. Samples from each are listed below.

The xmulti.out file contains the ionization and capture cross sections for each requested charge state (or for every charge state if the beam's initial charge state is selected as -1). Also included are multiple ionization cross sections as discussed in section 5.4.10. A sample xmulti.out output file is listed below from the calculations generated by the above input file. It provides the cross section values for a neutral lead beam upon impact with BeF_2, as specified by the input deck. The 'Multiplicity' column signifies multiplicity of multiple ionization, listing cross section values for single through quintuple ionization of the lead projectile.

```
Charge state = 0
Total Ionization Cross Section [cm2] 0.913D-15
Total Capture Cross Section [cm2] 0.000D+00
Multiplicity Cross Section [cm2]
1            0.442D-15
2            0.136D-15
3            0.130D-15
4            0.401D-16
5            0.302D-16
```

The xlist.out file contains a list of the total ionization and recombination cross sections for the beam, per collision with a target molecule. For the run produced by the

x.inp input deck considered here, the following output is generated by the x code in the xlist.out file:

Charge	Ionization	Capture
.00000D+00	.91327D-15	.00000D+00
.10000D+01	.77454D-15	.79007D-25
.20000D+01	.61272D-15	.93992D-24
.30000D+01	.62526D-15	.65743D-23
.40000D+01	.48404D-15	.18426D-22
.50000D+01	.41719D-15	.59463D-22
.60000D+01	.37854D-15	.12069D-21
.70000D+01	.34385D-15	.22155D-21
.80000D+01	.30378D-15	.37594D-21
.90000D+01	.27699D-15	.60142D-21
.10000D+02	.25326D-15	.91764D-21
.11000D+02	.23177D-15	.13819D-20
.12000D+02	.24029D-15	.19620D-20
...		
.61000D+02	.19156D-17	.15500D-17
.62000D+02	.20006D-17	.16448D-17
.63000D+02	.14778D-17	.17383D-17
.64000D+02	.10903D-17	.19613D-17
.65000D+02	.93518D-18	.20670D-17
.66000D+02	.79078D-18	.21820D-17
.67000D+02	.64999D-18	.23001D-17
.68000D+02	.52513D-18	.24213D-17
.69000D+02	.28789D-18	.25285D-17
.70000D+02	.30143D-18	.26544D-17
.71000D+02	.20376D-18	.27792D-17
.72000D+02	.11047D-18	.29573D-17
.73000D+02	.92112D-19	.30844D-17
.74000D+02	.75309D-19	.32143D-17
.75000D+02	.59203D-19	.33473D-17
.76000D+02	.45027D-19	.34833D-17
.77000D+02	.32197D-19	.36196D-17
.78000D+02	.20464D-19	.37613D-17
.79000D+02	.99761D-20	.39060D-17
.80000D+02	.26443D-21	.40592D-17
.81000D+02	.12463D-21	.42242D-17
.82000D+02	.00000D+00	.43933D-17

(Some points were omitted for brevity.) This file lists the total ionization and capture cross sections for each requested beam charge state, given in cm^2. The first column contains the charge state, the second contains the ionization cross section and the last contains the capture cross section. Note that this file can be used to identify the equilibrium charge state for this beam-target configuration. It occurs between projectile charge state 62 and 63 as judged by the balance of ionization and capture between those points. This happens to be very near the value predicted by the Bohr cold target fit for a lead beam at this energy. The first dozen of these ionization cross sections are identical to the ones which appear in table 7.1.

A key file exists called 'x.inp.key' which contains more information about the input file and it is found in the xinp directory. Please refer to this file for any updates about the code's operation.

C.2 zstop

The code **zstop** exists in a FORTRAN77 form called 'zstop.f'. The compiled version should be called **zstop** . Its associated input file must be named 'zstop.inp' and must exist in a subdirectory called 'zinp'.

A sample input file and output analysis for this code are presented below. Its input structure is very similar to that of the **x** code, but with some modifications to suite the code's different purpose. The following input file provides the instructions necessary to simulate the deposition of a 20MeV/u lead beam into a gold target of density $1g/cm^3$ at 300eV.

```
82,208
-20.0D6
300.0, 1.0 1
79,197,1.0,27.4,1560.
0.01
```

The first line contains the atomic number and atomic mass number, Z_p and A_p respectively, of the projectile species. The second line contains the beam energy (with 'D' for exponential values signifying double-precision). The energy is negative, which means it is interpreted as energy per atomic mass unit. The value is $20\text{MeV}/u$ in this case. Note that no initial charge state is required to be specified for the projectile species since the code treats the incident ions as being in instantaneous equilibrium, which is calculated by the code itself. The next line contains the target's temperature and density, respectively, which are 300eV and 1.0g/cm^3 in this case. The **zstop** code is an average atom code, so it treats every atom or ion in the target as having the same properties. The following line, containing 1, tells the code that there is just one target atomic constituent. The following line gives the properties of that one constituent. The five values on line 5 are target atomic number and atomic mass number, fraction of that species in the target (being 1.0 if there is only one target constituent), the average charge state of the target and the average ionization potential of the target's remaining bound electrons. The values for this gold target are taken from section 3.1.10. The last line contains the ϵ tolerance value discussed in section 6.1.2. A value of $0.01 = 1\%$ was used here and throughout the calculations in this dissertation.

The output file generated by **zstop** is called 'zstop.out'. It contains data whose

columns represent different physical parameters of the problem and whose rows represent values taken at each numerical step. The lines below contain a sample line from the data output of the calculation generated by the input file above.

```
Energy/amu   Speed        Charge   -dE/dx       -dE/dR       Depth        Range        Time
HeV          cm/s         State    HeV/cm       HeV/mg/cm2   cm           mg/cm2       sec
...
0.5009D+01   0.3097D+10   43       0.6844D+05   0.6844D+02   0.5001D-01   0.5001D+02   0.1071D-10
...
```

The full plot of the projectile's energy deposition rate as a function of the total range of penetration into the target (column 5 *vs.* 7) appears in figure 7.23. This line was taken from a point at which the range of the lead projectile was about 50mg/cm^2 (column 7). The energy at this point was about 5.0MeV/amu, as shown in column 1. The 'Time' column lists total deposition time of the beam into the target. At the point shown here, the beam has been deposited for about 1 nanosecond (being the value 0.10710×10^{-10} in column 8).

C.3 zstopx

The operation of the **zstopx** code is very similar to that of the **zstop** code. The primary difference is that the beam's charge state evolution is calculated from first principles, from the individual ionization and capture reaction rates, and not from a simple formula. The input file necessary to run this code is called 'zstopx.inp' and it must exist in a subdirectory 'zxinp'. Since this code calculates the actual charge state evolution of the beam, the initial charge state of the beam must be provided in the input deck. An sample use of the **zstopx** code is presented below. The input deck which would be used to

simulate the deposition of a 20MeV/u lead beam into a carbon plasma of density 0.01g/cm^3 at 300eV is as follows:

```
82,208
-20.0D6, 10
300.0, 0.01 1
6,12,1.0,5.9,1024.
0.01
```

This case was examined in section 7.3.2 and displayed in figure 7.10. Notice that the only structural difference between this input file and the one required for the **zstop** code is the second data point on line 2 for the beam's initial charge state. In this case the value is 10. The charge state quickly changes from this initial state, and its value does not affect the output of the code in this case.

The **zstopx** code generates an output file called 'zstopx.out'. A representative output line from that file, generated by the above input file, is listed below. This particular beam-target configuration was examined in the body of the dissertation to establish that an HIF driver beam's charge state during its penetration into a hohlraum target would be equal to the equilibrium charge state at each point in the deposition. The sample output line printed below was chosen at a point in the deposition when the beam's velocity was near 2×10^9cm/s (in column 2). The charge state of the beam is found in column 3. The charge state of the incident lead beam at this point in the beam's deposition is calculated to be 40.

```
Energy/amu   Speed        Charge   -dE/dx       -dE/dR       Depth        Range        Time
```

```
MeV          cm/s          State    MeV/cm       MeV/mg/cm2   cm           mg/cm2       sec
...
0.2099D+01   0.2009D+10    40       0.2883D+04   0.2883D+03   0.1948D+01   0.1948D+02   0.4538D-09 ...
```

C.4 Listing of x.f code

The following is a listing of the x.f source code for the **x** cross section calculation code.

```
c
c "x" x.f by MSA 2000
c This program calculates ionization and
c recombination cross sections in a beam penetrating a target
c Contact author at msarmel@lbl.gov or through
c advisor Prof. Per Peterson peterson@nuc.berkeley.edu
c or through the Dept. of Nuclear Eng. at UCBerkeley
c See MSA's dissertation "Atomic Processes for Heavy Ion Inertial Fusion"
c for more info about code
c****************Variables and Inputs********
        common zp,ap,ztarg,atarg,ibart,scr,ttargev,eb,nti,nmt,nenl,ng,lg,nmax,lmax,ntc,ipp,ipt

        real*16 mp
        real*16 scr(1:100,1:7,0:6),ttargev,nit,nmt,nfe,nti(1:10,0:100)
        real*16 eb(1:100,1:7,0:6), ibart(1:100), ipp(0:100), ipt(1:10,0:100)
        integer zp,ap,ztarg(1:10),atarg(1:10),ntc
        integer nenl(1:100,1:7,0:6), ng(1:100), lg(1:100), nmax(1:100), lmax(1:100)

        real*16 c,me,meev,amu,amev,pi,e,a0,alpha,hbar
        parameter (c=2.998D10, me=9.108D-28, meev=5.11D5, amu=1.66D-24)
        parameter (amev=931.502D6, pi=3.1415927, e=4.803D-10, a0=0.529D-8, alpha=7.3D-3, hbar=1.054D-27)

        real*16 tp,tp0
        real*16 rate1,rate2
        real*16 tpev
        real*16 ttarg,rho,eblow
        real*16 v1,v0,v1fit,veth,vpc,vprel
        real*16 mua,muz
        real*16 ttargk
        real*16 fs,nesum,bsaha,csaha,coefs,hold,gsaha
        real*16 mpev,vp,ne
        real*16 r0,tq
        real*16 xp,tt
        real*16 theta, again, alose
        real*16 sigma(1:10)
        real*16 ftarg(1:10),fqtarg(1:10,0:100)
        real*16 ftsum

        integer ni,zmax
        integer qtarg(1:10)
        integer nl,tn,tl
        integer qp,zpp,zp0
        integer ztrk0, ztrk1, ztrk2
        integer printz,fch

cfffffffffff formats ffffffffffffffff
4       format(2I10)
5       format(D10.4,I10)
6       format(2D10.3)
7       format(2D10.3, I10)
9       format(2I10,D10.3)
10      format(2I10,D10.3,I10)
11      format(I10)
12      format(2I10,2D10.4)
13      format(D10.3)
14      format(I10,D10.3)
20      format(5D10.3)

ciiiiiiiiiii--Reading problem input data--iiiiiiiiiiiiiiiiiiii
        open(8,file="xinp/x.inp")
c       ----------Projectile
        read(8,4)zp,ap
        read(8,5)tp,zp0
c       --------------Target
        read(8,7)ttargev,rho,fch
        read(8,11)ntc
        ftsum = 0.
        do 25 i=1,ntc
                if (fch.ge.3) then
                        read (8,9)ztarg(i),atarg(i),ftarg(i)
                else
                        read(8,10)ztarg(i),atarg(i),ftarg(i),qtarg(i)
                endif
                ftsum = ftsum + ftarg(i)
                if (fch.eq.2) then
                        do 24 ii=0,qtarg(i)
                                read(8,13)fqtarg(i,ii)
24                      continue
                endif
                if (fch.eq.1) read(8,13)sigma(i)
25      continue
        close (8,status="keep")

c#######--Conversions, initializations, and important variable set-ups--##########
        xp=0.
        tt=0.
        tq = 0.
        theta = 0.
        rate1 = 0.
        rate2 = 0.
        if (zp.gt.ztarg(ntc)) then
                zmax = zp
        else
                zmax = ztarg(ntc)
        endif
        do 34 i=1,100
                do 33 n=1,7
                        do 32 l=0,n-1
```

```
                                nenl(i,n,l)=0
32                      continue
33              continue
34      continue

        if (tp.lt.0.0) tp=abs(tp*ap)
        tp = tp*1.602D-12
        tp0=tp
        mpev=amev*ap
        mp=ap*amu
        ttarg=ttargev*1.602D-12
        ttargk = ttargev*11605.
        veth = sqrt(2.0*ttarg/me)
        tpev = tp/1.602D-12
        vpc = sqrt(2.0*tp/mp)
        vprel = c*sqrt(1.0 - (1. + tpev/(ap*amev))**-2.0)
        if ((tpev/ap).gt.30.) then
                vp = vprel
        else
                vp = vpc
        endif
        mua=0.
        muz=0.
        do 35 i=1,ntc
                mua=mua + atarg(i)*ftarg(i)/ftsum
                muz=muz + ztarg(i)*ftarg(i)/ftsum
35      continue
        do 38 i=1,ntc
                do 37 j=0,ztarg(i)
                        nti(i,j) = 0.
37              continue
38      continue
        if (rho.lt.0.0) then
                nmt = abs(rho)
                nit = ftsum*nmt
                rho = nit*mua*amu
        else
                nit = rho/(mua*amu)
                nmt = nit/ftsum
        endif
        ne=muz*nit
        qp=zp0
        alphtint=0.0
        probz=exp(-1.0*alphtint)
        r0=(3./(4.*pi*nit))**(1./3.)
        v0 = c/137.
        v1 = v0*(zp**0.6666)
        v1fit = v0*(zp**0.6666)
        ztrk0=-1
        ztrk1=qp
        ztrk2=qp
        printz=0

cooooooooooo--Open output files--ooooooooooooooooooooooooooooooo
        open(18,file="xmulti.out")
        open(19,file="x.out")
        write(18,27)
        write(18,28)
27      format("Z       Energy  Energy/amu          Speed     Charge")
28      format("        [MeV]   [MeV]               [cm/s]    State")

c###Print Info###############
        write(18,319)zp, tp/1.0D6/1.602D-12, tp/1.0D6/1.602D-12/ap, vp, qp
319     format(I3, "    ",D10.4," ", D10.4,"    ", D10.4," ",I10)

c%%%%%%%%%%%%%%%%%%%%%%%%%%%%%%%%%%%%%%%%%%%%GLOBAL ATOMIC PHYSICS%%%%%%%%%%%%%%%%%%%%%%%%%%%%%%%%%%%%%%%%%%%%
ciiiiiiiiiiiiiii--Reading electron structure, binding energies and screening constants--iiiiiiiiiiiiiiii
ciiiiiiiiiiiiiiiiii--Also read atomic radii and density profile--iiiiiiiiiiiiiiiiiiii
        open(81,file="estruct.dat")
c       read in values for all species <= maximum Z
        do 50 i=1,zmax
c       -------------electronic structure
                read(81,4)zpp,nl
                eblow=1.D9
                do 48 ii=1,nl
                        read(81,5081)tn,tl,nenl(i,tn,tl),eb(i,tn,tl),scr(i,tn,tl)
                        if (eb(i,tn,tl).lt.eblow) then
                                ng(i)=tn
                                lg(i)=tl
                                eblow = eb(i,tn,tl)
                        endif
48              continue
                nmax(i)=tn
                lmax(i)=tl
50      continue
        close(81,status="keep")
5081    format(3I10,2G10.6)
c%%%%%%%%%%%%%%%%%%%%%%%%%%%%%%%%%%%%%%%%%%%%%%%%%%%%%%%%%%%%%%%%%%%%%%%%%%%%%%%%%%%%%%%%%%%%%%%%%%%%%%%%%%%%%5

c Note: Even though I use scaling laws to determine inner binding energies for ionized
c species, I will still use pre-determined (outer electron) ionization potentials when
c possible (one may as well use real*16 values over scaled ones whenever possible).
c
ciiiiiiiiiiiiiii--Reading target ionization potentials--iiiiiiiiiiiiiii
        open(81,file="ionpot.dat")
        do 59 i=1,ntc
53              read(81,*)zpp
                if (-1*zpp.ne.ztarg(i)) goto 53
```

```
                zpp = -1*zpp
                do 58 j=0,zpp-1
                        read(81,13)ipt(i,j)
                        ipt(i,j)=ipt(i,j)*1000.
58              continue
59      continue
        close(81,status="keep")

ciiiiiiiiiiiiiii--Reading projectile ionization potentials--iiiiiiiiiiiiiii
        open(81,file="ionpot.dat")
60      read(81,*)zpp
        if (-1*zpp.ne.zp) goto 60
        zpp = -1*zpp
        do 69 j=0,zpp-1
                read(81,13)ipp(j)
                ipp(j)=ipp(j)*1000.
69      continue
        close(81,status="keep")


ciiiiiiiiiiiiiiiiiiiii---Average target ionization potentials--iiiiiiiiiiiiiiiiiiii
        open(81,file="ibar.dat")
        do 79 i=1,92
                read(81,*)zpp
                read(81,13)ibart(i)
79      continue
        close(81,status="keep")

c%%%%%%%%%%%%%%%%%%%%%%%%%%%%%%%%%%%%%%%%%%%%%%%%--TARGET ATOMIC PHYSICS--%%%%%%%%%%%%%%%%%%%%%%%%%%%%%%%%%%%%%%%%%%%%%%%%
c___________________Charge State distribution___________________
c_____________________________Delta, Gaussian or Saha_____________________
        nfe=0.
        do 94 jj=1,ntc
                if (fch.eq.3) then
c                       ------------------------Saha Equation-------------------
                        coefs = 2.*3.02D21*(ttargev**1.5)
c                       coefs = (1.305D26*ttarg)**1.5
                        nti(jj,0)=nit*ftarg(jj)/ftsum
                        nesum = 0.
                        do 86 ii=1,ztarg(jj)
                                fs = coefs*exp(-1.*ipt(jj,ii-1)/ttargev)
                                nesum = 0.
                                if (ii.gt.1) then
                                        do 85 ni = 1,ii-1
                                                nesum = nesum + ni*nti(jj,ni)
85                                      continue
                                endif
                                bsaha = nesum + fs
                                csaha = fs*nti(jj,ii-1)
                                gsaha = 0.5*(-1.0 + sqrt(1. + 4.*csaha/(bsaha*bsaha)))
c                               ____________________ Must be careful with numerics _____________________
                                if (gsaha.lt.1.) then
                                        hold = nti(jj,ii-1)
                                        nti(jj,ii-1) = hold*gsaha/(1. + gsaha)
                                        nti(jj,ii) = hold - nti(jj,ii-1)
                                else
                                        nti(jj,ii) = 0.5*bsaha*(-1.0 + sqrt(1. + 4.*csaha/(bsaha*bsaha)))
                                        nti(jj,ii-1) = nti(jj,ii-1) - nti(jj,ii)
                                endif
86                      continue
                        do 88 ii=0,ztarg(jj)
                                nfe=nfe+ii*nti(jj,ii)
88                      continue
                endif
c               ------------------Average Atom--------------------------
                if (fch.eq.0) then
                        nti(jj,qtarg(jj)) = nit*ftarg(jj)/ftsum
                        nfe = nfe + qtarg(jj)*nti(jj,qtarg(jj))
                endif
c               ------------------Gaussian-----------------------------------
                if (fch.eq.1) then
                        do 90 ii=0,ztarg(jj)
                                nti(jj,ii)=(nit*(ftarg(jj)/ftsum)/(sigma(jj)*sqrt(2.*pi)))*exp( -((1.*ii - qtarg
(jj)*1.)**2)/(2.*sigma(jj)*sigma(jj)) )
                                if ( int(abs(1.*ii - 1.*qtarg(jj))).gt.int(2*sigma(jj)) ) nti(jj,ii)=0.
                                nfe=nfe+ii*nti(jj,ii)
90                      continue
                endif
c               ----------------------Manual---------------------------
                if (fch.eq.2) then
                        do 92 ii=0,qtarg(jj)
                                nti(jj,ii) = ftarg(jj)*nit*fqtarg(jj,ii)/ftsum
                                nfe = nfe + ii*nti(jj,ii)
92                      continue
                endif
94      continue

c ***************************************************************************************************************
*
c ***************************************************************************************************************
*
c                       This is the main calculation routine.
c ***************************************************************************************************************
*
c ***************************************************************************************************************
*

c$$$Call charge routine$$$
```

```
        call dcharge(qp,tp,again,alose)

c$$$$$$Close output files
        close(18,status="keep")
        close(19,status="keep")


6660    format(D10.4," ",D10.4,"  ",D10.4,"  ",D10.4," ",D10.4,"  ",D10.4,"  ")

c$$$$$$Go home
        end

c *_*_*_*_*_*_*_*_*_*_*_*_*_*_*_*_*_*_*_*_*_*_*_*_*_*_*  dpz/dt  *_*_*_*_*_*_*_*_*_*_*_*_*_*_*_*_*_*_*_*
c Calculating dpz, the change in the charge state probablilty
c%%%%%%%%%%%%%%%%%%%%%%%%%%%%%
        subroutine dcharge(qps,tps,again,alose)
        common zp,ap,ztarg,atarg,ibart,scr,ttargev,eb,nti,nmt,nenl,ng,lg,nmax,lmax,ntc,ipp,ipt

        real*16 mp
        real*16 scr(1:100,1:7,0:6),ttargev,nit,nfe,nti(1:10,0:100),nmt
        real*16 eb(1:100,1:7,0:6), ibart(1:100), ipp(0:100), ipt(1:10,0:100)
        integer zp,ap,ztarg(1:10),atarg(1:10),ntc
        integer nenl(1:100,1:7,0:6), ng(1:100), lg(1:100), nmax(1:100), lmax(1:100)

        real*16 c,me,meev,amu,amev,pi,e,a0,alpha,hbar
        parameter (c=2.998D10, me=9.108D-28, meev=5.11D5, amu=1.66D-24)
        parameter (amev=931.502D6, pi=3.1415927, e=4.803D-10, a0=0.529D-8, alpha=7.3D-3, hbar=1.054D-27)

        real*16 tps,tpev,ntis,snuc
        real*16 adom,rnl(0:100), ziont2, bnl(0:100)
        real*16 re,gamma,beta,vpc,vprel
        real*16 vp,ttarg,veth,vr,v0,h,hbev,r0,prhonl
        real*16 alose,ibnlev,ibnl,zeft
        real*16 av,bv,v,cv,gvgryz,gvggv
        real*16 gv1,gv2,gv3,gv4
        real*16 fnl,vnl,zeffnl
        real*16 sfe,sdr,srec
        real*16 snl,snlbethe,snlbohr,snlgryz
        real*16 cbohr, bohrsum, fvbethe
        real*16 vbohr, arect, srect
        real*16 qenc, bmin, ecoul, gvlotz
        real*16 snllotz
        real*16 bete,gamme
        real*16 rright,rleft,fmin
        real*16 er,erev,step,ev
        real*16 arec,aa,g1,ebind,hn,srn,sc,coef
        real*16 eta,arec2,kappa,srec2
        real*16 a3br,s3br
        real*16 act,sct,ekev,ekit,ekfp,heta,ep,vi
        real*16 eika,eikb,eikc,aeik,ct1,ct2,scti
        real*16 enl,ipc
        real*16 adr,coe,ipi,ipj,s,t,fst,ipv
        real*16 fij1,fji1,fvi1,fiv1
        real*16 gx,glp,gd,gn0,gl,aa1,ar1,aa1jive,aa1vije,ar1vi
        real*16 adrnlij,aav
        real*16 ei,ej,ek,en
        real*16 again, bminmax, atot, anuc
        real*16 zef,zefm, zbart
        real*16 ibar,scsum,scavg,coef2,bmax,bmaxmax
        real*16 snlggv
        real*16 prob(0:100), probnot
        real*16 sigion, sigrec, sigmult(1:100)
        real*16 ptot, sigtot
        real*16 aionmax, sionmax, ra
        real*16 flow, fyes, dsig, hold
        real*16 probsum,impactsum
        real*16 sct2,act2

        integer zmockp,zmockt,qloop,qtargs
        integer qps,ztargs,atargs,tcis
        integer jj,n,ngp,nv,glj,gnj,nmaxp,lgp
        integer ljavg,nlj
        integer nc,ni,lc,li,lv,nnl
        integer nj,nnli,nep,nsum,njsum
        integer llow,nval, forder
        integer iq, q
        integer nin,ntn,nout

        nit = 0.
        nfe = 0.
        do 28 i = 1,ntc
                do 25 ii = 0,ztarg(i)
                        nfe = nfe + ii*nti(i,ii)
                        nit = nit + nti(i,ii)
25              continue
28      continue

        v0=c/137.D0
        h=4.13570D-15*1.602D-12
        hbev=6.58217D-16
        r0=(3.D0/(4.D0*pi*nit))**(1.D0/3.D0)
        re = e*e/(me*c*c)

        mp = ap*amu
        ttarg=ttargev*1.602D-12
9       tpev = tps/1.602D-12
        vpc = sqrt(2.0*tps/mp)
```

```
        vprel = c*sqrt(1.0 - (1. + tpev/(ap*amev))**-2.0)
        vp = vpc/(exp((tps-mp*c*c)/(0.1*mp*c*c)) + 1.) + vprel/(exp((mp*c*c-tps)/(0.1*mp*c*c)) + 1.)
        if ((tpev/ap).gt.30.) then
                vp = vprel
                beta = vp/c
                gamma = (1. - beta*beta)**(-0.5)
                ek = (gamma-1.)*me*c*c
        else
                vp = vpc
                beta = vp/c
                gamma = 1.
                ek = 0.5*me*vp*vp
        endif
        ekev=6.242D11*ek
        veth = sqrt(2.*ttarg/me)
        vr=sqrt(vp*vp + veth*veth)
        er = 0.5*me*vr*vr
        erev = er*6.242D11

        if (qps.lt.0) then
                qloop = 1
                qps = 0
        endif

10      nep = zp-qps
        zmockp=zp-qps

c00000000000000Initialize000000000000000000
        adom = 0.
        arect=0.
        anuc = 0.
        afe = 0.
        alose = 0.
        arec = 0.
        arec2 = 0.
        a3br = 0.
        act = 0.
        adr = 0.
        again = 0.
        act2 = 0.
        sfe = 0.
        srec=0.
        srec2 = 0.
        s3br=0.
        sct=0.
        sct2 = 0.
        sdr=0.
        snuc = 0.
        aionmax = 0.
        do 53 i=0,nep
                rnl(i) = 0.
                bnl(i) = 0.
                prob(i) = 0.
53      continue

        if (zmockp.eq.0) then
                ibar = 0.
                nmaxp = 0
                bmax = 0.
                goto 60
        endif
        ngp = ng(zmockp)
        lgp = lg(zmockp)
        nmaxp = nmax(zmockp)
c       ========Get Ibar for projectile===============
        ibar = ibart(zmockp)
        scsum = 0.
        nsum = 0
        do 55 n=1,nmax(zmockp)
                do 54 l=0,n-1
                        scsum = scsum + nenl(zmockp,n,l)*scr(zmockp,n,l)
                        nsum = nsum + nenl(zmockp,n,l)
54              continue
55      continue
        scavg = scsum/nsum
c       ----------Final form----------
        coef2 = ( (1.*zp - scavg)/(1.*zmockp - scavg) )**2.0
        ibar=1.602D-12*ibar*coef2
        bmax = vp*hbar/ibar

c       ****************************Loop for each target constituent****************
60      do 699 tcis=1,ntc
                ztargs=ztarg(tcis)
                atargs=atarg(tcis)
c       ----------------------Ionization by Target Nuclear Charge and Bound electrons----------------
100             if (qps.eq.zp) goto 351
c               vvvvvvvvvvvvvvvvvvvvvvvvFor each target charge statevvvvvvvvvvvvvvvvvvvvvvvv
                do 190 jj=0,ztargs
                        qtargs=jj
                        if (nti(tcis,jj).eq.0) goto 190
                        zmockt = ztargs-jj
c                       ----------Target effective ionization potential---------
c                       ...get avg screening constant...
                        scavgt = 0.
                        do 120 ni=1,nmax(zmockt)
                                do 110 li=0,nmax(zmockt)-1
                                        scavgt = scavgt + nenl(zmockt,ni,li)*scr(zmockt,ni,li)
110                             continue
```

```
120                     continue
                        scavgt = scavgt/zmockt
                        coef = ((1.*ztargs - scavgt)/(1.*zmockt - scavgt))**2.0
                        ibartjj = ibart(zmockt)*coef
c                       vvvvvvvvvvvvvvvvvvvvvvvvFor each projectile electron/shellvvvvvvvvvvvvvvvvvvvvvvvvvvvvvvv
                        bminmax = 0.
                        bmaxmax = 0.
                        ei = 0
                        nout = nep
                        do 180 n=1,nmaxp
c                               ----------Radius of n-shell----
                                nin = nep - nout
                                ntn = 0
                                do 122 l=0,n-1
                                        ntn = ntn + nenl(zmockp,n,l)
122                             continue
                                nout = nout - ntn
                                ra = n*n*a0/(zp*1. - 0.9*nin - 0.264*ntn - 0.1*nout)
                                if (ra.gt.1.5D-8) ra = 1.5D-8

c                               write(18,19)n*1.,ra

                                do 170 l=0,n-1
                                        if (nenl(zmockp,n,l).eq.0) goto 170
                                        sc = scr(zmockp,n,l)
                                        zeffnl = zp*1. - sc
c                                       --------Alternative radius------
c                                       ra = n*n*a0/zeffnl

                                        vbohr  = zeffnl*alpha/n
c                                       -------------Scaled nl's binding energy
                                        coef = (zeffnl/(1.*zmockp - sc))**2.0
                                        ibnlev = eb(zmockp,n,l)*coef

c                                       if ((n.eq.ngp).and.(l.eq.lgp)) ibnlev = ipp(qps)
                                        ibnl = ibnlev*1.602D-12
c                                       ---------nl's velocity ----------
                                        gamme = 1. + ibnlev/5.11D5
                                        if ((ibnlev/5.11D5).lt.1.0D-2) then
                                                vnl = (2.*ibnl/me)**0.5
                                                bete = vnl/c
                                        else
                                                bete = (1. + gamme**-2.)**0.5
                                                vnl = bete*c
                                        endif
c                                       ++++++++++++++++++++++++Velocity ratio++++++++++++++++++
                                        v = vp*n/(c*alpha*zeffnl)
c                                       !!!!!!!!!!!!!!K-shell correction for nuclear enhancement!!!!!!
c                                       if (n.eq.1) v = vp*n/(c*alpha*(zeffnl + 0.5*qtargs))

c                                       ----------------------Calculate zeft-----------------------------------
                                        if (jj.eq.ztargs) then
                                                zeft = ztargs*1.
                                                bmin = zeft*e*e/ibnl
                                                bminmax = bmin
                                                goto 128
                                        endif
                                        if ((jj*e*e/r0).gt.ibnl) goto 170
                                        rright=r0
                                        rleft = a0/1.0D6
125                                     bmin = 0.5*(rright+rleft)
                                        call qsubr(ztargs,jj,bmin,qenc)
                                        zeft = 1.*ztargs - qenc
                                        ecoul = zeft*e*e/bmin
                                        fmin = ecoul - ibnl
                                        if (abs(fmin/ecoul).gt.0.01) then
                                                if (fmin.gt.0.) then
                                                        rleft = bmin
                                                        goto 125
                                                else
                                                        rright = bmin
                                                        goto 125
                                                endif
                                        endif

128                                     ziont2 = zeft**2. + 1.*(ztargs - jj)

c                               --------Calculate individual ionization cross sections from a variety of methods
--------------
c                               --------Bethe----------------------
                                        if (n.gt.1) then
                                                fnl = 0.28/((n*1.)**0.415) - (l*1./(n*1.-1.))*(0.28/((n*1.)**0.4
15) - 0.28/((n*1.)**1.11))
                                        else
                                                fnl = 0.28
                                        endif
                                        fvbethe = fnl*log(4.*v*v)/(v*v)
                                        if (fvbethe.lt.0.) fvbethe = 0.
                                        snlbethe = (6.50D-14)*ziont2*fvbethe/(ibnlev**2.)

c                                       ----------Bohr----------------------
                                        cbohr =  4.*pi*((a0*alpha/beta)**2.)
                                        if ( (13.6/ibnlev).lt.(1./(2.*5.11D5*beta*beta)) ) then
                                                bohrsum = 0.
                                        else
                                                bohrsum = (13.6/ibnlev - 1./(2.*5.11D5*beta*beta) )
                                        endif
                                        snlbohr = cbohr*ziont2*bohrsum
```

```
c                               ------------GGV BEM-----------------------
c                                       ============GGV (Vriens,Armel) Velocity Dependence=======
                                        av = 1./(1. + v*v)
                                        cv = 0.75*v
                                        bv = 1./(1. + cv*cv)
                                        gv1 = 35./6. + 35*atan(cv)/(3.*pi) + (128./(9.*pi))*((v*bv)**3. -bv**1.5
) + (cv*bv/(3.*pi))*(35. - 58.*bv/3. - 8.*bv*bv/3.)
                                        gv2 = (2./(3.*pi))*v*av*bv*((5.-4.*v*v)*(3.*av*av + 1.5*av*bv+bv*bv) - c
v*v*(15./2. + 9.*av + 5.*bv))
                                        gv3 = (16./pi)*v*(av**4.)*log(4.*v*v+1.)
                                        gv4 = v*v*av*(1. + (2./pi)*atan(cv))*(5./2. + 3.*av + 4.*av*av + 8.*av*a
v*av)
                                        if (v.ge.1.) then
                                                gvggv = (1./(4.*v*v))*(gv1 + gv2 - gv3 - gv4)
                                        else
c                                               ====================================
                                                gvggv = 0.696/(exp((0.585-v)/0.096) + 1.)
c                                               ==============My fit=================
                                        endif
                                        snlggv = (6.50D-14)*ziont2*gvggv/(ibnlev**2.)

c                               --------Gryzinski BEM--------------------------
                                        av = v*v/(1. + v*v)
                                        bv = 1./(4.*v*(1. + v))
                                        if (v.ge.0.206) then
                                                gvgryz = (av**1.5)*(av + (2./3.)*(1.+bv)*log(2.7 + v))*(1.-bv)*(
1.- bv**(1.+v*v))/(v*v)
                                        else
                                                gvgryz = (4.*v**4.)/15.
                                        endif
c                                       ##################################
                                        if (v.gt.7.6) gvgryz = 0.615*log(v*v)/(v*v)
c                                       ##############################
                                        snlgryz = (6.50D-14)*ziont2*gvgryz/(ibnlev**2.)

c                               ================Final Choice=====================
                                        snl = snlgryz

c                               ================================================

c                               %%%%%%%%%%%%%%%%%%%Adjustment for indirect ionization%%%%%%%%%%%%%%%
c                                       if ( ((tpev/ap).gt.1.D6).and.(nit.le.1.D17).and.(qps.gt.1) ) snl = snl*1
.4

c                               -)-)-)-)-)-)-)-)-)-)-)-)-)-)-)-)-)-)-)-)-)-)-)-)-)-)-)-)-)-)-)-)-)-)-)-)-)-)-)-)
                                        snuc = snuc + nenl(zmockp,n,l)*snl*nti(tcis,jj)/nmt
                                        asnl = nenl(zmockp,n,l)*snl*nti(tcis,jj)*vp
                                        if (asnl.gt.aionmax) aionmax = asnl

c                                       write(18,19)tcis*1.,ztargs*1.,nti(tcis,jj)/nmt,snl,n*1.,l*1.,ziont2,v,bm
in,gvgryz,ibnlev,vp
c                                       write(18,19)qps*1.,n*1.,l*1.,vp,v,ibnlev,sc,zeffnl,coef

                                        anuc = anuc + asnl

                                        do 165 i=1,nenl(zmockp,n,l)
                                                ei = ei + 1
                                                rnl(ei) = ra
                                                bnl(ei) = 1.4*ra
                                                prob(ei) = snl/(pi*bnl(ei)*bnl(ei))
c                                               write(18,19)ei*1.,prob(ei),snl,(pi*rnl(ei)*rnl(ei)),ra,bnl(ei),v
165                                     continue
170                             continue
180                     continue
c               ^^^
```

```
                        prhonl = 1.
c                       pppppppppppppppppppppppppppppppppppppppppppppppp
                        arec2 = arec2 + prhonl*( 1. - 1.*nnl/(2*n*n) )*srn*vr*ntis
                        srec2 = srec2 + prhonl*( 1. - 1.*nnl/(2*n*n) )*srn
390             continue

c-----------Charge Transfer by eikonal OBK-----------------------------
500             if (qps.eq.0) goto 1001
                do 580 jj=0,ztargs-1
                        if (nti(tcis,jj).eq.0) goto 580
                        scti = 0.
                        zmockt = ztargs - jj
c                       iiiiiiiiiiiiiiiii Initial electron shell in target iiiiiiiiiiiii
                        do 560 ni=1,nmax(zmockt)
                                do 550 li=0,ni-1
                                        if (nenl(zmockt,ni,li).eq.0) goto 550
c                                       ######Scale initial electron binding energy
                                        sc = scr(zmockt,ni,li)
                                        zef = 1.*ztargs - sc
                                        zefm = 1.*zmockt - sc
                                        coef = (zef/zefm)**2.0
                                        ekit = eb(zmockt,ni,li)*coef
c                                       vvvvvvvvvvvvvvvvvvvvvvv final shell n vvvvvvvvvvvvvvvvvvvvvvvvvvv
                                        do 540 n=1,30
                                                nnl = 0
                                                if (n.le.nmaxp) then
                                                        do 505 l=0,n-1
                                                                if (zmockp.gt.0) nnl = nnl + nenl(zmockp,n,l)
505                                                     continue
                                                endif
                                                if (nnl.eq.2*n*n) goto 540
                                                if (nnl.gt.0) then
                                                        ebind = ipp(qps-1)
                                                else
                                                        ebind = 13.6*qps*qps/(1.*n*n)
                                                endif
                                                ekfp=ebind
                                                heta=alpha/beta
                                                ep=(ekfp-ekit)/13.6
                                                vi=sqrt(ekit/13.6)
                                                eika=pi*heta*vi/sinh(pi*heta*vi)
                                                eikb=-2.*heta*vi*atan((0.5*vp-ep*heta)/vi)
                                                eikc=(23./48. + (vi*vi/6.+5.*ep/6.)*heta*heta + 5.*ep*ep*(heta**
4.)/12.)

                                                aeik=eika*exp(eikb)*eikc
                                                ct1=((qps*e*e*6.242D11)**0.4)*(ekit**0.5)*(ekfp**0.3)*(ekev**0.8
)

                                                ct2=(ekev*ekev + 2.0*ekev*(ekit+ekfp) + (ekit-ekfp)**2.0)
c                                               ------pppppppppppdensity correctionpppppppppppppp----------
c                                               prhonl=(1. + 5.0D-18*(ztargs**2.)*nit*(n**5.)/((zp**6.0)*beta/al
pha))**-1.0

                                                prhonl = 1.
c                                               ************************
                                                snl = prhonl*(1. - 1.*nnl/(2.*n*n))*4.1D4*nenl(zmockt,ni,li)*aei
k*(ct1/ct2)**5.0

                                                if (snl.lt.1.0D-40) snl = 0.
c                                               write(18,19)qps*1.,ni*1.,li*1.,n*1.,snl,ct1,ct2,aeik,ekit,1.
c                                               write(18,19)prhonl,aeik,nit
c                                               ************************
                                                scti = scti + snl
540                                     continue
550                             continue
560                     continue
                        act=act+nti(tcis,jj)*scti*vp
580             continue
                if (act.gt.adom) adom = act

c-----------Charge Transfer2 (Projectile -> Target)------------------------------
1001            if (qps.eq.zp) goto 699
                do 1080 jj=1,ztargs
                        if (nti(tcis,jj).eq.0) goto 1080
                        sct2i = 0.
                        zmockt = ztargs - jj
                        if (zmockt.eq.0) then
                                nmaxt = 0
                        else
                                nmaxt = nmax(zmockt)
                        endif
c                       iiiiiiiiiiiiiiiii Initial electron shell in projectile iiiiiiiiiiiii
                        do 1060 ni=1,nmaxp
                                do 1050 li=0,ni-1
                                        if (nenl(zmockp,ni,li).eq.0) goto 1050
c                                       ######Scale initial electron binding energy
                                        sc = scr(zmockp,ni,li)
                                        zef = 1.*qps - sc
                                        zefm = 1.*zmockp - sc
                                        coef = (zef/zefm)**2.0
                                        ekit = eb(zmockp,ni,li)*coef
c                                       vvvvvvvvvvvvvvvvvvvvvvv final shell n in targetvvvvvvvvvvvvvvvvvvvvvvvvv
vvvvv
                                        do 1040 n=1,30
                                                nnl = 0
                                                if (n.le.nmaxt) then
                                                        do 1005 l=0,n-1
                                                                if (zmockt.gt.0) nnl = nnl + nenl(zmockt,n,l)
1005                                                    continue
                                                endif
                                                if (nnl.eq.2*n*n) goto 1040
```

```
                                                if (nnl.gt.0) then
                                                        ebind = ipt(tcis,ztargs-1)
                                                else
                                                        ebind = 13.6*ztargs*ztargs/(n*n)
                                                endif
                                                ekfp=ebind
                                                heta=alpha/beta
                                                ep=(ekfp-ekit)/13.6
                                                vi=sqrt(ekit/13.6)
                                                eika=pi*heta*vi/sinh(pi*heta*vi)
                                                eikb=-2*(heta*vi*atan((0.5*vp-ep*heta)/vi))
                                                eikc=(23./48. + (vi*vi/6.+5.*ep/6.)*heta*heta + 5.*ep*ep*(heta**
4.)/12.)

                                                aeik=eika*exp(eikb)*eikc
                                                ct1=((ztargs*e*e*6.242D11)**0.4)*(ekit**0.5)*(ekfp**0.3)*(ekev**
0.8)

                                                ct2=(ekev*ekev + 2.0*ekev*(ekit+ekfp) + (ekit-ekfp)**2.0)
c                                               ------pppppppppppdensity correctionpppppppppppp----------
c                                               prhonl=(1. + 5.0D-18*(ztargs**2.)*nit*(n**5.)/((zp**6.0)*beta/al
pha))**-1.0

                                                prhonl = 1.
c                                               ************************
                                                snl = prhonl*(1. - 1.*nnl/(2.*n*n))*4.1D4*nenl(zmockp,ni,li)*aei
k*(ct1/ct2)**5.0

                                                if (snl.lt.1.0D-40) snl = 0.
c                                               write(18,19)qps*1.,ni*1.,li*1.,n*1.,snl,ct1,ct2,aeik,ekit,ekfp,e
kev,2.
c                                               write(18,19)eikb,heta,vi,ekfp,ekit,atan((0.5*vp-ep*heta)/vi),-2*
heta
c                                               write(18,19)snl,eikb
c                                               ************************
                                                sct2i = sct2i + snl
1040                                    continue
1050                            continue
1060                    continue
                        act2 = act2 + nti(tcis,jj)*sct2i*vp
1080            continue
                if (act2.gt.adom) adom = act2
                sct2 = act2/(nmt*vp)


c****************************************
699     continue
c****************************

c---------Free Electron Collision Ionization--------
200     if (qps.eq.zp) goto 300
        if (nfe.eq.0.) goto 300
        er = 0.5*me*(vr*vr)
        erev = er*6.242D11
c       xxxxxxxxxxxxx For each projectile electron nl xxxxxxxxxxxxxxxxxxxx
        ei = 0
        do 250 n=1,nmaxp
                do 230 l=0,n-1
                        if (nenl(zmockp,n,l).eq.0) goto 230
c               ######Scale binding energy
                        sc = scr(zmockp,n,l)
                        zef = 1.*zp - sc
                        zefm = 1.*zmockp - sc
                        coef = (zef/zefm)**2.0
                        ibnlev = eb(zmockp,n,l)*coef
                        ibnl = ibnlev*1.602D-12
                        if ((n.eq.ngp).and.(l.eq.lgp)) ibnlev = ipp(qps)
                        zeffnl = zp*1. - scr(zmockp,n,l)
                        step=(abs(erev-ibnlev) + (erev-ibnlev))/(2.0*(erev-ibnlev))
c                       ------nl's scaled orbital radius------
                        ra = (n**2.)*a0/zeffnl

                        if ((vp*hbar/ibnl).gt.bmaxmax) bmaxmax = vp*hbar/ibnl
c                       ---------nl's velocity ----------
                        gamme = 1. + ibnlev/5.11D5
                        if ((ibnlev/5.11D5).lt.1.0D-2) then
                                vnl = (2.*ibnl/me)**0.5
                                bete = vnl/c
                        else
                                bete = (1. + gamme**-2.)**0.5
                                vnl = bete*c
                        endif

c                       write(19,19)n*1.,l*1.,vnl,c*(1. + gamme**-2.)**0.5,(2.*ibnl/me)**0.5,zeffnl*alpha*c/n,ib
nlev/5.11D5

c                       ###################Velocity Ratio#########################3
                        v = sqrt(vp*vp + veth**2.)*n/(c*alpha*zeffnl)

c                       v=1.
c228                    v = v + 0.01
c               ------------Lotz-----------------------------
                        if (v.lt.(1.0)) then
                                gvlotz = 0.
                        else
                                gvlotz = 0.615*log(v*v)/(v*v)
                        endif
                        snllotz = 6.50D-14*step*gvlotz/ibnlev**2.
c               #-----------------Make Final Choice-------------------#
c               ------These are the semi-empirical adjustments discussed in Dissertation
229                     if ((v.lt.1.3).and.(qps.gt.0)) snl = 10.*snllotz
                        if ((v.ge.1.3).and.(v.lt.2.0).and.(qps.gt.0)) snl = 2.*snllotz
```

```
                        if ((v.ge.2.0).and.(qps.gt.0)) snl = snllotz
                        if (qps.eq.0) snl = snllotz

c2295                   goto 228
c-------------------------------------------------------------------------------
                        sfe = sfe + nenl(zmockp,n,l)*snl
                        asnl = nenl(zmockp,n,l)*snl*nfe*vr
                        if (asnl.gt.aionmax) aionmax = asnl

                        do 225 i=1,nenl(zmockp,n,l)
                                ei = ei + 1
                                prob(ei) = prob(ei) + (nfe/nit)*snl/(pi*bnl(ei)*bnl(ei))
225                     continue

                        afe = afe + asnl
230             continue
250     continue

c----------Free Electron Radiative Electron Capture--------------
300     if (qps.eq.0) goto 399
        if (nfe.eq.0.) goto 399
        aa=2.11D-22
        g1=1.1
        er = 0.5*me*vr*vr
        erev = er*6.242D11
c       ~~~~~~~~~~~~Find possible landing sites in 'n' shell~~~~~~~~~~~~~~~~~~~
        do 350 n=1,10
                nnl = 0
                if (n.le.nmaxp) then
                        do 305 l=0,n-1
                                if (zmockp.gt.0) nnl = nnl + nenl(zmockp,n,l)
305                     continue
c                       --------Is it full?--------->
                        if ((nnl.eq.2*n*n).or.(n.eq.1)) goto 350
                        ebind = ipp(qps-1)
                else
                        ebind = 13.6*qps*qps/(n*n)
                endif
                hn = erev + ebind
c               ************
                srn=aa*ebind*ebind*g1*n/(erev*hn)
c               write(18,19)qps*1.,n*1.,l*1.,ebind,srn
c               ***************
c               ppppppppppp Density correction pppppppppppp
                prhonl=(1. + 5.D-18*(ztargs**2.)*nit*(n**5.)/((zp**6.)*beta/alpha))**-1.
                prhonl = 1.
c               ppppppppppppppppppppppppppppppppppppppppppppp
                arec = arec + prhonl*( 1. - 1.*nnl/(2*n*n) )*srn*vr*nfe
                srec = srec + prhonl*( 1. - 1.*nnl/(2*n*n) )*srn
350     continue

c----------Combine REC rates
399     arect = arec + arec2
        srect = srec + srec2
        if (arect.gt.adom) adom = arect

c----------Three Body Recombination---------------------
400     if (qps.eq.0) goto 600
        if (nfe.eq.0.) goto 600
        a3br=a3br + (nfe*(qps**3.0)) * (4.048D-4*(vr/v0))**9.0
        s3br = a3br/(nfe*vr)
        if (a3br.gt.adom) adom = a3br

c-----------------------------------------Dielectronic Recombination-----------------------------------------
---------
c                       ---- Incoming free electron lands in shell n, transferring some of its energy to an
c                            electron bound in shell i which bumps to shell j ---
600     if (nfe.eq.0) goto 700
        if (qps.eq.0) goto 700
        if (qps.eq.zp) goto 700
        coe=nfe*((1.304D26*ttarg)**-1.5)
c       vvvvvvvvvvvvvvvvvv nc loop Captured electron shell# vvvvvvvvvvvvvvvvvvvvvvvvvvvvvvvvvvvvvvv
        do 690 nc=nmaxp+1,50
c               vvvvvvvvvvvvvvvvvvvvvvvv lc loop vvvvvvvvvvvvvvvvvvvvvvvvvvvvvvvvvvvvvvvvvvvvvvvv
                lcavg = 0
                do 610 lc=0,nc-1
                        glc = 2*(2*lc + 1)
                        lcavg = lcavg + glc*lcavg
610             continue
                lcavg = int(lcavg/(2*nc*nc))
c               )))) energy of electron captured ((((
                ipc=13.598*qps*qps/(nc*nc)
                en = -1.*ipc
c       vvvvvvvvvvvvvvvvvvvvvvv Inner electron to receive excess energy - i loop vvvvvvvvvvvvvvvvv
                do 670 ni=1,nmaxp
c               vvvvvvvvvvvvvvvvvvv li loop to get average li and energy vvvvvvvvvvvvvvvvvvvvvv
                        do 660 li = 0,ni-1
                                nnli = nenl(zmockp,ni,li)
c                               ---------->>
                                if (nnli.eq.0) goto 660
c                       ..........Determine i electron energy using screening....
                                sc = scr(zmockp,ni,li)
                                zef = 1.*zp - sc
                                zefm = 1.*zmockp - sc
                                coef = (zef/zefm)**2.0
                                ipi = eb(zmockp,ni,li)*coef
                                if ((ni.eq.ngp).and.(li.eq.lgp)) ipi = ipp(qps)
                                ei = -ipi
```

```
c                               vvvvvvvvvvvvvvvvvvvvvvv Landing site of recipient electron - nj loop vvvvvvvvvvvv
vvvvvvvvvvvvvvvv
                                do 650 nj=ni+1,20
                                        ljavg = 0
                                        njsum = 0
                                        gnj = 2*nj*nj
                                        do 645 lj = 0,nj-1
                                                glj = 2*(2*lj+1)
                                                if (nj.le.nmaxp) then
                                                        nlj = nenl(zmockp,nj,lj)
                                                else
                                                        nlj = 0
                                                endif
                                                njsum = njsum + nlj
                                                ljavg = ljavg + lj*(glj - nlj)
645                                     continue
                                        if (njsum.eq.gnj) goto 650
                                        ljavg = int(ljavg/(gnj - njsum))
                                        if (nj.le.nmaxp) then
c                                               ---Find lowest populated l level and use its energy----
                                                llow = nj-1
620                                             if (nenl(zmockp,nj,llow).eq.0) then
                                                        llow = llow-1
                                                        if (llow.gt.0) goto 620
                                                endif
                                                sc = scr(zmockp,nj,llow)
                                                enl = eb(zmockp,nj,llow)
                                                zef = 1.*zp - sc + 0.8
                                                zefm = 1.*zmockp - sc
                                                coef = (zef/zefm)**2.0
                                                ebind = enl*coef
                                                if ((nj.eq.ngp).and.(llow.eq.lgp)) ebind = ipp(qps-1)*((zp*1. -
sc + 0.8)/(zp*1. - sc))**2.
                                                if (eb(zmockp,ni,li).le.eb(zmockp,nj,llow)) goto 650
                                        else
                                                ebind = 13.6*qps*qps/(nj*nj)
                                        endif
                                        ipj = ebind
                                        ej = -1.*ipj
c                               ........Prevent imaginary radical.................
                                        if ((ej-ei+en).lt.0.) goto 650
                                        if (ipi.lt.ipj) goto 650
c                               ))))))) function resonance f ((((((((((((
                                        s=((ej-ei+en)/ttargev)**0.5
                                        t=(0.5*me*vp*vp/ttarg)**0.5
                                        fst = exp(-1.*((s-t)**2.))/(4.*s*t) - exp(-1.*((s+t)**2.))/(4.*s*t)
                                        if (fst.lt.1.D-40) then
                                                fst=0.
                                                goto 650
                                        endif
c                               -------------- oscilator strength -------------
                                        fij1 = 1.96*(nj**3.)*ni*(nj**2. - ni**2.)**-3.
                                        fji1 = 1.96*(ni**3.)*nj*(nj**2. - ni**2.)**-3.
c                               ------------------Gaunt Factor--------
                                        gl = 0.2/(2*nc*nc)
c                               ######!!!!!!!!Auto-Ionization and Radiative Decay rates!!!!!!################
                                        aa1=fij1*(8./sqrt(3.))*(13.6/hbev)*(nc**-3.)*(qps*qps*13.6/(ipi-ipj))/(2
*lcavg+1)
                                        ar1=fji1*(13.6/hbev)*(137.**-3.0)* ( ((ipj-ipi)/13.6)**2. )
c                               ################These are additional processes which may detract from true proce
ss##########
                                        aav = 0.
                                        aa1jive=0.
                                        aa1vije=0.
                                        ar1vi=0.
                                        nv = ngp
                                        lv = lgp
                                        nval = nenl(zmockp,nv,lv)
                                        if (nval.eq.0) goto 640
c                                       ----------Find new valence energy-----------
                                        ipv = ipp(qps)*((zp*1. - sc + 0.8)/(zp*1. - sc))**2.
                                        ev = -1.*ipv
c                                       ----->
                                        if (ipv.ge.ipi) goto 640
                                        if (nv.le.ni) goto 640
c                                       ################j electron goes to i, valence electron bails############
###
c                                       ------------Gaunt--------
                                        gx=ek/ipv
                                        glp=(nv**0.66666)/(sqrt(1. + gx))
                                        gd=sqrt(1. + gx)/(2.5*nv)
                                        gn0=(0.4/sqrt(pi)) * sqrt(gd)/(2. - exp(-0.6/(sqrt(gd)*(nv**1.33333) )))
                                        gl=gn0*exp(-1.*gd*(1.*lv-glp)**2.)
                                        aa1jive = nval*fij1*gl*(8./sqrt(3.0))*(13.6/hbev)*(nv**-3.)*(qps*qps*13.
6/(ipi-ipj))/(2*lcavg+1)
c                                       -------Oscillator Strngths-----
                                        fiv1 = 1.96*(nv**3.)*ni*(nv**2. - ni**2.)**-3.
                                        fvi1 = 1.96*(ni**3.)*nv*(nv**2. - ni**2.)**-3.
c                                       ##############valence electron goes to i, j electron bails###############
                                        gl = 0.2
                                        aa1vije = fiv1*gl*(8./sqrt(3.0))*(13.6/hbev)*(nj**-3.)*(qps*qps*13.6/(ip
i-ipv))/(2*ljavg+1)
c                                       ################j, n electrons remain, valence returns to i, photon rele
ased############
                                        ar1vi = fvi1*(13.6/hbev)*(137.0**-3.0)*( ((ipi-ipv)/(13.6))**2.0 )
c                                       ################Total#############
640                                     aav = aav + (aa1jive + aa1vije + ar1vi)
c                               ppppppppppppppppDensity suppression factorpppppppppppppppp
```

```
                                        prhonl=1.0
c                                       prhonl=prhonl*(1. + 5.D-18*jj*jj*nit*lcavg*lcavg*(nc**5.0)/((qps**6.0)*v
p*137.0/c))**-1.
c                                       prhonl=prhonl*(1. + 5.D-18*jj*jj*nit*ljavg*ljavg*(nj**5.0)/((qps**6.0)*v
p*137.0/c))**-1.
c                       !!!!!!!!!!!!!!!!!!!!!!!!!!!!!!!!!!!!!!!!!!!!!!!!Final Expression!!!!!!!!!!!!!!!!!!!!!!!!!!!!!!
!!!!
c                                       *********************************
                                        adrnlij = prhonl*coe*nnli*((gnj-njsum)/(1.*gnj))*(2*lcavg+1)*fst*ar1*aa1
/(ar1 + aa1 + aav)
                                        adr = adr + adrnlij
c                                       write(18,19)qps*1.,nc*1.,ni*1.,nj*1.,adrnlij,en,ei,ej,ev,ar1,aa1,aav,aa1
vije,aa1jive,ar1vi,fst
c                                       write(18,19)qps*1.,nc*1.,ni*1.,nj*1.,nv*1.,aav,ar1*aa1/(ar1 + aa1),ar1*a
a1/(ar1 + aa1 + aav)
c                                       write(18,19)13.6/(ipi-ipj),( ((ipj-ipi)/13.6)**2. ),fij1
c                                       write(18,19)fij,fiv,((gnj-njsum)/gnj)*1.,(2*lcavg+1)*1.,fst,ar1*aa1/(ar1
 + aa1 + aav)
c                                       write(18,19)nc*1.,lc*1.,ni*1.,li*1.,nj*1.,aa1jive,aa1vije,ar1vi,fiv,fij
                                        sdr = sdr + adr/(nfe*vr)
650                                     continue
c                               ^^^^^^^end of nj loop^^^^^^^^
660                             continue
c                       ^^^^^^^^^^^^^^^^ li loop ^^^^^^^^^^^^^^^^
670             continue
c               ^^^^^^^end of ni loop^^^^^^^
690     continue
c       ^^^^^^^^end of nc loop^^^^^^^
        if (adr.gt.adom) adom = adr

c-------------------------------------------------------------------------------------------------------------------
-----

c       ###################### Put all rates together ##########################
700     alose = anuc + afe
        again = arect + act + adr + a3br
        atot = (alose - again)
        sigion = alose/(nmt*vp)
        sigrec = again/(nmt*vp)
        sionmax = aionmax/(nmt*vp)

c       ))))))))))))))))))))Probability of no reaction((((((((((
        probnot = 1.
        probsum=0.
        impactsum=0.
        do 710 i=1,nep
                impactsum = impactsum + pi*bnl(i)*bnl(i)
                probsum = probsum + prob(i)
                probnot = probnot*(1. - prob(i))
710     continue
        ptot = 1. - probnot
        pgross = probsum/nep

        write(18,19)

c       @@@@@@@@@@@@@@@@@@@@@@@@@@@@@@@@@@@@@Compute Multiple Probabilities and Xsections@@@@@@@@@@@@@@@@@@@@@@@@@@
@
        do 799 i=1,4
                sigmult(i) = 0.
799     continue

c       xxxxxxxxxxxxxxxxxxxxArrange values in order of impact parameterxxxxxxxxxxxxxxx
        i=1
        forder = 0
711     if (bnl(i).gt.bnl(i+1)) then
c               .....Impact regime
                hold = bnl(i)
                bnl(i) = bnl(i+1)
                bnl(i+1) = hold
c               ......shell radius
                hold = rnl(i)
                rnl(i) = rnl(i+1)
                rnl(i+1) = hold
c               .........probability
                hold = prob(i)
                prob(i) = prob(i+1)
                prob(i+1) = hold
                forder = 1
        endif
        i = i+1
        if (i.lt.nep) goto 711
        if (forder.eq.1) then
                forder=0
                i=1
                goto 711
        endif


        write(18,16)
        write(18,17)sigion,pgross
c       write(18,17)sigion
c       write(18,17)sigion,sigion/impactsum
16      format("Total Ionization Cross Section [cm2]      Gross Probability")
17      format("   ",D10.3,"            ",D10.3)

        write(18,19)
        write(18,22)
        write(18,21)sigrec
```

```
22      format("Total Capture Cross Section [cm2]")

        write(18,19)
        write(18,20)
        write(18,21)bnl(nep),rnl(nep)
20      format("Max Impact Radius [cm]    <r> [cm]")
21      format("  ",D10.3,"      ",D10.3)

        goto 1101
c       ((((((This section is skipped in favor of the alternative mutliple method
c       shown below))))))))))))))))
c       ================Here's one way to do multiples================
c       ------Single-----------------
        do 1100 i=1,nep
                dsig = 0.
                fyes = prob(i)/(1. - prob(i))
                flow = 1.
                do 720 q=1,i
                        flow = flow/(1. - prob(q-1))
                        dsig = dsig + pi*(bnl(q)**2. - bnl(q-1)**2.)*probnot*fyes*flow
c                       write(18,19)i*1.,q*1.,dsig,bnl(q),bnl(q-1),(bnl(q)**2. - bnl(q-1)**2.),probnot,fyes,flow
720             continue
                sigmult(1) = sigmult(1) + dsig
c               ------Double----------------
                do 1000 j = i+1,nep
                        dsig = 0.
                        fyes = fyes*prob(j)/(1. - prob(j))
                        flow = 1.
                        do 730 q=1,i
                                flow = flow/(1. - prob(q-1))
                                dsig = dsig + pi*(bnl(q)**2. - bnl(q-1)**2.)*probnot*fyes*flow
730                     continue
                        sigmult(2) = sigmult(2) + dsig
c                       -------Triple---------------------
                        do 900 k = j+1,nep
                                dsig = 0.
                                fyes = fyes*prob(k)/(1. - prob(k))
                                flow = 1.
                                do 740 q=1,i
                                        flow = flow/(1. - prob(q-1))
                                        dsig = dsig + pi*(bnl(q)**2. - bnl(q-1)**2.)*probnot*fyes*flow
740                             continue
                                sigmult(3) = sigmult(3) + dsig
c                               --------Quadruple--------------------
                                do 800 l = k+1,nep
                                        dsig = 0.
                                        fyes = fyes*prob(l)/(1. - prob(l))
                                        flow = 1.
                                        do 750 q=1,i
                                                flow = flow/(1. - prob(q-1))
                                                dsig = dsig + pi*(bnl(q)**2. - bnl(q-1)**2.)*probnot*fyes*flow
750                                     continue
                                        sigmult(4) = sigmult(4) + dsig
800                             continue
900                     continue
1000            continue
1100    continue

1101    write(18,19)

        write(18,19)
        sigtot = 0.
        do 1300 i=1,4
                sigtot = sigtot + i*sigmult(i)
1300    continue

c%%%%%%%%%%%%%%%%%%  Or, here is a simpler way to do multiples%%%%%%%%%%%%%%%%%%%%%%
        sigmult(1) = sigion/(1. + 2.*pgross + 3.*pgross*pgross + 4.*pgross*pgross*pgross + 5.*pgross*pgross*pgro
ss*pgross)
        sigmult(2) = sigmult(1)*pgross
        sigmult(3) = sigmult(2)*pgross
        sigmult(4) = sigmult(3)*pgross
        sigmult(5) = sigmult(4)*pgross

        write(18,15)
        do 1310 i=1,5
                write(18,14)i,sigmult(i)
1310    continue

14      format(I5,"     ",D10.3)
15      format("Multiplicity   Cross Section [cm2]")

c       ========Possible choices of x.out output lines================
        write(19,19)qps*1.,alose/(nmt*vp),again/(nmt*vp)
c       write(19,19)qps*1.0,alose/(nmt*vp),again/(nmt*vp),anuc/(nmt*vp),afe/(nmt*vp),act2/(nmt*vp),arect/(nmt*vp
),act/(nmt*vp),adr/(nmt*vp)
c       write(19,19)(tps/ap/1.602D-6),qps*1.,alose/(nmt*vp),again/(nmt*vp),anuc/(nmt*vp),afe/(nmt*vp),arect/(nmt
*vp),act/(nmt*vp),adr/(nmt*vp)
19      format(D10.5," ",D10.5," ",D10.5," ",D10.5," ",D10.5," ",D10.5," ",D10.5," ",D10.5," ",D10.5," ",D10.5,"
",D10.5," ",D10.5)
c       write(19,19)(tps/ap/1.602D-6),qps*1.,alose*1.D24/(nmt*vp),again*1.D24/(nmt*vp)
c       write(19,19)qps*1.,snuc,sfe,srect,scti,sdr
c       write(19,19)qps*1.,anuc,afe,arec,act,adr,a3br

c&&&&&&&&&&&&&&&&&&&&&&&&&&&&&&&&
c       These loops are for projectile charge state and energy variation
c       if requested
        if ((qloop.eq.1).and.(qps.lt.zp)) then
```

```
                qps = qps+1
                goto 10
        endif

c       if (tps.gt.0.) then
c               tps = tps *0.99
c               goto 9
c       endif

        return
        end
c *_*_*_*_*_*_*_*_*_*_*_*_*_*_*_*_*_*_*_*_*_*_*_*_*_*_*_*_*_*_*_*_*_*_*_*_*_*

cvvvvvvvvvvvvvvvvvQenc(r)vvvvvvvvvvvvvvvvvvvvvvvvvvvvvvv
c       *****This subroutine calculates the average number of electrons enclosed within
c       a given radius about an atom or ion.***********

        subroutine qsubr(ztargss,jjs,r,qenc)
        common zp,ap,ztarg,atarg,ibart,scr,ttargev,eb,nti,nmt,nenl,ng,lg,nmax,lmax,ntc,ipp,ipt

        real*16 mp
        real*16 scr(1:100,1:7,0:6),ttargev,nit,nfe,nti(1:10,0:100),nmt
        real*16 eb(1:100,1:7,0:6), ibart(1:100), ipp(0:100), ipt(1:10,0:100)
        real*16 ntot
        integer zp,ap,ztarg(1:10),atarg(1:10),ntc
        integer nenl(1:100,1:7,0:6), ng(1:100), lg(1:100), nmax(1:100), lmax(1:100)

        real*16 c,me,meev,amu,amev,pi,e,a0,alpha,hbar
        parameter (c=2.998D10, me=9.108D-28, meev=5.11D5, amu=1.66D-24)
        parameter (amev=931.502D6, pi=3.1415927, e=4.803D-10, a0=0.529D-8, alpha=7.3D-3, hbar=1.054D-27)

        integer ztargss, jjs, zef, nin, lin, ntnin
        integer ntout, nout,lout
        real*16 r, qenc, rn, cn, r0, az

        nit = 0.
        nfe = 0.
        do 28 i = 1,ntc
                do 25 ii = 0,ztarg(i)
                        nfe = nfe + ii*nti(i,ii)
                        nit = nit + nti(i,ii)
25              continue
28      continue

        mp = ap*amu
        zef = ztargss - jjs

        qenc=0.
        r0 = (3./(4.*pi*nit))**0.333333
        az = a0*(zp**-0.33333)

c...........diagnostic.....
c       r = 0.01D-8

29      ntot = 0.

c-------------------------------------------------------------------------
        do 150 n=1,nmax(zef)
                ntn=0
                ntnin = 0
                ntout = 0
c               --------tally electrons in shells within 'n'--------
                do 140 nin = 1,n-1
                        do 130 lin = 0,nin-1
                                ntnin = ntnin + nenl(zef,nin,lin)
130                     continue
140             continue
c               ----------tally electrons in 'n'---------
                do 145 l = 0,n-1
                        ntn = ntn + nenl(zef,n,l)
145             continue
c               ---------And electrons in outer shells...----
                do 147 nout = n+1,nmax(zef)
                        do 146 lout = 0,nout-1
                                ntout = ntout + nenl(zef,nout,lout)
146                     continue
147             continue
c               ------------radius of max of r^2 rho(r,n)----------
                rn = n*n*a0/(1.*ztargss - 0.9*ntnin - 0.264*ntn - 0.1*ntout)
                cn = ntn/(4.*pi*rn*rn*(1. - (1. + (r0/rn))*exp(-r0/rn)))
                qenc = qenc + 4.*pi*cn*rn*rn*(1. - (1. + r/rn)*exp(-r/rn))

                ntot = ntot + cn*exp(-r/rn)/r

c               write(18,151)ztargss*1.,jjs*1.,n*1.,nin*1.,ntn*1.,rn,cn,r,qenc,(1. - (1. + r/rn)*exp(-r/rn))

150     continue
151     format(10D10.3)

c       write(18,151)r/1.D-8,4.*pi*ntot*r*r*1.D-8
c       r=r+0.01D-8
c       goto 29

        return
        end
c^^^^^^^^^^^^^^^^^^^^^^^^^^^^^^^^^^^^^^^^^^^^^^^^^^^^^^^^^^^^^^^^^^^^^^^
```